

**Protein-Protein Interaction Analysis: Expanded Hydrogen/Deuterium Exchange  
Tandem Mass Spectrometry and Host Cell Protein Characterization**

by

Qingyi Wang

A dissertation submitted in partial fulfillment  
of the requirements for the degree of  
Doctor of Philosophy  
(Chemistry)  
in the University of Michigan  
2019

Doctoral Committee:

Professor Kristina I. Håkansson, Chair  
Professor Heather Carlson  
Professor Robert T. Kennedy  
Professor Brandon T. Ruotolo

Qingyi Wang

qywang@umich.edu

ORCID iD: 0000-0003-0949-0969

© Qingyi Wang 2019

**To My Beloved Family**

## Acknowledgements

I would like to express my appreciation to many people, who have supported and helped me throughout these years at Michigan for studying/working toward my Ph.D. degree.

I appreciate the opportunity that the Michigan Chemistry Department and Rackham Graduate School have offered me. Thank my PI, Dr. Kristina “Kicki” Håkansson. Her guidance and care have always been a source of strength for me to get through difficulties in my research and my life. Special thanks go to all my previous and current lab mates: Dr. Ning Wang, Dr. Wendi Hale, Dr. Tao Jiang, Dr. Phil McClory, Dr. Kevin Ileka, Dr. Hye Kyong Kweon, Dr. Nick Borotto, Dr. Isaac Agyekum, Eunju Jang, Nhat Le, and Carson Szot. It has been a pleasure working with and learning from you guys. Together we went through a lot of stories. There were ups and downs, and they are precious memories to me. Hope we may see each other again very soon.

Thank all the financial sources – NIH and NSF funding, department fellowship, and Rackham Travel Grant. Thank Phil Andrews’ group for allowing me doing experiments on their instrument. And I appreciate the time and efforts that my committee has put on me for helping me fulfill the graduation requirements.

Also, I would like to thank the mass spectrometry group at Bristol-Myers Squibb, Hopewell, NJ, where I did a six-month co-op in my fifth year. Specially, I want to thank Dr. Tom Slaney, my manager, for providing instructions on my work and all kinds of supports. Inspiring discussions with Dr. Li Tao, Dr. Richard Ludwig, Dr. Wei Wu, and Tom helped me achieve continuous progress on my project.

To my friends in China, Ann Arbor, and other places around the U.S., I cannot say

enough thanks to you – you have been brightening my spirit and inspiring my life. To my boyfriend, Jialiu, you helped me through every frustrating moment, with all your heart and soul – thank you so much for love and support. I hope in future we can take our time to enjoy this life. To my parents, Junhua and Minli, you are the people I love and admire the most in the world, and I just wish I could spend more time with you. It always means a lot to me hearing you say you are proud of me.

Thanks to all of you, I can be in the position where I am today. I will always look forward and move forward, for the best is yet to come. So, stay tuned. ☺

Qingyi (Emma) Wang

March 23rd, 2019

Ann Arbor, MI

## Table of Contents

<b>Dedication .....</b>	<b>ii</b>
<b>Acknowledgements .....</b>	<b>iii</b>
<b>List of Figures.....</b>	<b>x</b>
<b>List of Tables.....</b>	<b>xv</b>
<b>List of Abbreviations.....</b>	<b>xvii</b>
<b>Abstract.....</b>	<b>xx</b>
<b>Chapter 1 Introduction.....</b>	<b>1</b>
1.1 Mass Spectrometry-Based Protein Structural Analysis .....	1
1.1.1 Biotherapeutic Proteins .....	1
1.1.2 Mass Spectrometry-Based Structural Biology Tools .....	3
1.1.3 Characterization of Host Cell Proteins in Biopharmaceuticals.....	4
1.2 Techniques and Strategies in Modern Proteomics .....	6
1.2.1 Bottom-up vs. Top-down Proteomic Strategies .....	6
1.2.2 Liquid Chromatography Mass Spectrometry (LC/MS) .....	7
1.2.3 Fourier Transform Mass Spectrometry (FT MS) .....	8
1.2.4 Tandem Mass Spectrometry (MS/MS) .....	13
1.2.4.1 Slow-Heating Fragmentation .....	15
1.2.4.2 Electron-Based Fragmentation.....	16
1.2.5 Charging and Supercharging.....	18
1.2.5.1 Electrospray Ionization (ESI) .....	18

1.2.5.2 Supercharging Strategies .....	19
1.3 Hydrogen/Deuterium Exchange Mass Spectrometry (HDX MS) .....	22
1.3.1 HDX Kinetics.....	22
1.3.2 HDX MS approaches .....	24
1.3.2.1 Bottom-up HDX MS.....	24
1.3.2.2 Top-down HDX MS.....	28
1.3.3 Hydrogen/Deuterium (H/D) Scrambling in HDX MS/MS .....	29
1.4 Dissertation Overview .....	32
1.5 References.....	33
<b>Chapter 2 Gas-Phase Hydrogen/Deuterium Scrambling in Negative-Ion Mode Tandem</b>	
<b>Mass Spectrometry .....</b>	<b>52</b>
2.1 Introduction.....	52
2.2 Experimental .....	53
2.2.1 Materials .....	53
2.2.2 Peptide Derivatization.....	54
2.2.3 Deuterium/hydrogen Exchange .....	54
2.2.4 Mass Spectrometry.....	55
2.2.5 Data Analysis .....	57
2.3 Results and Discussion .....	58
2.3.1 H/D Scrambling in Collision Induced Dissociation of Electrosprayed Deprotonated Peptides .....	62
2.3.2 H/D Scrambling in Radical-Driven Dissociation of Peptide Anions.....	68
2.4 Conclusions.....	74
2.5 Acknowledgements .....	75
2.6 References.....	75

**Chapter 3 Supercharging for Improved Electron Capture/Transfer Dissociation (ECD/ETD)-based Hydrogen/Deuterium Exchange Mass Spectrometry..... 80**

3.1 Introduction.....	80
3.2 Experimental.....	83
3.2.1 Materials.....	83
3.2.2 Hydrogen/Deuterium Exchange and Proteolysis.....	83
3.2.3 Liquid Chromatography.....	84
3.2.4 Mass Spectrometry.....	85
3.2.5 Data Analysis.....	86
3.3 Results and Discussion.....	87
3.3.1 Supercharging of peptic peptides.....	87
3.3.2 Post-column addition of supercharging reagent for improved liquid chromatography.....	95
3.3.3 Supercharging with varying <i>m</i> -NBA concentrations and with other supercharging reagents.....	98
3.3.4 Supercharging in LC ECD MS/MS of peptic peptides.....	102
3.3.5 <i>m</i> -NBA supercharging in HDX LC/MS.....	105
3.4 Conclusion.....	108
3.5 Acknowledgements.....	109
3.6 References.....	109

**Chapter 4 The Presence of *b* ions in Electron Capture/Transfer Dissociation (ECD/ETD) of Supercharged Peptides.....114**

4.1 Introduction.....	114
4.2 Experimental.....	116
4.2.1 Reagents and Sample Preparation.....	116
4.2.2 Liquid Chromatography.....	117

4.2.3 Mass Spectrometry.....	117
4.2.4 Data Analysis .....	118
4.3 Results and Discussion .....	119
4.3.1 ECD and ETD of peptides with few or no basic amino acid residues.....	119
4.3.2 ECD and ETD of the 4+, 5+, and 6+ charge states of melittin.....	122
4.3.3 <i>b</i> ions observed in ECD and ETD of tryptic and peptic peptides with varying charge states .....	125
4.3.4 Possible mechanisms for the formation of <i>b</i> ions from supercharged peptides upon ECD and ETD.....	127
4.4 Conclusions.....	132
4.5 Acknowledgements .....	133
4.6 References.....	133

**Chapter 5 Off-line HILIC Sample Preparation for Improved Detection of Host Cell Proteins in Drug Substances ..... 137**

5.1 Introduction.....	137
5.2 Experimental .....	139
5.2.1 Materials .....	139
5.2.2 Offline HILIC Sample Preparation.....	140
5.2.3 HILIC Separation Parameters and Fraction Collection .....	140
5.2.4 Trypsin Digestion.....	142
5.2.5 UPLC-MS/MS Analysis of Tryptically Digested HILIC Fractions.....	142
5.2.6 Database Search Parameters .....	143
5.3 Results and Discussion .....	143
5.3.1 Separation Profiles of HCPs and Therapeutic mAb Using HILIC .....	145
5.3.2 HCP Detection with Spiked Samples.....	147
5.3.3 HCP Detection with NISTmAb .....	150

5.3.4 HCP Detection with Fusion Protein.....	156
5.4 Conclusions.....	157
5.5 References.....	158
<b>Chapter 6 Conclusions and Future Directions .....</b>	<b>160</b>
6.1 Dissertation Summary.....	160
6.2 Future Directions .....	163
6.2.1 Hydrogen scrambling mechanisms in negative ion mode MS/MS.....	163
6.2.2 Supercharging combined with ECD HDX MS/MS for elucidation of structural changes of a modular polyketide synthase during its catalytic cycle .....	164
6.2.3 Investigation of the occurrence of <i>b</i> -type ions in ECD/ETD of supercharged peptides .....	166
6.2.4 Further characterization and optimization of the offline HILIC method and the potential of utilizing HDX MS to investigate interactions between HCPs and biotherapeutic proteins.....	170
6.3 References.....	171

## List of Figures

<b>Figure 1.1</b> Cyclotron motion of a positively charged ion in the plane perpendicular to the magnetic field lines .....	10
<b>Figure 1.2</b> Schematic diagram of a 7-T SolariX quadrupole-FT-ICR mass spectrometer (Bruker Daltonics).....	11
<b>Figure 1.3</b> Schematic diagram of an LTQ Orbitrap XL hybrid FT mass spectrometer (Thermo Fisher Scientific).....	12
<b>Figure 1.4</b> Schematic diagram of an Orbitrap Fusion Lumos tribrid mass spectrometer (Thermo Fisher Scientific).....	13
<b>Figure 1.5</b> Nomenclature for peptide fragment ions in MS/MS .....	15
<b>Figure 1.6</b> Diagram of protein HDX MS and MS/MS workflows with the use of LC and/or gas-phase fragmentation techniques .....	25
<b>Figure 1.7</b> Diagram of online pepsin digestion setup. The pepsin column can be placed either inside or outside the cooling chamber .....	26
<b>Figure 1.8</b> Principle of measuring H/D scrambling by gas-phase fragmentation of selectively labeled model peptides. The figure accounts for C-terminal $y$ -type ions and thus the sequence is read from right to left.....	30
<b>Figure 2.1</b> Illustration of a selectively deuterated peptide undergoing gas-phase dissociation with (left) and without (right) H/D scrambling. Blue and orange curves illustrate theoretical 0 and 100% scrambling levels, respectively, for a hypothetical series of $y$ -type ions ( $y_2$ - $y_{11}$ ) .....	59
<b>Figure 2.2</b> Deuteration levels of ECD-derived $c$ -type fragment ions after tuning the ion source for gentle transmission. Data were collected on a Bruker SolariX FT-ICR mass spectrometer...	60
<b>Figure 2.3</b> Deuteration levels of ETD-derived $c$ -type fragment ions after gentle ion transfer and selection conditions. Data were collected on a Thermo Scientific Orbitrap Fusion Lumos mass spectrometer .....	60
<b>Figure 2.4</b> nCID MS/MS spectrum of doubly deprotonated P1 (HHHHHHIIKIIK). * indicates internal fragments .....	63
<b>Figure 2.5</b> Observed isotopic distributions of $c_3$ (A) and $y_9$ (C) fragment ions from nCID of the	

natural and deuterated peptide P1 (HHHHHHIHKIHK). The weighted average  $m/z$  value for each species is illustrated by a solid green (natural) or grey (deuterated) line. Theoretical deuteration levels for 100 and 0% scrambling are denoted with dashed orange (100%) and blue (0%) lines, respectively. Deuteration levels for all measured P1 nCID-derived  $c$ - (B) and  $y$ -type (D) fragment ions. Blue and orange lines represent expected deuteration levels for 0 and 100% scrambling, respectively ..... 64

**Figure 2.6** Deuteration levels of nCID-derived  $y$ -type fragment ions from the peptide P2 (H\*HHHHHIHK\*IHK\* in which \* denotes sites of acetylation) ..... 65

**Figure 2.7** nCID MS/MS spectrum of doubly deprotonated P3 (DDDDDDIIEIIE). \* indicates internal fragments ..... 66

**Figure 2.8** Deuteration levels observed for  $y$ -type ions from nCID of the peptide P3 (DDDDDDIIEIIE) as well as expected deuteration levels for 0% and 100% scrambling, respectively ..... 66

**Figure 2.9** nCID-generated P1 deuteration levels overlaid with 0% and 100% scrambling curves with the 100% curve being adjusted to account for hydrogen exchange at histidine C-2 carbon atoms (A) and adjusted to account for both histidine C-2 and  $C_\beta$  hydrogen atom exchange (B). 67

**Figure 2.10** nFRIPS MS/MS spectrum of singly deprotonated P1 (HHHHHHIHKIHK). Subscripted “r” denotes presence of cleaved TEMPO label..... 69

**Figure 2.11** EDD MS/MS spectrum of doubly deprotonated P3 (DDDDDDIIEIIE).  $v_3$  = third harmonic ..... 70

**Figure 2.12** Deuteration levels of nFRIPS-generated  $z$ -type fragment ions (A) and EDD-generated  $a$ -type ions (B) from the peptide P3 as well as predicted 0% and 100% scrambling curves. EDD was performed after both “soft” and “harsh” ion source conditions .... 70

**Figure 2.13** niECD MS/MS spectra of (A) P3 (DDDDDDIIEIIE) and (B) P4 (DDDDDIIEI).  $v_3$  = third harmonic.  $v_5$  = fifth harmonic. (A) was collected under the condition of pH = 7.5; (B) was collected under the condition of pH = 4.0 ..... 73

**Figure 3.1** Diagram of the HDX LC/MS set-up used in this work. The red arrow and dot indicates the point where supercharging reagents were introduced in the case of post-column injection..... 85

**Figure 3.2** FT-ICR mass spectra at 4.2(a)/3.9(b) and 4.7(c)/4.3(d) minutes from LC/MS of a myoglobin peptic digest in the absence (a, c) and presence (b, d) of 0.1%  $m$ -NBA. The observed earlier elution in the presence of  $m$ -NBA is due to the corresponding increased solvent strength. Average charge states for the peptides TALGGILKKKGHHEAEL (71-87) (a, b) and FRNDIAAKYKELGFQG (139-154) (c, d) under the two LC conditions are indicated in the upper right of each panel..... 89

**Figure 3.3** Bar charts showing the shift in charge-state distributions for three  $\alpha$ -casein peptic peptides; FVAPFPEVFGKEKVNEL (top), LRLKKYKVPQL (middle), and YYVPLGTQYTDA

(bottom), upon addition of 0.1% *m*-NBA ..... 92

**Figure 3.4** Bar charts showing the charge state distributions for peptic peptides from myoglobin, cytochrome c,  $\alpha$ -casein, and  $\beta$ -casein without (left) and with 0.1% (right) *m*-NBA in the mobile phase solvent. The calculated average charge states for peptic peptides from each protein are shown on the upper-right, respectively ..... 94

**Figure 3.5** (a) Base peak chromatograms from peptically digested myoglobin and extracted ion chromatograms for one peptide (inset) without (top) and with (bottom) 0.1% *m*-NBA in the mobile phase solvents. The shaded yellow areas on the BPCs indicate the retention time of the peptide in each case. (b) Base peak chromatograms from peptically digested  $\alpha$ -casein (top) and  $\beta$ -casein (bottom) and extracted ion chromatogram for one peptide from each protein (insets) without and with 0.1% *m*-NBA added through a post-column mixing tee. The latter set-up eliminated retention time shifts. The shaded yellow areas on the overlaid BPCs indicate the same retention time of either peptide with and without 0.1% *m*-NBA. A simplified diagram of the latter set-up is shown in (c) ..... 97

**Figure 3.6** Average charge states of five myoglobin peptic peptides (a) as a function of *m*-NBA concentration in the ESI solvent and (b) when no supercharging reagent, 0.1% *m*-NBA, 5% propylene carbonate (PC), 20% DMSO, or 150 mM sulfolane were added to the ESI solvent, respectively ..... 100

**Figure 3.7** (a) Average charge states of four myoglobin peptic peptides as a function of DMSO concentration in the ESI solvent. (b) Average charge state increase percentages for ten peptic peptides (P1-P6 from  $\alpha$ -casein, P7-P10 from myoglobin) upon addition of 10% DMSO into the ESI solvent ..... 101

**Figure 3.8** ECD MS/MS spectra of the peptic peptide TALGGILKKKGHHEAEL (71-87) from myoglobin in precursor ion charge states (a) 2+, (b) 3+, and (c) 4+. The ECD MS/MS spectrum for the doubly charged precursor ions was collected without *m*-NBA in the ESI solution whereas the spectra for the triply and quadruply charged precursor ions were collected with 0.1% *m*-NBA in the ESI solutions ..... 102

**Figure 3.9** Differences in deuterium content for ten myoglobin peptic peptides in HDX LC/MS experiments with and without 0.1% *m*-NBA (green bars). The HDX incubation time was 10 min. Deuterium content standard deviations from triplicate measurements without and with *m*-NBA (blue and red bars, respectively). The deuterium content difference was smaller than the standard deviation for each peptide, except the peptide 139-154 (2+), indicating that the use of *m*-NBA had a minor effect on peptic peptide deuterium uptake levels ..... 106

**Figure 3.10** Deuterium uptake curves for two myoglobin peptic peptides, NVWGKVEA (13-20) (left) and KPLAQSHATKHKIPIKY (88-104) (right), at multiple charge states in the absence and presence of 0.1% *m*-NBA in the ESI solvent. Similar HDX behaviors were observed for the same peptide with or without *m*-NBA ..... 107

**Figure 3.11** Deuterium content for three myoglobin peptic peptides, GLSDGEW (2-8),

NVWGKVEADIAGHGQEV L (13-30), and FRNDIAAKYKELGFQ G (139-154), without *m*-NBA (A), and with 0.1% *m*-NBA introduced after the analytical column (B), or directly into the LC mobile phase (C). Bars in different colors indicate different charge states ..... 108

**Figure 4.1** (a) ECD and (b) ETD MS/MS spectra of doubly protonated CCK; (c) ECD and (d) ETD MS/MS spectra of doubly protonated Q<sup>8</sup>-LHRH. *b*-type fragment ions are highlighted in blue. *b*/*y*' product ions present prior to electron irradiation (ECD) or ion-ion reaction (ETD) as a result of peptide vibrational excitation are labeled with circles (°); \* = water loss; Δ = ammonia loss. Insets show expanded views of the charge reduced precursor ions..... 121

**Figure 4.2** (a)(c) ECD and (b)(d) ETD MS/MS spectra of the (a)(b) 4+ and (c)(d) 5+ charge states of melittin. Only the precursor ions, charge reduced species, and *b* ions are labeled..... 124

**Figure 4.3** (a) Relative abundance of *b*<sub>5</sub> through *b*<sub>9</sub> ions from doubly protonated desulfated caerulein upon ECD when the ECD lens voltage was set to 10 V (to promote electron injection, blue bars) and - 20 V (to preclude electron injection, red bars) respectively. (b)(c) *b* ion abundance partitioning for doubly protonated desulfated caerulein upon ECD with varying (b) ECD pulse length and (c) ECD bias voltage..... 129

**Figure 4.4** *b* ion relative abundance (% , blue bars) of doubly protonated Q<sup>8</sup>-LHRH (top) and desulfated caerulein (bottom) upon ECD co-plotted with the *b* ion onset voltage (V, red line) obtained by CID ..... 131

**Figure 5.1** Proposed protocol for our HILIC-enriched HCP LC/MS method..... 144

**Figure 5.2** 280 nm UV chromatograms from HILIC separation of 10.0 μg BMS mAb 1 drug substance with (red line) and without (black line) addition of 9.4 μg HCP standard from CHO null cell line. Blank (water, brown line) and null cell HCP material only (blue line) chromatograms are also shown for reference. A Waters UPLC BEH Glycoprotein Amide column (300 Å, 1.7 μm, 2.1 x 150 mm) was used ..... 145

**Figure 5.3** 280 nm UV chromatograms from HILIC separation of 5.0 μg BMS mAb 1 drug substance with (red line) and without (blue line) addition of 4.7 μg HCP standard from CHO null cell line. Blank (water, black line) and null cell HCP material only (green line) chromatograms are also shown for reference. A Waters XBridge HILIC column (5 μm, 4.6 x 150 mm) was used at an operating temperature of 45 °C. Mobile phase solvent A was 20 mM ammonium formate in water containing 0.1% formic acid and mobile phase solvent B was 20 mM ammonium formate in 90/10 acetonitrile/water containing 0.1% formic acid..... 146

**Figure 5.4** The 280 nm UV chromatogram following HILIC separation of 150 μg BMS mAb 1 drug substance spiked with 10k ppm HCPs. The LC eluate was collected as Fractions #1, #2, and #3 separately, as indicated by the different retention time ranges: 1.0–11.7 min for Fraction #1, 11.7–15.5 min for Fraction #2, and 15.5–24.0 min for Fraction #3 ..... 149

**Figure 5.5** 280 nm UV chromatograms following HILIC separation of 700 μg NISTmAb. Two control injections are indicated with a red line (water) and blue line (solvent blank, H<sub>2</sub>O/ACN/DMSO/TFA 28/66/5/1 (v/v)). The LC eluate was collected in Fractions #1, #2, and #3

separately, as indicated by the different retention time ranges: 1.0–11.9 min for Fraction #1, 11.9–17.3 min for Fraction #2, and 17.3–24.0 min for Fraction #3 ..... 151

**Figure 5.6** MS/MS spectra for two identified peptides from two novel HCPs detected in NISTmAb, (A) ubiquitin-60S ribosomal protein L40 (P62984) and (B) ATPase inhibitor, mitochondrial (O35143)..... 155

**Figure 5.7** 280 nm UV chromatogram from HILIC separation of 700 µg BMS fusion protein 1. The LC eluate was collected in Fraction #1, #2, and #3 separately, as indicated by the different retention time ranges: 1.0–12.0 min for Fraction #1, 12.0–19.0 min for Fraction #2, and 19.0–24.0 min for Fraction #3 ..... 157

**Figure 6.1** Charge-state distributions of apo-myoglobin with (bottom) and without (top) addition of 0.1% *m*-NBA into the ESI solvent (50/50/0.2 water/methanol/formic acid). The mass spectra were collected on a Solarix FT-ICR mass spectrometer ..... 165

**Figure 6.2** Backbone cleavages in apo-myoglobin upon ECD of the 17+ charge state (top) versus the 22+ charge state (bottom).  $a^*/x$ ,  $b/y'$ , and  $c/z^*$  fragment ions are color-coded as shown in the legend. The addition of 0.1% *m*-NBA into the ESI solvent promoted the generation of more highly-charged protein ions, improving sequence coverage from 59% (17+) to 72% (22+) ..... 166

**Figure 6.3** Diagram of proposed H/D scrambling behaviors of  $c^*$ ,  $z^*$ , and  $b$ -ions generated from ECD of a supercharged, selectively-deuterated peptide ion under “soft” and “harsh” conditions, respectively ..... 167

**Figure 6.4** ECD (top) and ETD (bottom) MS/MS spectra of a quadruply protonated monophosphorylated peptide from trypsin digestion of β-casein. This charge state is only observed following supercharging with *m*-NBA. In the ECD spectrum, only  $b$  ions and  $b$  ions with neutral loss are labeled (red) ..... 169

## List of Tables

<b>Table 2.1</b> Instrument parameters for ECD experiments: The SolariX Q-FT-ICR mass spectrometer was tuned to accomplish “harsh” (complete scrambling) and “soft” conditions (minimum scrambling) in ECD MS/MS experiments .....	56
<b>Table 2.2</b> Predicted intrinsic amide exchange rates of peptides P3 and P4.....	58
<b>Table 2.3</b> Instrument parameters for EDD experiments: Instrumental parameters of the SolariX Q-FT-ICR mass spectrometer were altered to create the “harsh” and “soft” conditions used in EDD MS/MS experiments .....	61
<b>Table 2.4</b> Instrument parameters for niECD experiments: Instrumental parameters of the SolariX Q-FT-ICR mass spectrometer used in niECD MS/MS experiments.....	61
<b>Table 2.5</b> Instrument parameters for nCID experiments: Relevant instrumental parameters for negative ion mode CID experiments on the LTQ Orbitrap XL mass spectrometer equipped with a Nanomate ion source.....	62
<b>Table 3.1</b> Overall protein sequence coverages of peptically digested myoglobin, cytochrome c, $\alpha$ -casein S1, and $\beta$ -casein following LC/MS experiments with and without 0.1% <i>m</i> -NBA in the mobile phase solvents, respectively. These data are based on duplicate measurements. The mass error for all assigned peptides was below 12 ppm.....	88
<b>Table 3.2</b> Charge-state distributions and calculated average charge states for myoglobin peptic peptides from LC/MS experiments using 0% and 0.1% <i>m</i> -NBA in the mobile phases, respectively .....	90
<b>Table 3.3</b> Example myoglobin peptic peptides observed in LC ECD MS/MS experiments with and without 0.1% <i>m</i> -NBA in the ESI solvent. Peptide abundances were normalized to charge. “Total analyte abd.” refers to the summed abundance of the precursor ions and ECD product ions post dissociation. The shift to more triply- (or higher) charged peptide ions is highly beneficial for both ECD fragmentation efficiency and peptide sequence coverage.....	105
<b>Table 4.1</b> Comparison of backbone fragmentation in ECD vs. ETD for three doubly protonated peptides lacking basic amino acid residues. <i>b</i> -type fragment ions are highlighted in red.....	122
<b>Table 4.2</b> Comparison of backbone fragmentation in ECD vs. ETD for the 4+, 5+, and 6+ charge	

states of melittin. Basic amino acids are highlighted in blue. Only *b*-type fragment ions are included in this table. \* indicates that the ECD/ETD experiment was performed following addition of 0.1% *m*-NBA into the ESI solvent..... 125

**Table 4.3** *b* ions generated from ECD vs. ETD of (a) tryptic peptides and (b) peptic peptides from myoglobin and  $\alpha$ -casein in different charge states. The basic amino acid residues in each peptide are highlighted in blue. \* indicates that the ECD/ETD experiment was performed with addition of 0.1% *m*-NBA into the ESI solvent..... 127

**Table 5.1** LC mobile phase gradient and flow rate used with the Waters XBridge HILIC column (data in Figure 5.3)..... 146

**Table 5.2** The numbers of HCPs identified in the three HILIC-enriched fractions compared with those identified by the mAb-precipitation method for BMS mAb 1 spiked with 1k and 10k ppm HCP standards, NISTmAb, and BMS fusion protein 1. The numbers in parentheses indicate how many HCPs were uniquely identified by the HILIC-enriched HCP method but not by the mAb-precipitation method for each sample..... 149

**Table 5.3** NISTmAb HCPs uniquely identified with our HILIC-enriched HCP LC/MS method. These HCPs were not observed with the mAb-precipitation method and, to our knowledge, have not been reported previously..... 152

**Table 5.4** A full list of identified HCPs in NISTmAb (RM 8671) using our HILIC-enriched HCP LC/MS method. For each identified HCP, the number of unique peptides observed, protein sequence coverage (%), and HILIC fraction are also listed..... 153

## List of Abbreviations

1,2-BC	1,2-Butylene Carbonate
ACN	Acetonitrile
APCI	Atmospheric Pressure Chemical Ionization
APPI	Atmospheric Pressure Photoionization
BPC	Base Peak Chromatogram
BSA	Bovine Serum Albumin
CEM	Charge Ejection Model
CID	Collision Induced Dissociation
CRM	Charge Residue Model
Cryo-EM	Cryogenic Electron Microscopy
CZE	Capillary Zone Electrophoresis
DDA	Data-dependent Acquisition
DIA	Data-independent Acquisition
DIGE	Difference Gel Electrophoresis
DMSO	Dimethyl Sulfoxide
ECD	Electron Capture Dissociation
EDD	Electron Detachment Dissociation
EIC	Extracted Ion Chromatogram
EID	Electron Ionization Dissociation
ELISA	Enzyme-Linked Immunosorbent Assay
ESI	Electrospray Ionization

ETD	Electron Transfer Dissociation
ETS	Electrothermal Supercharging
FA	Formic Acid
FRIPS	Free Radical Initiated Peptide Sequencing
FT MS	Fourier Transform Mass Spectrometry
FT-ICR	Fourier Transform-Ion Cyclotron Resonance
H/D	Hydrogen/Deuterium
HCD	High-Energy Collision Dissociation
HCP	Host Cell Protein
HDX	Hydrogen/Deuterium Exchange
HECD	Hot Electron Capture Dissociation
HILIC	Hydrophilic Interaction Chromatography
HPLC	High Performance Liquid Chromatography
i.d.	Inner Diameter
IEM	Ion Ejection Model
IRMPD	Infrared Multiphoton Dissociation
ISD	In-Source Decay
IVR	Intramolecular Vibrational-energy Redistribution
LC	Liquid Chromatography
LTQ	Linear Trap Quadrupole
$m/z$	Mass-to-Charge Ratio
mAb	Monoclonal Antibody
MALDI	Matrix-Assisted Laser Desorption/Ionization
<i>m</i> -NBA	<i>meta</i> -Nitrobenzyl Alcohol
MS	Mass Spectrometry
MS/MS	Tandem Mass Spectrometry
nCID	Negative-Ion Collision Induced Dissociation

nFRIPS	Negative-Ion Free Radical Initiated Peptide Sequencing
niECD	Negative-Ion Electron Capture Dissociation
NMR	Nuclear Magnetic Resonance
PC	Propylene Carbonate
PPI	Protein-Protein Interaction
PTM	Post-Translational Modification
RP	Reversed-Phase
S/N	Signal-to-Noise Ratio
SDS PAGE	Sodium Dodecyl Sulfate Polyacrylamide Gel Electrophoresis
SFC	Supercritical Fluid Chromatography
SWATH	Sequential Isolation Window Acquisition
TCEP	Tris(2-carboxyethyl)phosphine
TFA	Trifluoroacetic Acid
TIC	Total Ion Chromatogram
TOF	Time-of-Flight
UVPD	Ultraviolet Photodissociation
WB	Western Blot

## Abstract

Elucidating protein structures, dynamics, and interactions is critical for understanding their roles in health and disease. In the biopharmaceutical industry, bioanalytical science allows, e.g., insights into how these complex molecules interact, and enables their characterization to assure safety and consistency of biotherapeutic manufacturing. Mass spectrometry (MS)-based methods, such as hydrogen/deuterium exchange (HDX) MS, are powerful tools for structural proteomics. This dissertation presents analytical strategies for incorporating gas-phase fragmentation for improved structural resolution in HDX MS workflows in both positive and negative ion mode, and for improving host cell protein characterization in biopharmaceuticals.

HDX is typically performed in positive ion mode. In Chapter 2, the feasibility of several negative ion mode tandem mass spectrometry (MS/MS) techniques for HDX coupling is explored. Regio-selectively deuterated peptide anions were fragmented by negative-ion collision induced dissociation (nCID), negative-ion free radical initiated peptide sequencing (nFRIPS), electron detachment dissociation (EDD), and negative-ion electron capture dissociation (niECD) to determine the extent of H/D scrambling in each MS/MS technique. nCID induces extensive H/D scrambling involving histidine C-2 and C $\beta$ -hydrogen atoms for histidine-containing peptides. nFRIPS proceeds with complete hydrogen scrambling but without histidine participation, whereas EDD and niECD demonstrate moderate scrambling with slightly lower levels in niECD. However, improved ionization efficiency, ion transmission, and fragmentation efficiency under HDX quenching conditions are needed for routine application of niECD in HDX MS workflows.

Due to the acidic HDX quenching conditions, the acid protease pepsin is employed for protein digestion. However, resulting peptic peptides may not contain basic residues and

therefore carry less average charge than typical tryptic peptides. In Chapter 3, supercharging strategies are explored for combination with electron capture/transfer dissociation (ECD/ETD)-based HDX MS/MS in positive ion mode. These MS/MS techniques require analytes to carry at least two positive charges. The supercharging reagent *m*-NBA was found to enhance the average charge state for a variety of pepsin-derived peptides, thus increasing ECD/ETD fragmentation efficiency and peptide sequence coverage in bottom-up HDX liquid chromatography (LC)/MS workflows. Retention time shifts in the presence of *m*-NBA were avoided by injecting *m*-NBA through a mixing tee following the analytical column.

During these experiments, *b*-type ions were observed in ECD spectra of supercharged peptides. Such fragment ions are atypical in ECD but have been found at increased levels for peptides containing few or no basic residues. In Chapter 4, we find that such peptides also show abundant hydrogen atom loss from the charge-reduced radical species. We show that, upon ECD of supercharged peptides, the number and abundance of *b* ions increases with increasing charge state; *b* ions are prevalent in ECD spectra when the number of protons is higher than the number of basic sites. Under the same conditions, significantly less abundant *b* ions were seen in ETD than ECD. The observed difference between ECD and ETD is likely due to different internal energy prior to dissociation. We propose that *b* ions should be considered in ExD database searches for supercharged peptides in HDX MS/MS, and that ETD may be superior to ECD for minimizing deuterium scrambling in such experiments.

In Chapter 5, an offline hydrophilic interaction chromatography (HILIC) sample preparation method for improving detection of residual host cell proteins (HCPs) in biotherapeutic proteins by LC MS/MS is described. This method enriches HCPs while depleting high abundance biotherapeutic proteins, enabling detection of previously unobserved HCPs in drug substances.

## **Chapter 1**

### **Introduction**

#### **1.1 Mass Spectrometry-Based Protein Structural Analysis**

Proteins are an important group of large biological molecules that represent the functional aspect of gene activities in living cells. The term proteome, first introduced by Wilkins *et al.* [1] in 1995, denotes the total number of proteins expressed by a genome at any given time while the term proteomics typically refers to global identification and quantification of proteins. In order to perform their biological functions, one or more amino-acid chains fold into specific spatial conformations to form protein higher-order structure (i.e., secondary, tertiary, and quaternary), driven by a number of intramolecular non-covalent interactions. Intermolecular interactions between proteins (or between proteins and other biomolecules) are also prevalent, as proteins rarely act alone and their functions are regulated. This type of interaction between proteins is referred to as protein-protein interaction (PPI).

##### **1.1.1 Biotherapeutic Proteins**

Protein therapy, based on the protective properties of passive immunization, has become an increasingly important mode of medical treatment. Recombinant DNA technology enables the development of protein therapy by allowing mass production of homogenous proteins of interest from living cells following well-defined bioprocesses. Such biotherapeutic proteins are employed to treat a variety of diseases [2, 3].

A large number of biotherapeutic proteins are monoclonal antibodies (mAb) or

mAb-based modalities, such as antibody-drug conjugates (ADCs), bispecific antibodies, or domain antibodies [2]. Antibodies are immune system-related proteins, known as immunoglobulins. An antibody consists of four polypeptides, including two identical heavy chains (H) and two identical light chains (L). Heavy and light chains are joined by non-covalent interactions and covalent interchain disulfide bonds to form a “Y” shaped molecule. mAbs function therapeutically via several mechanisms, including by inducing apoptosis in cells that express the target (antigen), by blocking protein ligand binding to its receptor, and/or by modulating signaling pathways [3].

Fusion proteins are another type of biotherapeutic proteins. They are generated through the fusing of two or more genes, which originally code for separate proteins. One kind of fusion protein is produced by adding a half-life extension protein (e.g., albumin, transferrin, antibody Fc region) to small recombinant peptides/proteins (< 60 kDa), for increasing the half-life of these relatively small biotherapeutics [4]. Other kinds of fusion proteins aim to enable the targeting of a specific cell surface component for improved biological activity at the target site (e.g., antibody-cytokine fusion proteins) [5], to promote binding to the target (e.g., bivalent Fc fusion proteins) [6], or to confer bispecific functions.

Compared with small molecule drugs, biotherapeutic proteins are not only larger in molecular size but also show much more complex higher-order structure. The vast majority of biotherapeutic proteins are produced from prokaryotic- or eukaryotic-based expression systems [7]. One key factor for selecting an appropriate expression system is the post-translational modification (PTM) requirements for optimal extraction, stability, and drug activities. However, biotherapeutic proteins usually exist as complex heterogeneous mixtures containing variants with different PTMs and aggregation states, and are susceptible to further modifications. Undesirable PTMs may cause potential problems, e.g., reduced drug efficacy and unwanted toxicity [8, 9]. Elucidating PTM structure for biotherapeutic proteins aids protein engineering for improved therapeutic properties. It is also crucial to characterize the higher-order structure of biotherapeutic proteins to understand their stability, conformation, and functional activities.

### 1.1.2 Mass Spectrometry-Based Structural Biology Tools

Elucidating protein structures as well as PPIs is an essential prerequisite for understanding their roles in health and disease. X-ray crystallography [10, 11], cryo-electron microscopy (cryo-EM) [12, 13], and nuclear magnetic resonance (NMR) spectroscopy [14] are valuable techniques for protein structural studies and have been routinely applied. In addition, recent developments in modern mass spectrometry (MS) have resulted in structural proteomics techniques. Although each technique has its own strengths and limitations, mass spectrometry has unique advantages, including high throughput and high sensitivity [15-17] for studies of protein systems of varying levels of complexity; exceptional detection limits, down to zeptomoles [18], and localization of post-translational modifications (PTMs) via multi-stage MS ( $MS^n$ ) [19-21], while elucidating protein/peptide structures down to the single amino acid residue level [22]. Overall, MS performs not only as a qualitative but also a quantitative tool for large scale proteomics studies [23, 24].

MS-based structural biology tools have also been developed and applied to studies of biomolecular conformations, dynamics, and molecular interactions [25, 26]. Solution-phase labeling methods, such as hydrogen/deuterium exchange (HDX) [27], covalent labeling [28], and hydroxyl radical labeling [29], modify the analyte mass based on its three-dimensional structure in solution, thus reflecting structural information by mass shift of the molecular ion. Covalent cross-linking [30] reveals the distances between intramolecular and/or intermolecular pairs of functional groups, which can serve as characteristic features of protein conformational change. Limited proteolysis [31] detects the outermost regions of protein surfaces exposed to the active sites of proteolytic enzymes. The protein charge state distribution [32-34] generated by electrospray ionization (ESI) [35] can also be used to probe structural changes. Other MS approaches that can provide protein structural information include native ESI-MS [36] and ion mobility MS [37]. A combination of different types of structural MS techniques can yield complementary information.

### 1.1.3 Characterization of Host Cell Proteins in Biopharmaceuticals

A large portion of the biopharmaceuticals today are produced by recombinant DNA technology using a well-selected host cell system [38]. Besides the recombinant protein drug, host cells express a large number of their own proteins related to normal cell functions. Even after orthogonal purification steps, low levels (ranging from <1 to a few hundred ppm) of host cell proteins (HCPs) may still exist in the final drug product. These protein impurities may significantly affect drug efficacy and cause immunogenicity. Therefore, detection and quantification of residual HCPs as potential process-related impurities is important for biopharmaceutical companies to meet regulatory requirements [39].

The enzyme-linked immunosorbent assay (ELISA) [40], as a common form of immunoassay, is frequently used in the biopharmaceutical industry for HCP measurement due to its high sensitivity and high throughput. In principle, anti-HCP antibodies can be produced by injecting HCP mixtures into animals to induce immune response and develop a multi-analyte ELISA kit. However, there are a few limitations associated with this technique, such as less-than-ideal coverage, dilutional nonlinearity, signal biased by proteins of high abundance/immunogenicity. Other separation and visualization methods such as 1D/2D sodium dodecyl sulfate-polyacrylamide gel electrophoresis (SDS-PAGE) [41], 2D differential in-gel electrophoresis (DIGE) [42], western blot (WB) [43], *etc.*, remain useful tools as well. However, in general, current analytical methods suffer from long method development times, require prior knowledge of contaminant proteins, and lack the capability of detecting a wide range of protein concentrations. LC/MS-based proteomics provides a powerful alternative method for HCP characterization, a supplement to affinity-based techniques, and has become a routine approach in the pharmaceutical industry. However, HCP LC/MS analysis is a challenging workflow because a dynamic range up to 6 orders of magnitude is required to be able to detect low ppm concentrations of residual HCPs in the presence of biotherapeutic proteins, which is out of range of current mass spectrometers.

A couple of analytical strategies have been developed based on conventional bottom-up

LC/MS workflows aiming to overcome this dynamic range limitation. In addition, to be widely adopted by the biopharmaceutical industry, the analytical solution has to be highly robust and relatively fast. Monoclonal antibody (mAb) samples spiked with low abundance standard proteins in a series of concentrations is frequently used as a model to test assay sensitivity and dynamic range [44]. One approach to improve LC separation is to increase gradient length and/or column length. Waters Corporation (Milford, MA) introduced an online high-pH/low-pH RP/RP 2D-LC system for comprehensive peptide separations and HCP analysis for mAbs [45]. Ion mobility can also be integrated in this workflow as an additional separation dimension to separate targeted peptide precursors from other co-eluting precursors [46]. However, 2D LC generally suffers from low throughput (e.g., 1-2 samples/day) and detection of <10 ppm HCPs is still challenging. HCP enrichment/mAb depletion during sample preparation is another strategy for improving HCP detection. Recently, Eli Lilly (Indianapolis, IN) reported a simple and robust method to characterize HCPs in mAbs by adopting trypsin digestion under native conditions, followed by precipitation of undigested mAb with heat treatment [44]. Following this procedure, residual HCPs are mostly digested in solution while the antibody is minimally digested and can be removed through filtration prior to proteomics analysis, whereas heat-labile HCPs and HCPs co-precipitating with the mAb are also lost. In terms of data acquisition, DDA is widely used to sample peptide precursors for MS/MS sequencing analysis, e.g., “top ten” method. Currently, applications of DIA for HCP detection are mostly in the form of MS<sup>E</sup> or UDMS<sup>E</sup> coupled with 2D-LC developed by Waters [45, 46]. In accordance with LC/MS instrument type and data format, several software packages have been adopted for identification and quantification of HCPs, for example, PLGS (Protein Lynx Global Server; Waters), Proteome Discoverer (Thermo Scientific), Byonic and Byologic (Protein Metrics), *etc.* However, due to the sample complexity and low abundance, as well as the MS dynamic range limitation, HCP characterization in biotherapeutic protein preparations utilizing LC/MS strategies is still facing the issue of limited sensitivity.

## 1.2 Techniques and Strategies in Modern Proteomics

### 1.2.1 Bottom-up vs. Top-down Proteomic Strategies

Bottom-up, top-down, and middle-down are three main approaches for proteomic experiments with mass spectrometry [47-49]. In a bottom-up experiment, proteolytic digestion is involved to cleave intact proteins into peptide segments (< 3 kDa) and the resulting peptides are usually separated by reversed-phase liquid chromatography (RP LC) prior to mass analysis to improve detection sensitivity. The bottom-up approach is commonly used for peptide mass fingerprinting and tandem mass spectrometry (MS/MS) identification combined with database searching [50]. To improve digestion efficiency, more than one protease [47] may be used. In addition, reduction and alkylation are often performed before proteolysis to break disulfide bonds between cysteine residues and prevent reformation of these linkages. To date, bottom-up proteomics is routinely applied to identify thousands of proteins present in one sample, even though the method may provide ambiguous results if only few peptides are detected from a particular protein. Another drawback for bottom-up analysis is that protein digestion inevitably increases the complexity of the analyte pool, making 100% protein sequence coverage and accurate assignment of proteoforms [49] containing various PTMs difficult to achieve.

The top-down strategy [51, 52], a term first introduced by McLafferty and coworkers [53], addresses the aforementioned issues by bypassing the proteolysis step and instead performing fragmentation on intact proteins in the gas phase. The intact mass and fragment masses are then compared to a sequence database. This approach can provide information about PTMs as PTM-retainable MS/MS techniques are utilized, such as electron capture dissociation (ECD) [54] and electron transfer dissociation (ETD) [55]. Top-down proteomics is mostly performed with Fourier transform MS [49] that enables high resolution and high mass accuracy, yet is still limited by MS/MS fragmentation efficiency and sequence coverage and thus most applicable to small-to-medium size proteins (< 40 kDa) [51, 56]. Recently, the use of native ESI MS has shown promise for the characterization of intact protein complexes in the 100 kDa to 1 MDa regime [52].

The third approach, middle-down proteomics [51, 57], combines the advantages of the bottom-up and top-down strategies and has recently been adopted for characterization of large proteins, such as antibodies, and protein complexes. With the middle-down strategy, the analyte is less complex compared with the bottom-up method, while the strength of the top-down method, such as localization of proteoform-specific PTMs [58], can be maintained.

### **1.2.2 Liquid Chromatography Mass Spectrometry (LC/MS)**

High performance liquid chromatography (HPLC; or high-pressure liquid chromatography) [59] is a powerful separation technique applicable to a variety of analytes. The principle of separation is based on the distribution of the components in a liquid between two immiscible phases, i.e., stationary and mobile phases, when the mobile phase containing the analytes permeates through the stationary phase bed in a given direction under high pressure. Five common types of liquid chromatography include adsorption chromatography, partition chromatography, ion-exchange chromatography, size-exclusion chromatography, and affinity chromatography. Among these, the most widely used kind for peptide separation in proteomics is the reverse-phase (RP) mode of the partition chromatography, which utilizes a non-polar (hydrophobic) stationary phase covalently bonded with octadecyl (C18), octyl (C8), or phenyl (C4) groups, and a polar mobile phase [60-62]. As a result, hydrophobic molecules in the polar mobile phase adsorb more strongly to the hydrophobic stationary phase and hydrophilic molecules will pass through the column to be eluted first. Hydrophobic molecules can be eluted from the column by decreasing the polarity of the mobile phase using organic solvent. A solvent gradient, commencing at low organic concentration and increasing to high organic concentration, can effectively improve the separation of analytes. On the contrary, for hydrophilic interaction chromatography (HILIC) [63, 64], a variant of normal-phase liquid chromatography, the stationary phase is highly polar (e.g., silica, amide, diol, cyano, *etc.* [65]) and the mobile phase is composed of mostly non-polar organic solution with a minor portion of water. Adding a polar phase (water in this case) to a polar surface will result in the formation of a water layer. Polar analytes partition into and out of this adsorbed water layer. The water content of the mobile

phase increases with the decrease of the organic portion, resulting in retention and then elution of polar analytes such as amino acids, peptides, metabolites, saccharides, *etc.* [66].

LC/MS combines the physical separation capabilities of LC with the mass analysis capability of MS. This tandem technique has been widely used to analyze biochemical, organic, and inorganic compounds in complex samples [67-73]. Currently, the most common LC/MS interfaces are ESI, atmospheric pressure chemical ionization (APCI), and atmospheric pressure photo-ionization (APPI) [69]. These ion sources enable online transition of analytes from solution phase to the gas phase. Recent development in LC techniques has led to higher separation efficiency and lower detection limits by use of columns with smaller inner diameter and stationary particle size [74]; higher pressure resistance is therefore required for current LC systems. Ultrahigh performance liquid chromatography (UPLC or UHPLC) [75] and nanoflow LC (nLC) [76-78] were developed to accommodate these demands. Also, with the improvement of robust MS instrumentation and computational tools, LC/MS-based proteomics [79] has witnessed rapid advancements and growing applications in recent years.

### **1.2.3 Fourier Transform Mass Spectrometry (FT MS)**

Mass spectrometry (MS) measures the mass-to-charge ratio ( $m/z$ ) of charged molecules. Basic components of a mass spectrometer include an inlet for sample introduction (usually LC or direct infusion), an ion source, a mass analyzer, an ion detector and a data system to process the output data and generate a spectrum. Different types of mass analyzers vary in resolution, transmission, and mass limit. A high mass resolution is desired for high selectivity, i.e., ability to distinguish between two species of small mass difference.

In LC/MS proteomics experiments, high resolution MS enables accurate peptide ion and/or fragment ion annotation and PTM assignment, allowing for rapid identification of proteins via peptide mass fingerprinting and high quality MS/MS identification. Top-down proteomics is also based on high resolution tandem MS and is mostly performed with Fourier transform MS (FT MS) [49]. FT MS has received considerable attention for its ability to achieve both high resolution and high mass accuracy [80]. The next two sections will focus on two kinds

of well-known FT-based high resolution mass spectrometers: Fourier transform-ion cyclotron resonance (FT-ICR) mass spectrometers and Orbitrap mass spectrometers. These two types of MS systems were used to complete this dissertation.

FT-ICR mass spectrometers [81, 82] feature unprecedented resolution and mass accuracy compared with other types of mass analyzers such as time-of-flight (TOF), quadrupole (Q), or ion trap mass analyzers, as well as the capability of implementing various MS/MS fragmentation techniques. The theory of ion cyclotron resonance was developed by Lawrence in the 1930s [83]. However, it was not until 1978 that Comisarow and Marshall built the first FT-ICR MS instrument [84, 85]. A main component in FT-ICR MS is a superconducting magnet featuring high field strength. The resolution of the instrument improves as the magnetic field strength increases. Therefore, design of instruments with stronger fields is a current trend and recently a 21-Tesla magnetic field has been successfully applied to FT-ICR MS to achieve baseline isotopic resolution for antibodies [86, 87]. The ICR analyzer cell is another critical component, in which ions are trapped, mass analyzed, and detected. The “Infinity Cell” [88] design improves ion trapping although the more recent dynamically harmonized FT-ICR cell designed by Nikolaev *et al.* [89] further improves FT-ICR resolving power. In addition, ultra-high vacuum is required ( $10^{-9}$ – $10^{-10}$  Torr) when ions are detected to achieve high resolution.

Ion cyclotron motion is the basis for ICR mass analyzer. As indicated in Equation 1.1 and Figure 1.1, a moving ion experiences a Lorentz force in the presence of a magnetic field, resulting in periodic cyclotron motion whose frequency ( $f_c$ ) is determined by the charge of the ion,  $q$ , the magnetic field strength,  $B$ , and the mass of the ion,  $m$ , while independent of the ion kinetic energy.  $f_c$  typically falls in the range of tens of kilohertz (kHz) to megahertz (MHz) [80].  $B$  is held constant and the  $m/z$  of an ion ( $m/q$ ) is consequently determined by measuring its cyclotron frequency. In reality, a combination of three types of motion, i.e., cyclotron motion, trapping motion, and magnetron motion, complicates the actual trajectories of ion movement in the ICR cell [90]. In the FT-ICR MS system used in the Hakansson Lab (Figure 1.2), the ions to be analyzed undergo dipolar excitation [91] as a sinusoidal voltage is applied to a pair of

excitation plates in the ICR cell. Ions that are in resonance with the excitation frequency spiral outwards from the center of the cell into a larger cyclotron orbit. All ions with the same  $m/z$  are excited coherently and undergo cyclotron motion as a packet. A rapid frequency sweep [92], or r.f. chirp, is applied during the excitation event to achieve broadband detection. The ion package passes the detection plates and induces a sinusoidal image current whose frequency is almost equal to the frequency of the ion cyclotron motion. This image current can be amplified, digitized, and stored as a time domain transient, which is then converted to a mass spectrum by performing a Fourier transform. Mass resolution improves in correlation with the length of the transient [80].

**Equation 1.1**  $f_c = \frac{qB}{2\pi m}$

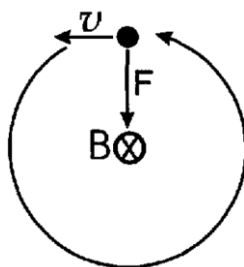


**Figure 1.1** Cyclotron motion of a positively charged ion in the plane perpendicular to the magnetic field lines.

The FT-ICR instrumentation platform in the Hakansson Lab (Figure 1.2) is equipped with an Apollo II ESI source, a dual ion funnel/skimmer, a chemical ionization source, a quadrupole mass filter, a hexapole collision cell, an ICR Infinity Cell, a hollow dispenser cathode, and a CO<sub>2</sub> IR laser. It allows ion-neutral, ion-electron, ion-ion, and ion-photon activation, including collision-induced dissociation (CID), electron capture/transfer dissociation (ECD/ETD), and infrared multiphoton dissociation (IRMPD). The unique capability of performing not only positive but also negative ion mode ion-electron fragmentation, such as electron detachment dissociation (EDD) and negative ion electron capture dissociation (niECD), makes the FT-ICR a superior tool for fundamental studies of gaseous radical chemistry. However, completion of a high-resolution mass spectrum scan (no lower than 512k data points) typically takes 0.5-1.0 s on our FT-ICR mass spectrometer, which results in fewer peptides being detected in typical LC/MS

workflows and, consequently, lower sequence coverage for proteomics experiments compared to Orbitrap or TOF MS.

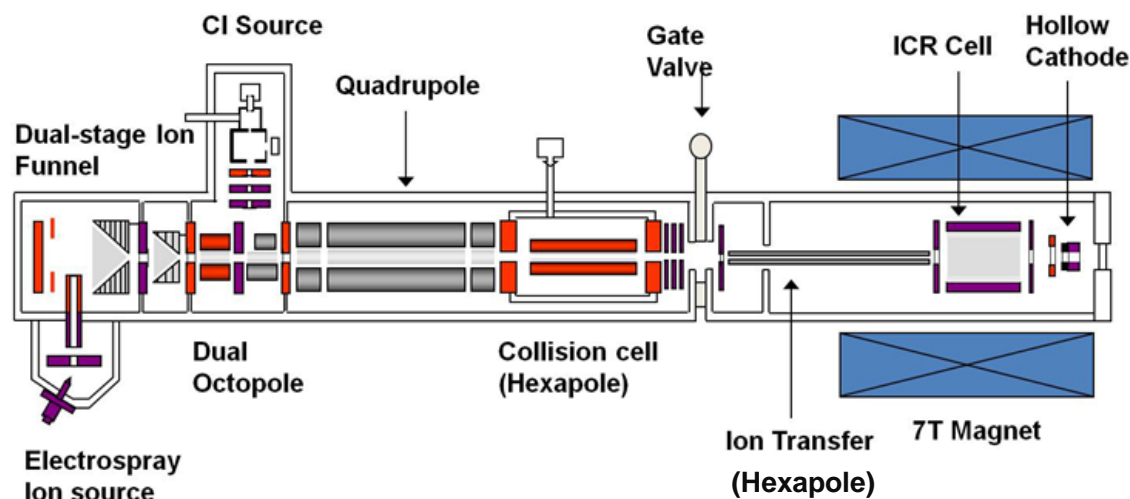


**Figure 1.2** Schematic diagram of a 7-T SolariX quadrupole-FT-ICR mass spectrometer (Bruker Daltonics).

The Orbitrap mass analyzer, developed from the work of Makarov [93], is a new member of the FT MS family [94-96]. The first commercial implementation was in 2005 in a hybrid instrument, LTQ Orbitrap, featuring a linear ion trap front-end [97]. Orbitrap mass spectrometers combine the principle of image current detection and the use of ion trapping in precisely defined electrode structures, while eliminating the necessity for a superconducting magnet as in FT-ICR. In both Orbitrap and FT-ICR MS, ions are trapped in ultrahigh vacuum to ensure very long mean free paths (tens to hundreds of kilometers) [80]. In addition, ions are detected based on their image current followed by FT processing. The digitized image current in the time domain is Fourier-transformed into the frequency domain in the same way as FT-ICR. However, in an Orbitrap instrument, the use of electric fields only for ion trapping makes it possible to implement on a bench top [98]. High-mass resolution can routinely be achieved with the Orbitrap MS in a relatively small amount of time (<1 s) that is compatible with UPLC. Thus, the Orbitrap type of mass spectrometers is widely used for current routine proteomics analysis [77, 98].

Figures 1.3 and 1.4 show two Orbitrap MS systems, LTQ Orbitrap XL and Orbitrap

Fusion Lumos. The LTQ Orbitrap features a linear ion trap enabling mass detection in front of the C-trap (a C-shaped rf-only quadrupole) and an octapole collision cell (HCD cell) following the C-trap [97]. As an ion storage device, the C-trap enables pulsed ion injection into Orbitrap, the second mass analyzer on the instrument that typically provides much higher mass resolution than the front-end ion trap. The Orbitrap Fusion Lumos is the state-of-the-art model in the Orbitrap family nowadays featuring a tribrid architecture including a front-end segmented quadrupole, a back-end dual-pressure ion trap, and an ultrahigh field Orbitrap mass analyzer.

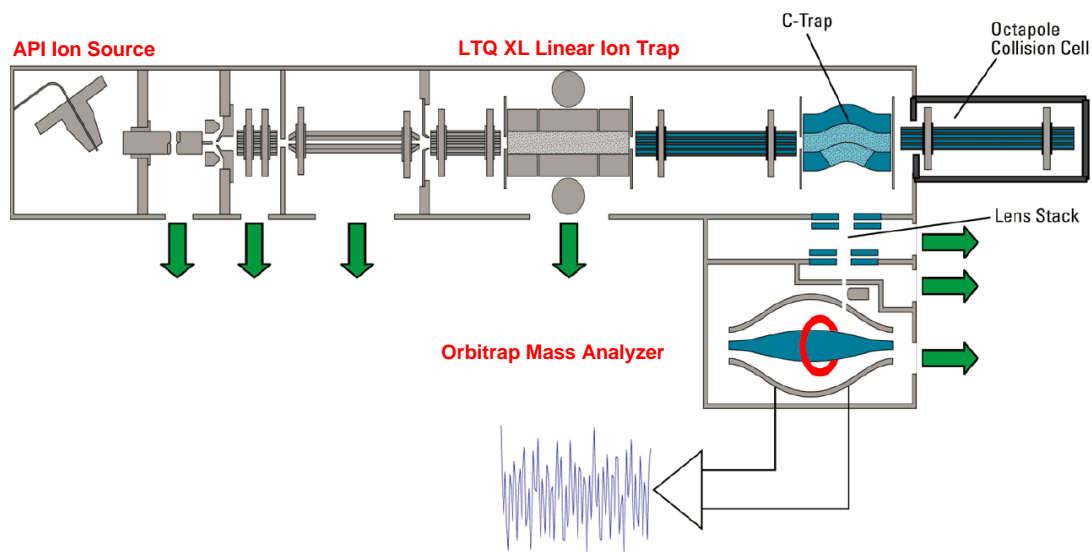


**Figure 1.3** Schematic diagram of an LTQ Orbitrap XL hybrid FT mass spectrometer (Thermo Fisher Scientific).

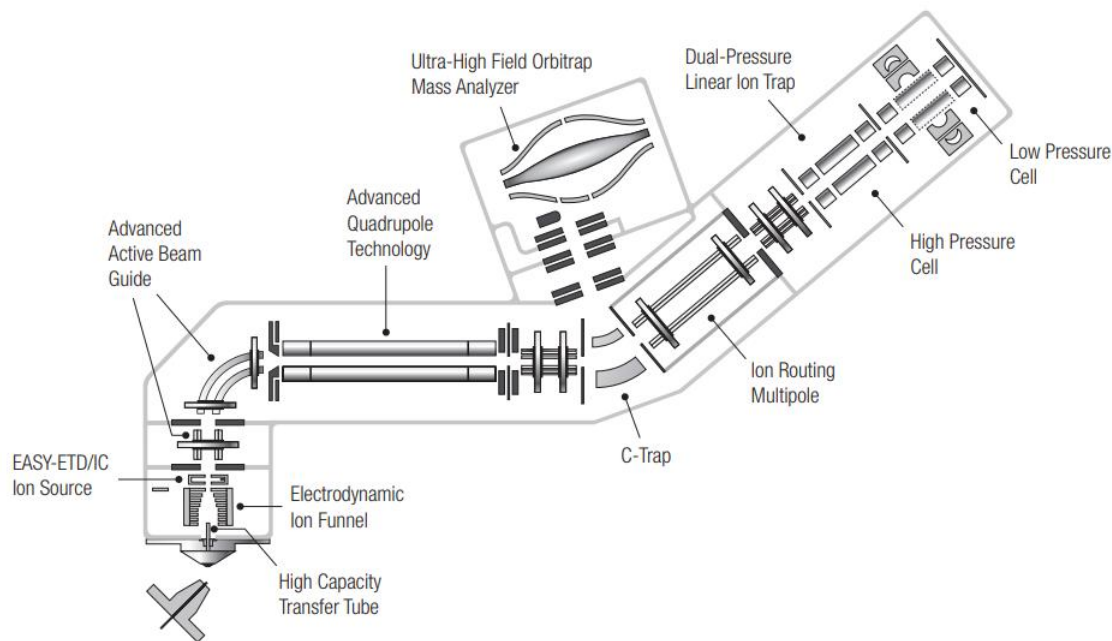


**Figure 1.4** Schematic diagram of an Orbitrap Fusion Lumos tribrid mass spectrometer (Thermo Fisher Scientific).

### 1.2.4 Tandem Mass Spectrometry (MS/MS)

The development of multi-stage and multi-functional hybrid instruments has enabled versatility of  $MS^n$  ( $n \geq 2$ ) experiments with FT MS instrumentation. MS/MS for peptide fragmentation and sequencing is crucial for MS-based proteomics. In typical bottom-up proteomics experiments, ESI-generated co-eluting peptide ions in one  $MS^1$  spectrum are a mixture of various peptide species and charge states. Ion species with a specific  $m/z$  value are typically mass filtered through a front-end quadrupole or ion trap using an isolation width of 1-5  $m/z$ . Isolated peptide ions (also called precursor ions or parent ions) then undergo inelastic collisions with neutral inert gas molecules such as helium or argon; the most common MS/MS technique referred to as collision-induced dissociation (CID) [99, 100], for peptide backbone fragmentation. All generated fragment ions (also called product ions or daughter ions) as well as undissociated precursor ions are then mass analyzed. Data-dependent acquisition (DDA) and data-independent acquisition (DIA) are two modes of data collection in MS/MS [101]. For DDA,

a fixed number of precursor ions whose  $m/z$  values are recorded in an MS<sup>1</sup> survey scan are selected sequentially and subjected to a second-stage MS/MS analysis [102]. DIA attempts to remedy the drawback of the DDA method that only a fixed number of ion species are subjected to fragmentation from one survey scan, potentially causing significant information loss in highly complex samples. For DIA, all ions within a selected  $m/z$  range are fragmented at one time and analyzed by second-stage MS/MS [103]; high resolution MS is thus essential to effectively resolve fragment ions generated from different peptide ions. SWATH [104] and MS<sup>E</sup> [105] are two commercial methods to reduce the complexity of DIA MS/MS spectra. In top-down experiments, a series of protein ions with multiple charge states is usually present together with other charged species such as contaminants, adducts, fragments, *etc.* Mass filtration is necessary to clean up the spectrum prior to fragmentation of certain species, given that dissociation of multiply charged protein ions typically generates overlapped MS/MS spectra consisting of fragment ions of multiple charge states. Fragmentation of proteins containing labile PTMs result in further complexity due to retention/loss of the modified functional groups.

ESI can be operated in both positive and negative ion modes. Based on the polarity of precursor ions, the combination of mass analyzers, and the incorporation of neutral gas molecules/radical ions/electrons/photons, different types of fragmentation techniques can be applied to proteins/peptides. The nomenclature of common types of peptide backbone fragment ions (or “sequence ions”) observed upon different fragmentation techniques is illustrated in Figure 1.5, as proposed by Roepstorff and Fohlman in 1984 [106] and later modified by Biemann [107].

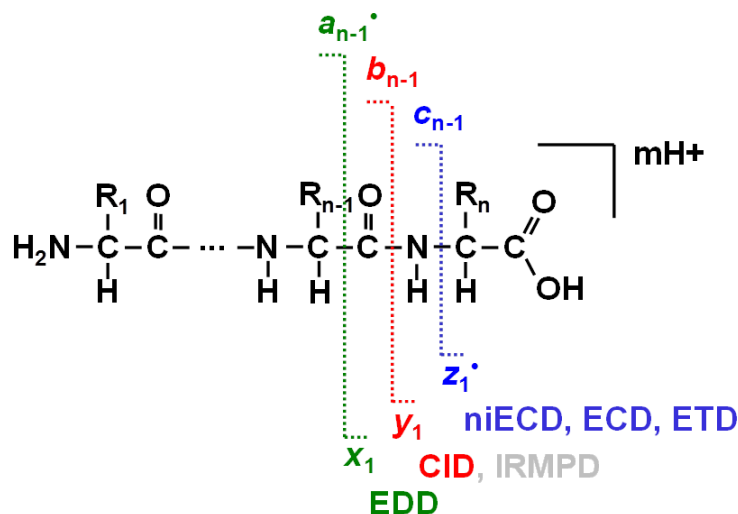


**Figure 1.5** Nomenclature for peptide fragment ions in MS/MS. Adapted from Roepstorff and Fohlman [106] and Biemann [107].

#### 1.2.4.1 Slow-Heating Fragmentation

The aforementioned CID technique involves slow heating [108], where positively or negatively charged protein/peptide ions are activated under low-energy collision conditions. Slow activation methods rely on multiple discrete activation events such as multiple collisions (e.g., CID) or multiple photon absorption (e.g., IRMPD) [108, 109]. The time scale for the multiple activation events can be long, on the order of ms or longer. The energy obtained by collisions is distributed through the peptide/protein ion via intramolecular vibrational energy redistribution (IVR) [110]. Dissociation of the weakest bonds in the molecule occurs once the internal energy of the vibrationally activated ion is raised above threshold and the lowest energy pathways will be followed. CID of protonated peptide ions mainly result in *b*- and *y*-type backbone fragment ions, while CID of deprotonated peptide ions typically result in *y*- and *c*-type fragment ions [111, 112]. In both cases, neutral losses from side chains such as water and phosphoric acid are also frequently observed.

Currently, the widely acknowledged framework to describe how protonated peptides dissociate upon collisional activation is termed the “mobile proton” model [113-116]. This model assumes that, for protonated peptide ions formed by soft ionization methods such as ESI, protons are initially localized on the most basic sites in the molecule, including the N-terminus and the

side chains of basic amino acid residues. During ion activation, these protons migrate to less basic sites provided that they are not sequestered by strongly basic amino acid side chains [117, 118]. It is known from the results of molecular orbital calculations that protonation of the amide nitrogen leads to considerable weakening of the amide bond [119], thus triggering charge-directed mechanisms [119-122] that provide mainly *b*- and *y*-ions, the two types of complementary fragment ions resulting from cleavage of the -CO-NH- peptide bond.

CID of deprotonated peptides has received less attention in proteomics studies. However, the mass spectra of negatively charged peptides can provide an important supplement to positive ion spectra in sequencing peptides [112, 123]. Bowie and coworkers described the fundamental backbone cleavages and the characteristic side-chain fragmentations for deprotonated peptides [111, 124, 125]. They suggested that the fragmentation pathways are often dependent on the specific peptide sequence and the side-chain structure of some amino acids.

#### 1.2.4.2 Electron-Based Fragmentation

As two commonly used electron-based fragmentation techniques, ECD [126] and ETD [127] can study non-covalent complexes [128] and preserve labile bonds to preclude the significant PTM losses typically observed in slow-heating methods [129-131]. Compared to CID, ECD and ETD often provide more peptide backbone cleavages and less side-chain losses. As indicated in Scheme 1.1(A), the principle of ECD is to react multiply protonated polypeptide cations with low-energy electrons. Capture of near-thermal free electrons results in charge-reduced radical intermediates that further fragment at the N-C<sub>α</sub> bond of the peptide backbone to produce *c*'- and *z*'-ions. *a*'- and *y*-ions are also observed in ECD mass spectra at lower abundance. In addition, ECD results in S-S bond cleavage [132]. The mechanism of N-C<sub>α</sub> peptide backbone bond cleavage upon electron capture is not fully understood; different mechanisms are currently proposed [126, 133-137]. ETD (2004) was introduced several years later than ECD (1998) [127]. Electrons in ETD are delivered by radical anions (e.g., fluoranthene), unlike the free electrons employed in ECD (Scheme 1.1(B)). Subsequent peptide backbone N-C<sub>α</sub> bond cleavage is assumed to proceed by the same mechanism as that in ECD

[134]. Unlike ECD, almost exclusively implemented on FT-ICR MS instruments, ETD can be implemented on relatively affordable, robust, and widespread ion trap mass spectrometers, which makes ETD more accessible than ECD, especially with instrumentation that deliver proteomics-grade performance such as high-resolution Orbitrap or TOF MS. Recently, the feasibility of performing ECD on benchtop MS instruments has also been explored [138].

- (A)  $[M + nH]^{n+} + e^{-} (< 1 \text{ eV}) \rightarrow [M + nH]^{(n-1)+\bullet} \rightarrow \text{Fragments}$   
 (B)  $[M + nH]^{n+} + A^{\bullet} \rightarrow [M + nH]^{(n-1)+\bullet} \rightarrow \text{Fragments}$   
 (C)  $[M - nH]^{n-} + e^{-} (> 10 \text{ eV}) \rightarrow [M - nH]^{(n-1)\bullet-} + 2e^{-} \rightarrow \text{Fragments}$   
 (D)  $[M - nH]^{n-} + e^{-} (\sim 2.5 - 6.5 \text{ eV}) \rightarrow [M - nH]^{(n+1)\bullet-} \rightarrow \text{Fragments}$

**Scheme 1.1** Fragmentation routes for (A) ECD, (B) ETD, (C) EDD, and (D) niECD.

Interaction of more energetic electrons ( $\sim 10$  eV) with multiply protonated peptide cations leads to increased efficiency of secondary fragmentation, a process known as hot ECD (HECD) [139]. In electron ionization dissociation (EID), involvement of electrons with even higher energy (up to 20-100 eV) may induce further ionization accompanied by extensive backbone fragmentation [140, 141]. Peptide backbone N-C $_{\alpha}$  bond cleavage is also possible for negatively charged peptide anions following capture of a slightly more energetic ( $\sim 2.5$ -6.5 eV) electron, a novel MS/MS technique termed negative ion electron capture dissociation (niECD) which was first discovered in the Hakansson Lab in 2011 [142, 143]. When multiply charged peptide anions interact with energetic electrons ( $> 10$  eV) in electron detachment dissociation (EDD), C $_{\alpha}$ -C backbone bond cleavage is a preferential fragmentation pathway to yield mainly  $a^{\bullet-}$  and  $x$ -ions for proteins and peptides [144, 145]. Both niECD and EDD are believed to proceed via radical-driven fragmentation mechanism and may find application in mass spectrometry for peptide sequencing and localization of labile PTMs, especially acidic ones that show improved ionization efficiency in negative ion mode, e.g., phosphorylation [142, 145, 146] and sulfation [143]. However, one drawback of niECD and EDD of polypeptides is their low fragmentation efficiency. Also, the use of highly energetic electrons in EDD may induce additional neutral losses and side-chain losses with less useful structural information, for example, the

characteristic CO<sub>2</sub> loss [144]. In this sense, niECD may mitigate the issue by utilizing less energetic electrons.

In addition to the aforementioned electron-based fragmentation methods, free radical initiated peptide sequencing (FRIPS) [147, 148] is an alternative radical-driven MS/MS technique. Different from the electron-mediated radical-driven mechanisms discussed above, radical initiation in FRIPS is accomplished through vibrational activation. A stable free radical initiator attached to free amines in protonated or deprotonated peptide ions undergo homolytic bond cleavage upon mild collisional activation to generate odd-electron species. The initiated radical is then propagated through the peptide ion to yield a variety of backbone fragments. FRIPS has shown potential to achieve localization of labile acidic modifications in negative ion mode [149].

### **1.2.5 Charging and Supercharging**

Mass spectrometers measure the  $m/z$  values of chemical species in gaseous form that carry a net charge. Thus, a key prerequisite is to ionize molecules of interest and transfer them into the gas phase. ESI [150] and matrix-assisted laser desorption/ionization (MALDI) [151] are by far the two most widely used “soft” ionization techniques for MS [152]. Both ESI and MALDI induce minor or no fragmentation. While MALDI typically forms singly charged ions, multiply charged ions are often formed via ESI, particularly for large analytes. ESI is thus the preferred method for coupling with mass analyzers of limited  $m/z$  range. In addition, ESI is a suitable ion source to couple LC with MS.

#### **1.2.5.1 Electrospray Ionization (ESI)**

The invention and application of ESI is a key milestone in the development of modern mass spectrometry [150]. ESI allows for biomolecules with varying sizes to be introduced into the gas phase carrying multiple charges. Under specific ESI conditions, proteins can be ionized without denaturation; thus non-covalent protein complexes can remain intact. ESI proceeds with the dispersal of a fine spray of charged droplets, from a Taylor cone formed at a small aperture capillary tip maintained at high voltage (e.g., 2.5-6.0 kV), followed by solvent evaporation,

droplet shrinkage, and ion formation from the highly charged nanodroplets [35, 153, 154]. The application of a nebulizing gas, e.g., nitrogen, which shears around the sample solution spray, assists rapid solvent evaporation and allows a higher sample flow rate, typically between one and several hundred  $\mu\text{L min}^{-1}$ . With the aid of an elevated source temperature and/or another stream of nitrogen drying gas, the shrinking droplets build up their charge density, until surface tension and Coulomb repulsion are balanced, a critical point termed the Rayleigh limit [18]. The Rayleigh limit predicts the maximum number ( $z_R$ ) of elementary charges  $e$  possible for a spherical droplet of radius  $R$ :

**Equation 1.2** 
$$z_R = \frac{8\pi\sqrt{\varepsilon_0\gamma R^3}}{e}$$

where  $\varepsilon_0$  is the vacuum permittivity and  $\gamma$  is the surface tension of the liquid. Gaseous analyte ions generated from ESI follow a pressure gradient and a potential gradient towards the analyzer region of the mass spectrometer.

Mechanisms for ESI are still under debate. Three major ion formation mechanisms are the ion evaporation model (IEM), charged residue model (CRM), and chain ejection model (CEM) [154, 155]. Low molecular weight species are believed to be ejected from droplet surfaces into the gas phase at the final stage of ESI, referred to as IEM. In CRM, nanodroplets that are close to Rayleigh limit and only contain one single analyte molecule evaporate to dryness. The nanodroplet transfers its charge to the analyte before it evaporates. It is widely accepted that large molecules with compact structures are released into the gas phase as described by CRM. Unfolded and hydrophobic proteins are believed to follow CEM ejected out of the droplet as a chain [156].

### 1.2.5.2 Supercharging Strategies

Back in 2001, Williams and coworkers discovered that addition of glycerol or *m*-nitrobenzyl alcohol (*m*-NBA) into electrospray solutions dramatically increased both the maximum observed charge state and the abundances of the high protein and peptide charge states [157]. Later, a number of studies were conducted to explore the mechanism of this charge-enhancing effect [158-162] and expand the application of the strategy, termed

“supercharging”. In addition to *m*-NBA [157], a number of molecules have been found to promote protein/peptide charging when added to ESI solvents (or LC mobile phases) in relatively low concentration, such as sulfolane [162, 163], dimethyl sulfoxide (DMSO) [164], propylene carbonate [32, 165], 1,2-butylene carbonate [166], *etc.* These low-volatility additives are referred to as “supercharging reagents”. Some supercharging reagents, such as *m*-NBA, have been found to be effective for both native (aqueous) [167] and denaturing (aqueous/organic) [168] ESI spray solutions. Novel supercharging reagents continue to be developed, including trivalent metal cations [169, 170]. Also, the extent of ESI supercharging in both ion modes has been investigated [171]. It was found that the same supercharging agents did not induce the same significant increase of charging for protein ions in negative ion mode ESI as observed in positive ion mode.

Over the past two decades, there have been discussions and debates over the mechanism of chemical supercharging. During evaporation, ESI droplets become enriched with the reagent due to its low volatility [158] and high boiling point (bp>180 °C) [157] relative to typical solvent molecules. In denaturing conditions in which proteins are more unfolded, retention of these reagent molecules causes an increase of the droplet surface tension and thus a higher charge density needed to reach Rayleigh limit [157]. More highly charged ions can be formed from droplets with a higher charge density. However, this argument contradicts the solution-phase properties of *m*-NBA ( $\gamma_{m\text{-NBA}} < \gamma_{\text{water}}$ ) [162]. Results from experiments using thermal activation [167], HDX MS [164, 172], traveling wave ion mobility MS (TWIMS MS) [173], and chemical cross-linking [174] indicated that chemical and/or thermal denaturation of the analyte in the ESI droplet is the primary reason for aqueous solution supercharging of proteins and complexes. Circular dichroism spectroscopy (CD) monitored the transition of protein structure from folded to unfolded states as sulfolane was added to the solution [171], consistent with this hypothesis. However, this unfolding mechanism was questioned with differential mobility analyzer-mass spectrometry (DMA-MS) data [175] and TWIMS data [173] indicating that supercharging occurred without extensive unfolding. Other investigations considered supercharging reagent-protein interactions [163, 176], as well as the supercharging reagent Bronsted acid/base

chemistry [159]. Meanwhile, ESI models (IEM, CRM and CEM) [155] have been frequently used to describe the supercharging process. Recent molecular dynamics (MD) simulations revealed that supercharging may be caused by a charge trapping mechanism [160, 161] for proteins electrosprayed from aqueous solution and released via the CRM, while charge carriers are ejected from the surface via the IEM with droplet shrinkage. Extended protein ions were shown to be formed by the CEM in supercharging ESI [156].

Benefits of charge enhancement through supercharging and other strategies are obvious for the performance of FT-based mass analyzers [93, 177] and the efficiency of tandem mass spectrometric techniques that require multiply charged precursors, such as ECD and ETD. Several studies reported on reduced fragmentation efficiency and limited sequence coverage for doubly charged peptides in ETD [178, 179]. Our group has also looked into the charge state effect on ECD performance using a variety of proteolytic peptides and demonstrated that triply protonated peptides show improved fragmentation efficiency than their doubly protonated counterparts [180]. Since the ECD/ETD fragmentation efficiency is greatest for  $\geq 3+$  peptide ions [180-182], it presents a problem in bottom-up proteomics strategies where proteins are enzymatically digested into peptides with limited size. Doubly charged peptide ions are reported to be the most abundant ion species from trypsin-digested proteins [183]. The problem with reduced ECD/ETD fragmentation is even more pronounced in bottom-up HDX experiments because pepsin-derived peptides [184] do not necessarily carry basic amino acid residues (protonation sites) at their C-terminus as trypsin-derived peptides [185] do.

McLuckey and coworkers have shown that elevated bath gas temperature can increase the overall sequence coverage for tryptic peptides containing more than seven residues [178]. Using proteases such as Lys-C or Asp-N is another approach to increase peptide ion charge states, since longer peptides (20-25 residues) are generated that tend to hold more charges (3-6) than tryptic peptides [127, 181]. Kjeldsen and coworkers found that by adding just 0.1% *m*-NBA to LC mobile phases in LC ETD MS/MS experiments, the average charge states for tryptic peptides were significantly increased, resulting in improved ETD fragmentation efficiency and,

consequently, improved peptide sequencing for regular peptides and phosphopeptides [168]. Furthermore, *m*-NBA has been adopted to promote charging for a variety of peptides derived from other proteases [186, 187]. In addition to chemical supercharging, electrothermal supercharging (ETS) [188, 189] was recently applied to native proteins by simply elevating the potential and the capillary temperature in a nanoESI source. It has been shown that protein denaturation occurring in ESI droplets is the primary mechanism for ETS [190].

### **1.3 Hydrogen/Deuterium Exchange Mass Spectrometry (HDX MS)**

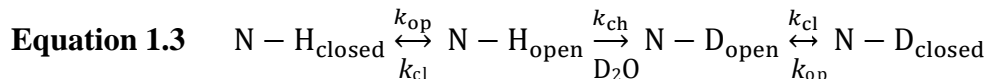
Protein HDX MS has evolved into a powerful method for investigation of protein conformation, folding/unfolding, dynamics, and interactions [191-195]. The traditional method for HDX studies has been two-dimensional NMR spectroscopy [196, 197]; however, HDX experiments have shifted mostly towards MS lately. Attractive features of HDX MS include great sensitivity, straightforward measurement, ideally unlimited size range, and capability to detect complex systems such as membrane proteins [198-200].

The HDX technique was first developed in the early 1950s by Kaj Linderstrom-Lang and coworkers [201]. They used density gradient tubes to monitor the protein mass increase as a result of hydrogen substitution for deuterium. Later, Englander and coworkers employed liquid scintillation counting to measure hydrogen/tritium exchange [202] and used NMR to examine HDX [197]. HDX was coupled to MS in the early 1990s [203], soon after the introduction of soft ionization methods. Rapid advances in this technique have been occurring ever since. This section exclusively focuses on commonly employed solution-phase HDX MS.

#### **1.3.1 HDX Kinetics**

HDX MS relies on the fact that exposure of a protein to D<sub>2</sub>O or other deuterated solvents can induce rapid amide hydrogen to deuterium exchange in disordered regions that lack stable hydrogen bonding. Tightly folded regions are much more protected from HDX, resulting in slower isotope exchange behavior [191, 193, 194]. The technique takes advantage of the inherent and spontaneous exchange of labile hydrogen atoms in a protein to serve as reporters of its global or local conformational environment. A general exchange mechanism for native proteins is

described as:



where  $k_{\text{op}}$  and  $k_{\text{cl}}$  are rate constants for the opening and closing transitions, and  $k_{\text{ch}}$  is the intrinsic rate constant for N-H  $\rightarrow$  N-D exchange determined for totally solvent-exposed amides, also referred to as the chemical rate constant. As indicated in Equation 1.3, HDX kinetics is strongly associated with the opening/closing (or unfolding/refolding) events of native proteins in solution. Isotopic labeling can only occur during short-lived transitions to an open state. The equilibrium between protein opening motion ( $k_{\text{op}}$ ) and closing motion ( $k_{\text{cl}}$ ) characterizes the populations of structurally open protein and structurally closed protein in solution. The overall (observed) HD exchange rate constant  $k_{\text{HDX}}$  can be described by Equation 1.4 [204]:

$$\text{Equation 1.4} \quad k_{\text{HDX}} = \frac{k_{\text{op}}k_{\text{ch}}}{k_{\text{cl}}+k_{\text{ch}}}$$

The corresponding protection factor [205] is defined by:

$$\text{Equation 1.5} \quad P = \frac{k_{\text{ch}}}{k_{\text{HDX}}}$$

The density of intramolecular hydrogen bonding and solvent access both contribute to protection of the amides [191]. If the unfolding/refolding event is much faster than the chemical exchange ( $k_{\text{cl}} \gg k_{\text{ch}}$ ), multiple openings and closings must take place before exchange occurs.  $k_{\text{HDX}}$  can thus be described as:

$$\text{Equation 1.6} \quad k_{\text{HDX}} = \frac{k_{\text{op}}k_{\text{ch}}}{k_{\text{cl}}}$$

This mechanism is termed EX2. If the protein refolds at a rate much slower than the chemical exchange ( $k_{\text{cl}} \ll k_{\text{ch}}$ ), amide labeling occurs during the very first opening event, following EX1 behavior:

$$\text{Equation 1.7} \quad k_{\text{HDX}} = k_{\text{op}}$$

In nature, most proteins follow EX2 behavior [191], although some proteins can be induced to undergo deuterium exchange by the EX1 mechanism by exposing the protein to denaturants [206]. Intermediate cases that exhibit aspects of both mechanisms have been reported as well

[204]. Bimodal isotope distributions are a signature for HDX that follows EX1 [206, 207]. However, one has to be careful in identifying EX1 behavior, as sometimes sample carryover during LC can lead to false EX1 characteristics [208].

HDX can proceed via catalysis by acid, base, and water. The pD dependence of  $k_{\text{ch}}$  is given by:

**Equation 1.8**  $k_{\text{ch}} = k_{\text{A}}[\text{D}^+] + k_{\text{B}}[\text{OD}^-] + k_{\text{W}}$

in which  $k_{\text{A}}$ ,  $k_{\text{B}}$ , and  $k_{\text{W}}$  are the acid-, base-, and water-catalyzed intrinsic rate constants. Basic catalysis is the dominant mechanism in near-neutral solution [209]. The exchange becomes minimal at pD ~2.5 and  $k_{\text{ch}}$  decreases ~4 orders of magnitude if pD is lowered from 7 to 2.5. In addition to pD, HDX depends on temperature, although the HDX rate is less sensitive to temperature change than pD change. A 10-fold change in exchange rate can be obtained by a change of one pH unit or ~22 °C in temperature [197]. Moreover, amide hydrogen exchange depends on the side chain structures of neighboring amino acid residues for unstructured polypeptides [209].

### 1.3.2 HDX MS approaches

#### 1.3.2.1 Bottom-up HDX MS

A typical procedure for HDX comprises isotope labeling, quench, proteolytic digestion, desalting/separation, and mass analysis [194]. HDX is usually initiated by dilution of the protein in deuterated buffer for each of several periods of time (continuous labeling), e.g., 1 min, 10 min, 1 h, *etc.* The dilution should be 10- to 20-fold to achieve at most 90-95% D labeling. The exchange is then quenched by lowering the solution pH to ~2.5 and the temperature to ~0 °C followed by enzymatic digestion either in solution [210] or on-column with an immobilized acid protease [211]. Alternatively, the digestion step can be skipped for global HDX analysis [190] or top-down HDX of intact proteins [212, 213]. Following proteolysis, the protein digests are desalted and separated through fast and chilled LC and then analyzed by MS (Figure 1.6). Because side chain deuteriums back-exchange for hydrogen during the LC step, only deuteriums

at the backbone amides are retained and measured, with the exception of proline residues which do not have backbone amide hydrogens [193, 195]. Because deuterium is twice as heavy as hydrogen, the exchange can be detected and quantified by mass shift. Deuterium content is calculated by subtracting the average mass of the undeuterated peptide (no HDX control) from that of the deuterated one at each incubation period. Comparison of deuterium uptake profiles under two sets of conditions provides insight into the protein conformational dynamics [191, 193, 214, 215].

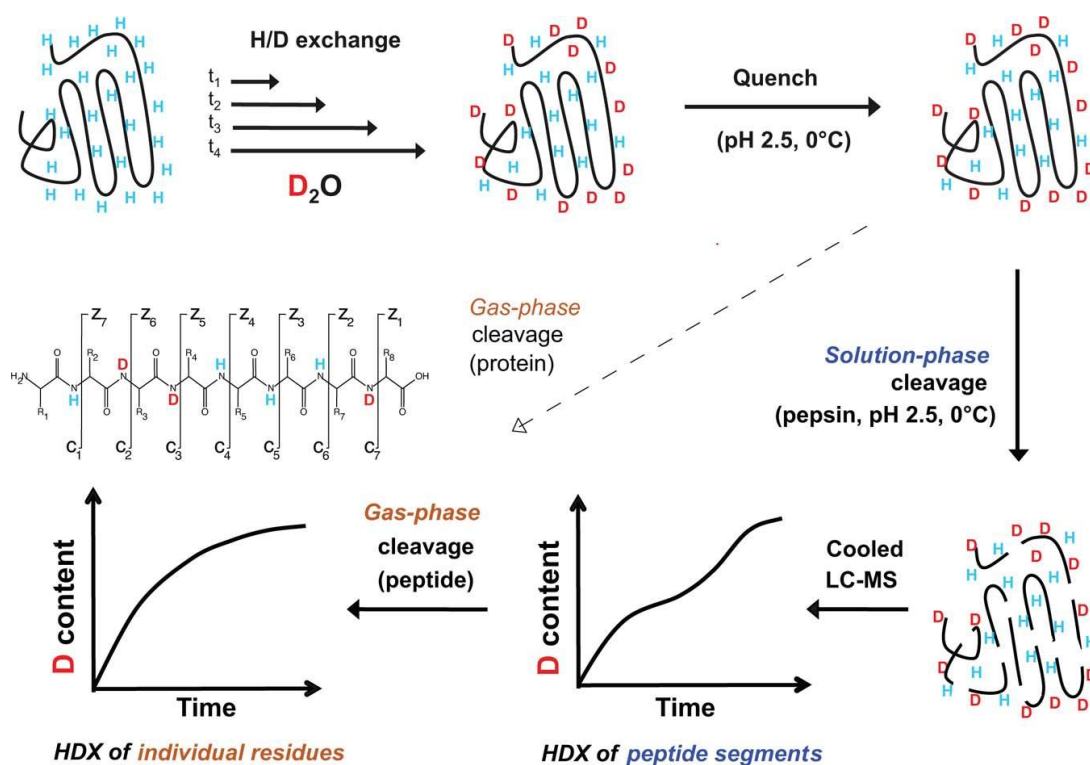


**Figure 1.6** Diagram of protein HDX MS and MS/MS workflows with the use of LC and/or gas-phase fragmentation techniques. Reprinted with permission from ref [230]. Copyright 2014 American Chemical Society.

In HDX MS experiments, conducting proteolytic digestion before LC/MS (bottom-up method) is helpful for monitoring conformational changes in small regions of a large protein. The acid protease commonly used in HDX is pepsin, which remains active under quenching conditions. In most cases, pepsin is added to a final level of 2:1 to 1:1 (w/w) protein:pepsin for in-solution digestion. Other acid-resistant proteases such as protease XIII and protease XVIII,

although less popular than pepsin, can yield complementary digestion patterns [184, 216, 217]. The use of more than one protease in HDX experiments [184] resulted in enhanced sequence resolution, as more overlapped peptide segments could be produced. However, due to the fairly non-selective cleavage pattern of pepsin and other acid proteases [216], tandem MS is usually suggested to confirm the identity of undeuterated peptides before HDX measurements. The use of denaturants (e.g., guanidine HCl or urea) [218] and/or disulfide bond reducing agents (e.g., tris(2-carboxyethyl)phosphine (TCEP)) [219] mixed with quenching solutions enables quenching of the HDX and simultaneous denaturing/reduction of the protein, thus improving digestion efficiency.

In addition to continuous labeling, one can also apply pulsed labeling to monitor rapid conformational changes in proteins in the presence of perturbant, such as denaturing agents, pH and/or temperature change, *etc.* In pulsed HDX, the exchange is only performed for a brief time (e.g., 10 s) [220-222]. Even shorter exposure time (milliseconds to seconds) was achievable on a more sophisticated labeling apparatus, such as a stopped-flow setup [223] or a microfluidic device [224].

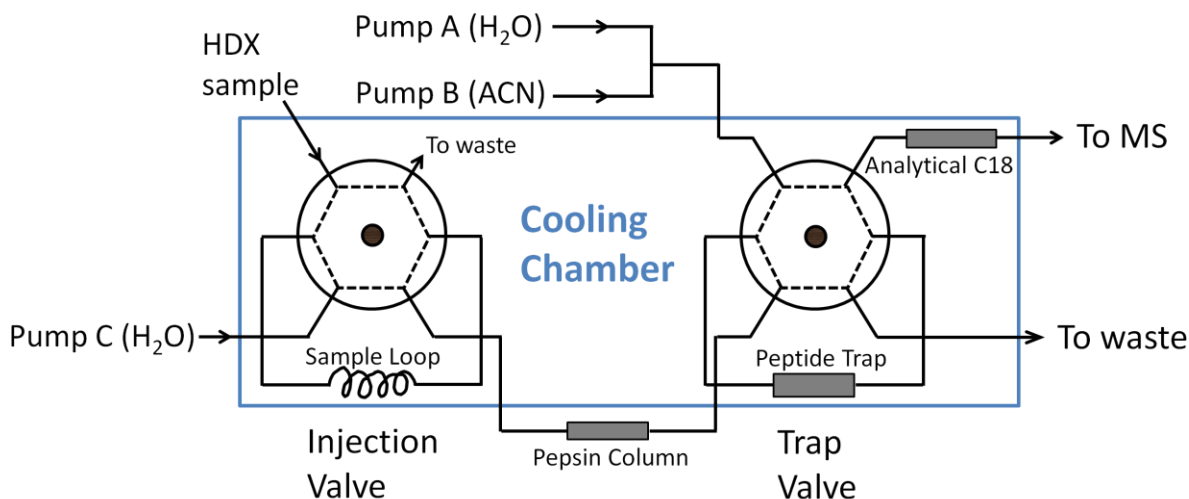


**Figure 1.7** Diagram of online pepsin digestion setup, modified from ref [194]. The pepsin column can be placed either inside or outside the cooling chamber.

Enzymatic digestion can also be achieved on-column if the protease is immobilized on a stationary phase (e.g., POROS beads [225, 226], ethyl-bridged hybrid particles [75]) packed into

a conventional stainless steel column. Attractive features of online digestion include that the effective protease concentration on-column is much larger than that in-solution, leading to higher digestion efficiency; the protease is not injected onto the analytical column, so a cleaner chromatogram can be created; and the reproducibility of protein digestion is improved compared with manual sample handling. To achieve online digestion, an LC setup incorporating an auxiliary pump and a binary solvent pump has been designed to couple the immobilized pepsin column with a C18 analytical column, in which a trap column is placed between the enzymatic column and the analytical column [75, 211, 225]. A diagram of the online pepsin digestion setup is shown in Figure 1.7. The additional auxiliary pump (Pump C in Figure 1.7) is to drive the protein through the pepsin column with aqueous solvent (usually water containing 0.1% formic acid). The digested sample is then carried to the peptide trap located on a second switch valve (the first switch valve is an injection valve for rapid sample loading). Following a short desalting period, the switch valve is set so that solvent from the binary pump (Pump A and Pump B in Figure 1.7) elutes peptides from the trap, enabling their separation and analysis by LC/MS. Although the pepsin column is usually used at ambient temperature, all other parts of the system are immersed in an ice bath or placed in a refrigerator to minimize deuterium loss. Nevertheless, one needs to be careful about back-exchange and carryover issues associated with immobilized pepsin columns [225].

In addition to online digestion, a number of efforts have been made to improve proteolysis in HDX due to the time limitation [210] and temperature requirement under quenching conditions. Mysling *et al.* demonstrated that electrochemical reduction of disulfide bonds is efficient under quench conditions [227]. New proteolytic enzymes suitable for HDX experiments have been investigated too [217, 228].

Strategies to improve separation and mass spectrometry analysis in HDX experiments include the use of UPLC [229] or supercritical fluid chromatography (SFC) [210, 230] instead of HPLC which performs poorly at 0 °C, a shorter yet efficient gradient compared to a conventional one [210], well-controlled refrigerated systems [231, 232], high resolution mass analyzers such

as FT-ICR [216, 233], appropriate tandem MS techniques [213], *etc.* The coupling of tandem MS to HDX is discussed in more detail in the following section.

Automation is another major trend in HDX MS. Recent development in automation of HDX sample handling has greatly improved throughput, increased reproducibility, reduced back-exchange during sample freezing/thawing, and eliminated human error. Waters Corporation (Milford, MA) developed a complete HDX setup composed of nanoAcquity solvent managers linked to an HDX manager (with cooling system) and a Synapt G2-S mass spectrometer. They also collaborated with Leap Technologies (Carrboro, NC) to provide an automated sample handling solution with a Leap robot. Thermo Scientific (La Jolla, CA) also introduced their first HDX setup in 2012. In addition, the demand for managing the large amount of data generated from an HDX experiment has provoked the development of automated or semi-automated data processing platforms. Software tools, such as HX-Express [234], Hydra [235], The Deuterator [236], HD Desktop [237], HeXicon [238], HDXFinder [239], *etc.*, provide a user-friendly interface to complete deuterium uptake calculation, data visualization and comparison. However, some of these packages require the file type(s) of MS raw data generated by a certain MS instrument manufacturer, thus are not universal solutions for all HDX practitioners.

### **1.3.2.2 Top-down HDX MS**

One drawback of the bottom-up HDX method is that spatial resolution is limited by the size of each proteolytic peptide, typically 5-10 residues in length [240]. In addition, the enzymatic cleavage events inevitably cause loss of HDX information at the two terminal residues. Even the combination of different proteases and generation of highly overlapped peptide segments cannot ensure a resolution of deuterium uptake down to single amino acid residue level [241]. Also, the proteolysis and chromatographic separation in bottom-up experiments are usually associated with the issue of back exchange [225].

Top-down MS/MS attempts to overcome these limitations by directly infusing deuterated proteins into a mass spectrometer and applying gas-phase fragmentation to the intact protein ions to yield complementary N- and C-terminal ion pairs, as indicated by the dashed line in Figure 1.6.

Higher spatial resolution can be obtained in top-down experiments, ideally to the single-residue level, because gas-phase fragmentation may generate the fragment ions that differ by one amino acid and the difference in deuterium contents of such adjacent ions can yield HDX information at a single backbone amide [54, 193]. Top-down HDX MS may also allow protein dynamics characterization in a conformer-specific fashion [242, 243]. However, top-down HDX MS had not enjoyed significant popularity until recently mainly due to several problems. One practical limitation is inadequate sequence coverage for larger polypeptides and proteins, which frequently results from limited fragmentation efficiency and/or limited resolving power of mass spectrometers for highly overlapped peaks, and leads to inferior spatial resolution. Incorporation of peptide ion fragmentation in the workflow of the bottom-up HDX MS measurements (Figure 1.6) attempts to overcome the size limitation of proteins studied associated with the top-down strategy and has shown potential for obtaining near-residue-level resolution in HDX MS/MS for proteins smaller than 30 kDa [187, 218, 240]. While incorrect determination of deuterium levels for fragment ions may result from fast LC/MS/MS and inadequate data acquisition time, a solution to address this problem is to enhance the quality of MS/MS of deuterated peptide ions by increasing the data acquisition window in high-resolution mass spectrometry (e.g., FT-ICR) while eliminating the LC step [244].

Another important fundamental problem that hinders widespread use of top-down HDX MS/MS and MS/MS coupled with bottom-up HDX workflows is the frequent occurrence of hydrogen/deuterium (H/D) scrambling upon protein and peptide ion activation prior to or during the dissociation event, further discussed in the following section.

### **1.3.3 Hydrogen/Deuterium (H/D) Scrambling in HDX MS/MS**

H/D scrambling refers to multiple reversible proton/deuteron transfers among all the labile sites in a gaseous peptide, i.e., all N-, S-, and O-linked hydrogen/deuterium atoms. The resulting, undesired, randomization of hydrogens and deuteriums in the gas phase distorts the labeling pattern from that obtained in solution and extensive H/D scrambling completely erases the information imprinted on a protein/peptide in solution. Therefore, H/D scrambling in the

gaseous peptide or protein ion is the main issue that has to be addressed prior to wider acceptance of MS/MS techniques to increase the spatial resolution in HDX MS experiments.

Comparison of the deuterium distribution patterns on a polypeptide/protein backbone obtained by HDX MS/MS and by NMR provides a straightforward manner to detect the occurrence and extent of H/D scrambling [190, 245, 246]. Another method is to use a polypeptide model system with well-characterized and selective deuterium labeling in solution; deviation from the expected, well-defined, exchange patterns of the series of fragment ions indicates the occurrence of H/D scrambling. These peptides can be prepared in a manner that ensures that the deuterium is exclusively or considerably retained at backbone amides of one half of the peptide prior to MS analysis [247-253]. Such regioselective deuterium labeling can be achieved either by higher-order structure effects [249, 251] or primary structure effects [250, 252, 253]. This method can also quantitate the H/D scrambling level during an MS/MS experiment by comparing the measured H/D distribution to the known solution pattern (0% scrambling) and the totally randomized distribution (100% scrambling), as indicated in Figure 1.8.

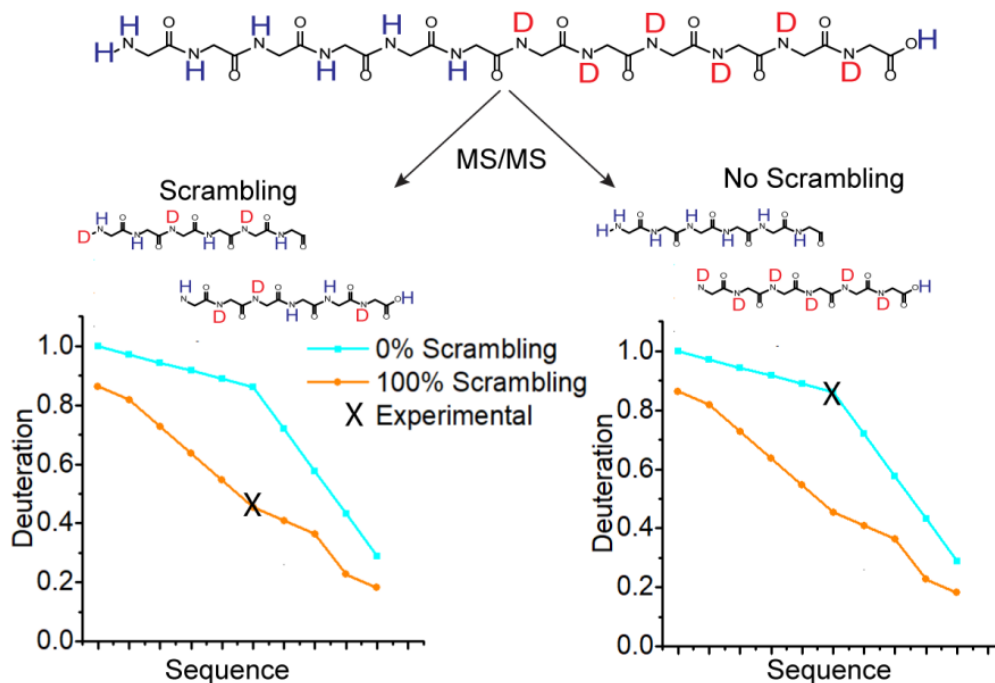


**Figure 1.8** Principle of measuring H/D scrambling by gas-phase fragmentation of selectively labeled model peptides. The figure accounts for C-terminal  $\gamma$ -type ions and thus the sequence is read from right to left.

Early studies on determinants of H/D scrambling in top-down HDX MS/MS utilizing CID for protein ions indicated that the occurrence of hydrogen scrambling is associated with both collision energy and protein ion structure in the gas phase [246, 254]. Low-energy CID is the most common fragmentation method for protein and peptide ions and is accessible on most commercial mass spectrometers. Unfortunately, several studies have demonstrated extensive H/D scrambling upon collisional activation of protonated peptides and proteins for both *b*- and *y*-ions [251, 252, 255, 256], consistent with the current theoretical framework developed to understand CID-type fragmentation of protonated peptides, known as the “mobile proton” model [113, 114]. In this charge-directed fragmentation mechanism, internal energy elevation through multiple energetic collisions ( $>\mu\text{s}$ ) facilitates intramolecular proton transfer from a basic site to a less basic backbone amide, which weakens the peptide bond to yield complementary *b*- and *y*-ions [114]. Protonation of the backbone amide is reversible in nature, which well explains the migration of deuteriums among labile sites in deuterated peptide ions. Negative ion mode CID has also been shown to induce complete hydrogen scrambling in deprotonated peptides using a MALDI ion source [249]. Overall, it has become a consensus that CID should not be used as a gas phase fragmentation technique in HDX MS experiments due to extensive H/D scrambling.

Electron-based fragmentation, on the other hand, may provide a solution to the scrambling problem. Based on an early suggestion that ECD proceeds in a nonergodic manner [126], it was hypothesized that ECD and ETD may induce minimal hydrogen scrambling [126, 247]. It is evident that these fragmentation techniques are gentle enough to cause peptide backbone fragmentation while retaining labile PTMs [129, 130]. Over the past decade, ECD and ETD have both been demonstrated to proceed with negligible intramolecular H/D migration in peptides [250, 253] and small intact proteins [213] (although recent work by Hamuro *et al.* implies that ETD fragmentation is accompanied by regioselective scrambling [257, 258]), thus allowing localization of deuteriums down to the single residue level without deviation from solution-phase labeling patterns. However, great care must be taken when conducting ECD/ETD-based HDX MS experiments, because careful optimization of the ion source and ion

transfer parameters is of vital importance to minimize H/D scrambling by vibrational excitation prior to the MS/MS event [250, 253, 259]. It is noteworthy that suitable parameters for ion source and ion transfer optics should be determined for each instrument type in order to find a compromise between minimal H/D scrambling levels and acceptable ion transmission efficiency and signal abundance [250, 253, 260].

In terms of other gas-phase fragmentation techniques for analysis of deuterated peptides, a rather limited number of studies have been conducted. MALDI in-source decay (ISD) was reported to yield minimum hydrogen scrambling [248]. IRMPD of intact protein ions following gas-phase HDX in an ICR cell showed a distribution of deuterium uptake different from the complete scrambling pattern, but the degree of scrambling increased as the laser power increased [261]. Recently, top-down HDX analysis of protein structures using ultraviolet photodissociation (UVPD) was achieved in positive ion mode on an Orbitrap Fusion Lumos Tribrid mass spectrometer equipped with a 213 nm laser [245]. UVPD is a recently developed fast-fragmentation technique based on irradiation of gaseous protein/peptide ions with far-UV light at a wavelength absorbable by peptide bonds [262, 263]. Fast radical-based mechanisms have been raised for understanding the UVPD process [262]. In this work, the lack of scrambling in UVPD was confirmed by comparing obtained deuteration data with NMR and X-ray crystallography results. In other recent work, quantitation of H/D scrambling during UVPD using a selectively labeled peptide was completed on a high-resolution Q-TOF mass spectrometer [264]. These results also showed that UVPD at 213 nm can proceed with limited H/D scrambling (<10% scrambling for *a/x* fragment ions) at mild ion source conditions. These findings indicate that UVPD fragmentation can be a valuable addition to the HDX MS toolbox for both bottom-up and top-down applications.

#### **1.4 Dissertation Overview**

This dissertation focuses on analytical strategy development for combining gas-phase fragmentation with HDX MS for protein structural analysis, and for improving host cell protein characterization in complex biopharmaceuticals. In Chapter 2, the feasibility of several negative

ion mode MS/MS techniques for improving HDX spatial resolution is explored, including nCID, nFRIPS, EDD, and niECD. Specifically, H/D scrambling levels associated with these techniques were measured and compared by use of basic and acidic regioselectively deuterium labeled model peptides. In Chapter 3, a supercharging strategy is described to facilitate ECD/ETD-based peptic peptide fragmentation to address the issue of limited charging in bottom-up HDX MS. The ability of the supercharging agent *m*-NBA to enhance average charging for short peptides frequently generated upon pepsin digestion is demonstrated and, consequently, improved ECD/ETD fragmentation efficiency, sequence coverage, and deuterium spatial resolution are achieved. Chapter 4 examines unconventional fragmentation behavior for supercharged peptides upon ECD/ETD. Standard peptides with few or no basic amino acid residues, a longer peptide (melittin), and proteolytically derived peptides are used to investigate the occurrence of atypical *b*-type fragment ions upon ECD and ETD, respectively, under supercharging conditions, providing insight into the different energetics of these two fragmentation methods that are often considered equivalent. Chapter 5 describes work I performed during a co-op program at Bristol-Myers Squibb (Hopewell, NJ) in 2018. An offline HILIC sample preparation method was developed for improving host cell protein detection in mAb and non-mAb biotherapeutic proteins by LC/MS. Finally, Chapter 6 summarizes all results and discusses future directions.

The work in Chapter 2 is currently in press for the *Journal of the American Society for Mass Spectrometry*. Chapters 3 through 5 are written in multiple manuscript format.

## 1.5 References

1. Wasinger, V.C., Cordwell, S.J., Cerpa-Poljak, A., Yan, J.X., Gooley, A.A., Wilkins, M.R., Duncan, M.W., Harris, R., Williams, K.L., Humphery-Smith, I.: Progress with gene-product mapping of the Mollicutes: *Mycoplasma genitalium*. *ELECTROPHORESIS*. **16**, 1090-1094 (1995)
2. Zhang, Y.J., Luo, L., Desai, D.D.: Overview on biotherapeutic proteins: impact on bioanalysis. *Bioanalysis*. **8**, 1-9 (2015)
3. Johnson, E.D.: Biotherapeutics: Challenges and Opportunities for Predictive Toxicology of Monoclonal Antibodies. *Int. J. Mol. Sci.* **19**, 3685 (2018)
4. Strohl, W.R.: Fusion Proteins for Half-Life Extension of Biologics as a Strategy to Make Biobetters. *BioDrugs*. **29**, 215-239 (2015)
5. Ortiz-Sánchez, E., Helguera, G., Daniels, T.R., Penichet, M.L.: Antibody-cytokine fusion

- proteins: applications in cancer therapy. *Expert Opin. Biol. Ther.* **8**, 609-632 (2008)
6. Brinkmann, U., Kontermann, R.E.: The making of bispecific antibodies. *mAbs.* **9**, 182-212 (2017)
  7. Owczarek, B., Gerszberg, A., Hnatuszko-Konka, K.: A Brief Reminder of Systems of Production and Chromatography-Based Recovery of Recombinant Protein Biopharmaceuticals. *BioMed Res. Int.* **2019**, 13 (2019)
  8. Taggart, C., Cervantes-Laurean, D., Kim, G., McElvaney, N.G., Wehr, N., Moss, J., Levine, R.L.: Oxidation of either methionine 351 or methionine 358 in  $\alpha$ 1-antitrypsin causes loss of anti-neutrophil elastase activity. *J. Biol. Chem.* **275**, 27258-27265 (2000)
  9. Prueksaritanont, T., Tang, C.: ADME of biologics-what have we learned from small molecules? *AAPS J.* **14**, 410-419 (2012)
  10. Cooper, J.B., Khan, G., Taylor, G., Tickle, I.J., Blundell, T.L.: X-ray analyses of aspartic proteinases: II. Three-dimensional structure of the hexagonal crystal form of porcine pepsin at 2.3Å resolution. *J. Mol. Biol.* **214**, 199-222 (1990)
  11. Holden, H.M., Ito, M., Hartshorne, D.J., Rayment, I.: X-ray structure determination of telokin, the C-terminal domain of myosin light chain kinase, at 2.8 Å resolution. *J. Mol. Biol.* **227**, 840-851 (1992)
  12. Jonic, S., V érien-Bryan, C.: Protein structure determination by electron cryo-microscopy. *Curr. Opin. Pharmacol.* **9**, 636-642 (2009)
  13. Murata, K., Wolf, M.: Cryo-electron microscopy for structural analysis of dynamic biological macromolecules. *Biochim. Biophys. Acta, Gen. Subj.* **1862**, 324-334 (2018)
  14. Mittermaier, A., Kay, L.E.: New Tools Provide New Insights in NMR Studies of Protein Dynamics. *Science.* **312**, 224 (2006)
  15. Reinders, J., Lewandrowski, U., Moebius, J., Wagner, Y., Sickmann, A.: Challenges in mass spectrometry-based proteomics. *PROTEOMICS.* **4**, 3686-3703 (2004)
  16. Aebersold, R., Mann, M.: Mass spectrometry-based proteomics. *Nature.* **422**, 198 (2003)
  17. Krastins, B., Prakash, A., Sarracino, D.A., Nedelkov, D., Niederkofler, E.E., Kiernan, U.A., Nelson, R., Vogelsang, M.S., Vadali, G., Garces, A., Sutton, J.N., Peterman, S., Byram, G., Darbouret, B., P érusse, J.R., Seidah, N.G., Coulombe, B., Gobom, J., Portelius, E., Pannee, J., Blennow, K., Kulasingam, V., Couchman, L., Moniz, C., Lopez, M.F.: Rapid development of sensitive, high-throughput, quantitative and highly selective mass spectrometric targeted immunoassays for clinically important proteins in human plasma and serum. *Clin. Biochem.* **46**, 399-410 (2013)
  18. Tang, K., Page, J.S., Kelly, R.T., Marginean, I.: Electrospray Ionization in Mass Spectrometry. In: Lindon JC, Tranter GE, Koppenaal DW (eds.). Academic Press, Oxford, (2017)
  19. Gault, J., Malosse, C., Dum énil, G., Chamot-Rooke, J.: A combined mass spectrometry strategy for complete posttranslational modification mapping of *Neisseria meningitidis* major pilin. *J. Mass Spectrom.* **48**, 1199-1206 (2013)
  20. Larsen, M.R., Jensen, O.N.: Posttranslational modification of proteins. *Encyclopedia of Genetics, Genomics, Proteomics and Bioinformatics.* (2005)

21. Eyers, C.E., Gaskell, S.J.: Mass Spectrometry to Identify Posttranslational Modifications. Wiley Encyclopedia of Chemical Biology. (2008)
22. Leurs, U., Mistarz, U.H., Rand, K.D.: Getting to the core of protein pharmaceuticals – Comprehensive structure analysis by mass spectrometry. *Eur. J. Pharm. Biopharm.* **93**, 95-109 (2015)
23. DeSouza, L.V., Siu, K.W.M.: Mass spectrometry-based quantification. *Clin. Biochem.* **46**, 421-431 (2013)
24. Božović, A., Kulasingam, V.: Quantitative mass spectrometry-based assay development and validation: From small molecules to proteins. *Clin. Biochem.* **46**, 444-455 (2013)
25. Henzler-Wildman, K., Kern, D.: Dynamic personalities of proteins. *Nature.* **450**, 964 (2007)
26. Robinson, C.V., Sali, A., Baumeister, W.: The molecular sociology of the cell. *Nature.* **450**, 973 (2007)
27. Oganessian, I., Lento, C., Wilson, D.J.: Contemporary hydrogen deuterium exchange mass spectrometry. *Methods.* **144**, 27-42 (2018)
28. Mendoza, V.L., Vachet, R.W.: Probing protein structure by amino acid-specific covalent labeling and mass spectrometry. *Mass Spectrom. Rev.* **28**, 785-815 (2009)
29. Zhang, B., Cheng, M., Rempel, D., Gross, M.L.: Implementing fast photochemical oxidation of proteins (FPOP) as a footprinting approach to solve diverse problems in structural biology. *Methods.* **144**, 94-103 (2018)
30. Fischer, L., Chen, Z.A., Rappsilber, J.: Quantitative cross-linking/mass spectrometry using isotope-labelled cross-linkers. *J. Proteomics.* **88**, 120-128 (2013)
31. Serpa, J.J., Patterson, A.P., Pan, J., Han, J., Wishart, D.S., Petrotchenko, E.V., Borchers, C.H.: Using multiple structural proteomics approaches for the characterization of prion proteins. *J. Proteomics.* **81**, 31-42 (2013)
32. Going, C.C., Williams, E.R.: Supercharging with m-Nitrobenzyl Alcohol and Propylene Carbonate: Forming Highly Charged Ions with Extended, Near-Linear Conformations. *Anal. Chem.* **87**, 3973-3980 (2015)
33. Kaltashov, I.A., Abzalimov, R.R.: Do ionic charges in ESI MS provide useful information on macromolecular structure? *J. Am. Soc. Mass. Spectrom.* **19**, 1239-1246 (2008)
34. Pan, J., Wilson, D.J., Konermann, L.: Pulsed Hydrogen Exchange and Electrospray Charge-State Distribution as Complementary Probes of Protein Structure in Kinetic Experiments: Implications for Ubiquitin Folding. *Biochemistry.* **44**, 8627-8633 (2005)
35. Kebarle, P., Verkerk, U.H.: Electrospray: From ions in solution to ions in the gas phase, what we know now. *Mass Spectrom. Rev.* **28**, 898-917 (2009)
36. Marcoux, J., Robinson, Carol V.: Twenty Years of Gas Phase Structural Biology. *Structure.* **21**, 1541-1550 (2013)
37. Ruotolo, B.T., Hyung, S.-J., Robinson, P.M., Giles, K., Bateman, R.H., Robinson, C.V.: Ion Mobility–Mass Spectrometry Reveals Long-Lived, Unfolded Intermediates in the Dissociation of Protein Complexes. *Angew. Chem. Int. Ed.* **46**, 8001-8004 (2007)
38. Eaton, L.C.: Host cell contaminant protein assay development for recombinant

- biopharmaceuticals. *J. Chromatogr. A.* **705**, 105-114 (1995)
39. Bracewell, D.G., Francis, R., Smales, C.M.: The future of host cell protein (HCP) identification during process development and manufacturing linked to a risk-based management for their control. *Biotechnol. Bioeng.* **112**, 1727-1737 (2015)
  40. Zhu-Shimoni, J., Yu, C., Nishihara, J., Wong, R.M., Gunawan, F., Lin, M., Krawitz, D., Liu, P., Sandoval, W., Vanderlaan, M.: Host cell protein testing by ELISAs and the use of orthogonal methods. *Biotechnol. Bioeng.* **111**, 2367-2379 (2014)
  41. Tait, A.S., Hogwood, C.E.M., Smales, C.M., Bracewell, D.G.: Host cell protein dynamics in the supernatant of a mAb producing CHO cell line. *Biotechnol. Bioeng.* **109**, 971-982 (2012)
  42. Jin, M., Szapiel, N., Zhang, J., Hickey, J., Ghose, S.: Profiling of host cell proteins by two-dimensional difference gel electrophoresis (2D-DIGE): Implications for downstream process development. *Biotechnol. Bioeng.* **105**, 306-316 (2010)
  43. Wang, X., Hunter, A.K., Mozier, N.M.: Host cell proteins in biologics development: Identification, quantitation and risk assessment. *Biotechnol. Bioeng.* **103**, 446-458 (2009)
  44. Huang, L., Wang, N., Mitchell, C.E., Brownlee, T., Maple, S.R., De Felippis, M.R.: A Novel Sample Preparation for Shotgun Proteomics Characterization of HCPs in Antibodies. *Anal. Chem.* **89**, 5436-5444 (2017)
  45. Schenauer, M.R., Flynn, G.C., Goetze, A.M.: Identification and quantification of host cell protein impurities in biotherapeutics using mass spectrometry. *Anal. Biochem.* **428**, 150-157 (2012)
  46. Doneanu, C.E., Anderson, M., Williams, B.J., Lauber, M.A., Chakraborty, A., Chen, W.: Enhanced Detection of Low-Abundance Host Cell Protein Impurities in High-Purity Monoclonal Antibodies Down to 1 ppm Using Ion Mobility Mass Spectrometry Coupled with Multidimensional Liquid Chromatography. *Anal. Chem.* **87**, 10283-10291 (2015)
  47. Switzar, L., Giera, M., Niessen, W.M.A.: Protein Digestion: An Overview of the Available Techniques and Recent Developments. *J. Proteome Res.* **12**, 1067-1077 (2013)
  48. Moradian, A., Kalli, A., Sweredoski, M.J., Hess, S.: The top-down, middle-down, and bottom-up mass spectrometry approaches for characterization of histone variants and their post-translational modifications. *PROTEOMICS.* **14**, 489-497 (2014)
  49. Tsybin, Y.O.: From High- to Super-resolution Mass Spectrometry. *Chimia.* **68**, 168-174 (2014)
  50. Bogdanov, B., Smith, R.D.: Proteomics by FTICR mass spectrometry: Top down and bottom up. *Mass Spectrom. Rev.* **24**, 168-200 (2005)
  51. Garcia, B.A.: What Does the Future Hold for Top Down Mass Spectrometry? *J. Am. Soc. Mass. Spectrom.* **21**, 193-202 (2010)
  52. Catherman, A.D., Skinner, O.S., Kelleher, N.L.: Top Down proteomics: Facts and perspectives. *Biochem. Biophys. Res. Commun.* **445**, 683-693 (2014)
  53. Kelleher, N.L., Lin, H.Y., Valaskovic, G.A., Aaserud, D.J., Fridriksson, E.K., McLafferty, F.W.: Top Down versus Bottom Up Protein Characterization by Tandem High-Resolution Mass Spectrometry. *J. Am. Chem. Soc.* **121**, 806-812 (1999)

54. Pan, J., Han, J., Borchers, C.H., Konermann, L.: Hydrogen/Deuterium Exchange Mass Spectrometry with Top-Down Electron Capture Dissociation for Characterizing Structural Transitions of a 17 kDa Protein. *J. Am. Chem. Soc.* **131**, 12801-12808 (2009)
55. Tsybin, Y.O., Fornelli, L., Stoermer, C., Luebeck, M., Parra, J., Nallet, S., Wurm, F.M., Hartmer, R.: Structural Analysis of Intact Monoclonal Antibodies by Electron Transfer Dissociation Mass Spectrometry. *Anal. Chem.* **83**, 8919-8927 (2011)
56. Fornelli, L., Toby, T.K., Schachner, L.F., Doubleday, P.F., Srzentić, K., DeHart, C.J., Kelleher, N.L.: Top-down proteomics: Where we are, where we are going? *J. Proteomics.* **175**, 3-4 (2018)
57. Garcia, B.A., Siuti, N., Thomas, C.E., Mizzen, C.A., Kelleher, N.L.: Characterization of neurohistone variants and post-translational modifications by electron capture dissociation mass spectrometry. *Int. J. Mass spectrom.* **259**, 184-196 (2007)
58. Gault, J., Malosse, C., Machata, S., Millien, C., Podglajen, I., Ploy, M.-C., Costello, C.E., Duménil, G., Chamot-Rooke, J.: Complete posttranslational modification mapping of pathogenic *Neisseria meningitidis* pilins requires top-down mass spectrometry. *PROTEOMICS.* **14**, 1141-1151 (2014)
59. Karger, B.L.: HPLC: Early and Recent Perspectives. *J. Chem. Educ.* **74**, 45 (1997)
60. Davis, M.T., Beierle, J., Bures, E.T., McGinley, M.D., Mort, J., Robinson, J.H., Spahr, C.S., Yu, W., Luethy, R., Patterson, S.D.: Automated LC–LC–MS–MS platform using binary ion-exchange and gradient reversed-phase chromatography for improved proteomic analyses. *J. Chromatogr. B: Biomed. Sci. Appl.* **752**, 281-291 (2001)
61. Qian, W.-J., Liu, T., Monroe, M.E., Strittmatter, E.F., Jacobs, J.M., Kangas, L.J., Petritis, K., Camp, D.G., Smith, R.D.: Probability-Based Evaluation of Peptide and Protein Identifications from Tandem Mass Spectrometry and SEQUEST Analysis: The Human Proteome. *J. Proteome Res.* **4**, 53-62 (2005)
62. Pinkse, M.W.H., Uitto, P.M., Hilhorst, M.J., Ooms, B., Heck, A.J.R.: Selective Isolation at the Femtomole Level of Phosphopeptides from Proteolytic Digests Using 2D-NanoLC-ESI-MS/MS and Titanium Oxide Precolumns. *Anal. Chem.* **76**, 3935-3943 (2004)
63. Alpert, A.J.: Hydrophobic interaction chromatography of peptides as an alternative to reversed-phase chromatography. *J. Chromatogr. A.* **444**, 269-274 (1988)
64. Buszewski, B., Noga, S.: Hydrophilic interaction liquid chromatography (HILIC)--a powerful separation technique. *Anal. Bioanal. Chem.* **402**, 231-247 (2012)
65. Liu, H., Guo, Y., Wang, X., Liang, X., Liu, X.: Amino-terminated ionic liquid modified graphene oxide coated silica composite stationary phase for hydrophilic interaction chromatography. *RSC Adv.* **4**, 37381-37388 (2014)
66. Nováková, L., Havlíková, L., Vlčková, H.: Hydrophilic interaction chromatography of polar and ionizable compounds by UHPLC. *TrAC, Trends Anal. Chem.* **63**, 55-64 (2014)
67. Shoji, Y., Yotsu-Yamashita, M., Miyazawa, T., Yasumoto, T.: Electrospray Ionization Mass Spectrometry of Tetrodotoxin and Its Analogs: Liquid Chromatography/Mass Spectrometry, Tandem Mass Spectrometry, and Liquid Chromatography/Tandem Mass Spectrometry.

- Anal. Biochem. **290**, 10-17 (2001)
68. Merrill, A.H., Sullards, M.C., Allegood, J.C., Kelly, S., Wang, E.: Sphingolipidomics: High-throughput, structure-specific, and quantitative analysis of sphingolipids by liquid chromatography tandem mass spectrometry. *Methods*. **36**, 207-224 (2005)
  69. Pitt, J.J.: Principles and applications of liquid chromatography-mass spectrometry in clinical biochemistry. *Clin. Biochem. Rev.* **30**, 19-34 (2009)
  70. Moco, S., Bino, R.J., Vorst, O., Verhoeven, H.A., de Groot, J., van Beek, T.A., Vervoort, J., de Vos, C.H.R.: A Liquid Chromatography-Mass Spectrometry-Based Metabolome Database for Tomato. *Plant Physiol.* **141**, 1205 (2006)
  71. Hird, S.J., Lau, B.P.Y., Schuhmacher, R., Krska, R.: Liquid chromatography-mass spectrometry for the determination of chemical contaminants in food. *TrAC, Trends Anal. Chem.* **59**, 59-72 (2014)
  72. Koehn, J., Ho, R.J.Y.: Novel Liquid Chromatography-Tandem Mass Spectrometry Method for Simultaneous Detection of Anti-HIV Drugs Lopinavir, Ritonavir, and Tenofovir in Plasma. *Antimicrob. Agents Chemother.* **58**, 2675 (2014)
  73. Ambati, C.R., Vantaku, V., Donepudi, S.R., Amara, C.S., Ravi, S.S., Mandalapu, A., Perla, M., Putluri, V., Sreekumar, A., Putluri, N.: Measurement of methylated metabolites using liquid chromatography-mass spectrometry and its biological application. *Anal. Methods*. **11**, 49-57 (2019)
  74. Richards, A.L., Hebert, A.S., Ulbrich, A., Bailey, D.J., Coughlin, E.E., Westphall, M.S., Coon, J.J.: One-hour proteome analysis in yeast. *Nat. Protoc.* **10**, 701 (2015)
  75. Ahn, J., Jung, M.C., Wyndham, K., Yu, Y.Q., Engen, J.R.: Pepsin Immobilized on High-Strength Hybrid Particles for Continuous Flow Online Digestion at 10 000 psi. *Anal. Chem.* **84**, 7256-7262 (2012)
  76. Saz, J.M., Marina, M.L.: Application of micro- and nano-HPLC to the determination and characterization of bioactive and biomarker peptides. *J. Sep. Sci.* **31**, 446-458 (2008)
  77. Thiede, B., Koehler, C.J., Strozynski, M., Treumann, A., Stein, R., Zimny-Arndt, U., Schmid, M., Jungblut, P.R.: High Resolution Quantitative Proteomics of HeLa Cells Protein Species Using Stable Isotope Labeling with Amino Acids in Cell Culture(SILAC), Two-Dimensional Gel Electrophoresis(2DE) and Nano-Liquid Chromatography Coupled to an LTQ-Orbitrap Mass Spectrometer. *Mol. Cell. Proteomics.* **12**, 529 (2013)
  78. Tyan, Y.-C., Wu, H.-Y., Lai, W.-W., Su, W.-C., Liao, P.-C.: Proteomic Profiling of Human Pleural Effusion Using Two-Dimensional Nano Liquid Chromatography Tandem Mass Spectrometry. *J. Proteome Res.* **4**, 1274-1286 (2005)
  79. Karpievitch, Y.V., Polpitiya, A.D., Anderson, G.A., Smith, R.D., Dabney, A.R.: Liquid Chromatography Mass Spectrometry-Based Proteomics: Biological and Technological Aspects. *Ann Appl Stat.* **4**, 1797-1823 (2010)
  80. Amster, I.J.: Fourier Transform Mass Spectrometry. *J. Mass Spectrom.* **31**, 1325-1337 (1996)
  81. Robinson, E.W.: Fourier-Transform Ion Cyclotron Resonance Mass Spectrometry (FT-ICR MS). In: Lindon JC (ed.). Academic Press, Oxford, (2010)

82. Marshall, A.G., Chen, T.: 40 years of Fourier transform ion cyclotron resonance mass spectrometry. *Int. J. Mass spectrom.* **377**, 410-420 (2015)
83. Lawrence, E.O., Livingston, M.S.: The Production of High Speed Light Ions Without the Use of High Voltages. *Phys. Rev.* **40**, 19-35 (1932)
84. Comisarow, M.B., Marshall, A.G.: Fourier transform ion cyclotron resonance spectroscopy. *Chem. Phys. Lett.* **25**, 282-283 (1974)
85. Wilkins, C.L.: A History of Ion Cyclotron Resonance (ICR) and Fourier Transform (FTICR) Mass Spectrometry. In: Gross ML, Caprioli RM (eds.). Elsevier, Boston, (2016)
86. Hendrickson, C.L., Quinn, J.P., Kaiser, N.K., Smith, D.F., Blakney, G.T., Chen, T., Marshall, A.G., Weisbrod, C.R., Beu, S.C.: 21 Tesla Fourier Transform Ion Cyclotron Resonance Mass Spectrometer: A National Resource for Ultrahigh Resolution Mass Analysis. *J. Am. Soc. Mass. Spectrom.* **26**, 1626-1632 (2015)
87. Shaw, J.B., Lin, T.-Y., Leach, F.E., Tolmachev, A.V., Tolić, N., Robinson, E.W., Koppenaal, D.W., Paša-Tolić, L.: 21 Tesla Fourier Transform Ion Cyclotron Resonance Mass Spectrometer Greatly Expands Mass Spectrometry Toolbox. *J. Am. Soc. Mass. Spectrom.* **27**, 1929-1936 (2016)
88. Caravatti, P., Allemann, M.: The ‘infinity cell’: A new trapped-ion cell with radiofrequency covered trapping electrodes for fourier transform ion cyclotron resonance mass spectrometry. *Org. Mass Spectrom.* **26**, 514-518 (1991)
89. N Nikolaev, E., N Vladimirov, G., Jertz, R., Baykut, G.: From Supercomputer Modeling to Highest Mass Resolution in FT-ICR. *Mass Spectrom.* **2**, S0010-S0010 (2013)
90. Marshall, A.G., Grosshans, P.B.: Fourier transform ion cyclotron resonance mass spectrometry: the teenage years. *Anal. Chem.* **63**, 215A-229A (1991)
91. Schweikhard, L., Marshall, A.G.: Excitation modes for Fourier transform-ion cyclotron resonance mass spectrometry. *J. Am. Soc. Mass. Spectrom.* **4**, 433-452 (1993)
92. Comisarow, M.B., Marshall, A.G.: Frequency-sweep fourier transform ion cyclotron resonance spectroscopy. *Chem. Phys. Lett.* **26**, 489-490 (1974)
93. Makarov, A.: Electrostatic Axially Harmonic Orbital Trapping: A High-Performance Technique of Mass Analysis. *Anal. Chem.* **72**, 1156-1162 (2000)
94. Hu, Q., Noll, R.J., Li, H., Makarov, A., Hardman, M., Graham Cooks, R.: The Orbitrap: a new mass spectrometer. *J. Mass Spectrom.* **40**, 430-443 (2005)
95. Perry, R.H., Cooks, R.G., Noll, R.J.: Orbitrap mass spectrometry: Instrumentation, ion motion and applications. *Mass Spectrom. Rev.* **27**, 661-699 (2008)
96. Olsen, J.V., de Godoy, L.M.F., Li, G., Macek, B., Mortensen, P., Pesch, R., Makarov, A., Lange, O., Horning, S., Mann, M.: Parts per Million Mass Accuracy on an Orbitrap Mass Spectrometer via Lock Mass Injection into a C-trap. *Mol. Cell. Proteomics.* **4**, 2010 (2005)
97. Makarov, A., Denisov, E., Kholomeev, A., Balschun, W., Lange, O., Strupat, K., Horning, S.: Performance Evaluation of a Hybrid Linear Ion Trap/Orbitrap Mass Spectrometer. *Anal. Chem.* **78**, 2113-2120 (2006)
98. Michalski, A., Damoc, E., Hauschild, J.-P., Lange, O., Wieghaus, A., Makarov, A., Nagaraj, N., Cox, J., Mann, M., Horning, S.: Mass Spectrometry-based Proteomics Using Q

- Exactive, a High-performance Benchtop Quadrupole Orbitrap Mass Spectrometer. *Mol. Cell. Proteomics*. **10**, M111.011015 (2011)
99. Hayes, R.N., Gross, M.L.: Collision-induced dissociation. Academic Press, (1990)
  100. McLuckey, S.A.: Principles of collisional activation in analytical mass spectrometry. *J. Am. Soc. Mass. Spectrom.* **3**, 599-614 (1992)
  101. Geromanos, S.J., Vissers, J.P.C., Silva, J.C., Dorschel, C.A., Li, G.-Z., Gorenstein, M.V., Bateman, R.H., Langridge, J.I.: The detection, correlation, and comparison of peptide precursor and product ions from data independent LC-MS with data dependant LC-MS/MS. *PROTEOMICS*. **9**, 1683-1695 (2009)
  102. Liu, H., Sadygov, R.G., Yates, J.R.: A Model for Random Sampling and Estimation of Relative Protein Abundance in Shotgun Proteomics. *Anal. Chem.* **76**, 4193-4201 (2004)
  103. Chapman, J.D., Goodlett, D.R., Masselon, C.D.: Multiplexed and data-independent tandem mass spectrometry for global proteome profiling. *Mass Spectrom. Rev.* **33**, 452-470 (2014)
  104. Braccia, C., Tomati, V., Caci, E., Pedemonte, N., Armirotti, A.: SWATH label-free proteomics for cystic fibrosis research. *J. Cystic Fibrosis*. (2018)
  105. Silva, J.C., Denny, R., Dorschel, C.A., Gorenstein, M., Kass, I.J., Li, G.-Z., McKenna, T., Nold, M.J., Richardson, K., Young, P., Geromanos, S.: Quantitative Proteomic Analysis by Accurate Mass Retention Time Pairs. *Anal. Chem.* **77**, 2187-2200 (2005)
  106. Roepstorff, P., Fohlman, J.: Letter to the editors. *Biomed. Mass Spectrom.* **11**, 601-601 (1984)
  107. Biemann, K.: Contributions of mass spectrometry to peptide and protein structure. *Biomed. Environ. Mass Spectrom.* **16**, 99-111 (1988)
  108. McLuckey, S.A., Goeringer, D.E.: SPECIAL FEATURE: TUTORIAL Slow Heating Methods in Tandem Mass Spectrometry. *J. Mass Spectrom.* **32**, 461-474 (1997)
  109. Little, D.P., Speir, J.P., Senko, M.W., O'Connor, P.B., McLafferty, F.W.: Infrared Multiphoton Dissociation of Large Multiply Charged Ions for Biomolecule Sequencing. *Anal. Chem.* **66**, 2809-2815 (1994)
  110. Stannard, P.R., Gelbart, W.M.: Intramolecular vibrational energy redistribution. *The Journal of Physical Chemistry*. **85**, 3592-3599 (1981)
  111. Bowie, J.H., Brinkworth, C.S., Dua, S.: Collision-induced fragmentations of the (M-H)<sup>-</sup> parent anions of underivatized peptides: An aid to structure determination and some unusual negative ion cleavages. *Mass Spectrom. Rev.* **21**, 87-107 (2002)
  112. Sugawara, N., Kawase, T., Oshikata, M., Imuro, R., Motoyama, A., Takayama, M.: Formation of c- and z-ions due to preferential cleavage at the NC bond of Xxx-Asp/Asn residues in negative-ion CID of peptides. *Int. J. Mass spectrom.* **383-384**, 38-43 (2015)
  113. Wysocki, V.H., Tsaprailis, G., Smith, L.L., Brechi, L.A.: Mobile and localized protons: a framework for understanding peptide dissociation. *J. Mass Spectrom.* **35**, 1399-1406 (2000)
  114. Paizs, B., Suhai, S.: Fragmentation pathways of protonated peptides. *Mass Spectrom. Rev.* **24**, 508-548 (2005)
  115. Boyd, R., Somogyi, Á.: The Mobile Proton Hypothesis in Fragmentation of Protonated

- Peptides: A Perspective. *J. Am. Soc. Mass. Spectrom.* **21**, 1275-1278 (2010)
116. Dongré A.R., Jones, J.L., Somogyi, Á., Wysocki, V.H.: Influence of Peptide Composition, Gas-Phase Basicity, and Chemical Modification on Fragmentation Efficiency: Evidence for the Mobile Proton Model. *J. Am. Chem. Soc.* **118**, 8365-8374 (1996)
  117. Tsapralis, G., Nair, H., Somogyi, Á., Wysocki, V.H., Zhong, W., Futrell, J.H., Summerfield, S.G., Gaskell, S.J.: Influence of Secondary Structure on the Fragmentation of Protonated Peptides. *J. Am. Chem. Soc.* **121**, 5142-5154 (1999)
  118. Gu, C., Tsapralis, G., Brechi, L., Wysocki, V.H.: Selective Gas-Phase Cleavage at the Peptide Bond C-Terminal to Aspartic Acid in Fixed-Charge Derivatives of Asp-Containing Peptides. *Anal. Chem.* **72**, 5804-5813 (2000)
  119. McCormack, A.L., Somogyi, A., Dongre, A.R., Wysocki, V.H.: Fragmentation of protonated peptides: surface-induced dissociation in conjunction with a quantum mechanical approach. *Anal. Chem.* **65**, 2859-2872 (1993)
  120. Johnson, R.S., Martin, S.A., Biemann, K.: Collision-induced fragmentation of  $(M + H)^+$  ions of peptides. Side chain specific sequence ions. *Int. J. Mass Spectrom. Ion Processes.* **86**, 137-154 (1988)
  121. Burlet, O., Yang, C.-Y., Gaskell, S.J.: Influence of cysteine to cysteic acid oxidation on the collision-activated decomposition of protonated peptides: Evidence for intraionic interactions. *J. Am. Soc. Mass. Spectrom.* **3**, 337-344 (1992)
  122. Tang, X.-J., Boyd, R.K., Bertrand, M.J.: An investigation of fragmentation mechanisms of doubly protonated tryptic peptides. *Rapid Commun. Mass Spectrom.* **6**, 651-657 (1992)
  123. Liang, Y., Neta, P., Yang, X., Stein, S.E.: Collision-Induced Dissociation of Deprotonated Peptides. Relative Abundance of Side-Chain Neutral Losses, Residue-Specific Product Ions, and Comparison with Protonated Peptides. *J. Am. Soc. Mass. Spectrom.* **29**, 463-469 (2018)
  124. Wang, T., Nha Tran, T.T., Andreazza, H.J., Bilusich, D., Brinkworth, C.S., Bowie, J.H.: Negative ion cleavages of  $(M-H)^-$  anions of peptides. Part 3. Post-translational modifications. *Mass Spectrom. Rev.* **37**, 3-21 (2018)
  125. Bilusich, D., Bowie, J.H.: Fragmentations of  $(M-H)^-$  anions of underivatized peptides. Part 2: Characteristic cleavages of Ser and Cys and of disulfides and other post-translational modifications, together with some unusual internal processes. *Mass Spectrom. Rev.* **28**, 20-34 (2009)
  126. Zubarev, R.A., Kelleher, N.L., McLafferty, F.W.: Electron Capture Dissociation of Multiply Charged Protein Cations. A Nonergodic Process. *J. Am. Chem. Soc.* **120**, 3265-3266 (1998)
  127. Syka, J.E.P., Coon, J.J., Schroeder, M.J., Shabanowitz, J., Hunt, D.F.: Peptide and protein sequence analysis by electron transfer dissociation mass spectrometry. *Proc. Natl. Acad. Sci.* **101**, 9528-9533 (2004)
  128. Zhang, H., Cui, W., Wen, J., Blankenship, R.E., Gross, M.L.: Native Electrospray and Electron-Capture Dissociation FTICR Mass Spectrometry for Top-Down Studies of Protein Assemblies. *Anal. Chem.* **83**, 5598-5606 (2011)
  129. Zubarev, R.A.: Reactions of polypeptide ions with electrons in the gas phase. *Mass*

- Spectrom. Rev. **22**, 57-77 (2003)
130. Chi, A., Huttenhower, C., Geer, L.Y., Coon, J.J., Syka, J.E.P., Bai, D.L., Shabanowitz, J., Burke, D.J., Troyanskaya, O.G., Hunt, D.F.: Analysis of phosphorylation sites on proteins from *Saccharomyces cerevisiae* by electron transfer dissociation (ETD) mass spectrometry. *Proc. Natl. Acad. Sci.* **104**, 2193 (2007)
  131. Cooper, H.J., Håkansson, K., Marshall, A.G.: The role of electron capture dissociation in biomolecular analysis. *Mass Spectrom. Rev.* **24**, 201-222 (2005)
  132. Zubarev, R.A., Kruger, N.A., Fridriksson, E.K., Lewis, M.A., Horn, D.M., Carpenter, B.K., McLafferty, F.W.: Electron Capture Dissociation of Gaseous Multiply-Charged Proteins Is Favored at Disulfide Bonds and Other Sites of High Hydrogen Atom Affinity. *J. Am. Chem. Soc.* **121**, 2857-2862 (1999)
  133. Syrstad, E.A., Tureček, F.: Toward a general mechanism of electron capture dissociation. *J. Am. Soc. Mass. Spectrom.* **16**, 208-224 (2005)
  134. Zhurov, K.O., Fornelli, L., Wodrich, M.D., Laskay, Ü.A., Tsybin, Y.O.: Principles of electron capture and transfer dissociation mass spectrometry applied to peptide and protein structure analysis. *Chem. Soc. Rev.* **42**, 5014-5030 (2013)
  135. Patriksson, A., Adams, C., Kjeldsen, F., Raber, J., van der Spoel, D., Zubarev, R.A.: Prediction of NC $\alpha$  bond cleavage frequencies in electron capture dissociation of Trp-cage dications by force-field molecular dynamics simulations. *Int. J. Mass spectrom.* **248**, 124-135 (2006)
  136. Sawicka, A., Skurski, P., Hudgins, R.R., Simons, J.: Model Calculations Relevant to Disulfide Bond Cleavage via Electron Capture Influenced by Positively Charged Groups. *J. Phys. Chem. B.* **107**, 13505-13511 (2003)
  137. Tureček, F., Chen, X., Hao, C.: Where Does the Electron Go? Electron Distribution and Reactivity of Peptide Cation Radicals Formed by Electron Transfer in the Gas phase. *J. Am. Chem. Soc.* **130**, 8818-8833 (2008)
  138. Fort, K.L., Cramer, C.N., Voinov, V.G., Vasil'ev, Y.V., Lopez, N.I., Beckman, J.S., Heck, A.J.R.: Exploring ECD on a Benchtop Q Exactive Orbitrap Mass Spectrometer. *J. Proteome Res.* **17**, 926-933 (2018)
  139. Kjeldsen, F., Haselmann, K.F., Budnik, B.A., Jensen, F., Zubarev, R.A.: Dissociative capture of hot (3–13 eV) electrons by polypeptide polycations: an efficient process accompanied by secondary fragmentation. *Chem. Phys. Lett.* **356**, 201-206 (2002)
  140. Zubarev, R.A., Yang, H.: Multiple Soft Ionization of Gas-Phase Proteins and Swift Backbone Dissociation in Collisions with  $\leq 99$  eV Electrons. *Angew. Chem. Int. Ed.* **49**, 1439-1441 (2010)
  141. Kalli, A., Grigorean, G., Håkansson, K.: Electron Induced Dissociation of Singly Deprotonated Peptides. *J. Am. Soc. Mass. Spectrom.* **22**, 2209-2221 (2011)
  142. Yoo, H.J., Wang, N., Zhuang, S., Song, H., Håkansson, K.: Negative-Ion Electron Capture Dissociation: Radical-Driven Fragmentation of Charge-Increased Gaseous Peptide Anions. *J. Am. Chem. Soc.* **133**, 16790-16793 (2011)
  143. Hersberger, K.E., Håkansson, K.: Characterization of O-Sulfopeptides by Negative Ion

- Mode Tandem Mass Spectrometry: Superior Performance of Negative Ion Electron Capture Dissociation. *Anal. Chem.* **84**, 6370-6377 (2012)
144. Budnik, B.A., Haselmann, K.F., Zubarev, R.A.: Electron detachment dissociation of peptide di-anions: an electron-hole recombination phenomenon. *Chem. Phys. Lett.* **342**, 299-302 (2001)
  145. Kjeldsen, F., Silivra, O.A., Ivonin, I.A., Haselmann, K.F., Gorshkov, M., Zubarev, R.A.:  $\alpha$ -C Backbone Fragmentation Dominates in Electron Detachment Dissociation of Gas-Phase Polypeptide Polyanions. *Chem. Eur. J.* **11**, 1803-1812 (2005)
  146. Song, H., Håkansson, K.: Electron Detachment Dissociation and Negative Ion Infrared Multiphoton Dissociation of Electrosprayed Intact Proteins. *Anal. Chem.* **84**, 871-876 (2012)
  147. Hodyss, R., Cox, H.A., Beauchamp, J.L.: Bioconjugates for Tunable Peptide Fragmentation: Free Radical Initiated Peptide Sequencing (FRIPS). *J. Am. Chem. Soc.* **127**, 12436-12437 (2005)
  148. Lee, M., Kang, M., Moon, B., Oh, H.B.: Gas-phase peptide sequencing by TEMPO-mediated radical generation. *Analyst.* **134**, 1706-1712 (2009)
  149. Borotto, N.B., Ilek, K.M., Tom, C.A.T.M.B., Martin, B.R., Håkansson, K.: Free Radical Initiated Peptide Sequencing for Direct Site Localization of Sulfation and Phosphorylation with Negative Ion Mode Mass Spectrometry. *Anal. Chem.* **90**, 9682-9686 (2018)
  150. Fenn, J.B., Mann, M., Meng, C.K., Wong, S.F., Whitehouse, C.M.: Electrospray Ionization for Mass Spectrometry of Large Biomolecules. *Science.* **246**, 64-71 (1989)
  151. Karas, M., Hillenkamp, F.: Laser desorption ionization of proteins with molecular masses exceeding 10,000 daltons. *Anal. Chem.* **60**, 2299-2301 (1988)
  152. Andersen, J.S., Svensson, B., Roepstorff, P.: Electrospray ionization and matrix assisted laser desorption/ionization mass spectrometry: Powerful analytical tools in recombinant protein chemistry. *Nat. Biotechnol.* **14**, 449-457 (1996)
  153. Ho, C.S., Lam, C.W.K., Chan, M.H.M., Cheung, R.C.K., Law, L.K., Lit, L.C.W., Ng, K.F., Suen, M.W.M., Tai, H.L.: Electrospray ionisation mass spectrometry: principles and clinical applications. *The Clinical biochemist Reviews.* **24**, 3-12 (2003)
  154. Konermann, L., Ahadi, E., Rodriguez, A.D., Vahidi, S.: Unraveling the Mechanism of Electrospray Ionization. *Anal. Chem.* **85**, 2-9 (2013)
  155. Polfer, N.C.: Supercharging Proteins: How Many Charges Can a Protein Carry? *Angew. Chem. Int. Ed.* **56**, 8335-8337 (2017)
  156. Donor, M.T., Ewing, S.A., Zenaidee, M.A., Donald, W.A., Prell, J.S.: Extended Protein Ions Are Formed by the Chain Ejection Model in Chemical Supercharging Electrospray Ionization. *Anal. Chem.* **89**, 5107-5114 (2017)
  157. Iavarone, A.T., Jurchen, J.C., Williams, E.R.: Supercharged Protein and Peptide Ions Formed by Electrospray Ionization. *Anal. Chem.* **73**, 1455-1460 (2001)
  158. Iavarone, A.T., Williams, E.R.: Mechanism of Charging and Supercharging Molecules in Electrospray Ionization. *J. Am. Chem. Soc.* **125**, 2319-2327 (2003)
  159. Ogorzalek Loo, R.R., Lakshmanan, R., Loo, J.A.: What Protein Charging (and

- Supercharging) Reveal about the Mechanism of Electrospray Ionization. *J. Am. Soc. Mass. Spectrom.* **25**, 1675-1693 (2014)
160. Metwally, H., McAllister, R.G., Popa, V., Konermann, L.: Mechanism of Protein Supercharging by Sulfolane and m-Nitrobenzyl Alcohol: Molecular Dynamics Simulations of the Electrospray Process. *Anal. Chem.* **88**, 5345-5354 (2016)
161. Metwally, H., Konermann, L.: Crown Ether Effects on the Location of Charge Carriers in Electrospray Droplets: Implications for the Mechanism of Protein Charging and Supercharging. *Anal. Chem.* **90**, 4126-4134 (2018)
162. Lomeli, S.H., Peng, I.X., Yin, S., Ogorzalek Loo, R.R., Loo, J.A.: New reagents for increasing ESI multiple charging of proteins and protein complexes. *J. Am. Soc. Mass. Spectrom.* **21**, 127-131 (2010)
163. Douglass, K.A., Venter, A.R.: Investigating the Role of Adducts in Protein Supercharging with Sulfolane. *J. Am. Soc. Mass. Spectrom.* **23**, 489-497 (2012)
164. Sterling, H.J., Prell, J.S., Cassou, C.A., Williams, E.R.: Protein Conformation and Supercharging with DMSO from Aqueous Solution. *J. Am. Soc. Mass. Spectrom.* **22**, 1178 (2011)
165. Teo, C.A., Donald, W.A.: Solution Additives for Supercharging Proteins beyond the Theoretical Maximum Proton-Transfer Limit in Electrospray Ionization Mass Spectrometry. *Anal. Chem.* **86**, 4455-4462 (2014)
166. Zenaidee, M.A., Donald, W.A.: Extremely supercharged proteins in mass spectrometry: profiling the pH of electrospray generated droplets, narrowing charge state distributions, and increasing ion fragmentation. *Analyst.* **140**, 1894-1905 (2015)
167. Sterling, H.J., Williams, E.R.: Origin of supercharging in electrospray ionization of noncovalent complexes from aqueous solution. *J. Am. Soc. Mass. Spectrom.* **20**, 1933-1943 (2009)
168. Kjeldsen, F., Giessing, A.M.B., Ingrell, C.R., Jensen, O.N.: Peptide Sequencing and Characterization of Post-Translational Modifications by Enhanced Ion-Charging and Liquid Chromatography Electron-Transfer Dissociation Tandem Mass Spectrometry. *Anal. Chem.* **79**, 9243-9252 (2007)
169. Flick, T.G., Williams, E.R.: Supercharging with Trivalent Metal Ions in Native Mass Spectrometry. *J. Am. Soc. Mass. Spectrom.* **23**, 1885-1895 (2012)
170. Feng, C., Commodore, J.J., Cassidy, C.J.: The Use of Chromium(III) to Supercharge Peptides by Protonation at Low Basicity Sites. *J. Am. Soc. Mass. Spectrom.* **26**, 347-358 (2015)
171. Sterling, H.J., Daly, M.P., Feld, G.K., Thoren, K.L., Kintzer, A.F., Krantz, B.A., Williams, E.R.: Effects of supercharging reagents on noncovalent complex structure in electrospray ionization from aqueous solutions. *J. Am. Soc. Mass. Spectrom.* **21**, 1762-1774 (2010)
172. Sterling, H.J., Williams, E.R.: Real-Time Hydrogen/Deuterium Exchange Kinetics via Supercharged Electrospray Ionization Tandem Mass Spectrometry. *Anal. Chem.* **82**, 9050-9057 (2010)
173. Sterling, H.J., Kintzer, A.F., Feld, G.K., Cassou, C.A., Krantz, B.A., Williams, E.R.:

- Supercharging Protein Complexes from Aqueous Solution Disrupts their Native Conformations. *J. Am. Soc. Mass. Spectrom.* **23**, 191-200 (2012)
174. Sterling, H.J., Cassou, C.A., Trnka, M.J., Burlingame, A.L., Krantz, B.A., Williams, E.R.: The role of conformational flexibility on protein supercharging in native electrospray ionization. *Phys. Chem. Chem. Phys.* **13**, 18288-18296 (2011)
  175. Hogan Jr, C.J., Ogorzalek Loo, R.R., Loo, J.A., Mora, J.F.d.l.: Ion mobility–mass spectrometry of phosphorylase B ions generated with supercharging reagents but in charge-reducing buffer. *Phys. Chem. Chem. Phys.* **12**, 13476-13483 (2010)
  176. Chingin, K., Xu, N., Chen, H.: Soft Supercharging of Biomolecular Ions in Electrospray Ionization Mass Spectrometry. *J. Am. Soc. Mass. Spectrom.* **25**, 928-934 (2014)
  177. Marshall, A.G., Hendrickson, C.L., Jackson, G.S.: Fourier transform ion cyclotron resonance mass spectrometry: A primer. *Mass Spectrom. Rev.* **17**, 1-35 (1998)
  178. Pitteri, S.J., Chrisman, P.A., McLuckey, S.A.: Electron-Transfer Ion/Ion Reactions of Doubly Protonated Peptides: Effect of Elevated Bath Gas Temperature. *Anal. Chem.* **77**, 5662-5669 (2005)
  179. Pitteri, S.J., Chrisman, P.A., Hogan, J.M., McLuckey, S.A.: Electron Transfer Ion/Ion Reactions in a Three-Dimensional Quadrupole Ion Trap: Reactions of Doubly and Triply Protonated Peptides with SO<sub>2</sub>•. *Anal. Chem.* **77**, 1831-1839 (2005)
  180. Kalli, A., Håkansson, K.: Comparison of the Electron Capture Dissociation Fragmentation Behavior of Doubly and Triply Protonated Peptides from Trypsin, Glu-C, and Chymotrypsin Digestion. *J. Proteome Res.* **7**, 2834-2844 (2008)
  181. Kalli, A., Håkansson, K.: Electron capture dissociation of highly charged proteolytic peptides from Lys N, Lys C and Glu C digestion. *Mol. BioSyst.* **6**, 1668-1681 (2010)
  182. Swaney, D.L., McAlister, G.C., Wirtala, M., Schwartz, J.C., Syka, J.E.P., Coon, J.J.: Supplemental Activation Method for High-Efficiency Electron-Transfer Dissociation of Doubly Protonated Peptide Precursors. *Anal. Chem.* **79**, 477-485 (2007)
  183. Nielsen, M.L., Savitski, M.M., Zubarev, R.A.: Improving Protein Identification Using Complementary Fragmentation Techniques in Fourier Transform Mass Spectrometry. *Mol. Cell. Proteomics.* **4**, 835 (2005)
  184. Cravello, L., Lascoux, D., Forest, E.: Use of different proteases working in acidic conditions to improve sequence coverage and resolution in hydrogen/deuterium exchange of large proteins. *Rapid Commun. Mass Spectrom.* **17**, 2387-2393 (2003)
  185. Vandermarliere, E., Mueller, M., Martens, L.: Getting intimate with trypsin, the leading protease in proteomics. *Mass Spectrom. Rev.* **32**, 453-465 (2013)
  186. Meyer, J.G., A. Komives, E.: Charge State Coalescence During Electrospray Ionization Improves Peptide Identification by Tandem Mass Spectrometry. *J. Am. Soc. Mass. Spectrom.* **23**, 1390-1399 (2012)
  187. Rand, K.D., Zehl, M., Jensen, O.N., Jørgensen, T.J.D.: Protein Hydrogen Exchange Measured at Single-Residue Resolution by Electron Transfer Dissociation Mass Spectrometry. *Anal. Chem.* **81**, 5577-5584 (2009)
  188. Cassou, C.A., Sterling, H.J., Susa, A.C., Williams, E.R.: Electrothermal Supercharging in

- Mass Spectrometry and Tandem Mass Spectrometry of Native Proteins. *Anal. Chem.* **85**, 138-146 (2013)
189. Mortensen, D.N., Williams, E.R.: Electrothermal supercharging of proteins in native MS: effects of protein isoelectric point, buffer, and nanoESI-emitter tip size. *Analyst.* **141**, 5598-5606 (2016)
  190. Going, C.C., Xia, Z., Williams, E.R.: Real-time HD Exchange Kinetics of Proteins from Buffered Aqueous Solution with Electrothermal Supercharging and Top-Down Tandem Mass Spectrometry. *J. Am. Soc. Mass. Spectrom.* **27**, 1019-1027 (2016)
  191. Wales, T.E., Engen, J.R.: Hydrogen exchange mass spectrometry for the analysis of protein dynamics. *Mass Spectrom. Rev.* **25**, 158-170 (2006)
  192. Pirrone, G.F., Jacob, R.E., Engen, J.R.: Applications of Hydrogen/Deuterium Exchange MS from 2012 to 2014. *Anal. Chem.* **87**, 99-118 (2015)
  193. Konermann, L., Pan, J., Liu, Y.-H.: Hydrogen exchange mass spectrometry for studying protein structure and dynamics. *Chem. Soc. Rev.* **40**, 1224-1234 (2011)
  194. Hoofnagle, A.N., Resing, K.A., Ahn, N.G.: Protein Analysis by Hydrogen Exchange Mass Spectrometry. *Annu. Rev. Biophys. Biomol. Struct.* **32**, 1-25 (2003)
  195. Huang, R.Y.C., Chen, G.: Higher order structure characterization of protein therapeutics by hydrogen/deuterium exchange mass spectrometry. *Anal. Bioanal. Chem.* **406**, 6541-6558 (2014)
  196. Englander, S.W., Mayne, L.: Protein folding studied using hydrogen-exchange labeling and two-dimensional NMR. *Annu. Rev. Biophys. Biomol. Struct.* **21**, 243-265 (1992)
  197. Krishna, M.M.G., Hoang, L., Lin, Y., Englander, S.W.: Hydrogen exchange methods to study protein folding. *Methods.* **34**, 51-64 (2004)
  198. Hebling, C.M., Morgan, C.R., Stafford, D.W., Jorgenson, J.W., Rand, K.D., Engen, J.R.: Conformational Analysis of Membrane Proteins in Phospholipid Bilayer Nanodiscs by Hydrogen Exchange Mass Spectrometry. *Anal. Chem.* **82**, 5415-5419 (2010)
  199. Pan, Y., Brown, L., Konermann, L.: Hydrogen/deuterium exchange mass spectrometry and optical spectroscopy as complementary tools for studying the structure and dynamics of a membrane protein. *Int. J. Mass spectrom.* **302**, 3-11 (2011)
  200. Rey, M., Mrázek, H., Pompach, P., Novák, P., Pelosi, L., Brandolin, G., Forest, E., Havlíček, V., Man, P.: Effective Removal of Nonionic Detergents in Protein Mass Spectrometry, Hydrogen/Deuterium Exchange, and Proteomics. *Anal. Chem.* **82**, 5107-5116 (2010)
  201. Hvidt, A., Linderstrøm-Lang, K.: Exchange of hydrogen atoms in insulin with deuterium atoms in aqueous solutions. *Biochim. Biophys. Acta.* **14**, 574-575 (1954)
  202. Englander, S.W., Englander, J.J.: Hydrogen—Tritium exchange. Academic Press, (1978)
  203. Zhang, Z., Smith, D.L.: Determination of amide hydrogen exchange by mass spectrometry: A new tool for protein structure elucidation. *Protein Sci.* **2**, 522-531 (1993)
  204. Konermann, L., Tong, X., Pan, Y.: Protein structure and dynamics studied by mass spectrometry: H/D exchange, hydroxyl radical labeling, and related approaches. *J. Mass Spectrom.* **43**, 1021-1036 (2008)
  205. Chetty, P.S., Mayne, L., Lund-Katz, S., Stranz, D., Englander, S.W., Phillips, M.C.: Helical

- structure and stability in human apolipoprotein A-I by hydrogen exchange and mass spectrometry. *Proc. Natl. Acad. Sci.* **106**, 19005 (2009)
206. Weis, D.D., Wales, T.E., Engen, J.R., Hotchko, M., Ten Eyck, L.F.: Identification and characterization of EX1 kinetics in H/D exchange mass spectrometry by peak width analysis. *J. Am. Soc. Mass. Spectrom.* **17**, 1498-1509 (2006)
  207. Urathamakul, T., Williams, N.K., Dixon, N.E., Beck, J.L.: EX1 hydrogen–deuterium exchange in an all-helical protein and its cyclized derivative at neutral pH. *Int. J. Mass spectrom.* **302**, 149-156 (2011)
  208. Fang, J., Rand, K.D., Beuning, P.J., Engen, J.R.: False EX1 signatures caused by sample carryover during HX MS analyses. *Int. J. Mass spectrom.* **302**, 19-25 (2011)
  209. Bai, Y., Milne, J.S., Mayne, L., Englander, S.W.: Primary structure effects on peptide group hydrogen exchange. *Proteins: Struct., Funct., Bioinf.* **17**, 75-86 (1993)
  210. Zhang, H.-M., Bou-Assaf, G.M., Emmett, M.R., Marshall, A.G.: Fast reversed-phase liquid chromatography to reduce back exchange and increase throughput in H/D exchange monitored by FT-ICR mass spectrometry. *J. Am. Soc. Mass. Spectrom.* **20**, 520-524 (2009)
  211. Wang, L., Pan, H., Smith, D.L.: Hydrogen Exchange-Mass Spectrometry. *Mol. Cell. Proteomics.* **1**, 132 (2002)
  212. Wang, G., Kaltashov, I.A.: Approach to Characterization of the Higher Order Structure of Disulfide-Containing Proteins Using Hydrogen/Deuterium Exchange and Top-Down Mass Spectrometry. *Anal. Chem.* **86**, 7293-7298 (2014)
  213. Abzalimov, R.R., Kaplan, D.A., Easterling, M.L., Kaltashov, I.A.: Protein conformations can be probed in top-down HDX MS experiments utilizing electron transfer dissociation of protein ions without hydrogen scrambling. *J. Am. Soc. Mass. Spectrom.* **20**, 1514-1517 (2009)
  214. Li, J., Rodnin, M.V., Ladokhin, A.S., Gross, M.L.: Hydrogen–Deuterium Exchange and Mass Spectrometry Reveal the pH-Dependent Conformational Changes of Diphtheria Toxin T Domain. *Biochemistry.* **53**, 6849-6856 (2014)
  215. Yan, Y., Grant, G.A., Gross, M.L.: Hydrogen–Deuterium Exchange Mass Spectrometry Reveals Unique Conformational and Chemical Transformations Occurring upon [4Fe-4S] Cluster Binding in the Type 2 l-Serine Dehydratase from *Legionella pneumophila*. *Biochemistry.* **54**, 5322-5328 (2015)
  216. Zhang, H.-M., Kazazic, S., Schaub, T.M., Tipton, J.D., Emmett, M.R., Marshall, A.G.: Enhanced Digestion Efficiency, Peptide Ionization Efficiency, and Sequence Resolution for Protein Hydrogen/Deuterium Exchange Monitored by Fourier Transform Ion Cyclotron Resonance Mass Spectrometry. *Anal. Chem.* **80**, 9034-9041 (2008)
  217. Kadek, A., Mrazek, H., Halada, P., Rey, M., Schriemer, D.C., Man, P.: Aspartic Protease Nepenthesin-1 as a Tool for Digestion in Hydrogen/Deuterium Exchange Mass Spectrometry. *Anal. Chem.* **86**, 4287-4294 (2014)
  218. Landgraf, R.R., Chalmers, M.J., Griffin, P.R.: Automated Hydrogen/Deuterium Exchange Electron Transfer Dissociation High Resolution Mass Spectrometry Measured at Single-Amide Resolution. *J. Am. Soc. Mass. Spectrom.* **23**, 301-309 (2012)

219. Bobst, C.E., Kaltashov, I.A.: Enhancing the Quality of H/D Exchange Measurements with Mass Spectrometry Detection in Disulfide-Rich Proteins Using Electron Capture Dissociation. *Anal. Chem.* **86**, 5225-5231 (2014)
220. Tsutsui, Y., Dela Cruz, R., Wintrode, P.L.: Folding mechanism of the metastable serpin  $\alpha$ 1-antitrypsin. *Proc. Natl. Acad. Sci.* **109**, 4467 (2012)
221. Pan, J., Han, J., Borchers, C.H., Konermann, L.: Characterizing Short-Lived Protein Folding Intermediates by Top-Down Hydrogen Exchange Mass Spectrometry. *Anal. Chem.* **82**, 8591-8597 (2010)
222. Konermann, L., Pan, J., Wilson, D.J.: Protein Folding Mechanisms Studied by Time-Resolved Electrospray Mass Spectrometry. *BioTechniques.* **40**, 135-141 (2006)
223. Mayne, L.: Hydrogen Exchange Mass Spectrometry. *Methods Enzymol.* **566**, 335-356 (2016)
224. Rob, T., Wilson, D.J.: Time-Resolved Mass Spectrometry for Monitoring Millisecond Time-Scale Solution-Phase Processes. *Eur. J. Mass Spectrom.* **18**, 205-214 (2012)
225. Wu, Y., Kaveti, S., Engen, J.R.: Extensive Deuterium Back-Exchange in Certain Immobilized Pepsin Columns Used for H/D Exchange Mass Spectrometry. *Anal. Chem.* **78**, 1719-1723 (2006)
226. Busby, S.A., Chalmers, M.J., Griffin, P.R.: Improving digestion efficiency under H/D exchange conditions with activated pepsinogen coupled columns. *Int. J. Mass spectrom.* **259**, 130-139 (2007)
227. Mysling, S., Salbo, R., Ploug, M., Jørgensen, T.J.D.: Electrochemical Reduction of Disulfide-Containing Proteins for Hydrogen/Deuterium Exchange Monitored by Mass Spectrometry. *Anal. Chem.* **86**, 340-345 (2014)
228. Yang, M., Hoepfner, M., Rey, M., Kadek, A., Man, P., Schriemer, D.C.: Recombinant Nepenthesin II for Hydrogen/Deuterium Exchange Mass Spectrometry. *Anal. Chem.* **87**, 6681-6687 (2015)
229. Wales, T.E., Fadgen, K.E., Gerhardt, G.C., Engen, J.R.: High-Speed and High-Resolution UPLC Separation at Zero Degrees Celsius. *Anal. Chem.* **80**, 6815-6820 (2008)
230. Emmett, M.R., Kazacic, S., Marshall, A.G., Chen, W., Shi, S.D.H., Bolaños, B., Greig, M.J.: Supercritical Fluid Chromatography Reduction of Hydrogen/Deuterium Back Exchange in Solution-Phase Hydrogen/Deuterium Exchange with Mass Spectrometric Analysis. *Anal. Chem.* **78**, 7058-7060 (2006)
231. Amon, S., Trelle, M.B., Jensen, O.N., Jørgensen, T.J.D.: Spatially Resolved Protein Hydrogen Exchange Measured by Subzero-Cooled Chip-Based Nanoelectrospray Ionization Tandem Mass Spectrometry. *Anal. Chem.* **84**, 4467-4473 (2012)
232. Pan, J., Zhang, S., Parker, C.E., Borchers, C.H.: Subzero Temperature Chromatography and Top-Down Mass Spectrometry for Protein Higher-Order Structure Characterization: Method Validation and Application to Therapeutic Antibodies. *J. Am. Chem. Soc.* **136**, 13065-13071 (2014)
233. Pan, J., Borchers, C.H.: Top-down structural analysis of posttranslationally modified proteins by Fourier transform ion cyclotron resonance-MS with hydrogen/deuterium

- exchange and electron capture dissociation. *PROTEOMICS*. **13**, 974-981 (2013)
234. Weis, D.D., Engen, J.R., Kass, I.J.: Semi-automated data processing of hydrogen exchange mass spectra using HX-Express. *J. Am. Soc. Mass. Spectrom.* **17**, 1700-1703 (2006)
235. Slysz, G.W., Baker, C.A.H., Bozsa, B.M., Dang, A., Percy, A.J., Bennett, M., Schriemer, D.C.: Hydra: software for tailored processing of H/D exchange data from MS or tandem MS analyses. *BMC Bioinf.* **10**, 162 (2009)
236. Pascal, B.D., Chalmers, M.J., Busby, S.A., Mader, C.C., Southern, M.R., Tsinoemas, N.F., Griffin, P.R.: The Deuterator: software for the determination of backbone amide deuterium levels from H/D exchange MS data. *BMC Bioinf.* **8**, 156 (2007)
237. Pascal, B.D., Chalmers, M.J., Busby, S.A., Griffin, P.R.: HD desktop: An integrated platform for the analysis and visualization of H/D exchange data. *J. Am. Soc. Mass. Spectrom.* **20**, 601-610 (2009)
238. Lindner, R., Lou, X., Reinstein, J., Shoeman, R.L., Hamprecht, F.A., Winkler, A.: Hexicon 2: Automated Processing of Hydrogen-Deuterium Exchange Mass Spectrometry Data with Improved Deuteration Distribution Estimation. *J. Am. Soc. Mass. Spectrom.* **25**, 1018-1028 (2014)
239. Miller, D.E., Prasanna, C.B., Villar, M.T., Fenton, A.W., Artigues, A.: HDXFinder: Automated Analysis and Data Reporting of Deuterium/Hydrogen Exchange Mass Spectrometry. *J. Am. Soc. Mass. Spectrom.* **23**, 425-429 (2012)
240. Rand, K.D.: Pinpointing changes in higher-order protein structure by hydrogen/deuterium exchange coupled to electron transfer dissociation mass spectrometry. *Int. J. Mass spectrom.* **338**, 2-10 (2013)
241. Kaltashov, I.A., Bobst, C.E., Abzalimov, R.R.: H/D Exchange and Mass Spectrometry in the Studies of Protein Conformation and Dynamics: Is There a Need for a Top-Down Approach? *Anal. Chem.* **81**, 7892-7899 (2009)
242. Wang, G., Abzalimov, R.R., Bobst, C.E., Kaltashov, I.A.: Conformer-specific characterization of nonnative protein states using hydrogen exchange and top-down mass spectrometry. *Proc. Natl. Acad. Sci.* **110**, 20087 (2013)
243. Pan, J., Han, J., Borchers, C.H., Konermann, L.: Conformer-Specific Hydrogen Exchange Analysis of A $\beta$ (1-42) Oligomers by Top-Down Electron Capture Dissociation Mass Spectrometry. *Anal. Chem.* **83**, 5386-5393 (2011)
244. Abzalimov, R.R., Bobst, C.E., Kaltashov, I.A.: A New Approach to Measuring Protein Backbone Protection with High Spatial Resolution Using H/D Exchange and Electron Capture Dissociation. *Anal. Chem.* **85**, 9173-9180 (2013)
245. Brodie, N.I., Huguet, R., Zhang, T., Viner, R., Zabrouskov, V., Pan, J., Petrotchenko, E.V., Borchers, C.H.: Top-Down Hydrogen-Deuterium Exchange Analysis of Protein Structures Using Ultraviolet Photodissociation. *Anal. Chem.* **90**, 3079-3082 (2018)
246. Hoerner, J.K., Xiao, H., Dobo, A., Kaltashov, I.A.: Is There Hydrogen Scrambling in the Gas Phase? Energetic and Structural Determinants of Proton Mobility within Protein Ions. *J. Am. Chem. Soc.* **126**, 7709-7717 (2004)
247. Rand, K.D., Zehl, M., Jørgensen, T.J.D.: Measuring the Hydrogen/Deuterium Exchange of

- Proteins at High Spatial Resolution by Mass Spectrometry: Overcoming Gas-Phase Hydrogen/Deuterium Scrambling. *Acc. Chem. Res.* **47**, 3018-3027 (2014)
248. Bache, N., Rand, K.D., Roepstorff, P., Jørgensen, T.J.D.: Gas-Phase Fragmentation of Peptides by MALDI in-Source Decay with Limited Amide Hydrogen (1H/2H) Scrambling. *Anal. Chem.* **80**, 6431-6435 (2008)
249. Bache, N., Rand, K.D., Roepstorff, P., Ploug, M., Jørgensen, T.J.D.: Hydrogen atom scrambling in selectively labeled anionic peptides upon collisional activation by MALDI tandem time-of-flight mass spectrometry. *J. Am. Soc. Mass. Spectrom.* **19**, 1719-1725 (2008)
250. Zehl, M., Rand, K.D., Jensen, O.N., Jørgensen, T.J.D.: Electron Transfer Dissociation Facilitates the Measurement of Deuterium Incorporation into Selectively Labeled Peptides with Single Residue Resolution. *J. Am. Chem. Soc.* **130**, 17453-17459 (2008)
251. Jørgensen, T.J.D., Gårdsvoll, H., Ploug, M., Roepstorff, P.: Intramolecular Migration of Amide Hydrogens in Protonated Peptides upon Collisional Activation. *J. Am. Chem. Soc.* **127**, 2785-2793 (2005)
252. Rand, K.D., Jørgensen, T.J.D.: Development of a Peptide Probe for the Occurrence of Hydrogen (1H/2H) Scrambling upon Gas-Phase Fragmentation. *Anal. Chem.* **79**, 8686-8693 (2007)
253. Rand, K.D., Adams, C.M., Zubarev, R.A., Jørgensen, T.J.D.: Electron Capture Dissociation Proceeds with a Low Degree of Intramolecular Migration of Peptide Amide Hydrogens. *J. Am. Chem. Soc.* **130**, 1341-1349 (2008)
254. Kaltashov, I.A., Eyles, S.J.: Crossing the phase boundary to study protein dynamics and function: combination of amide hydrogen exchange in solution and ion fragmentation in the gas phase. *J. Mass Spectrom.* **37**, 557-565 (2002)
255. Ferguson, P.L., Pan, J., Wilson, D.J., Dempsey, B., Lajoie, G., Shilton, B., Konermann, L.: Hydrogen/Deuterium Scrambling during Quadrupole Time-of-Flight MS/MS Analysis of a Zinc-Binding Protein Domain. *Anal. Chem.* **79**, 153-160 (2007)
256. Jørgensen, T.J.D., Bache, N., Roepstorff, P., Gårdsvoll, H., Ploug, M.: Collisional Activation by MALDI Tandem Time-of-flight Mass Spectrometry Induces Intramolecular Migration of Amide Hydrogens in Protonated Peptides. *Mol. Cell. Proteomics.* **4**, 1910 (2005)
257. Hamuro, Y.: Regio-Selective Intramolecular Hydrogen/Deuterium Exchange in Gas-Phase Electron Transfer Dissociation. *J. Am. Soc. Mass. Spectrom.* **28**, 971-977 (2017)
258. Hamuro, Y., E, S.Y.: Determination of Backbone Amide Hydrogen Exchange Rates of Cytochrome c Using Partially Scrambled Electron Transfer Dissociation Data. *J. Am. Soc. Mass. Spectrom.* **29**, 989-1001 (2018)
259. Duchateau, M., Jørgensen, T.J.D., Robine, O., Nicol, E., Malosse, C., Chamot-Rooke, J., van der Rest, G.: Ion source parameters and hydrogen scrambling in the ECD of selectively deuterated peptides. *Int. J. Mass spectrom.* **367**, 21-27 (2014)
260. Rand, K.D., Pringle, S.D., Morris, M., Engen, J.R., Brown, J.M.: ETD in a Traveling Wave Ion Guide at Tuned Z-Spray Ion Source Conditions Allows for Site-Specific

- Hydrogen/Deuterium Exchange Measurements. *J. Am. Soc. Mass. Spectrom.* **22**, 1784 (2011)
261. Freitas, M.A., Hendrickson, C.L., Marshall, A.G.: Correlation between solution and gas-phase protein conformation: H/D exchange, IRMPD, and ESI FT-ICR MS. *Proc. SPIE.* **3926**, 61-68 (2000)
262. Cui, W., Thompson, M.S., Reilly, J.P.: Pathways of Peptide Ion Fragmentation Induced by Vacuum Ultraviolet Light. *J. Am. Soc. Mass. Spectrom.* **16**, 1384-1398 (2005)
263. Shaw, J.B., Li, W., Holden, D.D., Zhang, Y., Griep-Raming, J., Fellers, R.T., Early, B.P., Thomas, P.M., Kelleher, N.L., Brodbelt, J.S.: Complete Protein Characterization Using Top-Down Mass Spectrometry and Ultraviolet Photodissociation. *J. Am. Chem. Soc.* **135**, 12646-12651 (2013)
264. Mistarz, U.H., Bellina, B., Jensen, P.F., Brown, J.M., Barran, P.E., Rand, K.D.: UV Photodissociation Mass Spectrometry Accurately Localize Sites of Backbone Deuteration in Peptides. *Anal. Chem.* **90**, 1077-1080 (2018)

## Chapter 2

### Gas-Phase Hydrogen/Deuterium Scrambling in Negative-Ion Mode Tandem Mass Spectrometry

#### 2.1 Introduction

Hydrogen/deuterium exchange (HDX) coupled with mass spectrometry (MS) is a powerful method for examining protein conformation and dynamics [1–5]. In HDX, protein amide hydrogen atoms are exchanged for deuterium (or vice versa). The location and rate of exchange depend on solvent accessibility and protection derived from hydrogen bonding and are thus indicative of protein three-dimensional structure and unfolding/refolding rate. When such deuterated samples are analyzed by a mass spectrometer, a mass shift of ~one Dalton is observed for each exchanged hydrogen atom. The structural resolution of this technique, however, is typically limited to the peptide level with pepsin being the proteolytic enzyme of choice due to quenching at low pH (where most enzymes are inactive) to minimize deuterium back exchange prior to and during MS analysis. Peptic peptides with overlapping sequences are required to measure H/D exchange rates at individual amino acid residues [6–9].

Alternatively, dissociation via tandem mass spectrometry (MS/MS) could potentially be used to improve structural resolution, either by fragmenting proteolytic peptide ions, or to enable top-down (intact) analysis of deuterated proteins. However, the most common MS/MS activation technique, positive-ion mode collision-induced dissociation (CID), has been reported to cause intramolecular hydrogen/deuterium (H/D) scrambling due to the increased vibrational

energy of protonated peptide/protein ions prior to dissociation and the up to millisecond time scale of CID [10–14]. Gas-phase H/D scrambling rearranges the deuteration pattern indicative of solution-phase protein structure/dynamics and, thus, erases the desired information.

Electron-based activation methods, e.g., electron-capture/transfer dissociation (ECD/ETD), have demonstrated the ability to induce peptide backbone dissociation with minimum levels of H/D scrambling at carefully tuned instrument settings [15, 16]. In addition to these electron-based techniques, ultraviolet photodissociation was recently reported to proceed with minimum H/D scrambling [17, 18]. ECD/ETD have seen increased utilization in HDX workflows [19–27], but are either incompatible or ineffective for low charge-state precursor ions such as the short peptides frequently generated upon pepsin digestion [28]. Furthermore, intramolecular hydrogen/deuterium migration upon ETD has recently been proposed to follow regio-selective behavior rather than a simple randomization process [29], thus further complicating spectral interpretation.

Negative-ion mode MS/MS is gaining interest for proteomic analysis due to the importance of acidic post-translational modifications [30–37]. While the use of HDX in this polarity has been limited, applications towards carbohydrates and MALDI-generated peptide anions have been reported [38, 39] with prevalent H/D scrambling observed in MALDI tandem time-of-flight CID of peptide anions [39]. However, intramolecular H/D scrambling behavior in electrospray-generated peptide anions has, to our knowledge, not been examined.

Here, we measure the extent of H/D scrambling in several negative-ion mode MS/MS techniques, including negative-ion mode CID (nCID), electron detachment dissociation (EDD) [40, 41], negative-ion electron capture dissociation (niECD) [34], and negative-ion mode free radical induced peptide sequencing (nFRIPS) [35, 42, 43]. Observed scrambling behaviors lend insight into the energetics of these processes.

## **2.2 Experimental**

### **2.2.1 Materials**

The model peptides P1 (HHHHHHIIKIIK) [44], P3 (DDDDDDIIEIIE), and P4

(DDDDDIIEII) were synthesized by GenicBio Limited (Shanghai, China). D<sub>2</sub>O (99.9 atom % D) was purchased from Sigma-Aldrich (St. Louis, MO). *o*-TEMPO-Bz-NHS was synthesized as described previously [35]. All other chemicals were obtained at HPLC grade from Thermo Fisher Scientific (Waltham, MA) and used without further purification.

### 2.2.2 Peptide Derivatization

Acetylation of P1 (here referred to as peptide P2) was achieved by mixing a 110 mM P1 solution in 30  $\mu$ L methanol with a 20  $\mu$ L 25% solution of acetic anhydride in methanol. Following three hour incubation at room temperature solvents were removed under vacuum.

*o*-TEMPO-Bz-NHS was dissolved in acetonitrile at a concentration of 22 mM. The P1 conjugation reaction was buffered with 100 mM triethylamine acetate (pH 8) and performed using a four-fold excess of label overnight at 37  $^{\circ}$ C. These selected conditions enabled targeted labeling of the N-terminus. The reaction solution was 60% acetonitrile which, after completion, was evaporated using a vacuum centrifuge followed by redissolution in water. The poor water solubility of *o*-TEMPO-Bz-NHS enabled crude extraction of the labeled peptide. For control experiments this purified stock solution was diluted to 1-5  $\mu$ M and directly infused into the instrument.

### 2.2.3 Deuterium/hydrogen Exchange

Deuterated peptides were prepared by dissolving unmodified peptides or diluting (1:20) derivatized peptides in D<sub>2</sub>O for a minimum of 18 h at 4  $^{\circ}$ C. The peptide concentration was 1,000  $\mu$ M, 500  $\mu$ M, 50  $\mu$ M, 100  $\mu$ M, and 200  $\mu$ M for nCID, nFRIPS, ECD, EDD, and niECD experiments, respectively. Deuterated peptides were diluted to 10-20  $\mu$ M using cooled protiated ESI solvents: 49:49:2 methanol:water:formic acid for ETD and nFRIPS and 45:45:10:0.1 water:methanol:isopropanol:formic acid for nCID and positive ion mode ECD, both solvents at approximately pH 2.5. Peptides P3 and P4 were diluted into 100 mM NH<sub>4</sub>HCO<sub>3</sub> in 50:50:0.3 H<sub>2</sub>O:isopropanol:formic acid (pH 4.0), or 45:45:10:0.05 H<sub>2</sub>O:methanol:isopropanol, ammonium hydroxide (pH 7.5) for niECD and EDD, respectively. These solutions were immediately transferred to a precooled syringe (Hamilton Co., Reno, NV) or to a Nanomate (Advion, Ithaca,

NY) cooled to 0 °C. For syringe infusion, the syringe was mounted on a pump and cooled with ice bags or dry ice. The flow rate was 10 µL/h for the Nanomate and 2-5.0 µL/min for the syringe pump.

#### **2.2.4 Mass Spectrometry**

Negative-ion mode CID MS/MS spectra were recorded on an Orbitrap-XL mass spectrometer (Thermo Fisher Scientific, Waltham, MA) equipped with a Nanomate nanoESI source. Doubly deprotonated precursor ions were isolated with an 18 m/z window and fragmented at a normalized collision energy of 30%. Fragment ions were acquired in profile mode with four microscans and mass-analyzed in the Orbitrap. Maximum ion injection times were set to 200 ms for MS/MS. The automatic gain control targets were set to  $1 \times 10^5$  for MS/MS in the Orbitrap. MS/MS data were gathered from m/z 210-1,600 in negative-ion mode.

ECD, niECD, and EDD MS/MS spectra were recorded on a 7 T SolariX Fourier transform ion cyclotron resonance (FT-ICR) mass spectrometer (Bruker Daltonics, Billerica, MA) equipped with an Apollo II ESI source. For ECD experiments, an accumulation time of 0.4-0.5 s was used to optimize ion abundance. Mass spectra were acquired from m/z 200-2,000 with 32 scans for an overall acquisition time of less than one minute. Instrument parameters, including drying gas temperature, capillary exit voltage, deflector plate voltage, funnel 1 voltage, skimmer 1 voltage, and quadrupole isolation width, were carefully tuned in order to define regimes of low and high scrambling levels (Table 2.1). ECD of triply protonated P1 ions was performed with a bias voltage of - 1.0 V and an irradiation time of 0.15 to 0.40 s. A lens electrode placed in front of the cathode was set at + 9-10 V. For negative-ion mode experiments on the SolariX, the nebulizing gas, drying gas, and temperature were set to 1 bar, 4.0 L/min, and 50-200 °C, respectively. Ions were accumulated for 3 s prior to EDD experiments. Doubly deprotonated P3 ions were irradiated at a cathode bias voltage of - 19 V for 2 s while the lens electrode was held at - 10 V. Mass spectra were acquired from m/z 200-2,000 with 32 averaged scans, accumulated over 2-3 minutes. For niECD experiments, the singly deprotonated peptides P3 and P4 were irradiated at a cathode bias voltage of - 4.7 V for 2 s while the lens electrode was held 1.0-1.5 V

lower than the cathode bias voltage to maximize the abundance of the charge-increased radical anion.

**Table 2.1** Instrument parameters for ECD experiments: The SolariX Q-FT-ICR mass spectrometer was tuned to accomplish “harsh” (complete scrambling) and “soft” conditions (minimum scrambling) in ECD MS/MS experiments.

	Instrumental parameters	"Harsh" conditions	"Soft" conditions
ESI source	Drying gas temperature	200 °C	40 °C
	Drying gas flow	2.0 L/min	3.5 L/min
	Nebulizing gas flow	2.0 bar	1.1 bar
	Capillary voltage (inlet)	-4.4 kV	-2.0 kV
	Capillary exit voltage	280 V	50 V
	Deflector plate voltage	260 V	40 V
	Funnel 1 voltage	110 V	10 V
	Skimmer 1 voltage	12 V	3 V
	Funnel 2 voltage	6.0 V	5.5 V
	Skimmer 2 voltage	5.0 V	5.0 V
Qh interface	Quadrupole focus lens	-82 V	-60 V
	Quadrupole isolation width	6 Da	30 Da
	Collision focus lens	-50 V	-35 V
	Collision voltage	-4.0 V	-0.5 V
	Ion accumulation time	0.4 sec	0.5 sec
ICR cell	Sweep excitation power	23.0%	18.5%
	Focusing lens 1	-47 V	-30 V
	Focusing lens 2	-8 V	-7 V
	Focusing lens 3	-33 V	-22 V
	DC Bias	-33 V	-18 V

Negative-ion mode FRIPS and positive-ion mode ETD and CID spectra were acquired on a Thermo Scientific Orbitrap Fusion Lumos (Waltham, MA). To minimize scrambling, positive ion mode ETD and CID experiments were collected under the “softest” settings that allowed for stable electrospray. The spray voltage, sheath gas, auxiliary gas, and RF lens were set to 3,600 V, 2.5 (Arb), 1.5, and 10 %, respectively. The 3+ charge state was isolated with a 10 m/z window and either reacted for 17 ms or subjected to 26% CID. In both experiments, the generated product ions were measured in the orbitrap. For nFRIPS, spectra were acquired with 2,700 V spray voltage, 7 sheath gas, 2 Aux gas, 150 °C ion transfer tube temperature, and 30% RF lens. For nFRIPS fragmentation, an MS<sup>3</sup> workflow was used: the precursor ion was first dissociated

with 17% HCD and the homolytically cleaved product was then isolated with a 10 m/z window and further activated at 25% HCD. The resulting product ions were measured in the orbitrap.

### 2.2.5 Data Analysis

Raw precursor and product ion deuterium contents were calculated by subtracting the observed weighted average natural isotopic distribution from the observed weighted average of deuterated equivalents (to yield  $\Delta m_{exp}$ ). Observed product ion raw deuterium contents, were then converted to deuteration levels using the following equation:

**Equation 2.1** Deuteration level =  $\Delta m_{exp}/(m_{100} - m_0)$

where  $m_{100}$  corresponds to the weighted average isotopic distribution of the deuterated intact precursor ion and  $m_0$  corresponds to the weighted average of its natural isotopic distribution, respectively. D/H exchange rates and predicted deuterium content curves under no scrambling conditions were calculated with the HXPep software (Zhongqi Zhang, Amgen, Thousand Oaks, CA), see Table 2.2 for peptides P3 and P4, unique to this work. Theoretical 100% scrambling product ion curves were calculated by multiplying equation (1) with the following factor:

**Equation 2.2** 100% scrambling factor =  $(H_{Frag}/H_{Pre})$

where  $H_{Frag}$  is the number of exchangeable hydrogen atoms in a given fragment ion and  $H_{Pre}$  is the total number of exchangeable hydrogen atoms in the precursor ion. Note that precursor ion charge states and the mechanism by which fragment ions were generated were both taken into consideration when calculating theoretical deuterium contents under complete scrambling conditions [34, 41, 45–49]. All experimental data are shown as the average of triplicate measurements. In cases where incomplete product ion series were observed, the level of H/D scrambling was calculated according to the following equation:

**Equation 2.3** Scrambling level =  $(\Delta m_{exp} - \Delta m_{0\%})/(\Delta m_{100\%} - \Delta m_{0\%}) \times 100\%$

where  $\Delta m_{100\%}$  and  $\Delta m_{0\%}$  are the theoretical mass increases of the corresponding species in the case of 100% scrambling and 0% scrambling, respectively.

**Table 2.2** Predicted intrinsic amide exchange rates of peptides P3 and P4.

P3		Amide HDX	Amide HDX	Amide HDX	P4		Amide HDX
Residues	Amide HDX rate	half-life	Amide HDX rate	half-life	Residues	Amide HDX rate	half-life
	$k(\text{min}^{-1})$	$t_{1/2}$ (min)	$k(\text{min}^{-1})$	$t_{1/2}$ (min)		$k(\text{min}^{-1})$	$t_{1/2}$ (min)
	pH 7.5	pH 7.5	pH 4.0	pH 4.0		pH 4.0	pH 4.0
D2	1628	0.0004	31	0.02	D2	31	0.02
D3	63	0.01	0.7	0.9	D3	0.7	0.9
D4	63	0.01	0.7	0.9	D4	0.7	0.9
D5	63	0.01	0.7	0.9	D5	0.7	0.9
D6	63	0.01	0.7	0.9	I6	0.04	19
I7	23	0.03	0.04	19	I7	0.007	103
I8	21	0.03	0.007	103	E8	0.06	12
E9	34	0.02	0.06	12	I9	0.03	27
I10	25	0.03	0.03	27	I10	0.007	103
I11	21	0.03	0.007	103			
E12	34	0.02	0.06	12			

<sup>a</sup> HDX rates of peptides P3 (DDDDDDIIEIIE) and P4 (DDDDDIIEII) were calculated at 0 °C, pH 7.5 and 4.0, using the HXPep software, based on an algorithm derived from Bai et al [50].

## 2.3 Results and Discussion

The exchange rate of backbone amide hydrogen atoms in unstructured peptides depends on pH, temperature, steric hindrance, and the inductive influence of neighboring side chains [15, 44, 50]. Utilizing these attributes, Rand *et. al.* designed the peptide HHHHHHIKIHK (P1) to investigate H/D scrambling [15, 16, 44]. The difference in intrinsic exchange rates of histidine and isoleucine residues promotes preferential retention of deuterium on C-terminal residues. The degree by which deuteriums migrate to N-terminal residues prior to backbone dissociation determines the applicability of an MS/MS technique for accurately determining deuterium location within this peptide (Figure 2.1). Implementing a similar approach, we investigated the prevalence of H/D scrambling in a series of negative-ion mode MS/MS techniques.

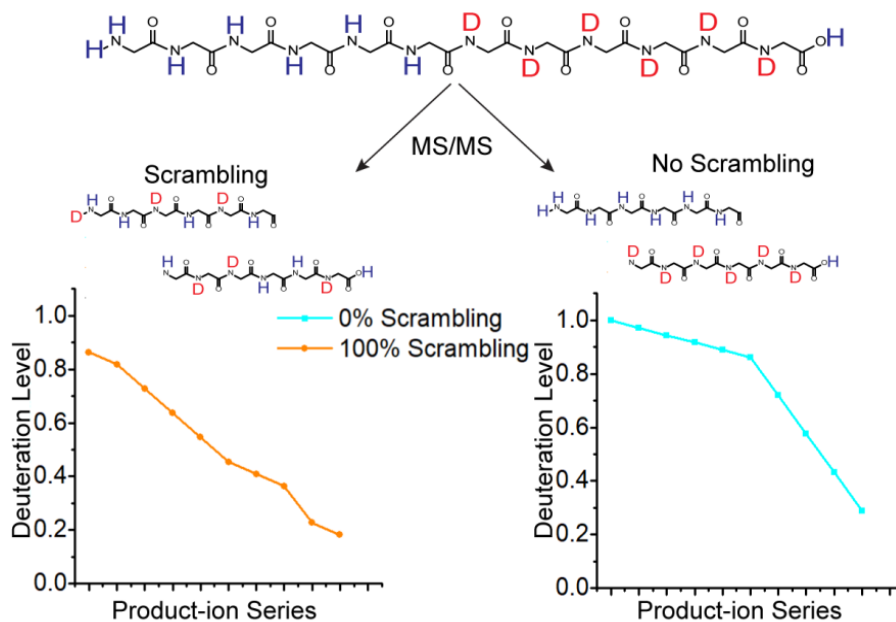


**Figure 2.1** Illustration of a selectively deuterated peptide undergoing gas-phase dissociation with (left) and without (right) H/D scrambling. Blue and orange curves illustrate theoretical 0 and 100% scrambling levels, respectively, for a hypothetical series of y-type ions ( $y_2$ - $y_{11}$ ).

Previous positive-ion mode work demonstrated that the ionization process itself as well as the ion transport conditions prior to MS/MS both have the potential to induce H/D scrambling [15]. That work also characterized the variables that must be adjusted to minimize these scrambling processes. Little is known about the conditions needed to minimize these processes in negative-ion mode; thus, on the utilized Bruker Solarix and Thermo Fusion Lumos instruments, settings were initially chosen that minimized scrambling in positive-ion mode as confirmed by ECD and ETD, respectively (Figures 2.2 and 2.3). These positive-ion mode settings were then ported to negative-ion mode and modified as necessary to achieve signal-to-noise ratios sufficient for analysis (Tables 2.3 and 2.4). The Orbitrap XL is not equipped with activation techniques capable of examining the extent of scrambling; thus, the energetics of its ion source and ion transport were minimized according to literature values [15; Table 2.5].

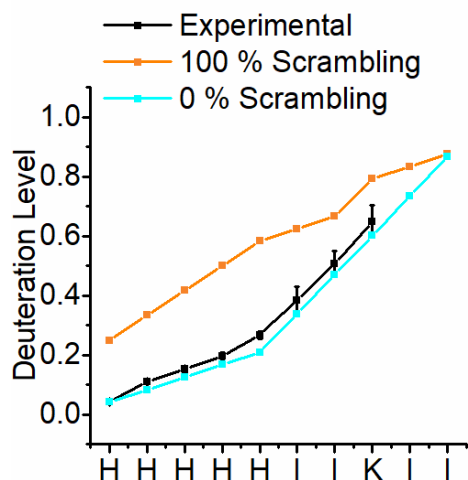


**Figure 2.2** Deuteration levels of ECD-derived *c*-type fragment ions after tuning the ion source for gentle transmission. Data were collected on a Bruker Solarix FT-ICR mass spectrometer.

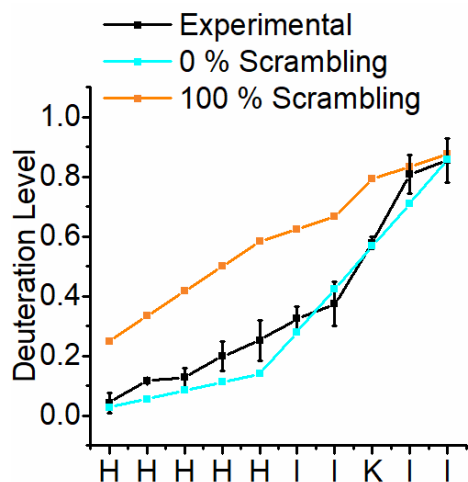


**Figure 2.3** Deuteration levels of ETD-derived *c*-type fragment ions after gentle ion transfer and selection conditions. Data were collected on a Thermo Scientific Orbitrap Fusion Lumos mass spectrometer.

**Table 2.3** Instrument parameters for EDD experiments: Instrumental parameters of the Solarix Q-FT-ICR mass spectrometer were altered to create the “harsh” and “soft” conditions used in EDD MS/MS experiments.

	Instrumental parameters	"Harsh" conditions	"Soft" conditions
ESI source	Drying gas temperature	200 °C	50 °C
	Drying gas flow	4.0 L/min	4.0 L/min
	Nebulizing gas flow	1.1 bar	1.1 bar
	Capillary voltage (inlet)	+3.6 kV	+3.6 kV
	Capillary exit voltage	-260 V	-190 V
	Deflector plate voltage	-240 V	-170 V
	Funnel 1 voltage	-120 V	-60 V
	Skimmer 1 voltage	-11 V	-6 V
	Funnel 2 voltage	-6.0 V	-6.0 V
	Skimmer 2 voltage	-5.0 V	-5.0 V
Qh interface	Quadrupole isolation width	8.0 Da	18.0 Da
	Collision voltage	4.0 V	2.5 V

**Table 2.4** Instrument parameters for niECD experiments: Instrumental parameters of the Solarix Q-FT-ICR mass spectrometer used in niECD MS/MS experiments.

	Instrumental parameters	Values
ESI source	Drying gas temperature	60 °C
	Drying gas flow	4.0 L/min
	Nebulizing gas flow	1.1 bar
	Capillary voltage (inlet)	+3.5 kV
	Capillary exit voltage	-210 V
	Deflector plate voltage	-195 V
	Funnel 1 voltage	-110 V
	Skimmer 1 voltage	-14 V
	Funnel 2 voltage	-6.0 V
	Skimmer 2 voltage	-5.0 V
Qh interface	Quadrupole isolation width	20.0 Da
	Collision voltage	3.0 V

**Table 2.5** Instrument parameters for nCID experiments: Relevant instrumental parameters for negative ion mode CID experiments on the LTQ Orbitrap XL mass spectrometer equipped with a Nanomate ion source.

		Standard values	Tuned ranges
Nanomate (nanoESI)	Gas Pressure*	0.40 psi	0.30 ~ 0.55 psi
	Voltage*	1.35 kV	1.25 ~ 1.50 kV
	Flow rate*	10 $\mu$ L/min	5 ~ 20 $\mu$ L/min
LTQ Orbitrap	Capillary temperature*	80 $^{\circ}$ C	50 ~ 200 $^{\circ}$ C
	Capillary voltage*	-40 V	-20 ~ -80 V
	Tube lens voltage*	-100 V	-50 ~ -200 V
	Normalized collision energy*	30	10 ~ 200
	Ion trap isolation window*	18.0 Da	1.0 ~ 20.0 Da
	Multipole 00 offset voltage	4.5 V	
	Lens 0 Voltage	4.5 V	
	Multipole 0 offset voltage	5.0 V	
	Lens 1 voltage*	9.0 V	8.0 ~ 36.0 V
	Gate lens voltage*	58.0 V	34.0 ~ 78.0 V
	Multipole 1 offset voltage*	9.5 V	6.0 ~ 12.0 V
	Multipole RF Amplitude	400 $V_{p-p}$	
Front lens	5.5 V		

\* Parameters which were altered during the course of this work.

### 2.3.1 H/D Scrambling in Collision Induced Dissociation of Electrosprayed Deprotonated Peptides

Upon nCID, the doubly deprotonated peptide P1 dissociated into a near complete series of *y*-type ( $y_4$ - $y_{11}$ ) and *c*-type fragment ions ( $c_2$ - $c_{10}$ ) (Figure 2.4). When deuterated P1 was dissociated, a corresponding set of isotopically enriched product ions was formed. Observed isotopic distributions for two representative fragment ions with and without deuterium incorporation are shown in Figures 2.5A ( $c_3$  fragment) and C ( $y_9$  fragment), respectively. The weighted average *m/z* values for the natural isotopic distributions are indicated with green solid lines and the weighted average *m/z* values for the deuterated species are indicated with grey solid lines. The dashed lines in Figures 2.5A and C represent the calculated weighted average *m/z* values under no scrambling (blue dashed line) and complete scrambling (orange dashed line) conditions, respectively. The N-terminal  $c_3$  fragment ion is expected to show a low deuteration level in the absence of scrambling whereas the C-terminal  $y_9$  fragment ion is expected to show a

high deuteration level. Near complete scrambling is evident for the  $c_3$  fragment ion whereas the  $y_9$  ion shows a deuteration level even lower than that expected for 100% scrambling. Figure 2.5B illustrates the deuteration level of all observed nCID-derived  $c$ -type ions (black line) as well as their expected deuteration levels in the absence (blue line for 0%) and presence (orange line for 100%) of scrambling. Similar to  $c_3$ , all  $c$ -type ions show deuterium contents indicative of high scrambling levels. Unlike the  $c$ -type ions but similar to the  $y_9$  ion, the deuteration level curve for the  $y$ -type ion series (Figure 2.5D, black line) does not follow the expected trend for 100% scrambling (Figure 2.5D, orange line). Unexpectedly, all these ions contain significantly less deuterium than previously observed for positive ion mode CID [51]. This apparent deuterium loss suggests that significantly more hydrogen atoms are participating in scrambling reactions in nCID compared with positive ion mode CID. Also, the slope differential between the experimental data and 100% scrambling curves in Figure 2.5D indicates deuterium enrichment onto the N-terminal side of the peptide rather than randomization of the deuterium content.

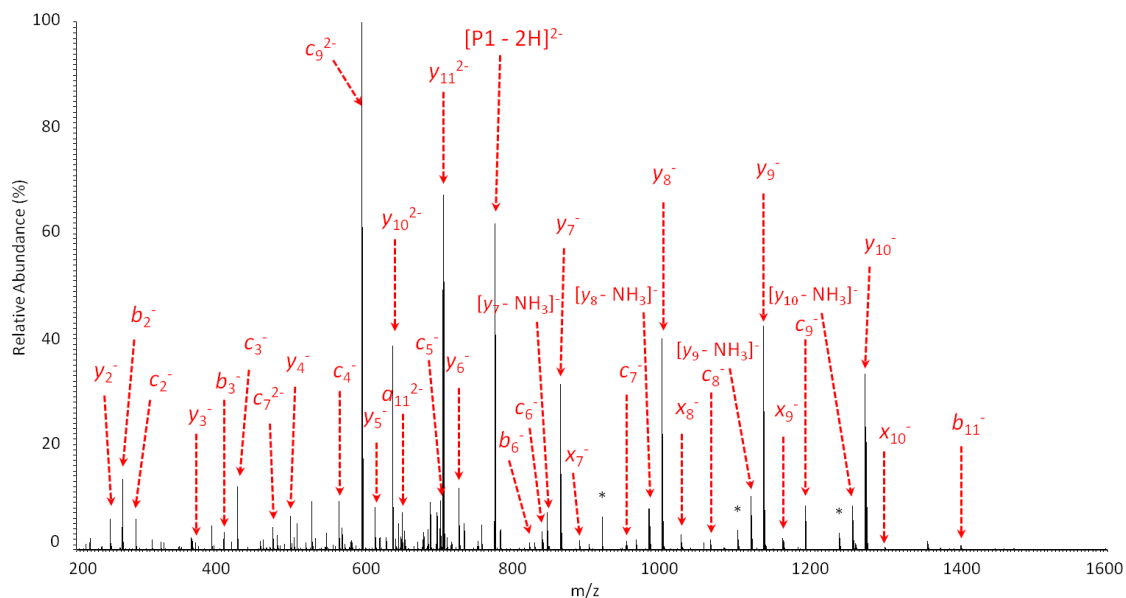


**Figure 2.4** nCID MS/MS spectrum of doubly deprotonated P1 (HHHHHHIIKIK). \* indicates internal fragments.

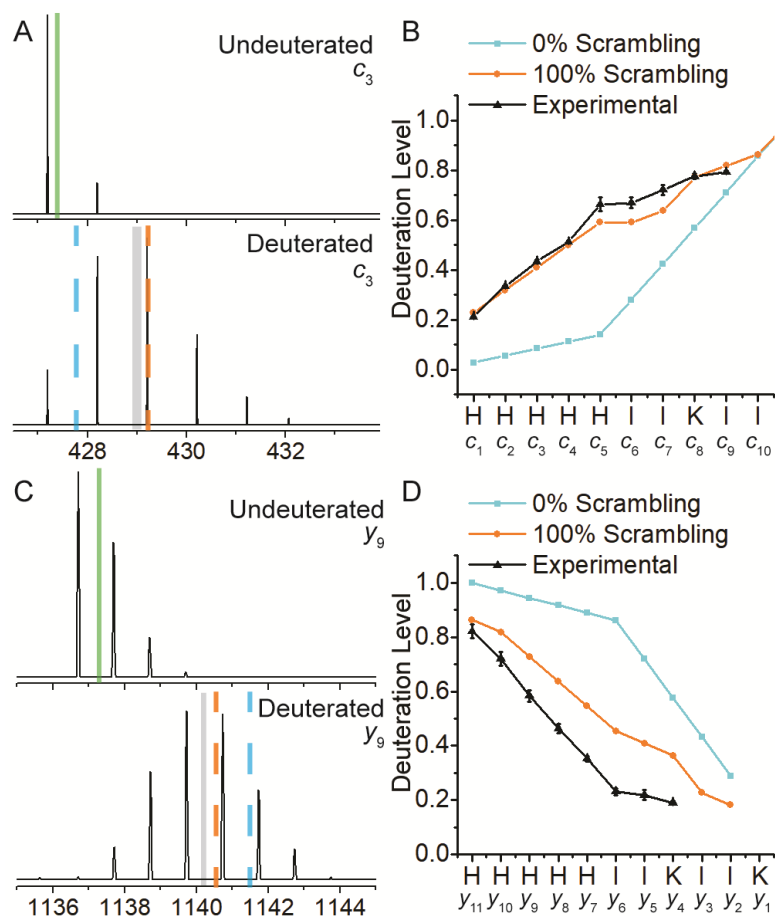


**Figure 2.5** Observed isotopic distributions of  $c_3$  (A) and  $y_9$  (C) fragment ions from nCID of the natural and deuterated peptide P1 (HHHHHHIHKIHK). The weighted average  $m/z$  value for each species is illustrated by a solid green (natural) or grey (deuterated) line. Theoretical deuterium levels for 100 and 0% scrambling are denoted with dashed orange (100%) and blue (0%) lines, respectively. Deuterium levels for all measured P1 nCID-derived  $c$ - (B) and  $y$ -type (D) fragment ions. Blue and orange lines represent expected deuterium levels for 0 and 100% scrambling, respectively.

To examine whether this aberrant scrambling behavior is mediated by the lysine residues, P1 was acetylated, resulting in modification of the N-terminus and both lysine residues. Deuterated doubly deprotonated \*HHHHHHIHK\*IHK\* (P2) was then subjected to nCID, yielding a near complete sequence of  $y$ -type fragment ions ( $y_4$ - $y_{11}$ , data not shown). Similar to P1, the P2  $y$ -ion series demonstrated deuterium enrichment onto the N-terminal amino acid residues (Figure 2.6), suggesting that primary amines do not mediate this unexpected H/D scrambling.

The histidine residues in P1/P2 constitute another possible source of excess hydrogen

atoms. Thus, a new model peptide, DDDDDDIIEIIE (P3), was designed. Similar to P1, P3 relies on substantially different intrinsic exchange rates of isoleucine and aspartic acid to concentrate deuterium to the C-terminal residues upon D/H exchange. Following nCID, *b*- and *y*-type fragment ions were observed (Figure 2.7). H/D scrambling for the *y*-type fragment ion series falls within the theoretical limit (Figure 2.8). This result is in direct contrast to nCID of deuterated P1 and suggests that the additional hydrogen atoms participating in the scrambling reaction for P1 originate from the histidine residues.

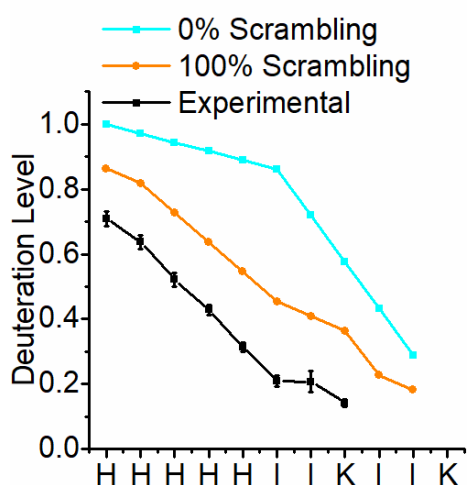


**Figure 2.6** Deuteration levels of nCID-derived *y*-type fragment ions from the peptide P2 (H\*HHHHHIK\*I\*K\* in which \* denotes sites of acetylation).

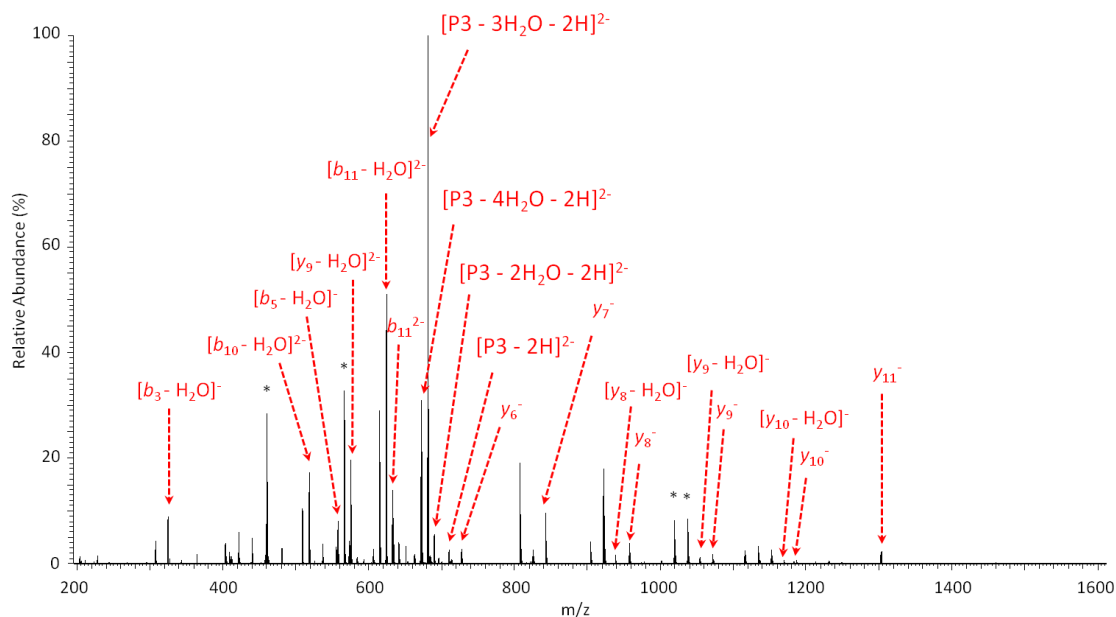


**Figure 2.7** nCID MS/MS spectrum of doubly deprotonated P3 (DDDDDDIIEIIE). \* indicates internal fragments.

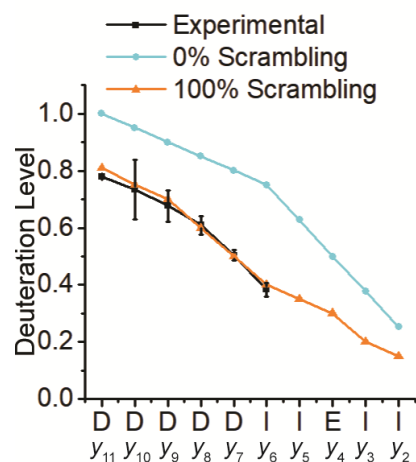


**Figure 2.8** Deuteration levels observed for  $y$ -type ions from nCID of the peptide P3 (DDDDDDIIEIIE) as well as expected deuteration levels for 0% and 100% scrambling, respectively.

The histidine C-2 hydrogen atom is known to undergo exchange reactions and has been utilized to examine local histidine environments [52, 53]. In the gas phase, however, previous work in positive-ion mode reported that these hydrogen atoms do not participate in scrambling reactions [54]. On the other hand, deprotonation of histidine residues has been shown to

promote this process [55] and critical energies for dissociating deprotonated peptides are known to be higher than those of protonated peptides [10, 56, 57]. Thus, histidine C-2 hydrogen atoms may undergo rearrangement in negative-ion mode. Accounting for these hydrogen atoms, the predicted 100% scrambling curve for P1  $\gamma$ -type ions (Figure 2.9A) is closer to the experimental nCID data (Figure 2.9A vs. 2.5D). However, the experimental curve (Figure 2.9A) is still beyond the theoretical deuterium migration limit and the slope differential between experimental data and predicted deuteration levels at 100% scrambling still suggests there are unaccounted hydrogen atoms participating in the scrambling process.

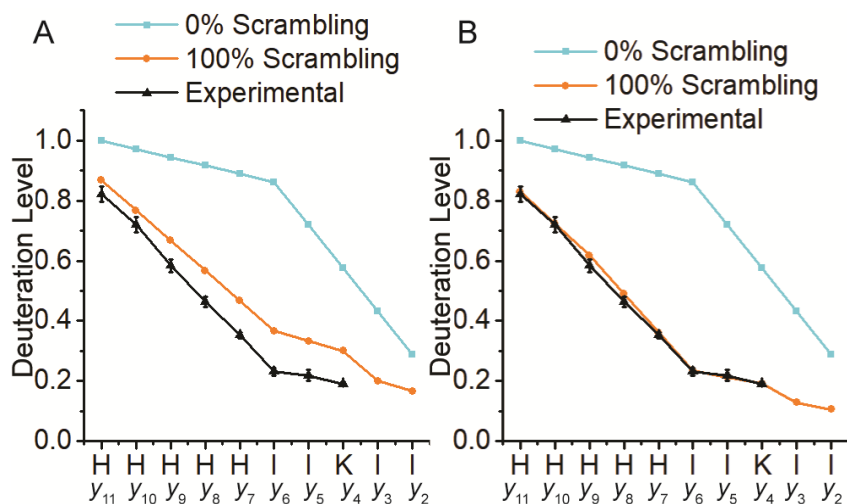


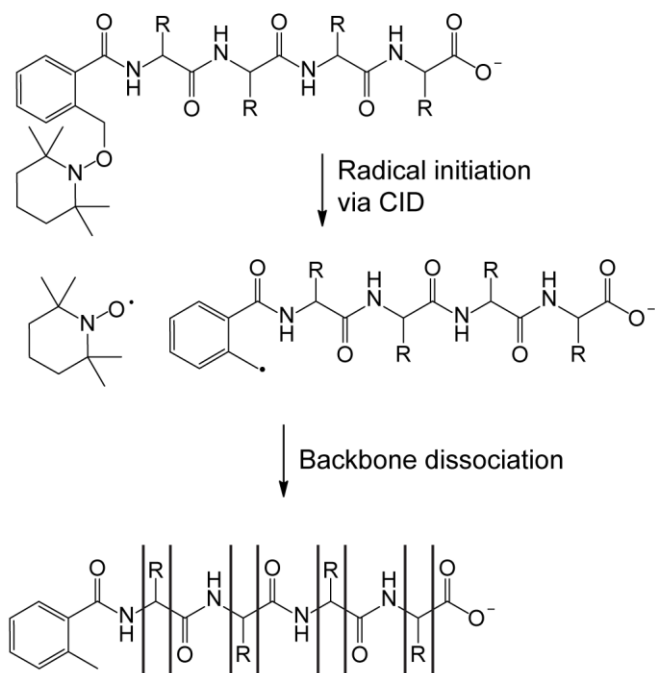
**Figure 2.9** nCID-generated P1 deuteration levels overlaid with 0% and 100% scrambling curves with the 100% curve being adjusted to account for hydrogen exchange at histidine C-2 carbon atoms (A) and adjusted to account for both histidine C-2 and C<sub>β</sub> hydrogen atom exchange (B).

nCID-driven  $\gamma$ -ion formation in the absence of deprotonated amino acid side chains has been proposed to involve hydrogen atom abstraction from  $\alpha$ -carbon atoms [46]. The energy required to abstract C <sub>$\alpha$</sub>  H atoms is in the same range as histidine C <sub>$\beta$</sub> -H bonds, which have the lowest bond dissociation energies (BDE) for C <sub>$\beta$</sub> -H bonds of any residue [58]. Additionally, when analyzing phenylalanine—another low C <sub>$\beta$</sub> -H BDE residue—containing peptides, Bowie *et al.* observed nCID derived products that could only be explained via abstraction of C <sub>$\beta$</sub> -H atoms [58, 59]. Thus, at the energies necessary to induce nCID dissociation, these C <sub>$\beta$</sub> -H atoms may also need to be considered when calculating the 100% scrambling curve. When both the

exchange of histidine C-2 and C $\beta$  hydrogen atoms are considered, the experimental data follows the 100% scrambling limit closely (Figure 2.9B). nCID of P3 does not demonstrate this effect; likely because aspartic acid C $\beta$ -H bonds have significantly higher BDEs and the  $y$ -type ions from this peptide are generated through a lower-energy aspartic acid-driven mechanism, analogous to the non-mobile proton positive-ion mode mechanism [48, 60]. The latter mechanism is supported by the extensive water loss observed for the  $b$ -type ion series (Figure 2.7), a hallmark of the aspartic acid-driven mechanism [48].

### 2.3.2 H/D Scrambling in Radical-Driven Dissociation of Peptide Anions

As with cations [10-14], the above data demonstrate that collisional activation of anions promotes extensive scrambling and is not amenable to improving the structural resolution of HDX experiments. Free radical initiated peptide sequencing (FRIPS) is a radical-driven technique that is achieved through derivatization of a peptide with a persistent radical-containing precursor [45, 61]. Upon low level collisional activation, this radical precursor undergoes homolytic cleavage, generating a radical that propagates throughout the peptide to yield a neutral loss, or an  $a$ - $x$ -,  $c$ -, or  $z$ -type ion (Scheme 2.1). TEMPO-assisted FRIPS was recently applied to peptide anions [35, 42] and was shown to allow backbone cleavage without loss of highly labile posttranslational modifications, e.g., sulfation [35], suggesting potential applicability towards deuterated peptides. nFRIPS of P1 generated a near complete set of  $z$ -type ions (Figure 2.10). When deuterated P1 was dissociated with nFRIPS, the generated  $z$ -type ions demonstrated near complete hydrogen randomization (Figure 2.12A). However, in contrast to nCID of this peptide, no imidazole C-2 hydrogen migration was observed. We recently calculated that TEMPO-assisted nFRIPS requires approximately 50 kcal mol<sup>-1</sup> to promote homolytic cleavage and subsequent backbone dissociation [35]. Our current result implies: **1**) that heteroatom-hydrogen scrambling requires less than 50 kcal mol<sup>-1</sup> to proceed, and **2**) that histidine C-2 and C $\beta$  hydrogen migration likely requires more than 50 kcal mol<sup>-1</sup>.



**Scheme 2.1** FRIPS-driven backbone dissociation.

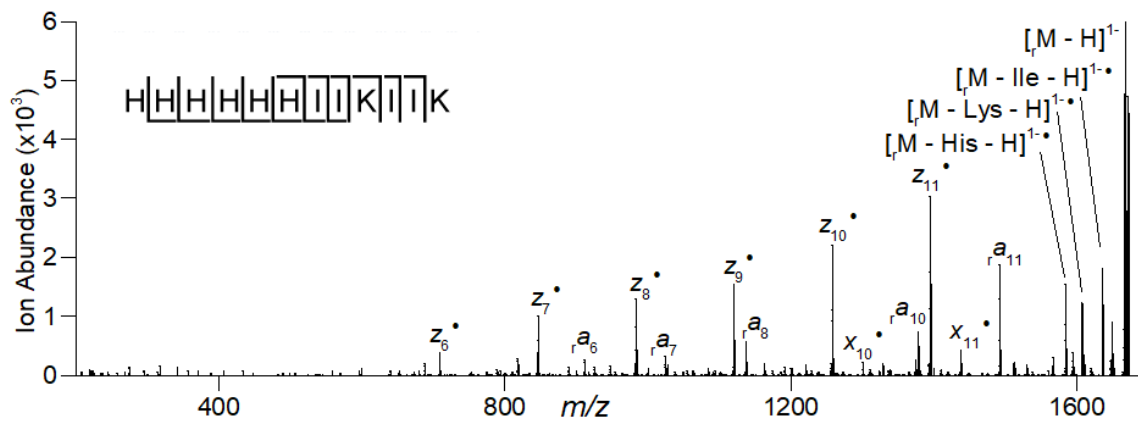


**Figure 2.10** nFRIPS MS/MS spectrum of singly deprotonated P1 (HHHHHHIHKIHK). Subscripted “r” denotes presence of cleaved TEMPO label [45].

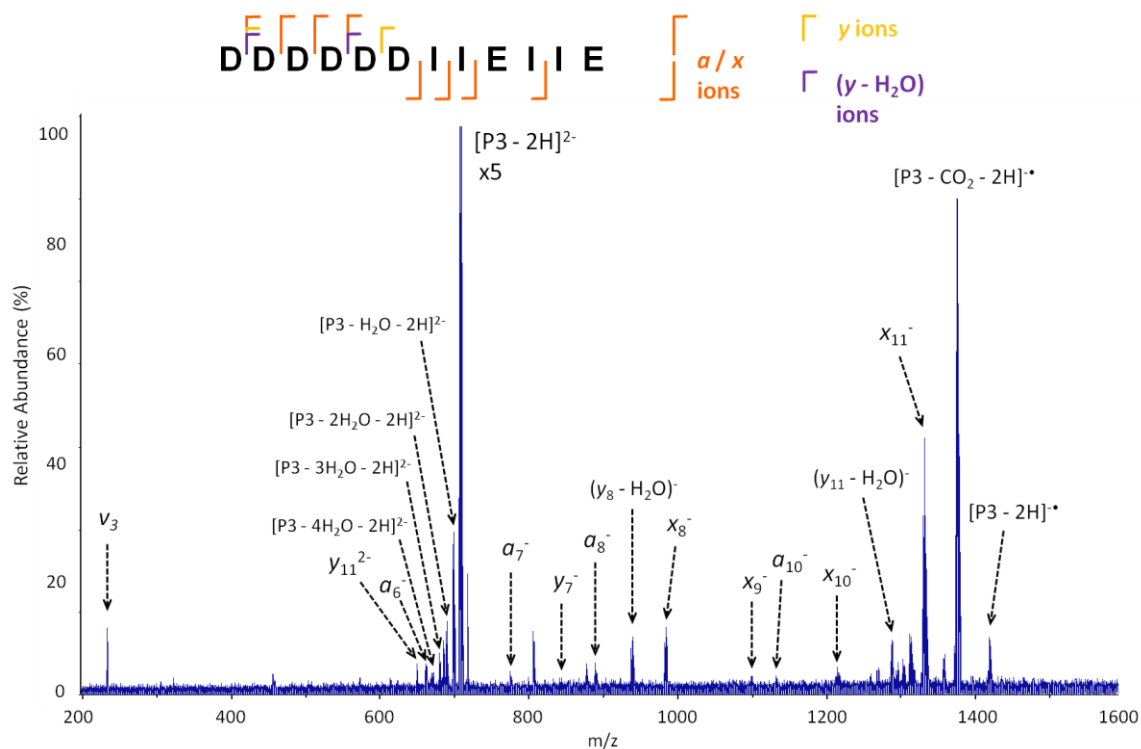


**Figure 2.11** EDD MS/MS spectrum of doubly deprotonated P3 (DDDDDDIIIEII).  $v_3$  = third harmonic.

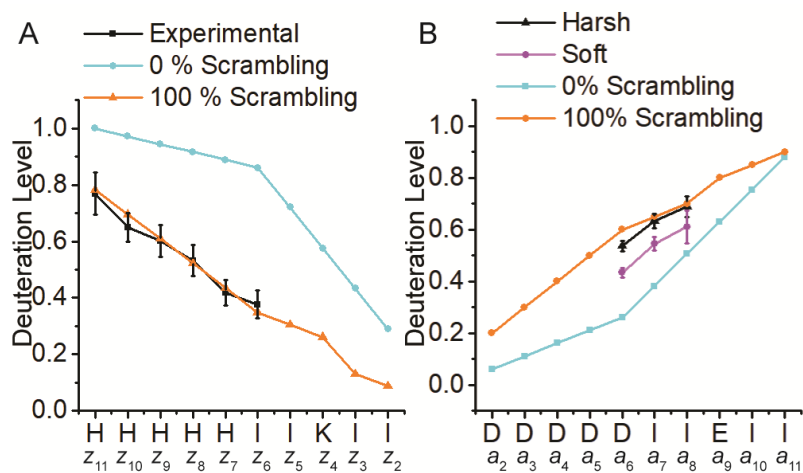


**Figure 2.12** Deuterium levels of nFRIPS-generated  $z$ -type fragment ions (A) and EDD-generated  $a$ -type ions (B) from the peptide P3 as well as predicted 0% and 100% scrambling curves. EDD was performed after both “soft” and “harsh” ion source conditions.

EDD was the first anion-electron reaction technique reported for peptide MS/MS and generates primarily  $a^{\bullet-}$  and  $x$ -type product ions [40, 41]. The seminal publication [41]

demonstrated that EDD is a “soft” dissociation technique, potentially allowing application towards deuterated peptides. When applied to P1, which lacks acidic amino acid residues, EDD did not promote backbone fragmentation (data not shown). Thus, we focused on the acidic peptide P3. Upon electron irradiation, doubly deprotonated P3 underwent fragmentation, generating characteristic  $a^{\bullet-}$  and  $x$ -type fragment ions (Figure 2.11). In particular,  $a^{\bullet 6-}$ ,  $a^{\bullet 8-}$ ,  $a^{\bullet 10-}$ , and  $x_{8-}$ - $x_{11-}$  were observed. However, upon deuterium incorporation, the low EDD fragmentation efficiency and resulting low fragment ion abundance, combined with signal dilution across broader isotopic envelopes, enabled the calculation of scrambling for only three  $a^{\bullet}$ -type product ions. Excitingly, these product ions demonstrated only moderate H/D scrambling (Figure 2.12B). The corresponding deuteration levels equate to a scrambling percentage of 51 for  $a^{\bullet 6-}$ , 61 for  $a^{\bullet 7-}$ , and 54 for  $a^{\bullet 8-}$ .

To ensure that this reduction in scrambling (as compared to nCID and nFRIPS) was accurate and not due to an unforeseen mechanism, the instrument parameters—particularly the ion source—were modified to promote “harsh” conditions (Table 2.3). The harsher source once again promoted extensive hydrogen migration (Figure 2.12B), increasing the scrambling percentages to 81, 94, and 95 for  $a^{\bullet 6-}$ ,  $a^{\bullet 7-}$ ,  $a^{\bullet 8-}$ , respectively. This result suggests that EDD is capable of limiting H/D scrambling for  $a$ -type ions. However, even under gentle ionization conditions scrambling levels are too high and the fragmentation efficiency is far too low to be feasible for HDX experiments. EDD utilizes ~20 eV electrons, which are significantly more energetic than the <1 eV electrons typically employed in ECD [41, 62]. It has been demonstrated that EDD involves both radical-driven fragmentation and vibrational excitation [63, 64]. Additionally, previous work demonstrated an uneven deuterium distribution in aspartic acid repeats following ETD [65]. This unexpected observation was attributed to the presence of nearby lysine residues. Although lysines are not present in the aspartic acid-rich model peptide studied here, it is possible that the observed H/D scrambling can also be attributed to this effect.

Negative-ion electron capture dissociation (niECD) is a radical-driven dissociation technique that is thought to occur through a similar mechanism as its positive-ion mode analogue.

In niECD, electron energies are considerably lower (3.5-6.5 eV) than in EDD. However, niECD is most compatible with low charge-state anions [34] and, under conditions suitable for HDX, the singly deprotonated P3 ion did not show sufficient abundance for analysis (Figure 2.13A). To increase the abundance of the desired singly deprotonated precursor ion, a truncated version of P3 was synthesized. Following ESI, the singly deprotonated species of the peptide DDDDDIIEII (P4) demonstrated significantly higher abundance, rendering it amenable to niECD. Electron irradiation of undeuterated P4 resulted in the formation of primarily *c*-type ions (Figure 2.13B). Similar to EDD, upon deuteration, the niECD efficiency was not widely compatible with the broad isotopic distributions observed following HDX and only the  $c_8^{2-}$ ,  $c_2$ ,  $c_3$ ,  $z_{\bullet 7} - \text{CO}_2$ ,  $z_{\bullet 8} - \text{CO}_2$ , and  $z_{\bullet 9} - \text{CO}_2$  product ions could be analyzed. Despite the utilization of low energy electrons, the *z*-type ion series demonstrated nearly 100% scrambling; 92, 84, and 100% for the  $z_{\bullet 7} - \text{CO}_2$ ,  $z_{\bullet 8} - \text{CO}_2$ , and  $z_{\bullet 9} - \text{CO}_2$  fragment ions respectively. niECD however, was able to minimize H/D scrambling to 32%  $\pm$ 8% for the  $c_2$  fragment ion and 30%  $\pm$ 4% for  $c_3$ .

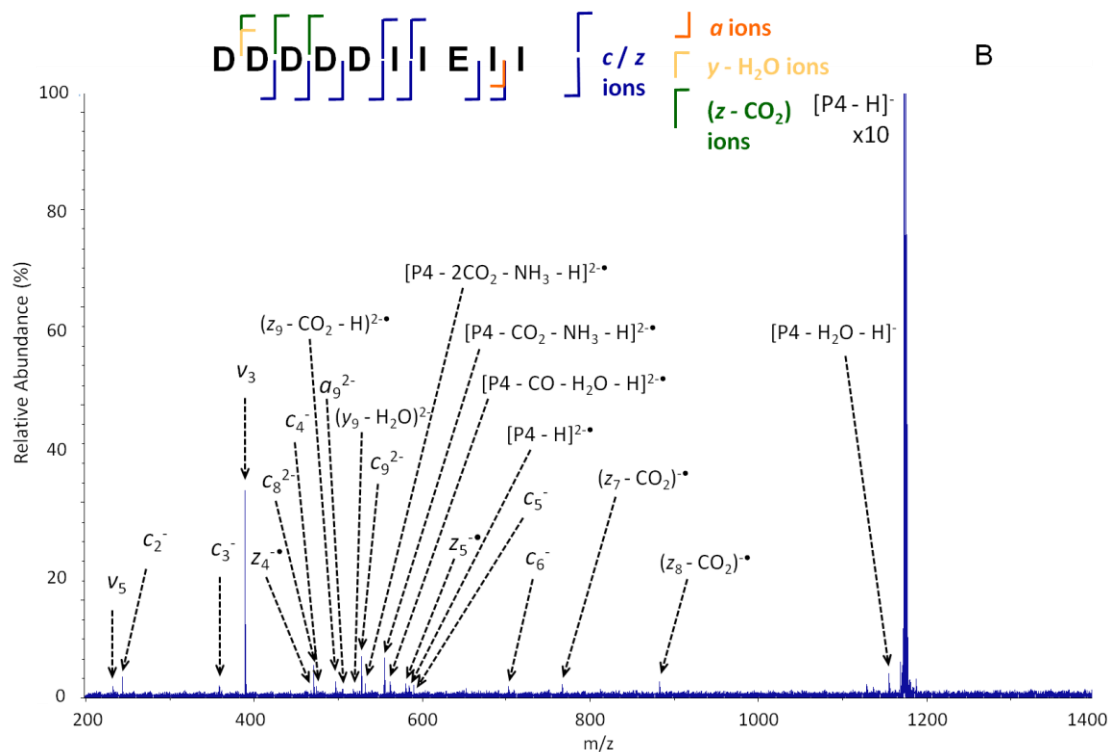
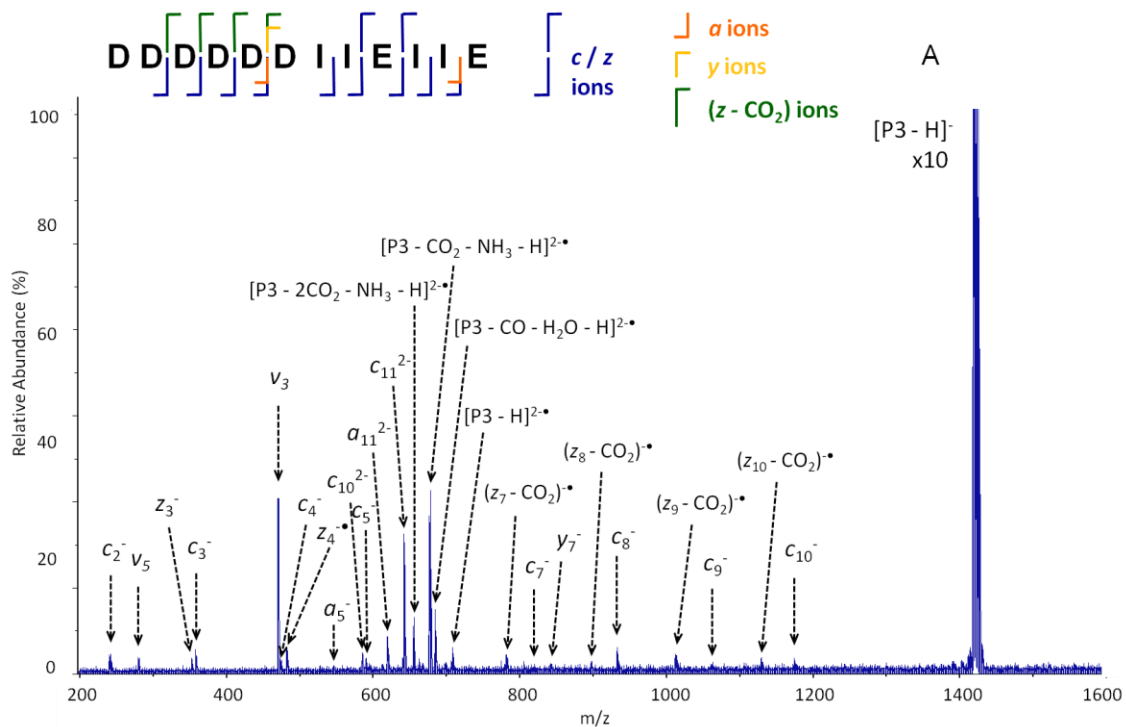


**Figure 2.13** niECD MS/MS spectra of (A) P3 (DDDDDDIIEIIE) and (B) P4 (DDDDDDIIEII).  $v_3$  = third harmonic.  $v_5$  = fifth harmonic. (A) was collected under the condition of pH = 7.5; (B) was collected under the condition of pH = 4.0.

Interestingly, the degree of H/D scrambling (96%  $\pm$ 30%) observed for  $c_8^{2-}$  fragment ion is much higher than that of the  $c_2$  and  $c_3$  ions. Similar inconsistencies were reported from ECD [15] and ETD [29], where the extent of scrambling appears to depend on the size of  $c$ -type ions with smaller  $c$ -ions demonstrating lower degrees of scrambling. This phenomenon may be related to the lifetime difference of the corresponding radical intermediates with their complementary  $z\bullet$ -type fragments [37].

## 2.4 Conclusions

To investigate H/D scrambling in negative-ion mode, several MS/MS techniques were applied towards regio-selectively deuterated peptide anions. We demonstrated that nCID mediated extensive H/D scrambling within all peptides examined. Furthermore, nCID promotes aberrant scrambling profiles in histidine-containing peptides. This unexpected behavior is potentially due to the scrambling of histidine C-2 and  $C_\beta$ -hydrogen atoms. Radical-driven fragmentation methods also promoted H/D scrambling: nFRIPS induced complete randomization of the deuterium profile whereas EDD and niECD proceeded with a moderate degree of H/D scrambling with niECD slightly outperforming EDD. Interestingly, the scrambling levels observed for different fragment ions from the same peptide upon EDD and niECD can be different, which may be attributed to the difference in chemical properties of exchangeable hydrogen sites and/or the conformation of the precursor peptide ions. Thus, more detailed analysis is needed to elucidate detailed mechanisms of intramolecular H/D migration. Overall, nCID, nFRIPS, EDD, and niECD under current experimental conditions are not amenable to HDX MS/MS experiments. For nCID, nFRIPS, and EDD, this incompatibility is likely due to the energetics associated with their mechanisms. For niECD, however, the energetics of the negative-ionization process itself may be too high. In addition, the acidic solution used for selective labeling is not ideal for negative-ion ESI due to inferior fragment ion abundance and the associated challenge of accurately determining deuterium content. Improving the negative-ion ESI efficiency under HDX quenching conditions is expected to improve the utility of negative-ion MS/MS techniques in HDX MS. Despite limited practical applications, the

observed H/D scrambling behavior provided insights into the energetics of these anion fragmentation techniques.

## 2.5 Acknowledgements

This work was supported by the National Science Foundation CHE 1609840 and the University of Michigan. The Thermo Scientific Orbitrap Fusion Lumos was acquired via National Institutes of Health grant S10 OD021619. We would also like to thank Z. Zhang for kindly providing the HXPEP software.

## 2.6 References

1. Pirrone, G.F., Jacob, R.E., Engen, J.R.: Applications of Hydrogen/Deuterium Exchange MS from 2012 to 2014. *Anal. Chem.* 87, 99–118 (2015).
2. Wales, T.E., Engen, J.R.: Hydrogen exchange mass spectrometry for the analysis of protein dynamics. *Mass Spectrom. Rev.* 25, 158–170 (2006).
3. Hoofnagle, A.N., Resing, K.A., Ahn, N.G.: Protein analysis by hydrogen exchange mass spectrometry. *Annu. Rev. Biophys. Biomol. Struct.* 32, 1–25 (2003).
4. Zhang, Z., Smith, D.L.: Determination of amide hydrogen exchange by mass spectrometry: a new tool for protein structure elucidation. *Protein Sci.* 2, 522–531 (1993).
5. Konermann, L., Pan, J., Liu, Y. H.: Hydrogen exchange mass spectrometry for studying protein structure and dynamics. *Chem. Soc. Rev.* 40, 1224–1234 (2011).
6. Brier, S., Maria, G., Carginale, V., Capasso, A., Wu, Y., Taylor, R.M., Borotto, N.B., Capasso, C., Engen, J.R.: Purification and characterization of pepsins A1 and A2 from the Antarctic rock cod *Trematomus bernacchii*. *FEBS J.* 274, 6152–6166 (2007).
7. Cravello, L., Lascoux, D., Forest, E.: Use of different proteases working in acidic conditions to improve sequence coverage and resolution in hydrogen/deuterium exchange of large proteins. *Rapid Commun. Mass Spectrom.* 17, 2387–2393 (2003).
8. Fajer, P.G., Bou-Assaf, G.M., Marshall, A.G.: Improved Sequence Resolution by Global Analysis of Overlapped Peptides in Hydrogen/Deuterium Exchange Mass Spectrometry. *J. Am. Soc. Mass Spectrom.* 23, 1202–1208 (2012).
9. Borotto, N.B., Zhang, Z., Dong, J., Burant, B., Vachet, R.W.: Increased  $\beta$ -Sheet Dynamics and D–E Loop Repositioning Are Necessary for Cu(II)-Induced Amyloid Formation by  $\beta$ -2-Microglobulin. *Biochemistry.* 56, 1095–1104 (2017).
10. Jørgensen, T.J.D., Gårdsvoll, H., Ploug, M., Roepstorff, P.: Intramolecular migration of amide hydrogens in protonated peptides upon collisional activation. *J. Am. Chem. Soc.* 127, 2785–2793 (2005).
11. Hoerner, J.K., Xiao, H., Dobo, A., Kaltashov, I.A.: Is there hydrogen scrambling in the gas phase? Energetic and structural determinants of proton mobility within protein ions. *J. Am. Chem. Soc.* 126, 7709–7717 (2004).

12. Hagman, C., Håkansson, P., Buijs, J., Håkansson, K.: Inter-molecular migration during collisional activation monitored by hydrogen/deuterium exchange FT-ICR tandem mass spectrometry. *J. Am. Soc. Mass Spectrom.* 15, 639–646 (2004).
13. Ferguson, P.L., Pan, J., Wilson, D.J., Dempsey, B., Lajoie, G., Shilton, B., Konermann, L.: Hydrogen/deuterium scrambling during quadrupole time-of-flight MS/MS analysis of a zinc-binding protein domain. *Anal. Chem.* 79, 153–160 (2007).
14. Hamuro, Y., Tomasso, J.C., Coales, S.J.: A Simple Test To Detect Hydrogen/Deuterium Scrambling during Gas-Phase Peptide Fragmentation. *Anal. Chem.* 80, 6785–6790 (2008).
15. Rand, K.D., Adams, C.M., Zubarev, R.A., Jørgensen, T.J.D.: Electron Capture Dissociation Proceeds with a Low Degree of Intramolecular Migration of Peptide Amide Hydrogens. *J. Am. Chem. Soc.* 130, 1341–1349 (2008).
16. Zehl, M., Rand, K.D., Jensen, O.N., Jørgensen, T.J.D.: Electron Transfer Dissociation Facilitates the Measurement of Deuterium Incorporation into Selectively Labeled Peptides with Single Residue Resolution. *J. Am. Chem. Soc.* 130, 17453–17459 (2008).
17. Brodie, N.I., Huguet, R., Zhang, T., Viner, R., Zabrouskov, V., Pan, J., Petrotchenko, E. V., Borchers, C.H.: Top-Down Hydrogen–Deuterium Exchange Analysis of Protein Structures Using Ultraviolet Photodissociation. *Anal. Chem.* 90, 3079–3082 (2018).
18. Mistrarz, U.H., Bellina, B., Jensen, P.F., Brown, J.M., Barran, P.E., Rand, K.D.: UV Photodissociation Mass Spectrometry Accurately Localize Sites of Backbone Deuteration in Peptides. *Anal. Chem.* 90, 1077–1080 (2018).
19. Pan, J., Zhang, S., Parker, C.E., Borchers, C.H.: Subzero Temperature Chromatography and Top-Down Mass Spectrometry for Protein Higher-Order Structure Characterization: Method Validation and Application to Therapeutic Antibodies. *J. Am. Chem. Soc.* 136, 13065–13071 (2014).
20. Wang, G., Kaltashov, I.A.: Approach to Characterization of the Higher Order Structure of Disulfide-Containing Proteins Using Hydrogen/Deuterium Exchange and Top-Down Mass Spectrometry. *Anal. Chem.* 86, 7293–7298 (2014).
21. Abzalimov, R.R., Bobst, C.E., Kaltashov, I.A.: A New Approach to Measuring Protein Backbone Protection with High Spatial Resolution Using H/D Exchange and Electron Capture Dissociation. *Anal. Chem.* 85, 9173–9180 (2013).
22. Pan, J., Heath, B.L., Jockusch, R.A., Konermann, L.: Structural Interrogation of Electrosprayed Peptide Ions by Gas-Phase H/D Exchange and Electron Capture Dissociation Mass Spectrometry. *Anal. Chem.* 84, 373–378 (2012).
23. Bobst, C.E., Kaltashov, I.A.: Enhancing the Quality of H/D Exchange Measurements with Mass Spectrometry Detection in Disulfide-Rich Proteins Using Electron Capture Dissociation. *Anal. Chem.* 86, 5225–5231 (2014).
24. Rand, K.D.: Pinpointing changes in higher-order protein structure by hydrogen/deuterium exchange coupled to electron transfer dissociation mass spectrometry. *Int. J. Mass Spectrom.* 338, 2–10 (2013).
25. Landgraf, R.R., Chalmers, M.J., Griffin, P.R.: Automated Hydrogen/Deuterium Exchange Electron Transfer Dissociation High Resolution Mass Spectrometry Measured at Single-

- Amide Resolution. *J. Am. Soc. Mass Spectrom.* 23, 301–309 (2012).
26. Going, C.C., Xia, Z., Williams, E.R.: Real-time HD Exchange Kinetics of Proteins from Buffered Aqueous Solution with Electrothermal Supercharging and Top-Down Tandem Mass Spectrometry. *J. Am. Soc. Mass Spectrom.* 27, 1019–1027 (2016).
  27. Masson, G.R., Maslen, S.L., Williams, R.L.: Analysis of phosphoinositide 3-kinase inhibitors by bottom-up electron-transfer dissociation hydrogen/deuterium exchange mass spectrometry. *Biochem. J.* 474, 1867–1877 (2017).
  28. Rand, K.D., Zehl, M., Jensen, O.N., Jørgensen, T.J.D.: Protein hydrogen exchange measured at single-residue resolution by electron transfer dissociation mass spectrometry. *Anal. Chem.* 81, 5577–5584 (2009).
  29. Hamuro, Y.: Regio-Selective Intramolecular Hydrogen/Deuterium Exchange in Gas-Phase Electron Transfer Dissociation. *J. Am. Soc. Mass Spectrom.* 28, 971–977 (2017).
  30. McAlister, G.C., Russell, J.D., Rumachik, N.G., Hebert, A.S., Syka, J.E.P., Geer, L.Y., Westphall, M.S., Pagliarini, D.J., Coon, J.J.: Analysis of the acidic proteome with negative electron-transfer dissociation mass spectrometry. *Anal. Chem.* 84, 2875–2882 (2012).
  31. Doerr, A.: Navigating the negative-mode proteome. *Nat. Methods.* 12, 808–808 (2015).
  32. Riley, N.M., Rush, M.J.P., Rose, C.M., Richards, A.L., Kwiecien, N.W., Bailey, D.J., Hebert, A.S., Westphall, M.S., Coon, J.J.: The Negative Mode Proteome with Activated Ion Negative Electron Transfer Dissociation. *Mol. Cell. Proteomics.* 14, 2644–2660 (2015).
  33. Robinson, M.R., Brodbelt, J.S.: Integrating Weak Anion Exchange and Ultraviolet Photodissociation Mass Spectrometry with Strategic Modulation of Peptide Basicity for the Enrichment of Sulfopeptides. *Anal. Chem.* 88, 11037–11045 (2016).
  34. Yoo, H.J., Wang, N., Zhuang, S., Song, H., Håkansson, K.: Negative-ion electron capture dissociation: Radical-driven fragmentation of charge-increased gaseous peptide anions. *J. Am. Chem. Soc.* 133, 16790–16793 (2011).
  35. Borotto, N.B., Ileka, K.M., Tom, C.A.T.M.B., Martin, B.R., Håkansson, K.: Free Radical Initiated Peptide Sequencing for Direct Site Localization of Sulfation and Phosphorylation with Negative Ion Mode Mass Spectrometry. *Anal. Chem.* 90, 9682–9686 (2018).
  36. Huzarska, M., Ugalde, I., Kaplan, D.A., Hartmer, R., Easterling, M.L., Polfer, N.C.: Negative electron transfer dissociation of deprotonated phosphopeptide anions: choice of radical cation reagent and competition between electron and proton transfer. *Anal. Chem.* 82, 2873–2878 (2010).
  37. Hersberger, K.E., Håkansson, K.: Characterization of O -Sulfopeptides by Negative Ion Mode Tandem Mass Spectrometry: Superior Performance of Negative Ion Electron Capture Dissociation. *Anal. Chem.* 84, 6370–6377 (2012).
  38. Kostyukevich, Y., Kononikhin, A., Popov, I., Nikolaev, E.: In-ESI Source Hydrogen/Deuterium Exchange of Carbohydrate Ions. *Anal. Chem.* 86, 2595–2600 (2014).
  39. Bache, N., Rand, K.D., Roepstorff, P., Ploug, M., Jørgensen, T.J.D.: Hydrogen Atom Scrambling in Selectively Labeled Anionic Peptides Upon Collisional Activation by MALDI Tandem Time-of-Flight Mass Spectrometry. *J. Am. Soc. Mass Spectrom.* 19, 1719–1725 (2008).

40. Kjeldsen, F., Silivra, O.A., Ivonin, I.A., Haselmann, K.F., Gorshkov, M., Zubarev, R.A.:  $\alpha$ -C backbone fragmentation dominates in electron detachment dissociation of gas-phase polypeptide polyanions. *Chem. Eur. J.* 11, 1803–1812 (2005).
41. Budnik, B.A., Haselmann, K.F., Zubarev, R.A.: Electron detachment dissociation of peptide di-anions: An electron-hole recombination phenomenon. *Chem. Phys. Lett.* 342, 299–302 (2001).
42. Lee, J., Park, H., Kwon, H., Kwon, G., Jeon, A., Kim, H.I., Sung, B.J., Moon, B., Oh, H. B.: One-step peptide backbone dissociations in negative-ion free radical initiated peptide sequencing mass spectrometry. *Anal. Chem.* 85, 7044–7051 (2013).
43. Hage, C., Ihling, C.H., Göze, M., Schäfer, M., Sinz, A.: Dissociation Behavior of a TEMPO-Active Ester Cross-Linker for Peptide Structure Analysis by Free Radical Initiated Peptide Sequencing (FRIPS) in Negative ESI-MS. *J. Am. Soc. Mass Spectrom.* 28, 56–68 (2017).
44. Rand, K.D., Jørgensen, T.J.D.: Development of a Peptide Probe for the Occurrence of Hydrogen (1 H/ 2 H) Scrambling upon Gas-Phase Fragmentation. *Anal. Chem.* 79, 8686–8693 (2007).
45. Lee, M., Kang, M., Moon, B., Oh, H. B.: Gas-phase peptide sequencing by TEMPO-mediated radical generation. *Analyst.* 134, 1706–1712 (2009).
46. Bowie, J.H., Brinkworth, C.S., Dua, S.: Collision-induced fragmentations of the (M-H)-parent anions of underivatized peptides: An aid to structure determination and some unusual negative ion cleavages. *Mass Spectrom. Rev.* 21, 87–107 (2002).
47. Brinkworth, C.S., Dua, S., McAnoy, A.M., Bowie, J.H.: Negative ion fragmentations of deprotonated peptides: Backbone cleavages directed through both Asp and Glu. *Rapid Commun. Mass Spectrom.* 15, 1965–1973 (2001).
48. Wysocki, V.H., Tsaprailis, G., Smith, L.L., Breci, L.A.: Mobile and localized protons: a framework for understanding peptide dissociation. *J. Mass Spectrom.* 35, 1399–1406 (2000).
49. Syrstad, E.A., Tureček, F.: Toward a general mechanism of electron capture dissociation. *J. Am. Soc. Mass Spectrom.* 16, 208–224 (2005).
50. Bai, Y., Milne, J.S., Mayne, L., Englander, S.W.: Primary structure effects on peptide group hydrogen exchange. *Proteins Struct. Funct. Genet.* 17, 75–86 (1993).
51. Jørgensen, T.J.D., Gårdsvoll, H., Ploug, M., Roepstorff, P.: Intramolecular migration of amide hydrogens in protonated peptides upon collisional activation. *J. Am. Chem. Soc.* 127, 2785–2793 (2005).
52. Miyagi, M., Wan, Q., Ahmad, M.F., Gokulrangan, G., Tomechko, S.E., Bennett, B., Dealwis, C.: Histidine hydrogen-deuterium exchange mass spectrometry for probing the microenvironment of histidine residues in dihydrofolate reductase. *PLoS One.* 6, e17055 (2011).
53. Dong, J., Callahan, Katie, L., Borotto, N.B., Vachet, R.W.: Identifying Zn-bound histidine residues in metalloproteins using hydrogen-deuterium exchange mass spectrometry. *Anal. Chem.* 86, 766–773 (2014).

54. Cebo, M., Kielmas, M., Adamczyk, J., Cebrat, M., Szewczuk, Z., Stefanowicz, P.: Hydrogen–deuterium exchange in imidazole as a tool for studying histidine phosphorylation. *Anal. Bioanal. Chem.* 406, 8013–8020 (2014).
55. Bradbury, J.H., Chapman, B.E., Pellegrino, F.A.: Hydrogen-deuterium exchange kinetics of the C-2 protons of imidazole and histidine compounds. *J. Am. Chem. Soc.* 95, 6139–6140 (1973).
56. Harrison, A.G.: Sequence-specific fragmentation of deprotonated peptides containing H or alkyl side chains. *J. Am. Soc. Mass Spectrom.* 12, 1–13 (2001).
57. Marzluff, E.M., Campbell, S., Rodgers, M.T., Beauchamp, J.L.: Low-Energy Dissociation Pathways of Small Deprotonated Peptides in the Gas Phase. *J. Am. Chem. Soc.* 116, 7787–7796 (1994).
58. Moore, B.N., Julian, R.R.: Dissociation energies of X-H bonds in amino acids. *Phys. Chem. Chem. Phys.* 14, 3148–3154 (2012).
59. Eckersley, M., Bowie, J.H., Hayes, R.N.: Collision-induced dissociations of deprotonated peptides, dipeptides and tripeptides with hydrogen and alkyl  $\alpha$  groups. An aid to structure determination. *Org. Mass Spectrom.* 24, 597–602 (1989).
60. Bulet, O., Yang, C.Y., Gaskell, S.J.: Influence of cysteine to cysteic acid oxidation on the collision-activated decomposition of protonated peptides: Evidence for intraionic interactions. *J. Am. Soc. Mass Spectrom.* 3, 337–344 (1992).
61. Hodyss, R., Cox, H.A., Beauchamp, J.L.: Bioconjugates for Tunable Peptide Fragmentation: Free Radical Initiated Peptide Sequencing (FRIPS). *J. Am. Chem. Soc.* 127, 12436–12437 (2005).
62. Axelsson, J., Palmblad, M., Håkansson, K., Håkansson, P.: Electron capture dissociation of substance P using a commercially available Fourier transform ion cyclotron resonance mass spectrometer. *Rapid Commun. Mass Spectrom.* 13, 474–477 (1999).
63. Wolff, J.J., Laremore, T.N., Aslam, H., Linhardt, R.J., Amster, I.J.: Electron-Induced Dissociation of Glycosaminoglycan Tetrasaccharides. *J. Am. Soc. Mass Spectrom.* 19, 1449–1458 (2008).
64. Kinet, C., Gabelica, V., Balbeur, D., De Pauw, E.: Electron detachment dissociation (EDD) pathways in oligonucleotides. *Int. J. Mass Spectrom.* 283, 206–213 (2009).
65. Rand, K.D., Lund, F.W., Amon, S., Jorgensen, T.J.D.: Investigation of amide hydrogen back-exchange in Asp and His repeats measured by hydrogen ( $^1\text{H}/^2\text{H}$ ) exchange mass spectrometry. *Int. J. Mass Spectrom.* 302, 110–115 (2011).

## Chapter 3

### Supercharging for Improved Electron Capture/Transfer Dissociation (ECD/ETD)-based Hydrogen/Deuterium Exchange Mass Spectrometry

#### 3.1 Introduction

Solution-phase hydrogen/deuterium exchange (HDX) coupled with mass spectrometry (MS) is widely used to reveal information about protein higher-order structure and dynamics [1-3]. Deuterium exchange rates, extracted from uptake curves of deuterium content *vs.* incubation time in D<sub>2</sub>O (exchange-in experiments) or H<sub>2</sub>O (exchange-out experiments), reflect both protein solvent accessibility and secondary structure stability (hydrogen bonds) [4]. HDX can outperform other solution-phase labeling techniques because it targets amide hydrogen atoms at every amino acid residue along protein backbones (except proline) and the exchange reaction is straightforward to conduct [2]. On the other hand, the reversible nature of H/D exchange allows deuterated proteins to undergo back exchange with solvent during the sample analysis time, causing undesired deuterium loss [5, 6]. Conventional HDX MS workflows include use of an acid protease (typically pepsin) to digest deuterium-labeled proteins prior to liquid chromatography (LC) separation and mass analysis. Pepsin digestion allows deuterium uptake to be assigned to distinct regions (i.e., peptide segments) of a protein [7, 8]. However; the deuterium content resolution is limited by the length of peptic peptides, typically 5-10 amino acid residues. When overlapping peptides are generated, e.g., due to the non-specific nature of pepsin, the deuterium uptake spatial resolution may increase based on the size of overlapping

regions from two peptides [9, 10]. In this situation, however, it is still unlikely to globally assign deuterium to individual amino acid amides.

In contrast to the aforementioned well-established “bottom-up” HDX approach, the “top-down” approach bypasses the proteolysis step. Instead, fragmentation of intact proteins take place in the gas phase [2]. Improved deuterium spatial resolution can be obtained in top-down experiments, down to the single amino acid level, because ladders of complementary fragment ion pairs can be generated [11, 12]. It is worth noting, however, that not all tandem mass spectrometry (MS/MS) activation techniques are applicable to measuring HDX rates of individual amino acid amides. H/D scrambling, which refers to multiple reversible proton/deuteron transfers among labile sites in a gaseous peptide or protein ion, is the main issue that needs to be addressed in order to utilize gas-phase dissociation to increase spatial resolution in HDX MS/MS experiments [13]. Slow heating methods, such as collision-induced dissociation (CID), widely used to fragment gaseous peptide and protein ions in commercial mass spectrometers, have been shown to generate extensive H/D scrambling and, therefore, completely randomize the deuteration pattern embedded in the protein backbone during solution-phase HDX [14, 15]. The observation of significant scrambling accompanied with HDX CID MS/MS is consistent with the mobile proton model of the CID process [13]. In contrast, H/D scrambling is much less pronounced when electron-based MS/MS techniques, e.g., electron capture dissociation (ECD) and electron transfer dissociation (ETD), are utilized to fragment intact proteins or larger peptides [12, 16-18]. Both ECD and ETD involve prompt fragmentation on a picosecond time scale [13, 19-21]. Although the detailed mechanism of peptide backbone N-C $\alpha$  bond cleavage in ECD/ETD is still under debate, it is widely acknowledged that these methods are gentle enough to yield peptide backbone fragmentation while retaining labile post-translational modifications (PTMs) [19, 22]. Accordingly, negligible H/D scrambling levels were observed in both ECD [16] and ETD [17], provided that collisional activation in the ion source and during ion transfer was kept at a minimum. Consequently, ECD/ETD are seeing increased utilization for generating accurate amide HDX information with close to single amino

acid residue resolution [7, 12, 23].

In HDX ECD/ETD MS/MS experiments, it is critical to generate highly charged protein/peptide ions for maximum fragmentation efficiency [24-26] and accompanying deuterium content resolution. ECD/ETD require at least doubly positively charged precursor ions [27]; however, our group reported that triply protonated species yield improved peptide sequence coverage and higher Mascot scores upon ECD compared to doubly protonated peptides [25]. Earlier ETD studies by McLuckey *et al.* suggested that elevated bath gas temperature can increase the overall sequence coverage for doubly protonated tryptic peptides [28]. In addition, supplemental collisional activation can efficiently improve ETD outcomes for doubly charged peptides, as reported by Coon *et al.* [29]. Acid is typically added to quench the HDX reaction along with decreasing the solution temperature by flash freezing in liquid nitrogen. Acidification boosts the charge states of peptide ions formed by positive ion mode electrospray ionization (ESI). Williams *et al.* showed in the early 2000's [30-32] that further enhanced charging is feasible for a variety of analytes by adding *m*-nitrobenzyl alcohol (*m*-NBA) to the ESI solvent. A number of subsequent studies showed that *m*-NBA can efficiently supercharge large molecules such as intact proteins [33-35] and polymers [31, 32]. Other organic additives, including sulfolane [36, 37], dimethyl sulfoxide (DMSO) [38, 39], propylene carbonate (PC) [33, 39, 40], and 1,2-butylene carbonate (1,2-BC) [41, 42] have also been reported to effectively supercharge proteins. Kjeldsen *et al.* showed that addition of as little as 0.1% *m*-NBA to the mobile-phase solvent is sufficient to shift the overall charge-state distributions for a variety of tryptic peptides in LC ESI ETD MS/MS experiments for improved fragmentation efficiency, sequence coverage, and peptide identification accuracy [26]. For example, the calculated average charge state for identified bovine serum albumin tryptic peptides was increased from 2.20 to 2.59. Similar improvements were reported by Sharp and co-workers for ETD-based quantification of hydroxyl radical protein footprinting [43]. Compared with tryptic peptides, peptic peptides can be even less compatible with ECD/ETD methods because they are often small and can lack basic residues (protonation sites). Rand *et al.* [23] reported the use of *m*-NBA in bottom-up HDX LC ETD

MS/MS of  $\beta_2$ -microglobulin. With the addition of 0.05% *m*-NBA to the HPLC solvents, the deuterium content of 60 out of 93 individual amide groups (65%) of the protein could be monitored, compared with only 45% sequence coverage in the absence of supercharging reagent. Sterling *et al.* [44] and Going *et al.* [45] also utilized chemical/electrothermal supercharging in top-down HDX ETD MS/MS for investigating real-time HDX kinetics of proteins from aqueous solution.

In this Chapter, we apply *m*-NBA to evaluate supercharging of a variety of peptic peptides generated from a bottom-up HDX workflow. Because addition of *m*-NBA to LC mobile-phase solvents reduces peptide retention times, we also explore post-column addition of *m*-NBA. Furthermore, we compare the peptic peptide supercharging performance of *m*-NBA to those of propylene carbonate (PC), dimethyl sulfoxide (DMSO), and sulfolane, all of which have been reported to effectively supercharge proteins and protein complexes [33-40].

## **3.2 Experimental**

### **3.2.1 Materials**

Myoglobin from equine heart, cytochrome c from bovine heart,  $\alpha$ -casein and  $\beta$ -casein from bovine milk, pepsin from porcine gastric mucosa, D<sub>2</sub>O (99.9 atom % D), *m*-NBA ( $\geq 99.5\%$ ), PC (99.7%), DMSO ( $\geq 99.7\%$ ), and sulfolane ( $\geq 99.8\%$ ) were purchased from Sigma-Aldrich (St. Louis, MO, USA). All other chemicals were obtained at HPLC or higher grade and used without further purification. All solution percent concentrations referred to in this work are volume/volume.

### **3.2.2 Hydrogen/Deuterium Exchange and Proteolysis**

All protein solutions were prepared from lyophilized solid without additional purification. For off-line digestion, a 20  $\mu$ M stock protein solution in 150 mM ammonium acetate buffer was mixed with pepsin in 2% formic acid solution at a substrate/protease molar ratio of 1:1 in an ice bath at 0  $^{\circ}$ C for 3 min (pH 2.5). The protein digests were then loaded onto a 10  $\mu$ L loop for manual injection LC MS(/MS). HDX experiments were performed by diluting stock protein

solutions (5  $\mu$ L, 400  $\mu$ M) into 95  $\mu$ L 150 mM ammonium acetate buffer in D<sub>2</sub>O for 1, 8, 10, 30, and 120 min at 0 °C before simultaneous quench and pepsin digestion. For the undeuterated control, the stock protein solutions were initially diluted into H<sub>2</sub>O instead of D<sub>2</sub>O. Each HDX reaction was quenched by adding pepsin solution in 2% formic acid at 1:1 (v/v) to decrease the final pH to ~2.5. The proteolysis reaction for HDX experiments followed the same steps as described above. All HDX runs were performed in triplicate.

### 3.2.3 Liquid Chromatography

An 1100 Agilent HPLC system coupled with two 6-port switching valves (VICI Valco, Houston, TX, USA), one for desalting and one for manual injection, was used for all experiments. Each protein digest was separated over a short C18 analytical column (Phenomenex Kinetex 5  $\mu$ m EVO 50 x 2.1 mm) at a flow rate of 0.2 mL/min. The LC gradient was 7 min long with 5% B for 0 to 1 min, 5 -75% B for 1 to 5 min, and 75% B for 5 to 7 min. The eluent within the first minute was directed to waste with subsequent eluent introduced into the mass spectrometer. Mobile phase A consisted of 5% acetonitrile (ACN) and 0.2% formic acid (FA) in water. Mobile phase B consisted of 5% water and 0.2% FA in ACN. 0.1% *m*-NBA was added to mobile phases A and B. *m*-NBA was dissolved in mobile phase B directly and in mobile phase A with the aid of ultrasound. In later experiments, *m*-NBA was added to the ESI solution via a post-column mixing tee with an additional syringe and pump (Fusion 400, Chemyx Inc., Stafford, TX, USA). ACN solution with various amounts of *m*-NBA was placed inside this additional syringe. The resulting *m*-NBA concentration in the ESI solution was altered by altering the infusion flow rate. DMSO, sulfolane, and PC were also explored as post column additives with the same device. Control runs were conducted with post-column injection of 100% ACN.

To minimize back exchange in all HDX experiments, LC mobile phases A and B were cooled through 0.02" i.d., 10-foot-long, coiled PEEK tubings (IDEX Health & Science, Oak Harbor, WA, USA) immersed in ice. These tubings were located after the HPLC binary pump. An external, cooled, mixing tee (IDEX Health & Science, Oak Harbor, WA, USA) was used to combine solvent A and B (Figure 3.1). Both solvent A and B were flowing through the cooling

tubings for at least 3.5 min to guarantee sufficient thermal exchange prior to making contact with the deuterated samples. The two switching valves were mounted on opposite sidewalls of an ice-filled aluminum box (20x20x20 cm, lidless) with their metallic heads pointing inward. This ice-filled box housed the HPLC solvent pre-cooling loops, the solvent A & B mixing tee, sample injection loop, and the analytical column (Figure 3.1). The syringe for post-column injection was pre-cooled in a separate ice bath.

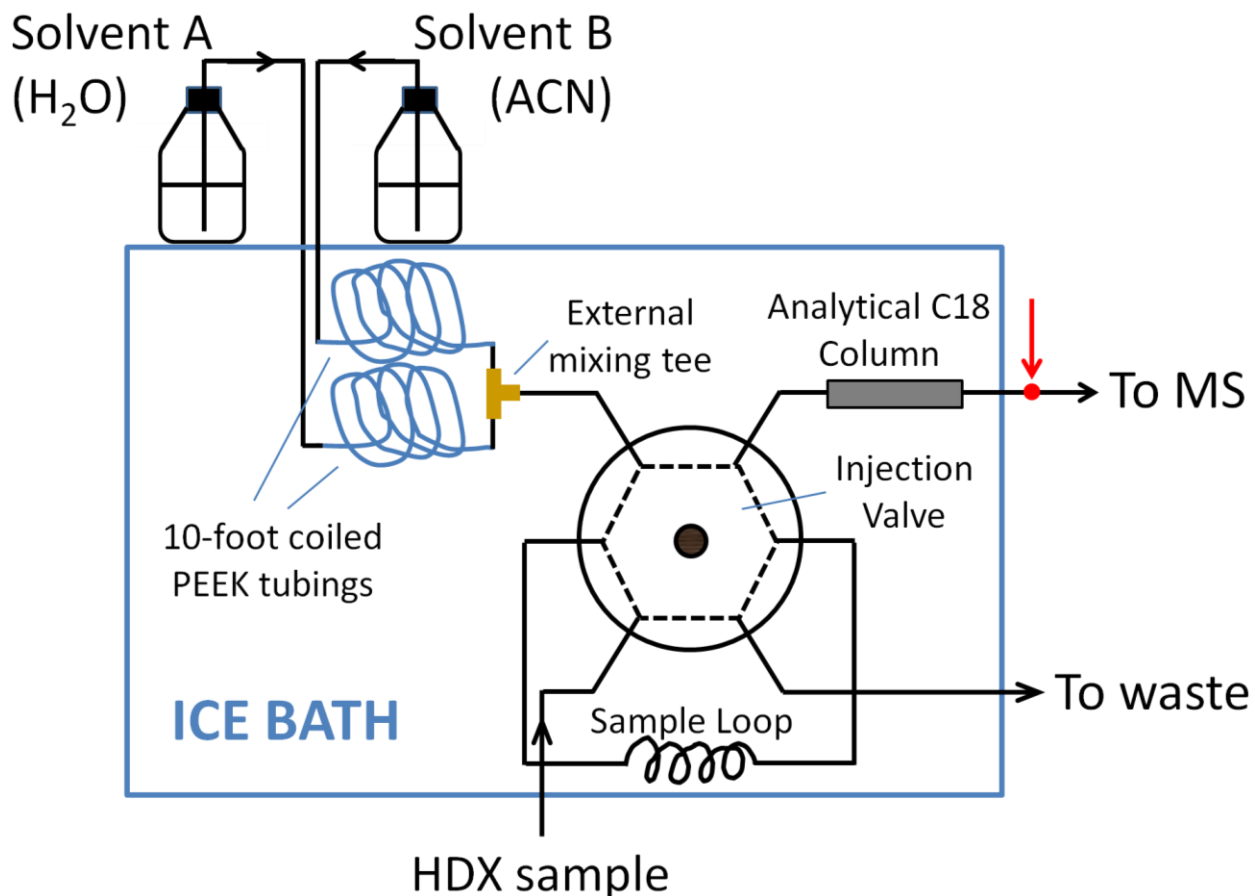


**Figure 3.1** Diagram of the HDX LC/MS set-up used in this work. The red arrow and dot indicates the point where supercharging reagents were introduced in the case of post-column injection.

### 3.2.4 Mass Spectrometry

All experiments were performed in positive ion mode on a 7 T Solarix quadrupole Fourier transform ion cyclotron resonance (FT-ICR) mass spectrometer (Bruker Daltonics, Billerica, MA, USA) equipped with an Apollo II ESI source. The capillary voltage, drying gas

flow rate, and drying gas temperature were set to 4,500 V, 3.8 L/min, and 130 °C respectively. A 0.25 s external accumulation time and a resolution of 512k were used. For the LC ECD MS/MS experiments, data-dependent acquisition with MS/MS boost was used. Accumulation times for MS and MS/MS scans were 0.15 and 0.50 s, respectively. Following an MS scan, a total of 3-4 precursors with charge states ranging from 2 to 5 were isolated (8 m/z window) and transferred to the FT-ICR cell for ECD (150 ms irradiation time, - 1.0 V ECD bias voltage, 1 scan for each MS/MS spectrum). An indirectly heated hollow dispenser cathode was used to perform ECD with a heating current of 1.6 A. Mass spectra were externally calibrated with sodium trifluoroacetate to <2 ppm error.

### 3.2.5 Data Analysis

Data analysis was performed manually using Bruker Data Analysis 4.4. Following replicate data collection, peptide matches were determined using an in-house Excel macro. Peptides were only assigned if the mass error was below 12 ppm. Variable modifications were set at 7 missed peptic cleavages, methionine oxidation, serine/threonine/tyrosine phosphorylation and N-terminal acetylation. N-terminal methionine loss was set as a fixed modification for myoglobin.

In the proceeding text and figures, the term “average charge state ( $q_{\text{avg}}$ )” describes the effect of *m*-NBA and other supercharging reagents on the peptide charge-state distribution, as determined from Equation 3.1:

**Equation 3.1** 
$$q_{\text{avg}} = \frac{\sum_i^N q_i W_i}{\sum_i^N W_i}$$

where  $N$  is the number of peptide charge states,  $q_i$  is the net charge of the  $i$ th charge state, and  $W_i$  is the ion abundance of the  $i$ th charge state. The ion abundance of multiply charged peptides was normalized to the net charge due to the nature of “image current” detection in the FT-ICR cell. Based on the relatively small molecular size of peptic peptides, only the monoisotopic peak abundances were considered.

ECD efficiency was determined as the ratio of the summed abundances of *c*- and *z*-type fragment ions with or without neutral losses, not including side chain cleavages, neutral losses,

or the charge reduced, undissociated species  $[M + nH]^{(n-1)+}$ , divided by the total ion abundance (Equation 3.2). All ion abundances were normalized to charge.

**Equation 3.2** 
$$\text{ECD frag eff.} = \frac{\sum \text{ECD product ions (c,z, and their neutral losses)}}{\sum \text{total ion abundance}}$$

For the HDX experiments, the deuterium content of a peptide ion was determined from the difference between the weighted average masses of the deuterated and undeuterated peptide. Weighted average masses were calculated by dividing the sum of the products of the mass and abundance of each isotopic peak by the total abundance of all observed isotopic peaks.

### 3.3 Results and Discussion

#### 3.3.1 Supercharging of peptic peptides

Protein sequence coverages of myoglobin, cytochrome c,  $\alpha$ -casein S1, and  $\beta$ -casein obtained from LC/MS experiments following pepsin digestion under the rapid and cold conditions required for HDX experiments are shown in Table 3.1 with and without addition of 0.1% *m*-NBA to the mobile phase solvents. The myoglobin sequence coverage reached 100% in both cases while addition of *m*-NBA resulted in slight sequence coverage decreases for cytochrome c (79% to 75%),  $\alpha$ -casein S1 (97% to 93%), and  $\beta$ -casein (91% to 85%). Even though addition of *m*-NBA resulted in detection of fewer peptic peptides, more multiply charged peptic peptide ions were generated in the presence of this supercharging reagent. For example, the mass spectra shown in Figure 3.2 illustrate the charge-state distribution of the myoglobin peptic peptides TALGGILKKKGHHEAEL and FRNDIAAKYKELGFQG, respectively, in the absence (a, c) and presence (b, d) of 0.1% *m*-NBA in the mobile phase. We chose 0.1% *m*-NBA as a starting concentration based on previous literature, which considered the balance between efficient supercharging and minimal chemical changes to the mobile phase [26, 46]. As demonstrated in Figure 3.2 (a, c), in the absence of *m*-NBA, doubly protonated species are dominant for both of these peptic peptides, showing average charge states of 2.2 and 2.0, respectively. With only 0.1% *m*-NBA (Figure 3.2 (b, d)) the charge-state distributions shift significantly towards higher average charge: the peptide TALGGILKKKGHHEAEL showed a

distribution of 67% doubly-protonated and 33% triply-protonated species without *m*-NBA, whereas 13% doubly-, 32% triply-, and 56% quadruply-protonated species were observed in the presence of *m*-NBA, corresponding to an average charge state of 3.2; an average increase of a whole unit of charge. Supercharging of the peptide FRNDIAAKYKELGFQG was not quite as dramatic but, nevertheless, highly effective with the average charge state increasing from 2.0 to 2.6. However; unfavorably, signal abundance decreased for both peptides upon addition of *m*-NBA.

**Table 3.1** Overall protein sequence coverages of peptically digested myoglobin, cytochrome c,  $\alpha$ -casein S1, and  $\beta$ -casein following LC/MS experiments with and without 0.1% *m*-NBA in the mobile phase solvents, respectively. These data are based on duplicate measurements. The mass error for all assigned peptides was below 12 ppm.

Overall protein sequence coverage	0% <i>m</i> -NBA	0.1% <i>m</i> -NBA
myoglobin	100%	100%
cytochrome c	79%	75%
$\alpha$ -casein S1	97%	93%
$\beta$ -casein	91%	85%

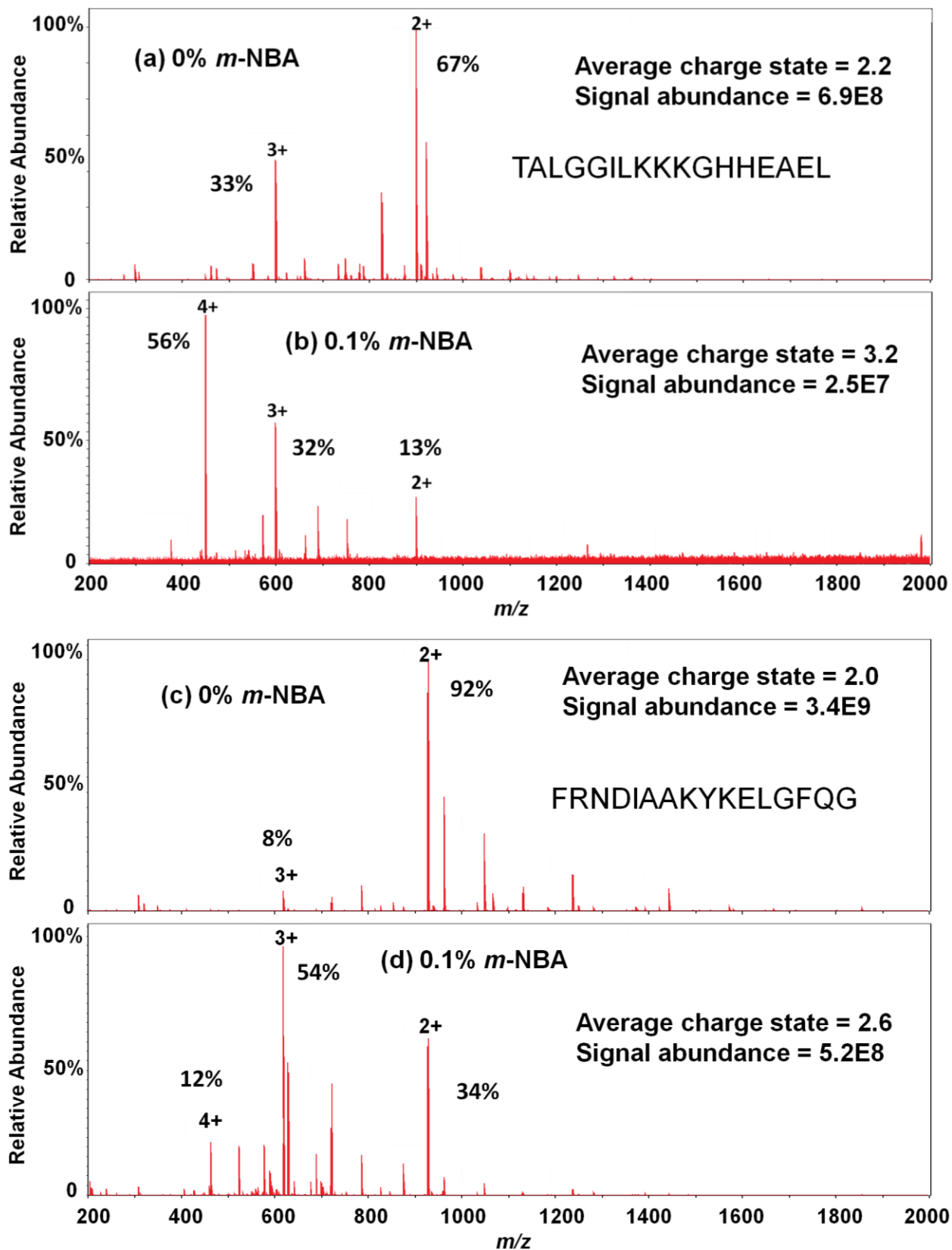


**Figure 3.2** FT-ICR mass spectra at 4.2(a)/3.9(b) and 4.7(c)/4.3(d) minutes from LC/MS of a

myoglobin peptic digest in the absence (a, c) and presence (b, d) of 0.1% *m*-NBA. The observed earlier elution in the presence of *m*-NBA is due to the corresponding increased solvent strength. Average charge states for the peptides TALGGILKKKGHHEAEL (71-87) (a,b) and FRNDIAAKYKELGFQG (139-154) (c, d) under the two LC conditions are indicated in the upper right of each panel.

**Table 3.2** Charge-state distributions and calculated average charge states for myoglobin peptides from LC/MS experiments using 0% and 0.1% *m*-NBA in the mobile phases, respectively.

Myoglobin			0% <i>m</i> -NBA					0.1% <i>m</i> -NBA							
Start	End	Peptide	Charge state distribution					Charge state distribution					diff in av CS		
			1+	2+	3+	4+	av CS	1+	2+	3+	4+	5+	6+	av CS	
2	8	GLSDGEW	100				1.00								
2+Acetyl	22	GLSDGEWQQVLNVWGKVEADI			100		3.00			35.8	64.2			3.64	0.64
9	12	QQVL	100				1.00	100						1.00	0.00
13	20	NVWGKVEA	100				1.00		100					2.00	1.00
13	30	NVWGKVEADIAGHGQEV		98.1	1.9		2.02			100				3.00	0.98
16	30	GKVEADIAGHGQEV	30.8	69.2			1.69		73.9	26.1				2.26	0.57
21	30	DIAGHGQEV	99.4	0.6			1.01		100					2.00	0.99
23	31	AGHGQEVLI	73.7	26.3			1.26		100					2.00	0.74
31	33	IRL	100				1.00								
31	41	IRLFTGHPETL	71.4	28.6			1.29		80.9	19.1				2.19	0.91
34	41	FTGHPETL	100				1.00		100					2.00	1.00
34	54	FTGHPETLEKFDKFKHLKTEA			100		3.00		19.6	27.5	31.8	17.2	3.9	3.58	0.58
55	70	EMKASEDLKKHGTVV		88.4	11.6		2.12			49.1	50.9			3.51	1.39
59	70	SEDLKKHGTVV		100			2.00			100				3.00	1.00
71	77	TALGGIL	100				1.00								
71	87	TALGGILKKKGHHEAEL		78.9	21.1		2.21			45.6	54.4			3.54	1.33
74	95	GGILKKKGHHEAELKPLAQSHA		3.7	90.9	5.4	3.02		16	26.5	37.5	20		3.62	0.60
86	104	ELKPLAQSHATKHKIPIKY		50.4	46.1	3.5	2.53			56.2	43.8			4.44	1.91
88	104	KPLAQSHATKHKIPIKY		71.9	26.6	1.5	2.30								
88	107	KPLAQSHATKHKIPIKYLEF		44.3	52.6	3.1	2.59			65.2	34.8			4.35	1.76
103	105	KYL	100				1.00	100						1.00	0.00
108	124	ISDAIIHVLHSHKHPGDF		73.6	26.4		2.26		20	48.6	31.4			3.11	0.85
108	126	ISDAIIHVLHSHKHPGDFGA		82.7	17.3		2.17			49	51			3.51	1.34
112	124	IIHVLHSHKHPGDF		94.7	5.3		2.05			63.2	36.8			3.37	1.32
112	128	IIHVLHSHKHPGDFGADA		93.6	6.4		2.06			61.1	38.9			3.39	1.33
112	131	IIHVLHSHKHPGDFGADAQGA		75.3	24.7		2.25			47.9	52.1			3.52	1.27
112	135	IIHVLHSHKHPGDFGADAQGAMTKA		45.5	50.3	4.2	2.59			17.9	42.5	39.6		4.22	1.63
125	136	GADAQGAMTKAL	100				1.00	98.6	1.4					1.01	0.01
125	139	GADAQGAMTKALELF							73.9	26.1				2.26	
136	138	LEL	100				1.00	100						1.00	0.00
139	145	FRNDIAA	100				1.00		100					2.00	1.00
139	152	FRNDIAAKYKELGF		96.1	3.9		2.04			86.5	13.5			3.14	1.10
139	154	FRNDIAAKYKELGFQG		94.2	5.8		2.06			86	14			3.14	1.08
140	152	RNDIAAKYKELGF		11.5	85.8	2.7	1.91			82	18			3.18	1.27
145	154	AKYKELGFQG		79.1	20.9		1.21								
146	154	KYKELGFQG	100				1.00		100					2.00	1.00
148	154	KELGFQG	100				1.00		100					2.00	1.00
Overall distribution			33%	36%	24%	7%		8%	24%	33%	24%	10%	1%		
Average							1.74							2.75	0.95
Standard deviation															0.49

Table 3.2 lists all myoglobin peptic peptides observed from LC/MS with and without *m*-NBA. The predominant charge states for these peptides in the absence of *m*-NBA were 1+ (33%) and 2+ (36%) with the remaining 31% having charge states of 3+ and higher. In the presence of *m*-NBA the predominant charge state was 3+ (33%) with 68% of peptides having a charge state of 3+ and higher. The calculated overall average charge state for all myoglobin peptic peptides observed in the LC/MS experiments increased from 1.74 without *m*-NBA to 2.75 with *m*-NBA. The average charge state increase for these 31 peptides (Table 3.2, rightmost column) was 0.95 with a standard deviation of 0.49. As previously discussed for tryptic peptides [26], this change in predominant charge state is quite important in data-dependent acquisition as 3+ and higher charge-state peptide ions are more likely to be selected for ECD/ETD, thus improving MS/MS outcome. A similar charge-enhancing effect was observed for  $\alpha$ -casein (average charge state increasing from 1.74 to 2.26) and  $\beta$ -casein (average charge state increasing from 1.88 to 2.34) upon addition of 0.1% *m*-NBA, although the average charge increase for these two proteins was lower than that of myoglobin. This result may be due to  $\alpha$ - and  $\beta$ -casein being phosphoproteins with a higher fraction of acidic amino acid residues than myoglobin. Acidic peptic peptides from these two proteins are less likely to carry multiple positive charges upon ESI. Nevertheless, notable shifts in charge state distributions for  $\alpha$ - and  $\beta$ -casein peptic peptides were observed, as shown in Figure 3.3 for the  $\alpha$ -casein peptides FVAPFPEVFGKEKVNEL, LRLKKYKVPQL, and YYVPLGTQYTDA. For example, the charge-state distribution of FVAPFPEVFGKEKVNEL was shifted from 70% 2+ ions/30% 3+ ions without *m*-NBA to 22% 2+ and 78% 3+ ions in the presence of 0.1% *m*-NBA. The peptide YYVPLGTQYTDA contains no basic amino acid residues and yielded almost exclusively singly charged ions (97%) without *m*-NBA; however, addition of supercharging reagent boosted the doubly charged ion abundance significantly, to 42%.

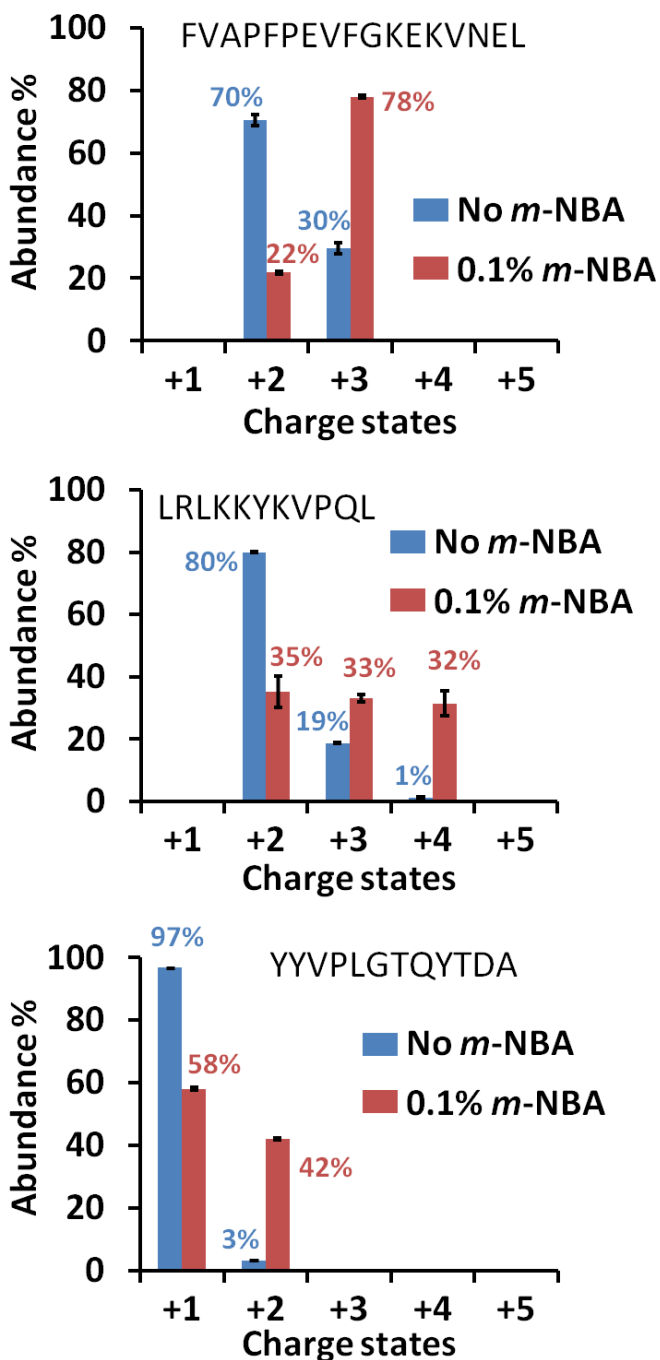


**Figure 3.3** Bar charts showing the shift in charge-state distributions for three  $\alpha$ -casein peptic peptides; FVAPFPEVFGKEKVNEL (top), LRLKKYKVPQL (middle), and YYVPLGTQYTDA (bottom), upon addition of 0.1% *m*-NBA.

Figure 3.4 shows the charge state distributions of all peptic peptides from myoglobin, cytochrome c,  $\alpha$ -casein S1, and  $\beta$ -casein observed under conventional ESI conditions (0% *m*-NBA) and with the addition of 0.1% *m*-NBA. Similar to myoglobin, cytochrome c peptic

peptides showed a high average charge state increase upon addition of *m*-NBA, from 2.16 to 3.02. Both myoglobin and cytochrome c have pI values higher than 7, thus a higher number of protonation sites are present compared with the casein proteins. Notably, no peptides were predominantly singly charged when electrosprayed with 0.1% *m*-NBA. This result is significant because ECD/ETD are not compatible with singly charged ions.

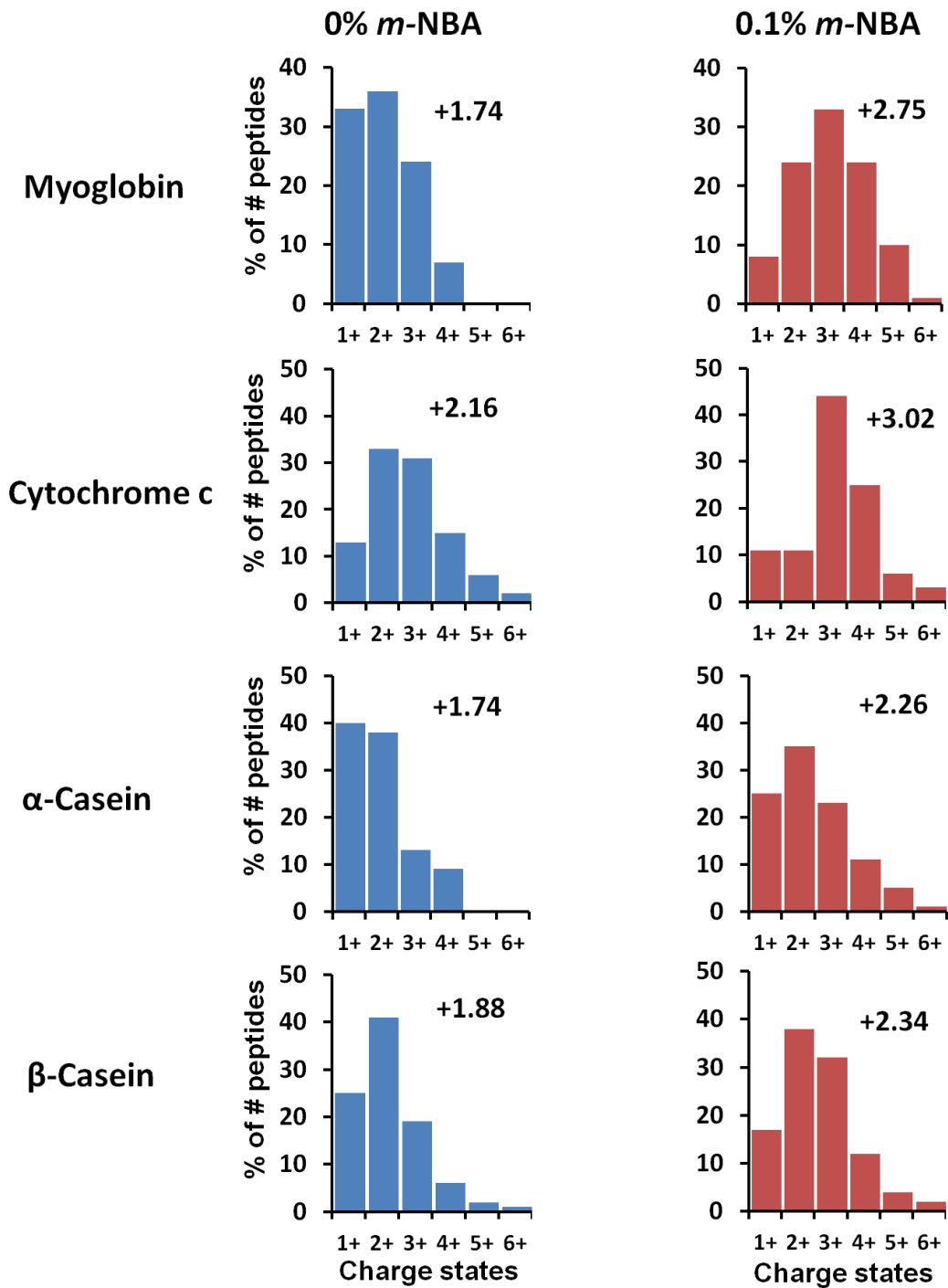


**Figure 3.4** Bar charts showing the charge state distributions for peptic peptides from myoglobin, cytochrome c,  $\alpha$ -casein, and  $\beta$ -casein without (left) and with 0.1% (right) *m*-NBA in the mobile phase solvent. The calculated average charge states for peptic peptides from each protein are shown on the upper-right, respectively.

### 3.3.2 Post-column addition of supercharging reagent for improved liquid chromatography

As previously reported, the presence of *m*-NBA in mobile phase solvents influences the retention time in reversed-phase chromatography [26, 46] with peptide retention inversely related to *m*-NBA concentration. Upon increasing the *m*-NBA concentration from 0% to 0.5%, the retention times of 19 BSA tryptic peptides all dropped linearly, although not to the same extent [26]. The same trend was observed here for peptic peptides from all four tested proteins when 0.1% *m*-NBA was added to the LC mobile phase. Base peak chromatograms (BPCs) from LC/MS of myoglobin peptide peptides with and without *m*-NBA are shown in Figure 3.5 (a). These BPCs are displayed on the same Y-axis scale, clearly illustrating that addition of 0.1% *m*-NBA results in lower peak abundances and, consequently, reduced sensitivity. In addition, the inset in Figure 3.5(a) demonstrates the retention time shift of a myoglobin peptic peptide ion, doubly-charged IRLFTGHPETL (31-41), upon addition of *m*-NBA: with 0.1% *m*-NBA, the peptide eluted at 4.3 min, while its elution time in the absence of *m*-NBA was 4.8 min. This observation is in agreement with the non-polar nature of *m*-NBA, resulting in stronger elution. Another possible explanation for the shortened peptide retention time is that *m*-NBA may adsorb to the non-polar column material, blocking peptide interactions sites and thus weakening the column retention ability.

To circumvent the problem of retention time shifting, as well as to avoid exposing the column to *m*-NBA, a post-column mixing tee and an additional syringe/pump were added to our LC set-up. Miladinovic *et al.* [47] introduced supercharging reagents directly into the ESI Taylor cone via a dual-sprayer ESI microchip and demonstrated average charge state increases for peptides and proteins. Their results suggest that the supercharging reaction can be accomplished on a short time scale, corresponding to ion formation from a droplet during the ESI process. Compared with their set-up, addition of supercharging reagents to the LC eluent through the post-column tee allowed much longer time for mixing with the analytes. Considering that *m*-NBA is quite viscous and dissolves poorly in water, *m*-NBA was dissolved in ACN and then transferred to the syringe for infusion. To ensure that the tee infusion flow rate was compatible

with the LC flow rate while maintaining ~0.1% *m*-NBA, the *m*-NBA concentration in ACN was kept low (5%). Figure 3.5(b) shows overlaid BPCs from LC/MS of  $\alpha$ -casein (top) and  $\beta$ -casein (bottom) peptic peptides with and without 0.1% *m*-NBA in the ESI solvent, as introduced via the post-column tee. The much improved overlap of BPCs generated with and without 0.1% *m*-NBA for each protein suggests that the retention time shifting issue was solved. Extracted ion chromatograms (EICs) for one peptide from each protein with and without 0.1% *m*-NBA (Figure 3.5(b) insets) confirm that retention times are unaffected when *m*-NBA is injected through the post-column tee. The *m*-NBA charge-enhancing effect reported in the preceding section was unchanged with the post-column addition set-up (data not shown). All remaining data in this Chapter were collected in this manner.

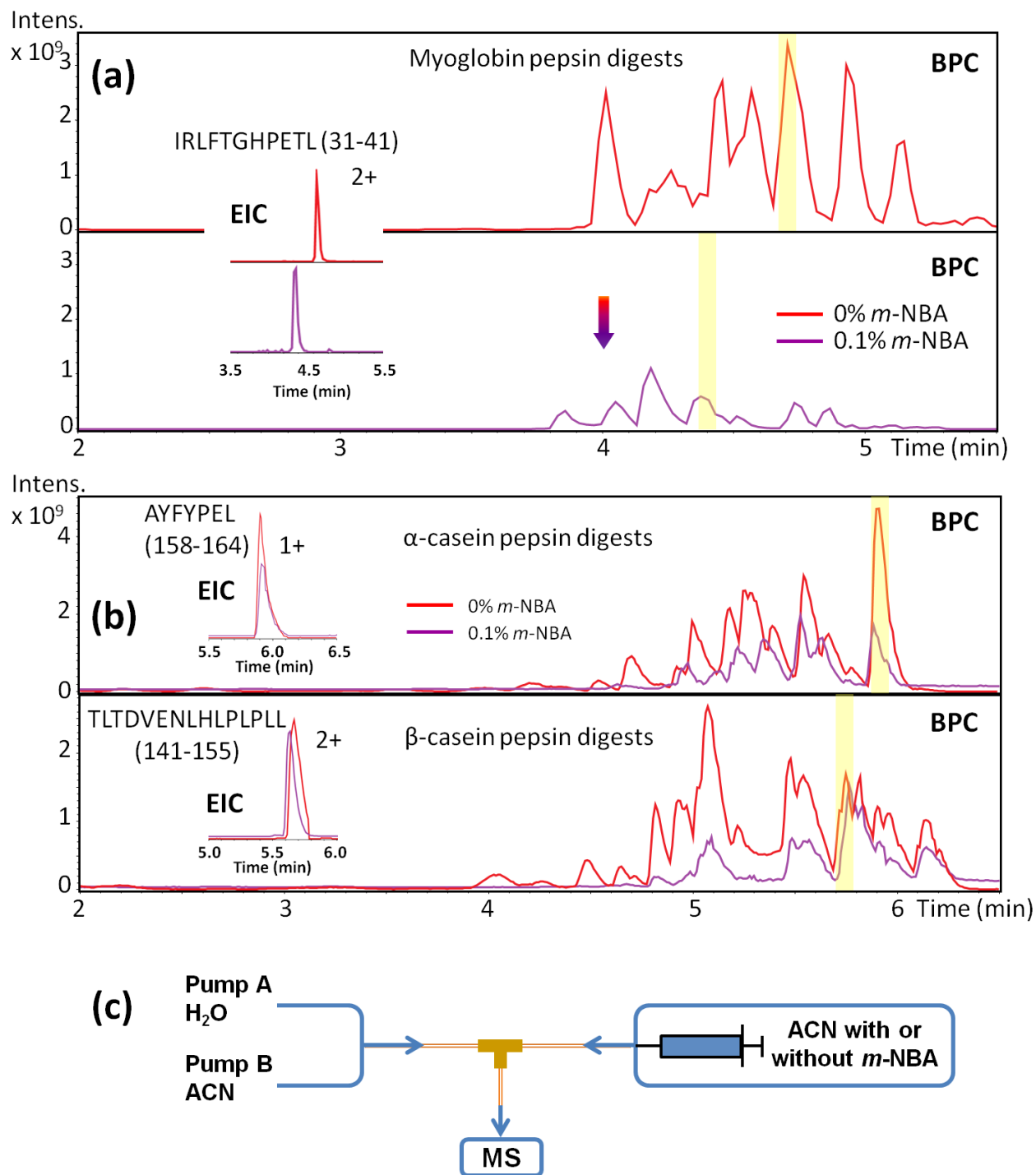


**Figure 3.5** (a) Base peak chromatograms from peptically digested myoglobin and extracted ion chromatograms for one peptide (inset) without (top) and with (bottom) 0.1% *m*-NBA in the mobile phase solvents. The shaded yellow areas on the BPCs indicate the retention time of the peptide in each case. (b) Base peak chromatograms from peptically digested  $\alpha$ -casein (top) and  $\beta$ -casein (bottom) and extracted ion chromatogram for one peptide from each protein (insets) without and with 0.1% *m*-NBA added through a post-column mixing tee. The latter set-up

eliminated retention time shifts. The shaded yellow areas on the overlaid BPCs indicate the same retention time of either peptide with and without 0.1% *m*-NBA. A simplified diagram of the latter set-up is shown in (c).

### 3.3.3 Supercharging with varying *m*-NBA concentrations and with other supercharging reagents

Including 0.1% *m*-NBA, five different concentrations were evaluated: 0, 0.05, 0.1, 0.2, and 0.4%. Figure 3.6(a) shows the average charge states of five myoglobin peptic peptides vs. *m*-NBA concentration, including NVWGKVEADIAGHGQEVL (13-30), IRLFTGHPETL (31-41), TALGGILKKKGHHEAEL (71-87), IIHVLHSHKHPGDFGADA (112-128), and FRNDIAAKYKELGFQG (139-154). With the mixing tee set-up for post-column addition, altering of *m*-NBA concentration was conveniently achieved by changing the flow rate of the infused *m*-NBA ACN solution. Notably, for all these five peptides, the average charge state increased steadily with increasing *m*-NBA concentration although not in the same manner. For peptides 13-30, 31-41, and 139-154, the average charge state dropped slightly as the *m*-NBA concentration increased from 0.1% to 0.2% and then stayed relatively unchanged as the *m*-NBA concentration doubled (to 0.4%). The average charge state of peptide 71-87 rose slightly at an *m*-NBA concentration of 0.2% compared with 0.1%; however, further increase to 0.4% did not boost the average charges state further. Interestingly, the average charge state of peptide 112-128 fluctuated more significantly but reached a maximum value at 0.1% *m*-NBA. One factor possibly influencing these results is the notable signal abundance decrease with increasing *m*-NBA concentration. The ESI efficiency may be lowered in the presence of *m*-NBA due to the increased viscosity of the solvent. Because the steepest increase in average charge state was observed up to 0.1% *m*-NBA, and to avoid signal abundance loss, 0.1% *m*-NBA appeared optimal also for post-column addition.

We also compared the charge-enhancing effect of *m*-NBA for peptic peptides with three other aprotic supercharging reagents; DMSO, PC, and sulfolane (Figure 3.6(b)). The concentrations of these reagents were chosen according to the literature [36-39, 46]. For the

same five myoglobin peptic peptides, 0.1% *m*-NBA showed the strongest overall charge-enhancing effect, with the exception of the peptide 139-154, which displayed the highest charge-state increase when electrosprayed with 150 mM sulfolane. However; 0.1% *m*-NBA was still the second most effective supercharging reagent for this peptide. Both 5% PC and 20% DMSO were inferior to 0.1% *m*-NBA and 150 mM sulfolane for supercharging peptic peptides; their presence did not generally alter the charge-state distribution for the examined peptides.

When further investigating DMSO as a supercharging reagent for peptic peptides, we observed that, at our ESI conditions, a minimum concentration of 20% DMSO was necessary to induce peptide supercharging. However; the supercharging effect of DMSO was quite varied for different peptides, independent of concentration. For example, addition of DMSO did not alter the charge-state distribution of myoglobin peptic peptides 13-30 and 31-41 (Figure 3.7(a)). With 10% DMSO, both charge increase and decrease was observed for a variety of peptides from pepsin digests of myoglobin and  $\alpha$ -casein S1 (Figure 3.7(b)), similar to previous results from Komives *et al.* [46].

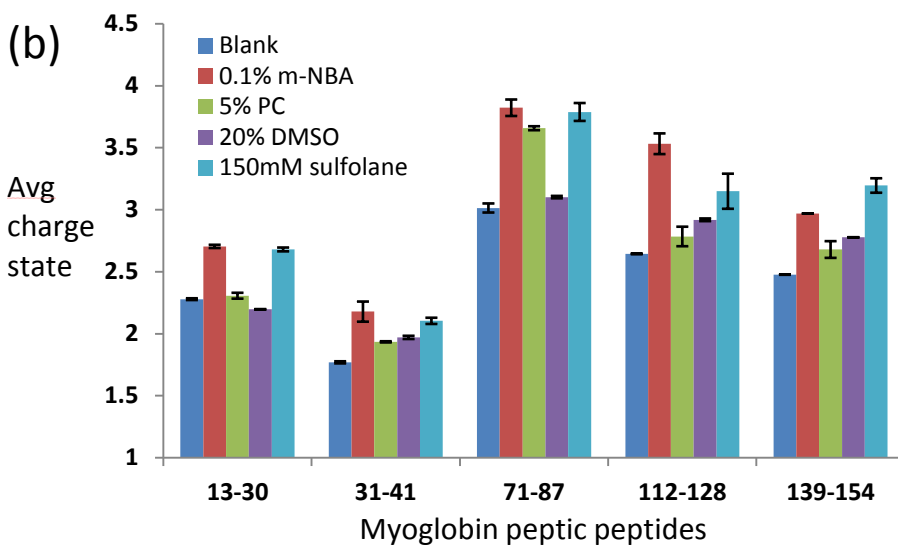
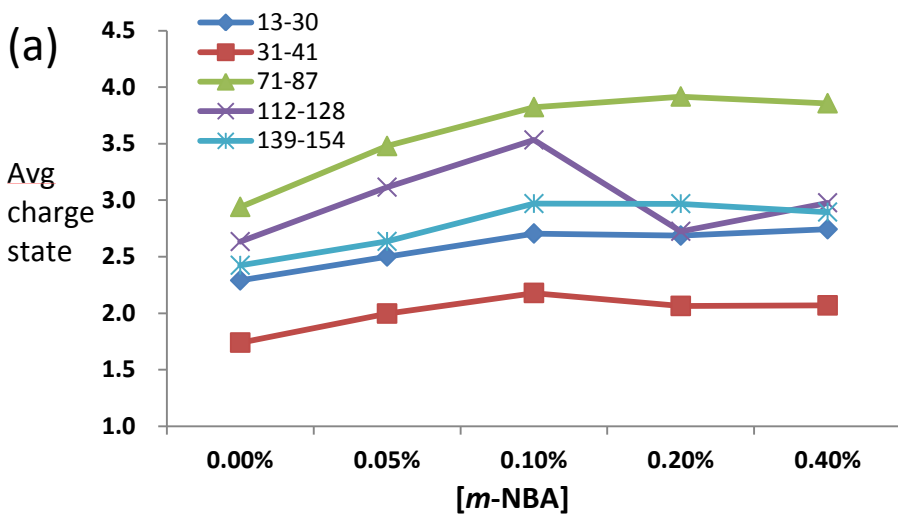


**Figure 3.6** Average charge states of five myoglobin peptic peptides (a) as a function of *m*-NBA concentration in the ESI solvent and (b) when no supercharging reagent, 0.1% *m*-NBA, 5% propylene carbonate (PC), 20% DMSO, or 150 mM sulfolane were added to the ESI solvent, respectively.

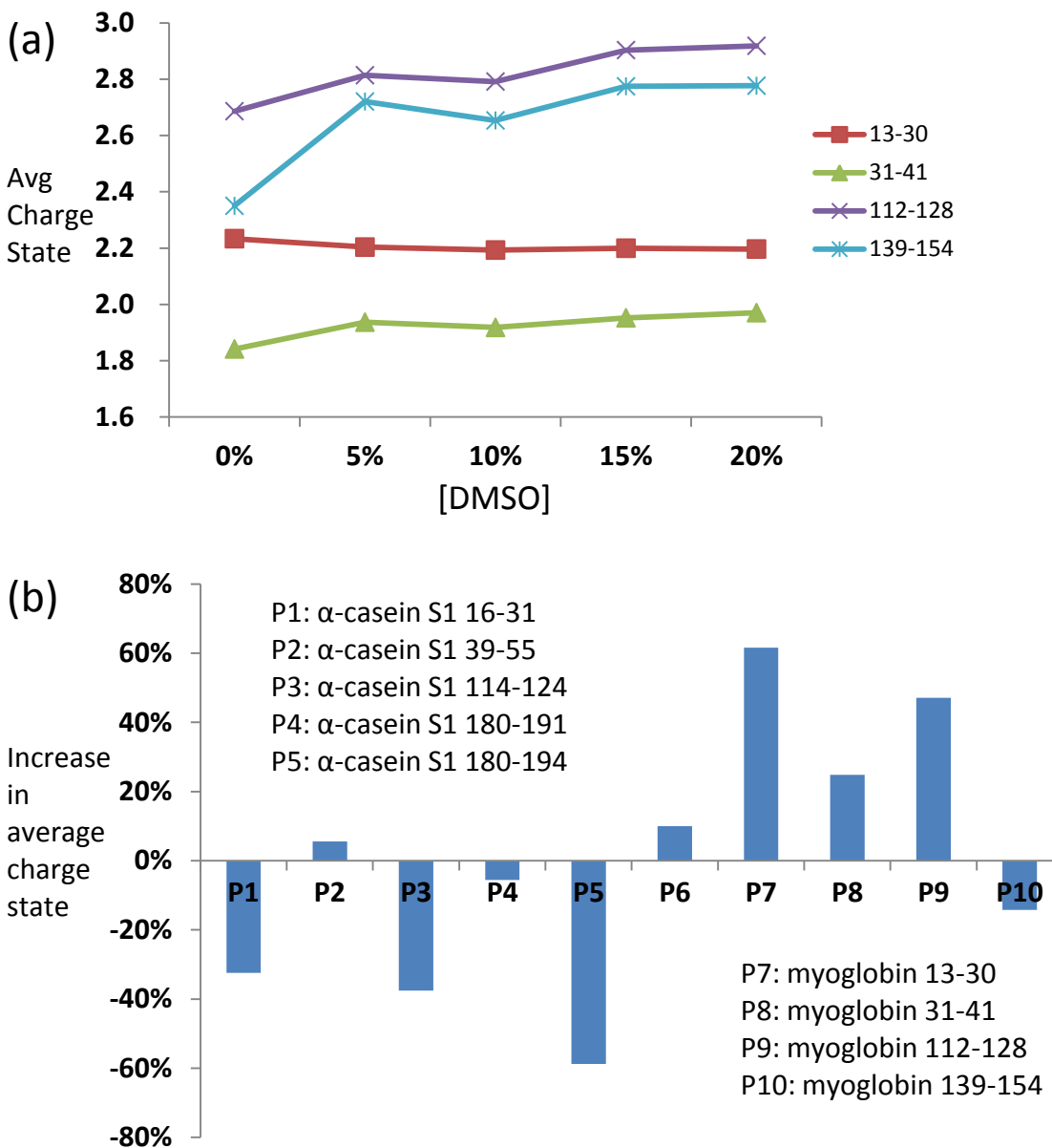


**Figure 3.7** (a) Average charge states of four myoglobin peptic peptides as a function of DMSO concentration in the ESI solvent. (b) Average charge state increase percentages for ten peptic peptides (P1-P6 from  $\alpha$ -casein, P7-P10 from myoglobin) upon addition of 10% DMSO into the ESI solvent.

### 3.3.4 Supercharging in LC ECD MS/MS of peptic peptides

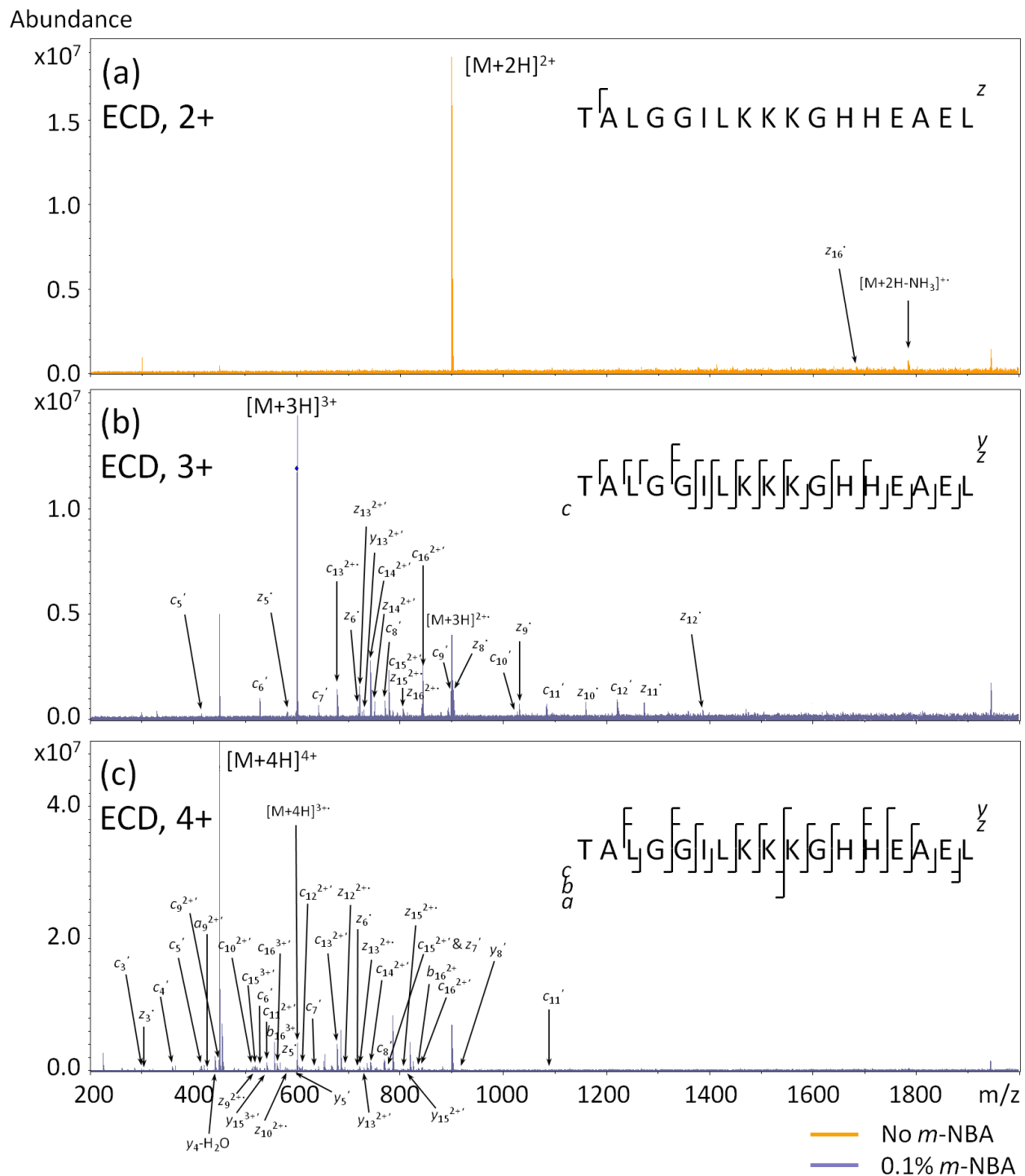


**Figure 3.8** ECD MS/MS spectra of the peptic peptide TALGGILKKKGHHEAEL (71-87) from myoglobin in precursor ion charge states (a) 2+, (b) 3+, and (c) 4+. The ECD MS/MS spectrum for the doubly charged precursor ions was collected without *m*-NBA in the ESI solution whereas the spectra for the triply and quadruply charged precursor ions were collected with 0.1% *m*-NBA

in the ESI solutions.

Charge enhancement of peptic peptides via supercharging was combined with ECD LC/MS/MS to assess effects on ECD fragmentation efficiency and peptide sequence coverage. ECD spectra of the doubly, triply, and quadruply charged peptide TALGGILKKKGHHEAEL from pepsin digestion of myoglobin are shown in Figure 3.8. For doubly charged precursor ions (Fig. 3.8 (a)), the ECD fragmentation efficiency was 12% and the peptide sequence coverage was only 6%. Due to the charge reduction occurring upon electron capture/transfer, ECD/ETD of 2+ ions only generate one fragment ion for each bond cleavage with the complementary fragment being neutral, thus preventing detection of complementary ion pairs. For peptide identification, the absence of such complementary fragments decreases peptide identification scores [25]. ECD of the triply charged precursor ions (Fig. 3.8 (b)) resulted in greatly improved fragmentation efficiency (72%) and peptide sequence coverage (100%) compared with the 2+ precursor ions: a total of 16 (out of 16) inter-residue bonds were cleaved, 7 of which yielded complementary *c/z* ion pairs. ECD of quadruply charged precursor ions for this peptide was only feasible upon addition of 0.1% *m*-NBA. The resulting spectrum (Fig. 3.8 (c)) showed extensive (though not the most extensive) fragmentation efficiency (63%) and sequence coverage (94%). The lower performance for the 4+ charge state may be attributed to its lower abundance (20.0%) compared with the 3+ charge state (37.9%) in the presence of 0.1% *m*-NBA. However; ECD of the quadruply charged precursor ions yielded 2 unique *c*-type ions ( $c_3'$ ,  $c_4'$ ) and 2 unique *z*-type ions ( $z_3^\bullet$ ,  $z_7^\bullet$ ) compared with ECD of the 3+ ions; thus, maximum sequence information is obtained by combining these spectra. Additional LC ECD MS/MS results for myoglobin peptic peptides are listed in Table 3.3. The precursor ion charge states were automatically selected with the AutoMSMS setting in SolariXControl. These pepsin digests were analyzed both with and without 0.1% *m*-NBA. In the absence of *m*-NBA, doubly charged precursor ions were selected for ECD (5 out of 5) and only one out of 5 peptides showed any ion population in a charge state higher than 2+ (TALGGILKKKGHHEAEL, 3+ at 47.1%). The ECD fragmentation efficiency and peptide sequence coverage for these 2+ precursor ions were below 25% and 50%,

respectively. When 0.1% *m*-NBA was added to the ESI solution, the shift in the charge-state distribution resulted in more 3+ precursor ions being selected for ECD. As expected, the shift to more triply charged peptide ions, in turn, resulted in more efficient ECD. For example, the peptide NVWGKVEADIAGHGQEV L showed a charge-state distribution of 71.2% 2+ and 28.8% 3+ compared with 80.5% 2+ and 19.5% 3+ in the absence of *m*-NBA. The total abundance of 3+ precursor ions and resulting product ions post dissociation was ~14 times higher than that of 2+ precursor ions ( $1.3 \times 10^8$  vs.  $9.6 \times 10^6$ ) upon addition of *m*-NBA. The resulting peptide sequence coverage was greatly improved from 53% (no *m*-NBA) to 100% (0.1% *m*-NBA). The peptide FTGHPETL is smaller in size and failed to generate a charge state higher than 2+ even in the presence of *m*-NBA. However, the 2+ ion abundance for this peptide was increased from 15.2% to 27.5% upon addition of 0.1% *m*-NBA, resulting in doubled sequence coverage (86% vs. 43%). Similarly, for the peptide FRNDIAAKYKELGFQG, the presence of 0.1% *m*-NBA increased the 3+ precursor ion abundance and, consequently, resulted in both improved fragmentation efficiency and peptide sequence coverage. Overall, fragmentation of  $\geq 3+$  peptide ions resulted in greater ECD efficiency and higher peptide sequence coverage. The *m*-NBA-generated charge enhancement increased the probability of  $\geq 3+$  peptide ions to be selected for fragmentation.

**Table 3.3** Example myoglobin peptic peptides observed in LC ECD MS/MS experiments with and without 0.1% *m*-NBA in the ESI solvent. Peptide abundances were normalized to charge. “Total analyte abd.” refers to the summed abundance of the precursor ions and ECD product ions post dissociation. The shift to more triply- (or higher) charged peptide ions is highly beneficial for both ECD fragmentation efficiency and peptide sequence coverage.

Myoglobin peptic peptides	0% <i>m</i> -NBA					0.1% <i>m</i> -NBA				
	Charge state distribution	Frag CS	Frag eff.	Seq cov	Total analyte abd.	Charge state distribution	Frag CS	Frag eff.	Seq cov	Total analyte abd.
NVWVGKVEADIAGHGQEVL	2+ (80.5%)	2+	20%	47%	1.1x10 <sup>8</sup>	2+ (71.2%)	2+	21%	41%	6.3x10 <sup>7</sup>
	3+ (19.5%)	3+	52%	53%	9.6x10 <sup>6</sup>	3+ (28.8%)	3+	59%	100%	1.3x10 <sup>8</sup>
FTGHPETL	1+ (84.8%)					1+ (72.5%)				
	2+ (15.2%)	2+	21%	43%	3.5x10 <sup>7</sup>	2+ (27.5%)	2+	24%	86%	9.0x10 <sup>7</sup>
TALGGILKKKGHHEAEL	2+ (40.8%)	2+	12%	6%	5.9x10 <sup>6</sup>	2+ (41.7%)				
	3+ (47.1%)	3+	68%	87%	2.6x10 <sup>7</sup>	3+ (37.9%)	3+	72%	100%	2.6x10 <sup>7</sup>
	4+ (12.1%)					4+ (20.0%)	4+	63%	94%	2.1x10 <sup>7</sup>
						5+ (0.4%)				
FRNDIAA	1+ (93.6%)					1+ (72.7%)				
	2+ (6.4%)	2+	0%	0%	3.1x10 <sup>6</sup>	2+ (27.3%)	2+	13%	67%	1.4x10 <sup>7</sup>
FRNDIAAKYKELGFQG	2+ (65.0%)	2+	17%	47%	1.3x10 <sup>8</sup>	2+ (57.8%)	2+	21%	47%	6.6x10 <sup>7</sup>
	3+ (35.0%)	3+	60%	86%	7.2x10 <sup>7</sup>	3+ (37.7%)	3+	71%	100%	1.8x10 <sup>8</sup>
						4+ (4.5%)				

### 3.3.5 *m*-NBA supercharging in HDX LC/MS

When combining ESI supercharging with bottom-up HDX MS, it is of great importance to ensure that no significant HDX information is lost due to H/D scrambling or back-exchange. *m*-NBA contains labile hydrogens and functional groups that may allow hydrogen bonding, aromatic interaction, and/or ionic interaction with the nitro group. Thus, its effect on overall HDX performance needs to be evaluated.

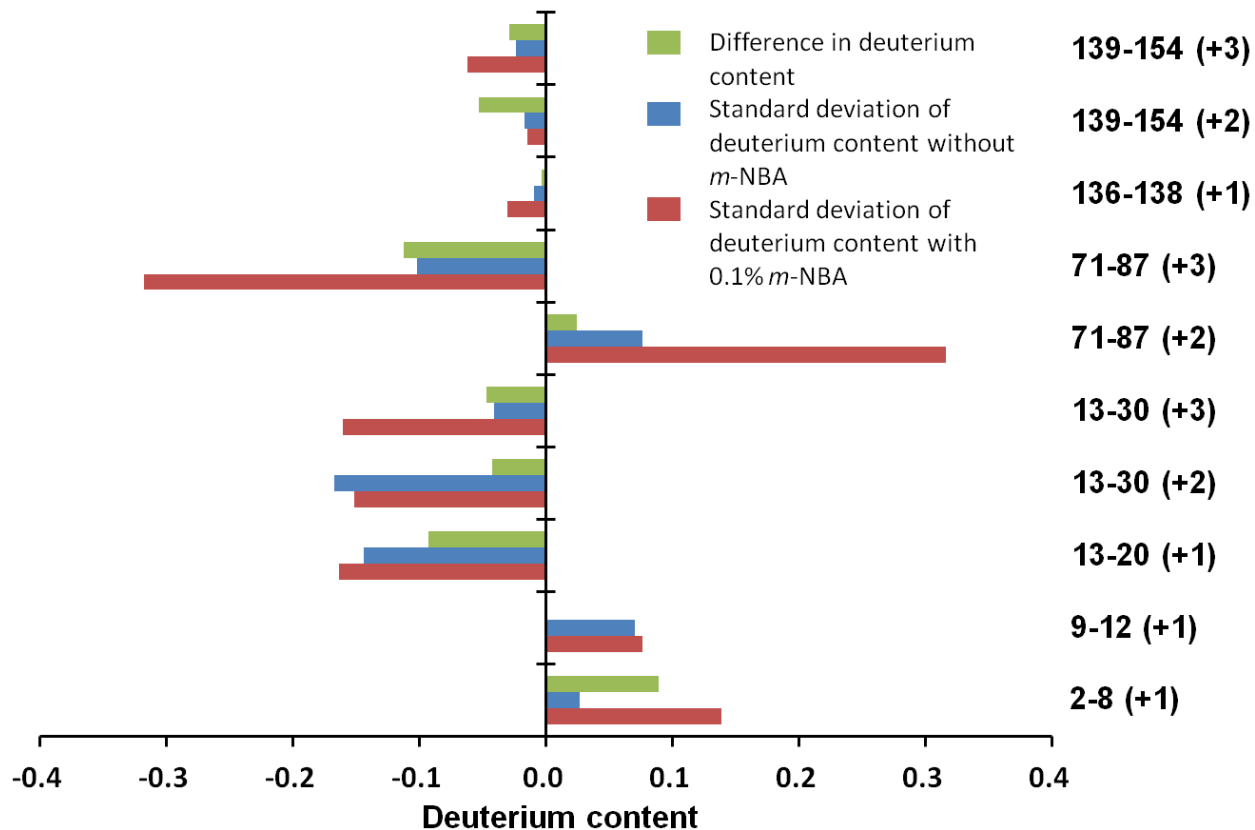


**Figure 3.9** Differences in deuterium content for ten myoglobin peptic peptides in HDX LC/MS experiments with and without 0.1% *m*-NBA (green bars). The HDX incubation time was 10 min. Deuterium content standard deviations from triplicate measurements without and with *m*-NBA (blue and red bars, respectively). The deuterium content difference was smaller than the standard deviation for each peptide, except the peptide 139-154 (2+), indicating that the use of *m*-NBA had a minor effect on peptic peptide deuterium uptake levels.

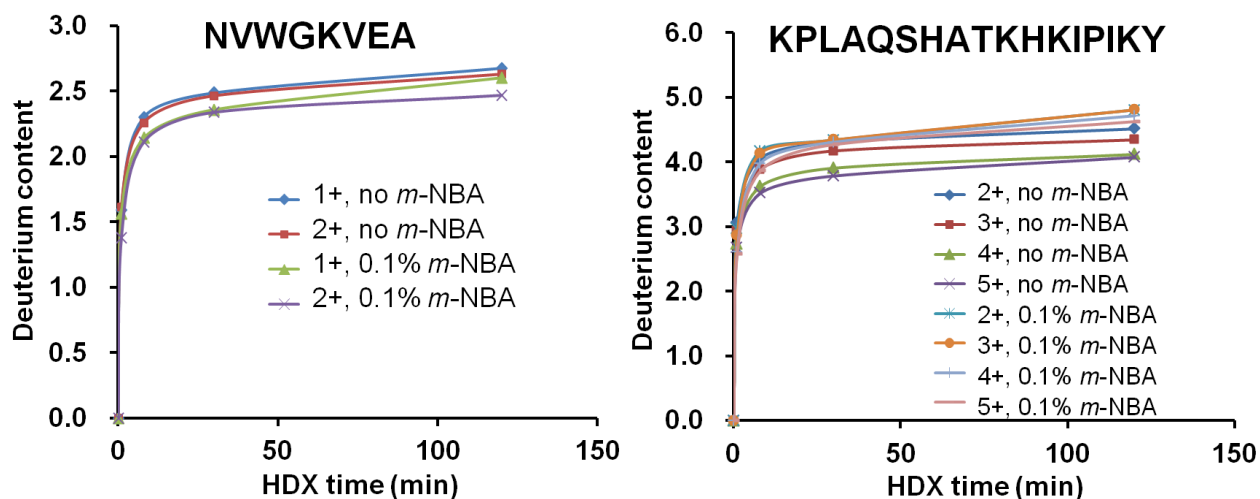


**Figure 3.10** Deuterium uptake curves for two myoglobin peptic peptides, NVWGKVEA (13-20) (left) and KPLAQSHATKHKIPIKY (88-104) (right), at multiple charge states in the absence and presence of 0.1% *m*-NBA in the ESI solvent. Similar HDX behaviors were observed for the same peptide with or without *m*-NBA.

Myoglobin peptic peptides were analyzed by HDX LC/MS with and without *m*-NBA (0.1%). The averaged deuterium contents and standard deviations were calculated based on triplicate measurements. Nine out of ten observed peptide ions (corresponding to 6 different peptides) showed deuterium content differences lower than the standard deviation between no *m*-NBA and 0.1% *m*-NBA, except the doubly charged peptide 139-154 (Figure 3.9). This observation indicates that addition of 0.1% *m*-NBA to the ESI solution did not change peptide deuterium levels beyond the experimental error. The deuterium uptake curves for two peptic peptides, NVWGKVEA (myoglobin 13-20) and KPLAQSHATKHKIPIKY (myoglobin 88-104), with different charge states for HDX incubation times ranging from 0 to 120 min are shown in Figure 3.10. Similarly, no significant variation in deuterium incorporation is observed in HDX LC/MS with and without 0.1% *m*-NBA.

We also explored whether introduction of *m*-NBA directly into the LC solvents vs. via the post-column tee differentially affects deuterium back exchange. Figure 3.11 shows the corresponding results for three myoglobin peptic peptides; 2-8, 13-30, and 139-154. A control experiment without *m*-NBA was also conducted in each case. For the peptide 2-8, only singly charged ions were observed with unvarying (within error) deuterium contents between the three

scenarios (0.1% *m*-NBA introduced pre- or post-column, and no *m*-NBA). For the 2+ and 3+ ions of the peptide 13-30, the deuterium content with *m*-NBA in the LC solvent was 3% higher than for the other cases. However, a deuteration level difference below 5% is typically insignificant [3, 5, 6]. For the peptide 139-154, nearly identical deuteration levels were observed between the three cases. Overall, neither the presence of 0.1% *m*-NBA, nor the manner of its introduction, appears to have a significant effect on peptic peptide deuterium levels.

It is worth noting, however, that higher charge-state peptide ions showed higher deuterium loss compared with their lower charge-state counterparts, e.g., the peptide 13-30, 3+ vs. 2+ ions. This effect is probably due to elevated kinetic energy at higher charge and lower barriers to proton migration during the desolvation process in the ion source. Similarly, limiting peptic peptide charge states to  $\leq 3+$  has been previously suggested for LC ECD/ETD experiments [23].

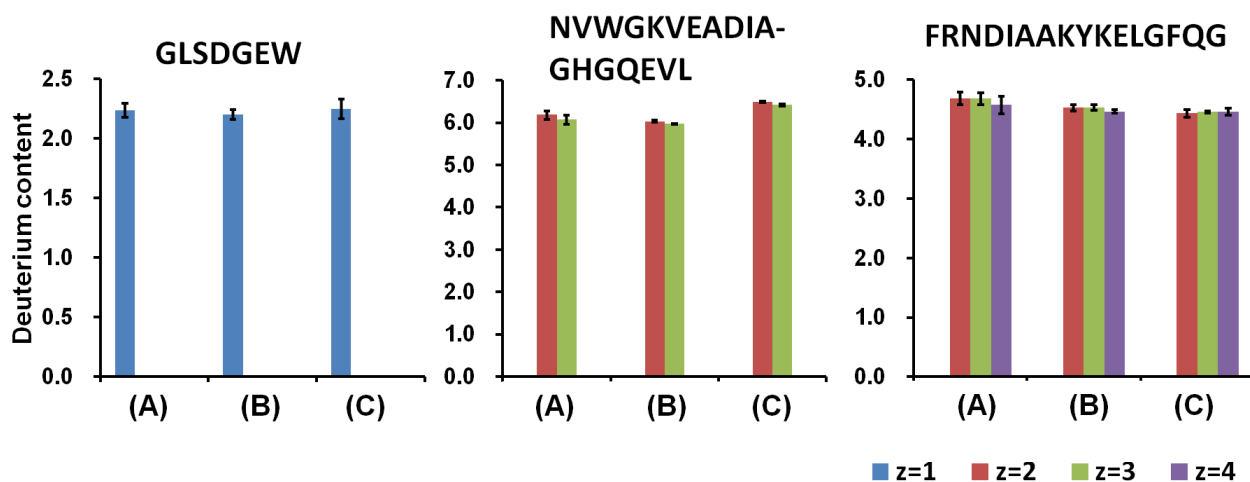


**Figure 3.11** Deuterium content for three myoglobin peptic peptides, GLSDGEW (2-8), NVWGKVEADIA-GHGQEVL (13-30), and FRNDIAAKYKELGFQG (139-154), without *m*-NBA (A), and with 0.1% *m*-NBA introduced after the analytical column (B), or directly into the LC mobile phase (C). Bars in different colors indicate different charge states.

### 3.4 Conclusion

We demonstrate the charge enhancing effect of *m*-NBA for a variety of peptic peptides from myoglobin, cytochrome c,  $\alpha$ -casein (S1), and  $\beta$ -casein. With the addition of as low as 0.1% *m*-NBA into the LC mobile-phase solvents, we achieved significant charge-state shifts for peptic

peptides in a bottom-up HDX LC/MS workflow, although adverse chromatographic effects were observed. Separation in the presence of 0.1% *m*-NBA generally decreased peptide retention times compared with the absence of *m*-NBA; however, these retention time shifts were circumvented by implementing post-column addition of *m*-NBA through an external mixing tee. With this device, the *m*-NBA concentration in the ESI solution can be changed simply by altering the infusion flow rate. 0.1% *m*-NBA appeared to be an optimal concentration in both implementations in terms of compromising between effective supercharging, and acceptable signal-to-noise ratios. We found that DMSO and PC were not effective supercharging reagents for peptic peptides. Sulfolane was also explored for charge enhancement of peptic peptides and was found to be similarly effective as *m*-NBA. As verified by LC ECD MS/MS experiments, *m*-NBA-based supercharging generates more triply (or higher) charged peptic peptide ions compared with the absence of *m*-NBA, resulting in enhanced ECD efficiency and peptide sequence coverage. Finally, we evaluated the effect of 0.1% *m*-NBA on the detected deuterium uptake levels of peptic peptide ions in HDX LC/MS experiments. The presence of 0.1% *m*-NBA did not skew the results. One advantage of sulfolane-based supercharging, despite the required higher concentration compared with *m*-NBA (150 mM or 1.43%, vs. 0.1%), is that addition of this supercharging reagent into the ESI solvent is not expected to alter deuterium content of deuterated peptides due to the absence of labile hydrogen in sulfolane. Our results suggest that both *m*-NBA and sulfolane can efficiently improve charging of peptic peptides in a bottom-up HDX LC/MS workflow. However; higher charge-state peptide ions were subjected to more deuterium loss compared with their lower charge counterparts, thus suggesting that a charge state of 3+ for peptic peptides is ideal in HDX ECD/ETD MS/MS.

### 3.5 Acknowledgements

The authors acknowledge financial support for this work from NSF grant CHE1609840. Dr. Phillip McClory is acknowledged for technical assistance and helpful suggestions.

### 3.6 References

1. Hoofnagle, A.N., Resing, K.A., Ahn, N.G.: Protein Analysis by Hydrogen Exchange Mass

- Spectrometry. *Annu. Rev. Biophys. Biomol. Struct.* **32**, 1-25 (2003)
2. Konermann, L., Pan, J., Liu, Y.-H.: Hydrogen exchange mass spectrometry for studying protein structure and dynamics. *Chem. Soc. Rev.* **40**, 1224-1234 (2011)
  3. Wales, T.E., Engen, J.R.: Hydrogen exchange mass spectrometry for the analysis of protein dynamics. *Mass Spectrom. Rev.* **25**, 158-170 (2006)
  4. Wales, T.E., Eggertson, M.J., Engen, J.R.: Considerations in the Analysis of Hydrogen Exchange Mass Spectrometry Data. *Methods Mol. Biol.* **1007**, 263-288 (2013)
  5. Zhang, H.-M., Bou-Assaf, G.M., Emmett, M.R., Marshall, A.G.: Fast reversed-phase liquid chromatography to reduce back exchange and increase throughput in H/D exchange monitored by FT-ICR mass spectrometry. *J. Am. Soc. Mass. Spectrom.* **20**, 520-524 (2009)
  6. Valeja, S.G., Emmett, M.R., Marshall, A.G.: Polar Aprotic Modifiers for Chromatographic Separation and Back-Exchange Reduction for Protein Hydrogen/Deuterium Exchange Monitored by Fourier Transform Ion Cyclotron Resonance Mass Spectrometry. *J. Am. Soc. Mass. Spectrom.* **23**, 699-707 (2012)
  7. Rand, K.D.: Pinpointing changes in higher-order protein structure by hydrogen/deuterium exchange coupled to electron transfer dissociation mass spectrometry. *Int. J. Mass spectrom.* **338**, 2-10 (2013)
  8. Li, J., Rodnin, M.V., Ladokhin, A.S., Gross, M.L.: Hydrogen–Deuterium Exchange and Mass Spectrometry Reveal the pH-Dependent Conformational Changes of Diphtheria Toxin T Domain. *Biochemistry.* **53**, 6849-6856 (2014)
  9. Cravello, L., Lascoux, D., Forest, E.: Use of different proteases working in acidic conditions to improve sequence coverage and resolution in hydrogen/deuterium exchange of large proteins. *Rapid Commun. Mass Spectrom.* **17**, 2387-2393 (2003)
  10. Zhang, H.-M., Kazazic, S., Schaub, T.M., Tipton, J.D., Emmett, M.R., Marshall, A.G.: Enhanced Digestion Efficiency, Peptide Ionization Efficiency, and Sequence Resolution for Protein Hydrogen/Deuterium Exchange Monitored by Fourier Transform Ion Cyclotron Resonance Mass Spectrometry. *Anal. Chem.* **80**, 9034-9041 (2008)
  11. Wang, G., Kaltashov, I.A.: Approach to Characterization of the Higher Order Structure of Disulfide-Containing Proteins Using Hydrogen/Deuterium Exchange and Top-Down Mass Spectrometry. *Anal. Chem.* **86**, 7293-7298 (2014)
  12. Pan, J., Han, J., Borchers, C.H., Konermann, L.: Hydrogen/Deuterium Exchange Mass Spectrometry with Top-Down Electron Capture Dissociation for Characterizing Structural Transitions of a 17 kDa Protein. *J. Am. Chem. Soc.* **131**, 12801-12808 (2009)
  13. Rand, K.D., Zehl, M., Jørgensen, T.J.D.: Measuring the Hydrogen/Deuterium Exchange of Proteins at High Spatial Resolution by Mass Spectrometry: Overcoming Gas-Phase Hydrogen/Deuterium Scrambling. *Acc. Chem. Res.* **47**, 3018-3027 (2014)
  14. Rand, K.D., Jørgensen, T.J.D.: Development of a Peptide Probe for the Occurrence of Hydrogen (1H/2H) Scrambling upon Gas-Phase Fragmentation. *Anal. Chem.* **79**, 8686-8693 (2007)
  15. Bache, N., Rand, K.D., Roepstorff, P., Ploug, M., Jørgensen, T.J.D.: Hydrogen atom scrambling in selectively labeled anionic peptides upon collisional activation by MALDI

- tandem time-of-flight mass spectrometry. *J. Am. Soc. Mass. Spectrom.* **19**, 1719-1725 (2008)
16. Rand, K.D., Adams, C.M., Zubarev, R.A., Jørgensen, T.J.D.: Electron Capture Dissociation Proceeds with a Low Degree of Intramolecular Migration of Peptide Amide Hydrogens. *J. Am. Chem. Soc.* **130**, 1341-1349 (2008)
  17. Zehl, M., Rand, K.D., Jensen, O.N., Jørgensen, T.J.D.: Electron Transfer Dissociation Facilitates the Measurement of Deuterium Incorporation into Selectively Labeled Peptides with Single Residue Resolution. *J. Am. Chem. Soc.* **130**, 17453-17459 (2008)
  18. Abzalimov, R.R., Kaplan, D.A., Easterling, M.L., Kaltashov, I.A.: Protein conformations can be probed in top-down HDX MS experiments utilizing electron transfer dissociation of protein ions without hydrogen scrambling. *J. Am. Soc. Mass. Spectrom.* **20**, 1514-1517 (2009)
  19. Zubarev, R.A.: Reactions of polypeptide ions with electrons in the gas phase. *Mass Spectrom. Rev.* **22**, 57-77 (2003)
  20. McLuckey, S.A., Goeringer, D.E.: SPECIAL FEATURE: TUTORIAL Slow Heating Methods in Tandem Mass Spectrometry. *J. Mass Spectrom.* **32**, 461-474 (1997)
  21. Pan, J., Han, J., Borchers, C.H., Konermann, L.: Electron Capture Dissociation of Electrosprayed Protein Ions for Spatially Resolved Hydrogen Exchange Measurements. *J. Am. Chem. Soc.* **130**, 11574-11575 (2008)
  22. Chi, A., Huttenhower, C., Geer, L.Y., Coon, J.J., Syka, J.E.P., Bai, D.L., Shabanowitz, J., Burke, D.J., Troyanskaya, O.G., Hunt, D.F.: Analysis of phosphorylation sites on proteins from *Saccharomyces cerevisiae* by electron transfer dissociation (ETD) mass spectrometry. *Proc. Natl. Acad. Sci.* **104**, 2193 (2007)
  23. Rand, K.D., Zehl, M., Jensen, O.N., Jørgensen, T.J.D.: Protein Hydrogen Exchange Measured at Single-Residue Resolution by Electron Transfer Dissociation Mass Spectrometry. *Anal. Chem.* **81**, 5577-5584 (2009)
  24. Cooper, H.J., Håkansson, K., Marshall, A.G.: The role of electron capture dissociation in biomolecular analysis. *Mass Spectrom. Rev.* **24**, 201-222 (2005)
  25. Kalli, A., Håkansson, K.: Comparison of the Electron Capture Dissociation Fragmentation Behavior of Doubly and Triply Protonated Peptides from Trypsin, Glu-C, and Chymotrypsin Digestion. *J. Proteome Res.* **7**, 2834-2844 (2008)
  26. Kjeldsen, F., Giessing, A.M.B., Ingrell, C.R., Jensen, O.N.: Peptide Sequencing and Characterization of Post-Translational Modifications by Enhanced Ion-Charging and Liquid Chromatography Electron-Transfer Dissociation Tandem Mass Spectrometry. *Anal. Chem.* **79**, 9243-9252 (2007)
  27. Zhurov, K.O., Fornelli, L., Wodrich, M.D., Laskay, Ü.A., Tsybin, Y.O.: Principles of electron capture and transfer dissociation mass spectrometry applied to peptide and protein structure analysis. *Chem. Soc. Rev.* **42**, 5014-5030 (2013)
  28. Pitteri, S.J., Chrisman, P.A., McLuckey, S.A.: Electron-Transfer Ion/Ion Reactions of Doubly Protonated Peptides: Effect of Elevated Bath Gas Temperature. *Anal. Chem.* **77**, 5662-5669 (2005)

29. Swaney, D.L., McAlister, G.C., Wirtala, M., Schwartz, J.C., Syka, J.E.P., Coon, J.J.: Supplemental Activation Method for High-Efficiency Electron-Transfer Dissociation of Doubly Protonated Peptide Precursors. *Anal. Chem.* **79**, 477-485 (2007)
30. Iavarone, A.T., Jurchen, J.C., Williams, E.R.: Supercharged Protein and Peptide Ions Formed by Electrospray Ionization. *Anal. Chem.* **73**, 1455-1460 (2001)
31. Iavarone, A.T., Williams, E.R.: Supercharging in electrospray ionization: effects on signal and charge. *Int. J. Mass spectrom.* **219**, 63-72 (2002)
32. Iavarone, A.T., Williams, E.R.: Mechanism of Charging and Supercharging Molecules in Electrospray Ionization. *J. Am. Chem. Soc.* **125**, 2319-2327 (2003)
33. Going, C.C., Williams, E.R.: Supercharging with m-Nitrobenzyl Alcohol and Propylene Carbonate: Forming Highly Charged Ions with Extended, Near-Linear Conformations. *Anal. Chem.* **87**, 3973-3980 (2015)
34. Sterling, H.J., Daly, M.P., Feld, G.K., Thoren, K.L., Kintzer, A.F., Krantz, B.A., Williams, E.R.: Effects of supercharging reagents on noncovalent complex structure in electrospray ionization from aqueous solutions. *J. Am. Soc. Mass. Spectrom.* **21**, 1762-1774 (2010)
35. Sterling, H.J., Kintzer, A.F., Feld, G.K., Cassou, C.A., Krantz, B.A., Williams, E.R.: Supercharging Protein Complexes from Aqueous Solution Disrupts their Native Conformations. *J. Am. Soc. Mass. Spectrom.* **23**, 191-200 (2012)
36. Zhang, J., Loo, R.R.O., Loo, J.A.: Increasing fragmentation of disulfide-bonded proteins for top-down mass spectrometry by supercharging. *Int. J. Mass spectrom.* **377**, 546-556 (2015)
37. Douglass, K.A., Venter, A.R.: Investigating the Role of Adducts in Protein Supercharging with Sulfolane. *J. Am. Soc. Mass. Spectrom.* **23**, 489-497 (2012)
38. Sterling, H.J., Prell, J.S., Cassou, C.A., Williams, E.R.: Protein Conformation and Supercharging with DMSO from Aqueous Solution. *J. Am. Soc. Mass. Spectrom.* **22**, 1178 (2011)
39. Ogorzalek Loo, R.R., Lakshmanan, R., Loo, J.A.: What Protein Charging (and Supercharging) Reveal about the Mechanism of Electrospray Ionization. *J. Am. Soc. Mass. Spectrom.* **25**, 1675-1693 (2014)
40. Teo, C.A., Donald, W.A.: Solution Additives for Supercharging Proteins beyond the Theoretical Maximum Proton-Transfer Limit in Electrospray Ionization Mass Spectrometry. *Anal. Chem.* **86**, 4455-4462 (2014)
41. Zenaidee, M.A., Donald, W.A.: Extremely supercharged proteins in mass spectrometry: profiling the pH of electrospray generated droplets, narrowing charge state distributions, and increasing ion fragmentation. *Analyst.* **140**, 1894-1905 (2015)
42. Zenaidee, M.A., Donald, W.A.: Electron capture dissociation of extremely supercharged protein ions formed by electrospray ionisation. *Anal. Methods.* **7**, 7132-7139 (2015)
43. Li, X., Li, Z., Xie, B., Sharp, J.S.: Supercharging by m-NBA Improves ETD-Based Quantification of Hydroxyl Radical Protein Footprinting. *J. Am. Soc. Mass. Spectrom.* **26**, 1424-1427 (2015)
44. Sterling, H.J., Williams, E.R.: Real-Time Hydrogen/Deuterium Exchange Kinetics via

- Supercharged Electrospray Ionization Tandem Mass Spectrometry. *Anal. Chem.* **82**, 9050-9057 (2010)
45. Going, C.C., Xia, Z., Williams, E.R.: Real-time HD Exchange Kinetics of Proteins from Buffered Aqueous Solution with Electrothermal Supercharging and Top-Down Tandem Mass Spectrometry. *J. Am. Soc. Mass. Spectrom.* **27**, 1019-1027 (2016)
  46. Meyer, J.G., A. Komives, E.: Charge State Coalescence During Electrospray Ionization Improves Peptide Identification by Tandem Mass Spectrometry. *J. Am. Soc. Mass. Spectrom.* **23**, 1390-1399 (2012)
  47. Miladinović, S.M., Fornelli, L., Lu, Y., Piech, K.M., Girault, H.H., Tsybin, Y.O.: In-Spray Supercharging of Peptides and Proteins in Electrospray Ionization Mass Spectrometry. *Anal. Chem.* **84**, 4647-4651 (2012)

## Chapter 4

### The Presence of *b* Ions in Electron Capture/Transfer Dissociation (ECD/ETD) of Supercharged Peptides

#### 4.1 Introduction

Electron capture dissociation (ECD) is a powerful tandem mass spectrometry (MS/MS) technique that involves reactions between multiply charged analyte cations and low-energy (<1 eV) electrons [1-5]. ECD of multiply protonated polypeptide ions can provide valuable sequence information in proteomics, particularly for peptides and proteins containing labile post-translational modifications (PTMs) [5-7]. By contrast conventional slow-heating activation methods such as the most commonly employed MS/MS approach, collision induced dissociation (CID), often fail to locate such PTMs as they are preferentially lost [8-10].

The primary product ions in ECD of peptides and proteins are *c'*- and *z'*-type fragment ions derived from cleavage of backbone N-C<sub>α</sub> bonds [2, 11], complementary to the *b*- and *y'*-type ions that are predominant in CID MS/MS spectra [12, 13]. In addition, a minor ECD fragmentation channel yields *a'*- and *y'*-type ions [3, 4]. More unconventional ECD fragments have also been reported. For example, Cooper was the first to report the presence of *b*-type ions in some ECD MS/MS spectra [14]. She proposed that the type of charge carrier (arginine vs. lysine protonation) is significant in determining the preferred ECD fragmentation channels. The position of such basic residues within a peptide sequence may also affect the ECD outcome. Specifically, peptides containing lysine charge carrier(s) yielded more *b* ions upon ECD than

those containing arginine. However; *b* ions were not detected for peptides with N-terminal Lys or Arg, possibly due to gas-phase structural differences. Haselmann and Schmidt reported examination of a series of custom peptides as probes for *b* ion formation in ECD [15]. For these peptides, ECD spectra containing *b* ions also showed abundant losses of hydrogen radicals from the charge reduced precursor ions. Less abundant *b* ions were observed in ECD of the peptide *H*-Lys-Ala<sub>4</sub>-Lys-Ala<sub>4</sub>-NH<sub>2</sub> compared with its N-terminally acetylated form. This result was explained through the “mobile proton” framework in which *b* ion formation upon collisional activation proceeds through backbone amide protonation. Upon N-terminal acetylation, one basic site (primary amine) is removed, increasing the probability of one proton being located at the peptide backbone. Lee *et al.* showed that, for peptide cations containing a lysine homologue, *b* ion formation was more prevalent with decreasing length and proton affinity of the primary amine side chain, both resulting in increased probability of backbone protonation [16]. Thus, the formation of *b* ions can be explained in the framework of the mobile proton model [17, 18]. Ab initio direct dynamics calculations by Uggerud *et al.* also revealed that *b*-type ions can be generated from electron capture at a protonated backbone amide nitrogen [19]. Our group examined ECD of doubly protonated peptides with one or no basic amino acid residues and observed the presence of abundant *b* ions [20]. Li *et al.* also reported abundant *b* ions in ECD of the doubly protonated peptide GSNKGAIIGLM containing only one basic amino acid residue, including high abundance *b*<sub>8</sub> and *b*<sub>10</sub> ions [21], in agreement with our observations [20]. However, they also reported low abundance *b* ions from electron transfer dissociation (ETD) of doubly and triply protonated peptides [21], but these may have resulted from vibrational excitation due to supplemental CID activation [22, 23]. We proposed that protonation of backbone amide nitrogens (due to the lack of basic side chains) is a prerequisite for *b* ion formation in ECD [20].

Supercharging [24-28] is an increasingly employed strategy in electron capture/transfer dissociation (ECD/ETD) experiments because at least doubly charged precursor ions are required but a precursor ion charge  $\geq 3+$  yields much improved fragmentation efficiencies [22, 29-33].

Kjeldsen *et al.* reported that the average charge states of tryptic peptides, particularly phosphopeptides, were significantly increased by adding 0.1% *m*-nitrobenzyl alcohol (*m*-NBA) to liquid chromatography (LC)/MS solvents [34]. The charge-enhancing ability of *m*-NBA benefited both peptide sequencing and PTM characterization in LC ETD MS/MS experiments due to improved ETD efficiency. A similar strategy was used by Rand *et al.* in bottom-up ETD hydrogen/deuterium exchange (HDX) MS/MS experiments [35] to enhance peptide sequence coverage and HDX spatial resolution. However, supercharged peptides and proteins result in more complex ECD/ETD spectra [34, 36]. We hypothesize that additional fragment ions detected in ECD/ETD of supercharged peptides may correspond to *b* ions, because, when the number of protons increases, backbone protonation becomes more likely. A mixture of *a*-, *b*-, *c*-, *x*-, *y*-, and *z*- ions was observed from ECD of extremely supercharged protein ions formed by electrospray ionization (ESI) [36]. However, to our knowledge, unconventional fragments from ECD or ETD of supercharged peptides have not been previously reported.

Here, we apply ECD towards a variety of peptides, with or without basic amino acid residues, and with and without supercharging to particularly investigate *b* ion formation under such conditions. In addition, we examine ETD of the same peptides. ETD generally results in highly analogous fragmentation to ECD and involves a similar fragmentation mechanism [5, 37]. However, to our knowledge, the presence of *b* ions in ETD spectra has not previously been noted in the absence of supplemental activation.

## 4.2 Experimental

### 4.2.1 Reagents and Sample Preparation

Unless otherwise specified, all chemicals, peptides, and proteins were purchased from Sigma-Aldrich (St. Louis, MO, USA) and used without further purification. Three groups of peptides were examined; first peptides containing few or no basic amino acid residues, including cholecystokinin fragment 26-33 (CCK = H-DYMGWMDF-NH<sub>2</sub>), desulfated caerulein (DC = pEQDYTGWMDF-NH<sub>2</sub>), avian luteinizing hormone releasing hormone (Q<sup>8</sup>-LHRH = pEHWSYGLQPG-NH<sub>2</sub>), (pGlu<sup>5</sup>, D-Trp<sup>7,9,10</sup>)-substance P fragment 5-11 (TrpSP =

pEQWFWWM-NH<sub>2</sub>), and oxytocin (OT = H-CYFQNCPLG-NH<sub>2</sub>, 1-5 disulfide bond). Desulfated caerulein was purchased from Bachem (Torrance, CA, USA) and Q<sup>8</sup>-LHRH was obtained from Abcam (Cambridge, MA, USA). Melittin (H-GIGAVLKVLTTGLPALISWIKRKRQQ-NH<sub>2</sub>) is the only peptide in the second group. The third group contained peptides derived from proteolytic digestion of equine heart myoglobin and  $\alpha$ -casein from bovine milk. Both porcine pepsin and porcine trypsin (mass spectrometry grade, Promega, Madison, WI, USA) were used for digestion.

Pepsin digestion was performed by mixing protein and pepsin 1:1 in water with 0.3% formic acid (0 °C, pH~2.5) followed by 2 min incubation prior to LC/MS analysis. Trypsin digestion was performed by mixing trypsin with protein at a 1:100 molar ratio in 50 mM ammonium bicarbonate buffer (pH adjusted to ~7.8 with ammonium hydroxide and formic acid) and incubating overnight at 37 °C followed by heating at 100 °C for 5 min to denature the protease. The digests were then diluted to 5-10  $\mu$ M and directly infused via ESI in 1:1 H<sub>2</sub>O/methanol, 0.2% formic acid, with or without 0.1% *m*-NBA.

#### 4.2.2 Liquid Chromatography

An Agilent 1100 HPLC system coupled with a 6-port switching valve (VICI Valco, Houston, TX, USA) was used for LC ECD MS/MS experiments of peptic mixtures from myoglobin or  $\alpha$ -casein. The protein digests were separated over a C18 reversed-phase analytical column (Phenomenex Kinetex 5  $\mu$ m EVO 50 x 2.1 mm) at a flow rate of 0.2 mL/min. Mobile phase A was 95/5 water/acetonitrile with 0.2% formic acid and mobile phase B was 5/95 water/acetonitrile with 0.2% formic acid. 0.1% *m*-NBA was added to the LC eluate via a post-column mixing tee with a syringe and pump when necessary. The 7-min-long LC gradient started at 5% B, held for 1 min, then linearly increased to 75% B for 4 min, and kept at 75% B for another 2 min. Eluate within the first minute was directed to waste. The injection volume was 6-8  $\mu$ L.

#### 4.2.3 Mass Spectrometry

All mass spectra were acquired in positive ion mode on a 7-T SolariX quadrupole Fourier

transform ion cyclotron resonance (Q-FT-ICR) mass spectrometer (Bruker Daltonics, Billerica, MA) equipped with an Apollo II ESI source. Duplicate measurements were performed for all experiments. ECD was performed in the ICR cell using an indirectly heated hollow dispenser cathode (1.6 A) at a bias voltage at - 1.0 V and an irradiation time of 100-200 ms. ETD was performed in the hexapole collision cell where both analyte ions and radical anionic fluoranthene reagent ( $m/z$  202) were accumulated. Reagent accumulation time was set to 160-180 ms and the reaction time was kept at 0. Following electron transfer events in the collision cell, product ions were transferred to the ICR cell and detected as an image current. For both ECD and ETD, precursor ions were mass-selectively filtered by the quadrupole using a 4-6  $m/z$  isolation window, then accumulated in the collision cell for 0.2-0.3 s prior to MS/MS. The collision voltage was kept at a low level (- 0.1 to + 0.1 V) to minimize supplemental collisional activation. ECD and ETD MS/MS spectra were acquired with 512k or 1M data points averaged over 16 or 32 scans in an  $m/z$  range from 200 to 1,800. Peptide standards and proteolytic mixtures were electrosprayed at a flow rate of 100  $\mu\text{L}/\text{h}$ . The nebulizer gas pressure, drying gas flow rate, and drying gas temperature for ESI were kept at 1.0 bar, 4.0 L/min, and 150  $^{\circ}\text{C}$ , respectively. For LC/MS, the capillary voltage, drying gas flow rate, and drying gas temperature were set to 4,500 V, 3.8 L/min, and 130  $^{\circ}\text{C}$ , respectively. Data dependent acquisition with MS/MS boost were used for auto ECD with an ion accumulation time of 0.15 s for MS scans and 0.50 s for MS/MS scans. For each MS scan, the four most abundant species with charge states ranging from 2 to 5 were selected for ECD (8  $m/z$  isolation width, 150 ms irradiation time, -1.0 V bias voltage, 1 scan for each ECD spectrum). A series of CID experiments were also performed with stepwise increased collision voltage in an increment of 0.5 V to determine the onset voltage for CID-based generation of *b* ions. Mass spectra were externally calibrated with sodium trifluoroacetate to <2 ppm error.

#### 4.2.4 Data Analysis

All data analysis was performed manually using Bruker Data Analysis 4.4. Reference masses of all precursor and fragment ions were determined by the MS Product function (<http://prospector.ucsf.edu/prospector/cgi-bin/msform.cgi?form=msproduct>) in Protein

Prospector. Only peak assignments with a mass accuracy better than 20 ppm and observed in duplicate measurements were accepted. Ion abundance was determined based on the monoisotopic peak with charge-state normalization. *b* ion relative abundance was defined as the ratio of the *b* ion abundance versus the precursor ion abundance upon isolation in the quadrupole (prior to dissociation). *b* ion partitioning was determined as the percentage of the *b* ion abundance among all product ions, including backbone fragments, neutral losses, and internal fragments, but not including the charge reduced species  $[M + nH]^{(n-1)+}$ .

## 4.3 Results and Discussion

### 4.3.1 ECD and ETD of peptides with few or no basic amino acid residues

Several peptides with few or no basic amino acid residues were examined to perform a side-by-side comparison between ECD and ETD. Our previous work with a different FT-ICR mass spectrometer (Apex-Q) showed that the peptides CCK, DC, Q<sup>8</sup>-LHRH, TrpSP, and OT all yielded abundant *b* ions upon ECD of their doubly protonated forms [20]. Figure 4.1(a) shows the ECD spectrum of doubly protonated CCK from our newer SolariX instrument. *b*-type ions (highlighted in blue) are abundant, including *b* ions with water loss (labeled with asterisks). By contrast no *b* ions were generated in ETD of the same peptide (Figure 4.1(b)). Interestingly, the *c'*- and *z'*-type product ions typical of ExD are prevalent in ETD but significantly less abundant than *b*-type ions in ECD. *b*<sub>5</sub> and *b*<sub>6</sub> ions, corresponding to the most abundant sequence ions upon ECD of  $[CCK + 2H]^{2+}$ , are present in the ETD spectrum at lower abundance (labeled with circles). However; control experiments performed with the same sample and ion source/transfer settings, including precursor ion quadrupole isolation, but without introducing ETD reagent showed that these *b* ions were already present at the same abundance prior to ETD, presumably due to the labile nature of this peptide. By contrast, their abundance increased significantly upon ECD and, thus, they are a result of electron irradiation in the latter case. The typical charge reduced species,  $[CCK + 2H]^{+}$ , was mostly absent in the ECD spectrum (Figure 4.1(a) inset). Instead the  $[CCK + H]^{+}$  species from hydrogen radical loss was prevalent, similar to the reports by Haselmann and Schmidt for ECD spectra with a significant *b* ion population [15]. A peak that

could correspond to hydrogen atom loss from the charge-reduced  $[\text{CCK} + 2\text{H}]^{++}$  species was also observed in the ETD spectrum (Figure 4.1(b) inset), but to a much lower degree compared with ECD. However, this peak can also be explained from proton transfer to the fluoranthene anion during the ETD reaction. Figures 4.1 (c)(d) show ECD (c) and ETD (d) spectra of doubly protonated  $\text{Q}^8\text{-LHRH}$ . ECD generated a mixture of different types of sequence ions, including  $c$ -,  $z$ -,  $b$ -,  $y$ -, and  $a$ -type ions (Figure 4.1(c)). Abundant hydrogen loss from the charge reduced  $[\text{Q}^8\text{-LHRH} + 2\text{H}]^{++}$  species was noted although a mixture of  $[\text{Q}^8\text{-LHRH} + \text{H}]^+$  and  $[\text{Q}^8\text{-LHRH} + 2\text{H}]^{++}$  is apparent for this peptide (Figure 4.1(c) inset). ETD, on the other hand, generated a less complex spectrum with mostly  $c'$ - and  $z'$ -type ions (Figure 4.1 (d)). A low abundance  $b_8$  ion was present prior to ETD (labeled with a circle). Hydrogen radical loss (or proton transfer) from the charge-reduced radical species was virtually absent for this peptide (Figure 4.1(d) inset). Three other peptides with few or no basic amino acid residues were subjected to ECD and ETD in their doubly protonated forms, as shown in Table 4.1. A number of  $b$  ions were exclusively observed from ECD of these peptides, as well as abundant hydrogen loss from the charge-reduced species. Neither outcome was apparent in ETD. Thus, as noted in previous ECD experiments, the occurrence of abundant  $b$  ions is related to preferred hydrogen loss from the charge-reduced radical [14-16, 20].

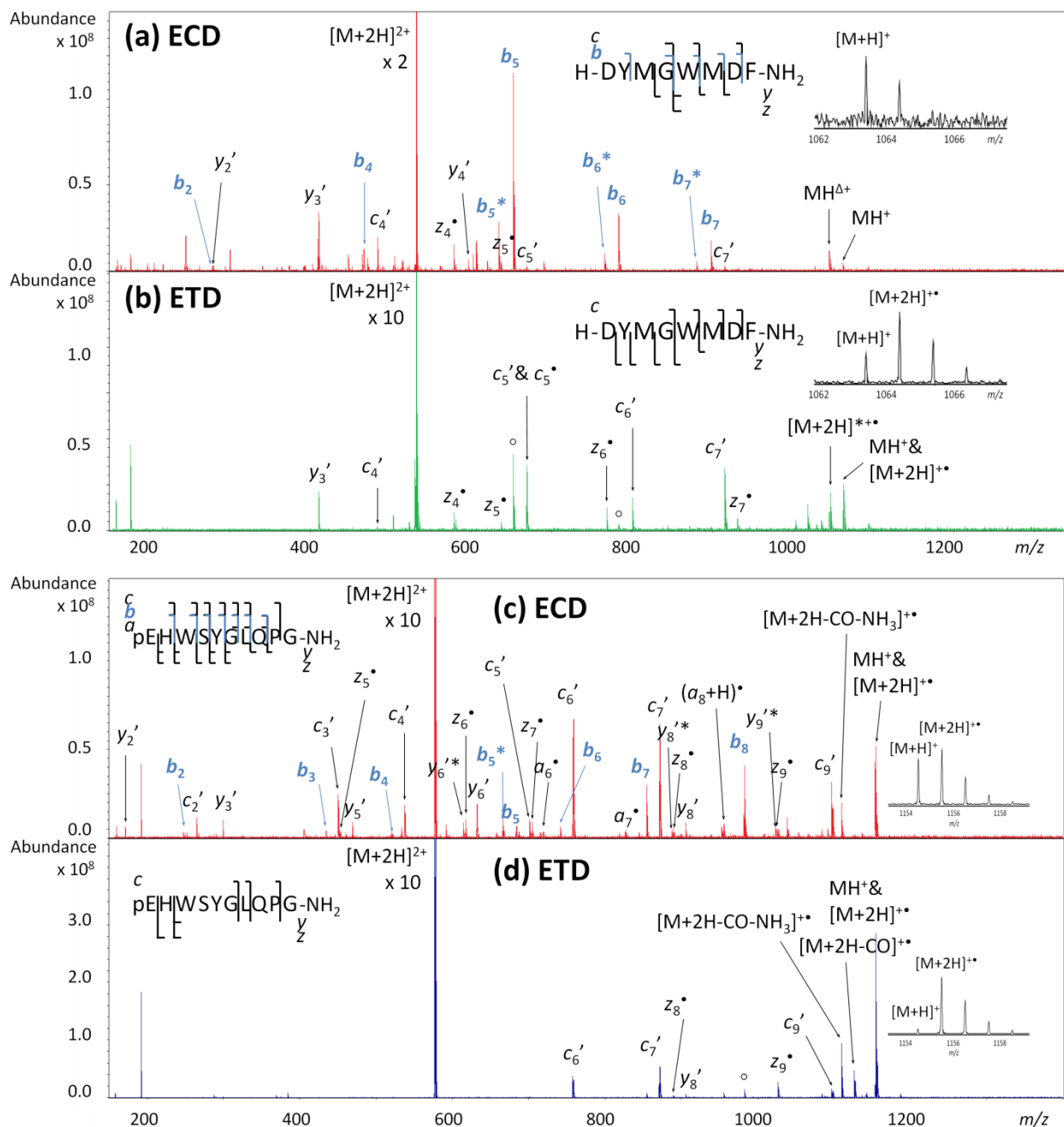


**Figure 4.1** (a) ECD and (b) ETD MS/MS spectra of doubly protonated CCK; (c) ECD and (d) ETD MS/MS spectra of doubly protonated  $Q^8$ -LHRH.  $b$ -type fragment ions are highlighted in blue.  $b/y'$  product ions present prior to electron irradiation (ECD) or ion-ion reaction (ETD) as a result of peptide vibrational excitation are labeled with circles ( $\circ$ );  $*$  = water loss;  $\Delta$  = ammonia loss. Insets show expanded views of the charge reduced precursor ions.

**Table 4.1** Comparison of backbone fragmentation in ECD vs. ETD for three doubly protonated peptides lacking basic amino acid residues. *b*-type fragment ions are highlighted in red.

Peptide name (charge state)	ECD	ETD
desulfated caerulein 2+		
(pGlu <sup>5</sup> , D-Trp <sup>7,9,10</sup> )- substance P fragment 5-11 (TrpSP) 2+		
oxytocin 2+		

#### 4.3.2 ECD and ETD of the 4+, 5+, and 6+ charge states of melittin

To further investigate the *b* ion formation in ExD, melittin carrying four and five protons was fragmented with ECD and ETD, respectively. For quadruply protonated melittin, only one minor *b* ion ( $b_{23}^{2+}$ ) was observed upon ECD (Figure 4.2 (a)). However; a large number of *b* ions were detected in ECD of the 5+ charge state (Figure 4.2 (c)). By contrast, ETD of the 4+ charge state did not result in any *b* ions (Figure 4.2 (b)) while the 5+ charge states yielded two minor *b* ions ( $b_{23}^{2+}$ ,  $b_{25}^{3+}$ ) from ETD (Figure 4.2 (d)). The striking difference between ECD and ETD spectra of the 5+ charge state of melittin in terms of the presence of *b* ions again clearly showed significant differences between these two activation methods. Our previous work [20] proposed that *b* ions should be expected for higher charge states when the number of protons is higher than the number of basic sites. This hypothesis is supported by the high number of *b* ions formed in ECD of quintuply protonated melittin but not in that of the quadruply protonated form. Melittin has six basic sites: the N-terminus and five basic amino acid residues (K<sup>7</sup>, KRKR<sup>21-24</sup>). Due to the consecutive order of the four basic residues KRKR<sup>21-24</sup> protonation of each one is thermodynamically unfavorable. Thus, it is quite likely that one proton in the 5+ charge state is located on a backbone amide nitrogen, consistent with the prevalent *b* ions.

By adding 0.1% *m*-NBA to the ESI solvent, the 6+ charge state of melittin could be isolated and subjected to ECD and ETD, respectively. Both spectra were rather complex (data not shown) with an even larger number of *b* ions generated in ECD of the 6+ charge state compared to the 5+ ion (Table 4.2). Interestingly, the ETD spectrum of the 6+ charge state of melittin showed several additional *b* ions not observed for the 5+ precursor ion (Table 4.2). The increased number of *b* ions in both ECD and ETD of the 6+ charge state of melittin is likely due to the even higher probability of backbone protonation compared with the 5+ charge state.

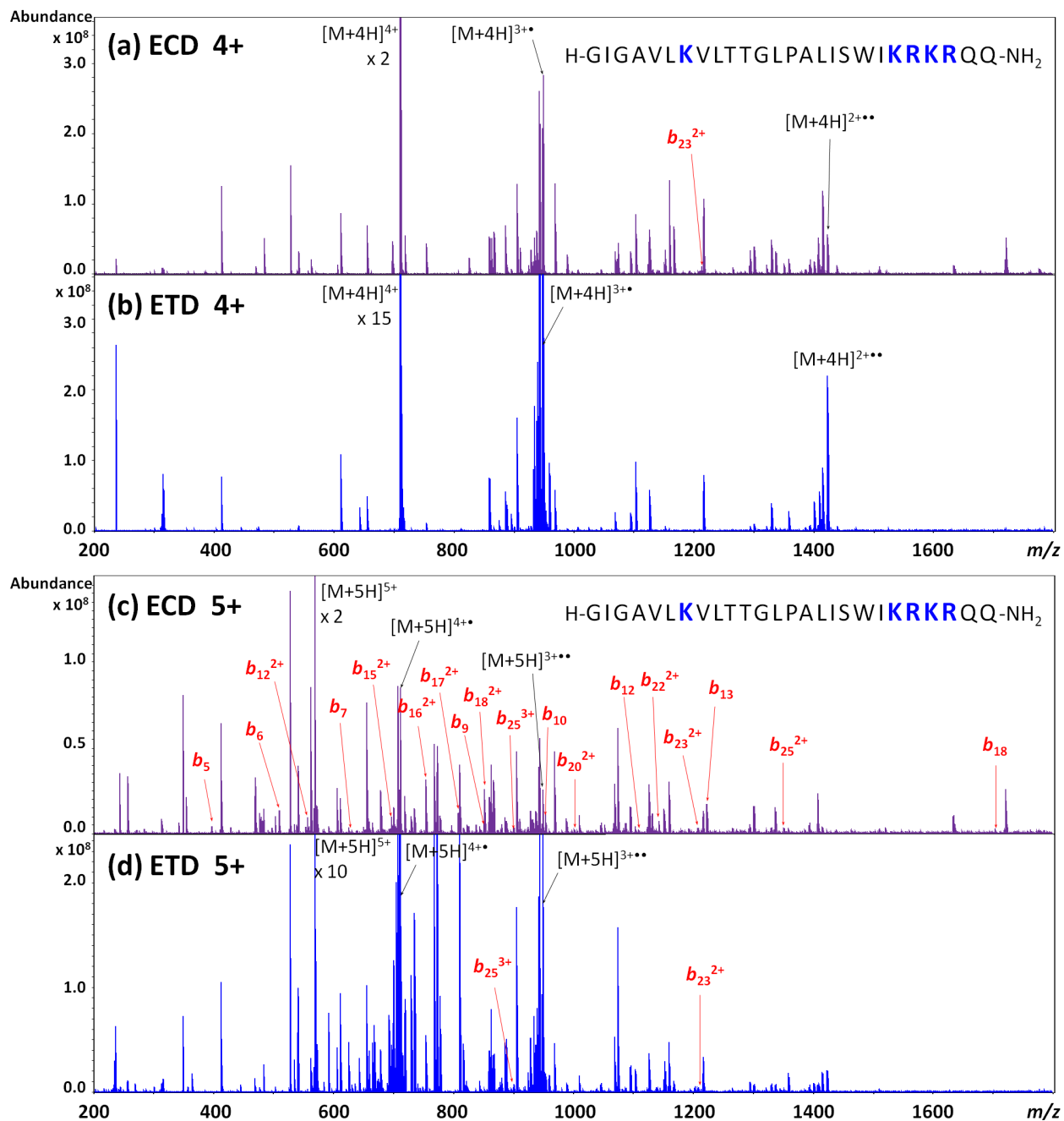


**Figure 4.2** (a)(c) ECD and (b)(d) ETD MS/MS spectra of the (a)(b) 4+ and (c)(d) 5+ charge states of melittin. Only the precursor ions, charge reduced species, and *b* ions are labeled.

**Table 4.2** Comparison of backbone fragmentation in ECD vs. ETD for the 4+, 5+, and 6+ charge states of melittin. Basic amino acids are highlighted in blue. Only *b*-type fragment ions are included in this table. \* indicates that the ECD/ETD experiment was performed following addition of 0.1% *m*-NBA into the ESI solvent.

Charge state	ECD	ETD
4+	<sup><i>b</i></sup> H-GIGAVL <b>K</b> VLT TGLPALISWIK <b>RKR</b> RQQ-NH <sub>2</sub>	H-GIGAVL <b>K</b> VLT TGLPALISWIK <b>RKR</b> RQQ-NH <sub>2</sub>
5+*	<sup><i>b</i></sup> H-GIGAVL <b>K</b> VLT TGLPALISWIK <b>RKR</b> RQQ-NH <sub>2</sub>	<sup><i>b</i></sup> H-GIGAVL <b>K</b> VLT TGLPALISWIK <b>RKR</b> RQQ-NH <sub>2</sub>
6+*	<sup><i>b</i></sup> H-GIGAVL <b>K</b> VLT TGLPALISWIK <b>RKR</b> RQQ-NH <sub>2</sub>	<sup><i>b</i></sup> H-GIGAVL <b>K</b> VLT TGLPALISWIK <b>RKR</b> RQQ-NH <sub>2</sub>

### 4.3.3 *b* ions observed in ECD and ETD of tryptic and peptic peptides with varying charge states

Table 4.3 shows *b* ions detected in ECD and ETD of myoglobin and  $\alpha$ -casein tryptic (a)/peptic (b) peptides. Doubly charged tryptic peptides are unlikely to be protonated at backbone amides. Accordingly, *b* ions were not detected in ECD of such species (Table 4.3(a)). The triply charged form of VEADIAGHGQEVLR generated one *b* ion in ECD but no *b* ions in ETD. The tryptic peptide LFTGHPETLEKFDKFK with two missed cleavage sites did not show any *b* ions upon ECD of the triply protonated form but the 4+ and 5+ charge states (generated via supercharging with *m*-NBA) yielded 2 and 11 *b*-type ions, respectively. However, no *b* ions were observed from ETD, even for the 5+ ions. This charge state may still preclude backbone protonation as there are five basic sites in this peptide (the N-terminus, histidine, and 3 lysines).

Peptic peptides do not, like tryptic peptides, contain basic amino acid residues at the C-terminus. Also, due to the less selective nature of pepsin, peptic peptides are often shorter than tryptic peptides. For these reasons, at higher charges states, peptic peptides may be more likely to include backbone protonation. Accordingly, *b* ions were observed from two doubly protonated peptic peptides upon ECD (Table 4.3(b)). One of these two peptides, FRQFYQL, also generated one *b* ion upon ETD. It is feasible that backbone protonation occurs in this peptide as there is an

arginine residue close to the N-terminus. Triply and quadruply protonated peptic peptides were generated with the aid of *m*-NBA-based supercharging. All such triply charged peptides, except **LRLKKYKVPQL**, generated *b* ions from ECD. The latter peptide, which contains five basic sites, was also present in a 4+ charge state, which did yield *b* ions from ECD. None of these peptides generated *b* ions upon ETD, again highlighting differences between these two activation methods.

**Table 4.3** *b* ions generated from ECD vs. ETD of (a) tryptic peptides and (b) peptic peptides from myoglobin and  $\alpha$ -casein in different charge states. The basic amino acid residues in each peptide are highlighted in blue. \* indicates that the ECD/ETD experiment was performed with addition of 0.1% *m*-NBA into the ESI solvent.

(a)

# basic amino acid residues	Charge states	ECD	ETD
2	2+	VEADIAGHGQEVLR	VEADIAGHGQEVLR
2	3+ *	<sup>b</sup> VEADIAGHGQEVLR	VEADIAGHGQEVLR
4	2+	LFTGHPETLEKFDKFK	LFTGHPETLEKFDKFK
4	3+	LFTGHPETLEKFDKFK	LFTGHPETLEKFDKFK
4	4+ *	<sup>b</sup> LFTGHPETLEKFDKFK	LFTGHPETLEKFDKFK
4	5+ *	<sup>b</sup> LFTGHPETLEKFDKFK	LFTGHPETLEKFDKFK

(b)

# basic amino acid residues	Charge states	ECD	ETD
0	2+ *	<sup>b</sup> YYVPLGTQYTDAPSF	YYVPLGTQYTDAPSF
1	2+ *	<sup>b</sup> FRQFYQL	<sup>b</sup> FRQFYQL
2	2+	NVWKGVEADIAGHGQEVLR	NVWKGVEADIAGHGQEVLR
2	3+ *	<sup>b</sup> NVWKGVEADIAGHGQEVLR	NVWKGVEADIAGHGQEVLR
3	2+	FRNDIAAKYKELGFQG	FRNDIAAKYKELGFQG
3	3+ *	<sup>b</sup> FRNDIAAKYKELGFQG	FRNDIAAKYKELGFQG
4	2+	LRLKKYKVPQL	LRLKKYKVPQL
4	3+	LRLKKYKVPQL	LRLKKYKVPQL
4	4+ *	<sup>b</sup> LRLKKYKVPQL	LRLKKYKVPQL

#### 4.3.4 Possible mechanisms for the formation of *b* ions from supercharged peptides upon

##### ECD and ETD

ECD and ETD are thought to share similar, if not identical, fragmentation mechanisms. Nevertheless, we observe a clear difference in the charge density threshold when *b* ions are formed from these activation methods. We propose that this difference is due to different initial

internal energy of the charge reduced radical intermediates upon electron capture/transfer [23] prior to dissociation. There are both fundamental and experimental differences that could account for this energy difference. First, the source of electrons in the two techniques is not the same; the recombination energy upon electron transfer (close to the electron affinity of the radical reagent anions [38]) is significantly lower compared to the recombination energy upon capture of free thermal electrons [1, 39-41]. Second, ETD is typically performed in an ion trapping device, *e.g.*, the collision cell on the Solarix FT-ICR mass spectrometer, at a pressure  $\sim 10^{-3}$  mbar, allowing for collisionally cooled precursor ions, whereas ECD takes place under ultra-high vacuum (UHV,  $\sim 10^{-10}$  mbar) in the absence of collision gas. In addition, the electron-emitting cathode used for ECD is heated to a high temperature, thus resulting in blackbody radiation within the ICR cell, a potential source of precursor ion vibrational excitation.

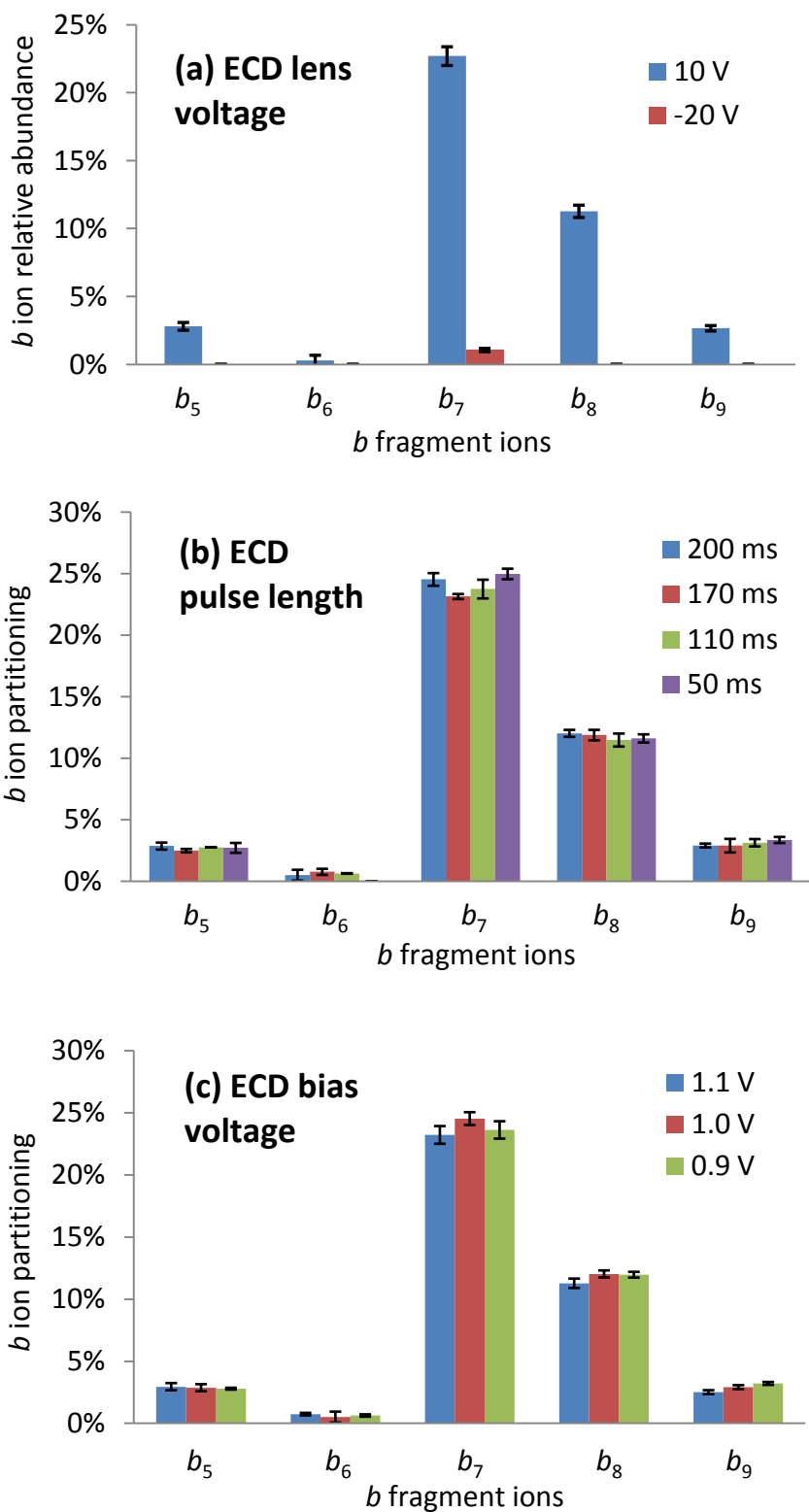


**Figure 4.3** (a) Relative abundance of  $b_5$  through  $b_9$  ions from doubly protonated desulfated caerulein upon ECD when the ECD lens voltage was set to 10 V (to promote electron injection, blue bars) and - 20 V (to preclude electron injection, red bars) respectively. (b)(c)  $b$  ion

abundance partitioning for doubly protonated desulfated caerulein upon ECD with varying (b) ECD pulse length and (c) ECD bias voltage.

To examine whether the increased ICR cell temperature at ECD conditions is directly responsible for the enhanced formation of *b* ions in ECD vs. ETD, a negative voltage (- 20 V) was applied to the ECD lens, located between the cathode and the ICR cell, to prevent electrons from entering the cell, while the cathode remained hot. The relative abundances of *b*<sub>5</sub>-*b*<sub>9</sub> ions detected from doubly protonated desulfated caerulein under ECD conditions at these two lens voltages are shown in Figure 4.3 (a). All *b* ions were significantly reduced or absent at the lens voltage preventing electrons from entering the ICR cell, with only the *b*<sub>7</sub> ion present at rather low abundance (1.5% relative to the precursor ion abundance) in the absence of electron irradiation. This result indicates that the formation of *b* ions in ECD is a radical-initiated process consistent with previous work [14]. We also found that the presence of *b* ions and their relative abundance among all ECD product ions are not affected by the ECD pulse length or ECD bias voltage (Figure 4.3 (b)(c)).

It has been reported that inelastic collisions with electrons can induce vibrational and/or electronic excitation, resulting in analyte fragmentation; a process termed electron impact excitation of ions from organics (EIEIO) [42, 43]. However; EIEIO typically employs significantly higher electron energy (70 eV) than typical ECD conditions. In hot ECD (HECD) experiments [44] at ~10 eV electron energy, *b*/*y*'-type ions are observed but this energy is still much higher than what is employed here. Cooper performed double resonance experiments to exclude that *b* ions result from secondary fragmentation of *c* ions [14]. The observation that abundant *b* ions are accompanied by abundant hydrogen radical loss from the charge reduced species suggests that such loss is favorable and results in peptide vibrational excitation. To further compare the ECD-generated *b* ions to those typically observed in CID, a series of CID experiments was performed on doubly protonated Q<sup>8</sup>-LHRH and desulfated caerulein, both of which generated abundant *b* ions upon ECD. These experiments gradually increased the collision energy to determine the onset voltage for formation of each *b* ion. As shown in Figure 4.4, an obvious inverse relationship between the *b* ion onset voltage determined by CID and the *b* ion

abundance in ECD was seen. For example,  $b_7$  and  $b_8$  ions from doubly protonated  $Q^8$ -LHRH were highly abundant upon ECD with an onset voltage close to 0, indicative of weak peptide bonds at  $LQ^{78}$  and  $QP^{89}$ .

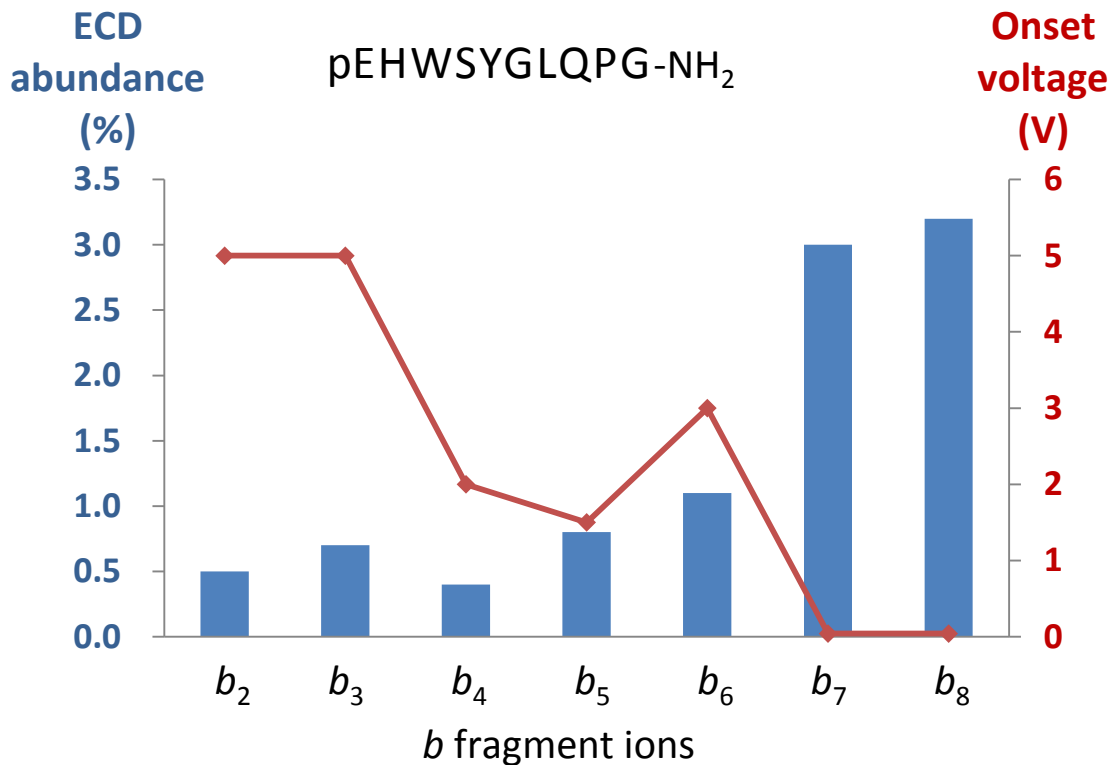


(Figure 4.4 continued on the next page)

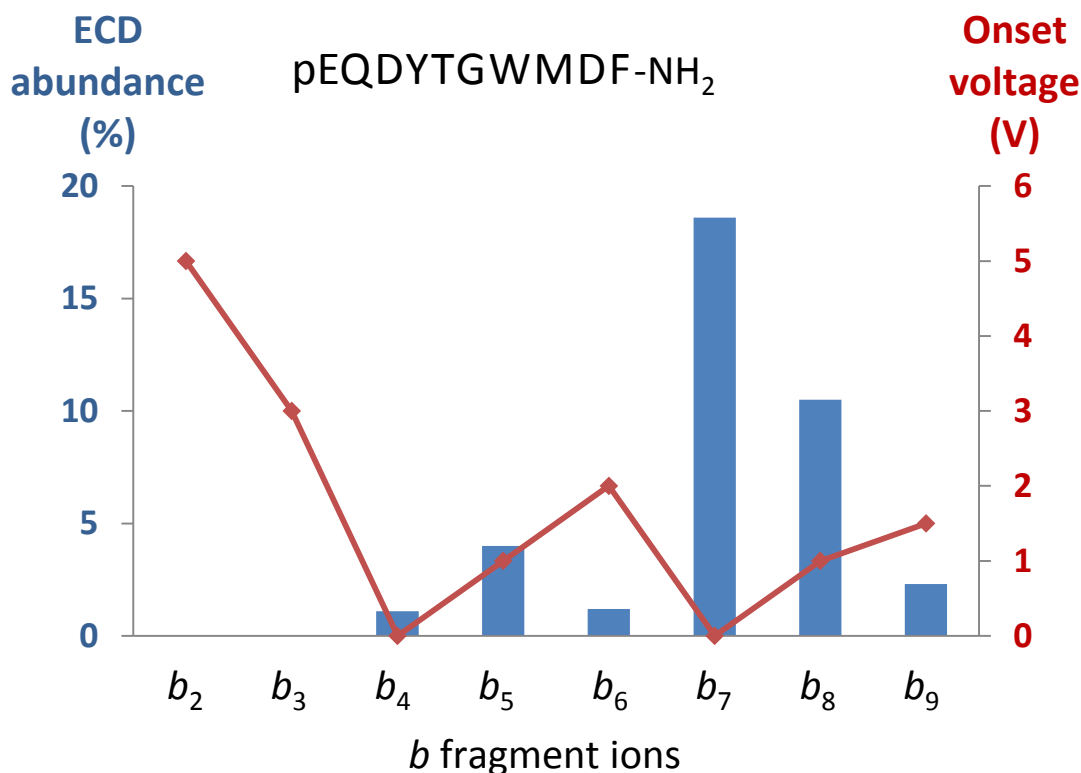


**Figure 4.4**  $b$  ion relative abundance (%), blue bars) of doubly protonated Q<sup>8</sup>-LHRH (top) and desulfated caerulein (bottom) upon ECD co-plotted with the  $b$  ion onset voltage (V, red line) obtained by CID.

In sum, a proposed pathway describing  $b$  ion formation in ExD involves electron capture/transfer by/to a peptide with at least one proton located at a backbone amide to form a hydrogen atom ( $H\bullet$ ). The associated recombination energy results in preferred loss of this hydrogen radical, leaving a vibrationally excited peptide ion that undergoes dissociation, forming  $b$ -type ions. The initial ion temperature upon electron capture/transfer appears to influence the probability of hydrogen atom ejection. This ejection probability is higher in ECD compared with ETD based on the local environment of each experiment (temperature and pressure). It is also enhanced for higher charge states, particularly those generated via supercharging strategies.

#### 4.4 Conclusions

In this work, the number and abundance of  $b$  ions generated in ECD are examined as a function of precursor ion charge state. As previously demonstrated,  $b$  ions are more prominent in

ECD spectra when the number of protons outnumber the basic sites. Interestingly, ETD, commonly believed to be analogous to ECD, generates much fewer *b* ions at the same charge state. Nevertheless, at high charge states, including those generated via supercharging, *b* ions are also seen in ETD spectra but at significantly lower levels than in ECD. This difference is related to the energetics and local environment of these two MS/MS experiments. We propose that, similar to the observations by Haselmann and Schmidt [15], *b* ions are formed following hydrogen atom ejection from charge-reduced precursor ions.

Supercharging is a useful strategy to enhance ECD/ETD-type peptide/protein sequencing; however, the occurrence of unconventional fragments, such as *b* ions, complicates spectral interpretation, may underestimate fragmentation efficiency, and may lead to lower peptide scores. Thus, *b* ions should be included in ExD database searches for higher charge states. In specialized tandem mass spectrometry experiments that require minimal vibrational activation, such as HDX MS/MS, ETD appears more appropriate than ECD.

#### 4.5 Acknowledgements

This work was supported by the National Science Foundation CHE1609840.

#### 4.6 References

1. Zubarev, R.A., Haselmann, K.F., Budnik, B., Kjeldsen, F., Jensen, F.: Towards An Understanding of the Mechanism of Electron-Capture Dissociation: A Historical Perspective and Modern Ideas. *Eur. J. Mass Spectrom.* **8**, 337-349 (2002)
2. Zubarev, R.A., Kelleher, N.L., McLafferty, F.W.: Electron Capture Dissociation of Multiply Charged Protein Cations. A Nonergodic Process. *J. Am. Chem. Soc.* **120**, 3265-3266 (1998)
3. Zubarev, R.A., Kruger, N.A., Fridriksson, E.K., Lewis, M.A., Horn, D.M., Carpenter, B.K., McLafferty, F.W.: Electron Capture Dissociation of Gaseous Multiply-Charged Proteins Is Favored at Disulfide Bonds and Other Sites of High Hydrogen Atom Affinity. *J. Am. Chem. Soc.* **121**, 2857-2862 (1999)
4. Breuker, K., Oh, H., Lin, C., Carpenter, B.K., McLafferty, F.W.: Nonergodic and conformational control of the electron capture dissociation of protein cations. *Proc. Natl. Acad. Sci. U. S. A.* **101**, 14011-14016 (2004)
5. Qi, Y., Volmer, D.A.: Electron-based fragmentation methods in mass spectrometry: An overview. *Mass Spectrom. Rev.* **36**, 4-15 (2017)
6. Molina, H., Horn, D.M., Tang, N., Mathivanan, S., Pandey, A.: Global proteomic profiling of phosphopeptides using electron transfer dissociation tandem mass spectrometry. *Proc.*

- Natl. Acad. Sci. U. S. A. **104**, 2199-2204 (2007)
7. Zubarev, R.A.: Electron-capture dissociation tandem mass spectrometry. *Curr. Opin. Biotechnol.* **15**, 12-16 (2004)
  8. Zhao, Y., Jensen, O.N.: Modification-specific proteomics: Strategies for characterization of post-translational modifications using enrichment techniques. *PROTEOMICS*. **9**, 4632-4641 (2009)
  9. Larsen, M.R., Trelle, M.B., Thingholm, T.E., Jensen, O.N.: Analysis of posttranslational modifications of proteins by tandem mass spectrometry. *BioTechniques*. **40**, 790-798 (2006)
  10. Hoffman, M.D., Sniatynski, M.J., Kast, J.: Current approaches for global post-translational modification discovery and mass spectrometric analysis. *Anal. Chim. Acta*. **627**, 50-61 (2008)
  11. Tureček, F.: NC $\alpha$  Bond Dissociation Energies and Kinetics in Amide and Peptide Radicals. Is the Dissociation a Non-ergodic Process? *J. Am. Chem. Soc.* **125**, 5954-5963 (2003)
  12. Syka, J.E.P., Coon, J.J., Schroeder, M.J., Shabanowitz, J., Hunt, D.F.: Peptide and protein sequence analysis by electron transfer dissociation mass spectrometry. *Proc. Natl. Acad. Sci. U. S. A.* **101**, 9528-9533 (2004)
  13. Mikhailov, V.A., Iniesta, J., Cooper, H.J.: Top-Down Mass Analysis of Protein Tyrosine Nitration: Comparison of Electron Capture Dissociation with “Slow-Heating” Tandem Mass Spectrometry Methods. *Anal. Chem.* **82**, 7283-7292 (2010)
  14. Cooper, H.J.: Investigation of the Presence of b Ions in Electron Capture Dissociation Mass Spectra. *J. Am. Soc. Mass. Spectrom.* **16**, 1932-1940 (2005)
  15. Haselmann, K.F., Schmidt, M.: Do b-ions occur from vibrational excitation upon H-desorption in electron capture dissociation? *Rapid Commun. Mass Spectrom.* **21**, 1003-1008 (2007)
  16. Lee, S., Chung, G., Kim, J., Oh, H.B.: Electron capture dissociation mass spectrometry of peptide cations containing a lysine homologue: a mobile proton model for explaining the observation of b-type product ions. *Rapid Commun. Mass Spectrom.* **20**, 3167-3175 (2006)
  17. Wysocki, V.H., Tsaprailis, G., Smith, L.L., Brei, L.A.: Mobile and localized protons: a framework for understanding peptide dissociation. *J. Mass Spectrom.* **35**, 1399-1406 (2000)
  18. Boyd, R., Somogyi, Á.: The mobile proton hypothesis in fragmentation of protonated peptides: A perspective. *J. Am. Soc. Mass. Spectrom.* **21**, 1275-1278 (2010)
  19. Bakken, V., Helgaker, T., Uggerud, E.: Models of Fragmentations Induced by Electron Attachment to Protonated Peptides. *Eur. J. Mass Spectrom.* **10**, 625-638 (2004)
  20. Liu, H., Håkansson, K.: Abundant b-Type Ions Produced in Electron Capture Dissociation of Peptides Without Basic Amino Acid Residues. *J. Am. Soc. Mass. Spectrom.* **18**, 2007-2013 (2007)
  21. Li, X., Lin, C., Han, L., Costello, C.E., O’Connor, P.B.: Charge remote fragmentation in electron capture and electron transfer dissociation. *J. Am. Soc. Mass. Spectrom.* **21**, 646-656 (2010)

22. Swaney, D.L., McAlister, G.C., Wirtala, M., Schwartz, J.C., Syka, J.E.P., Coon, J.J.: Supplemental Activation Method for High-Efficiency Electron-Transfer Dissociation of Doubly Protonated Peptide Precursors. *Anal. Chem.* **79**, 477-485 (2007)
23. Hamidane, H.B., Chiappe, D., Hartmer, R., Vorobyev, A., Moniatte, M., Tsybin, Y.O.: Electron capture and transfer dissociation: Peptide structure analysis at different ion internal energy levels. *J. Am. Soc. Mass. Spectrom.* **20**, 567-575 (2009)
24. Iavarone, A.T., Jurchen, J.C., Williams, E.R.: Supercharged Protein and Peptide Ions Formed by Electrospray Ionization. *Anal. Chem.* **73**, 1455-1460 (2001)
25. Iavarone, A.T., Williams, E.R.: Supercharging in electrospray ionization: effects on signal and charge. *Int. J. Mass spectrom.* **219**, 63-72 (2002)
26. Iavarone, A.T., Williams, E.R.: Mechanism of Charging and Supercharging Molecules in Electrospray Ionization. *J. Am. Chem. Soc.* **125**, 2319-2327 (2003)
27. Zhang, J., Ogorzalek Loo, R.R., Loo, J.A.: Increasing Fragmentation of Disulfide-Bonded Proteins for Top-Down Mass Spectrometry by Supercharging. *Int. J. Mass spectrom.* **377**, 546-556 (2015)
28. Meyer, J.G., A. Komives, E.: Charge State Coalescence During Electrospray Ionization Improves Peptide Identification by Tandem Mass Spectrometry. *J. Am. Soc. Mass. Spectrom.* **23**, 1390-1399 (2012)
29. Kjeldsen, F., Savitski, M.M., Adams, C.M., Zubarev, R.A.: Determination of the location of positive charges in gas-phase polypeptide polycations by tandem mass spectrometry. *Int. J. Mass spectrom.* **252**, 204-212 (2006)
30. Kalli, A., Håkansson, K.: Electron capture dissociation of highly charged proteolytic peptides from Lys N, Lys C and Glu C digestion. *Mol. BioSyst.* **6**, 1668-1681 (2010)
31. Cassou, C.A., Sterling, H.J., Susa, A.C., Williams, E.R.: Electrothermal Supercharging in Mass Spectrometry and Tandem Mass Spectrometry of Native Proteins. *Anal. Chem.* **85**, 138-146 (2013)
32. Kalli, A., Håkansson, K.: Comparison of the Electron Capture Dissociation Fragmentation Behavior of Doubly and Triply Protonated Peptides from Trypsin, Glu-C, and Chymotrypsin Digestion. *J. Proteome Res.* **7**, 2834-2844 (2008)
33. Vasicek, L., Brodbelt, J.S.: Enhanced Electron Transfer Dissociation through Fixed Charge Derivatization of Cysteines. *Anal. Chem.* **81**, 7876-7884 (2009)
34. Kjeldsen, F., Giessing, A.M.B., Ingrell, C.R., Jensen, O.N.: Peptide Sequencing and Characterization of Post-Translational Modifications by Enhanced Ion-Charging and Liquid Chromatography Electron-Transfer Dissociation Tandem Mass Spectrometry. *Anal. Chem.* **79**, 9243-9252 (2007)
35. Rand, K.D., Zehl, M., Jensen, O.N., Jørgensen, T.J.D.: Protein Hydrogen Exchange Measured at Single-Residue Resolution by Electron Transfer Dissociation Mass Spectrometry. *Anal. Chem.* **81**, 5577-5584 (2009)
36. Zenaidee, M.A., Donald, W.A.: Electron capture dissociation of extremely supercharged protein ions formed by electrospray ionisation. *Anal. Methods.* **7**, 7132-7139 (2015)
37. Zhurov, K.O., Fornelli, L., Wodrich, M.D., Laskay, Ü.A., Tsybin, Y.O.: Principles of

- electron capture and transfer dissociation mass spectrometry applied to peptide and protein structure analysis. *Chem. Soc. Rev.* **42**, 5014-5030 (2013)
38. Coon, J.J., Syka, J.E.P., Schwartz, J.C., Shabanowitz, J., Hunt, D.F.: Anion dependence in the partitioning between proton and electron transfer in ion/ion reactions. *Int. J. Mass spectrom.* **236**, 33-42 (2004)
  39. Zehl, M., Rand, K.D., Jensen, O.N., Jørgensen, T.J.D.: Electron Transfer Dissociation Facilitates the Measurement of Deuterium Incorporation into Selectively Labeled Peptides with Single Residue Resolution. *J. Am. Chem. Soc.* **130**, 17453-17459 (2008)
  40. Anusiewicz, I., Berdys-Kochanska, J., Simons, J.: Electron Attachment Step in Electron Capture Dissociation (ECD) and Electron Transfer Dissociation (ETD). *J. Phys. Chem. A.* **109**, 5801-5813 (2005)
  41. Gunawardena, H.P., He, M., Chrisman, P.A., Pitteri, S.J., Hogan, J.M., Hodges, B.D.M., McLuckey, S.A.: Electron Transfer versus Proton Transfer in Gas-Phase Ion/Ion Reactions of Polyprotonated Peptides. *J. Am. Chem. Soc.* **127**, 12627-12639 (2005)
  42. Cody, R.B., Freiser, B.S.: Electron impact excitation of ions from organics: an alternative to collision induced dissociation. *Anal. Chem.* **51**, 547-551 (1979)
  43. Wang, B.-H., McLafferty, F.W.: Electron impact excitation of ions from larger organic molecules. *Org. Mass Spectrom.* **25**, 554-556 (1990)
  44. Kjeldsen, F., Haselmann, K.F., Budnik, B.A., Jensen, F., Zubarev, R.A.: Dissociative capture of hot (3–13 eV) electrons by polypeptide polycations: an efficient process accompanied by secondary fragmentation. *Chem. Phys. Lett.* **356**, 201-206 (2002)

## Chapter 5

### Off-line HILIC Sample Preparation for Improved Detection of Host Cell Proteins in Drug Substances

#### 5.1 Introduction

Host cell proteins (HCPs) are native proteins from the host organism used to express a biotherapeutic antibodies. HCPs may be co-purified with the drug substance protein [1]. The presence of these impurities in biotherapeutics may potentially elicit immune responses in patients, affect drug efficacy, and cause product instability [2, 3]. Therefore, effective removal of these impurities needs to be achieved in the downstream purification process during manufacturing, and HCPs present must be monitored and characterized to understand potential risks [4, 5].

Enzyme-linked immunosorbent assay (ELISA) remains the most common technique used for HCP characterization in industry because of its high sensitivity, high throughput, and capability for quantification [1]. Generally, generic HCP ELISAs are developed using polyclonal antibodies raised against antigen proteins produced in culture from a process-representative null host cell line. However, achieving antibody coverage of all HCP species present within a certain manufacturing process is still a challenge, and even the best process-specific HCP ELISA cannot detect 100% of the HCPs for a given host cell line [5].

In addition to ELISA, protein separation and visualization methods, such as 1D and 2D sodium dodecyl sulfate-polyacrylamide gel electrophoresis (SDS-PAGE) [6], 2D-differential in-gel electrophoresis (2D-DIGE), western blotting (WB) [7], and capillary zone electrophoresis

(CZE), are valuable tools for HCP characterization. While protein-specific antibodies can be used effectively with ELISA and WB techniques, separation techniques alone do not enable protein identification, nor is it practical to raise specific antibodies for all HCPs.

LC/MS-based “shotgun” proteomics is a powerful method for HCP characterization to support downstream purification process development [8, 9] and is increasingly common throughout industry. In contrast to ELISA and 1D/2D gel electrophoresis methods, HCPs can be identified upon database searches against the entire proteome of the host organism. Approximate quantification of individual HCP species can also be achieved by spiking in known amounts of internal standard proteins in 2D-LC/MS<sup>E</sup> and by utilizing the “Hi-3” [4, 10] quantitative strategy, or more accurately quantified using specific peptide or protein standards. However, because HCPs contained within a biopharmaceutical product are typically at less than 100 ppm concentration (ng of HCP per mg biotherapeutic protein), a dynamic range of up to 6 orders of magnitude is required in order to detect these low abundance species within the overwhelming background of the drug substance, a challenge for even state-of-the-art mass spectrometers.

Strategies to circumvent this problem include chromatographically resolving HCP peptides from drug substance peptides by using long LC gradients, using multiple columns, and adding multiple separation dimensions such as 2D-LC [10, 11] and/or ion mobility [11]. The drawback of enhanced separation is that throughput can be greatly sacrificed, limiting the types of studies which can be supported. Other approaches include enriching residual HCPs by removing the monoclonal antibody (mAb) with affinity purification [9], precipitating the mAb after minimal digestion under native conditions [12]; and applying novel data acquisition methods allowing more peptide species to be fragmented by tandem mass spectrometry (for example, data-independent acquisition and MS<sup>E</sup>) [10, 11].

The native digestion/mAb-precipitation sample preparation method, first described in a recent publication by Huang *et al.* [12], mitigates this dynamic range issue by depletion of the mAb. The method relies on the hypothesis that the mAb will maintain its folded three-dimensional structure under native conditions (neutral pH, non-denaturing buffer) and resist protease digestion

when incubated with trypsin, while less-rigid HCPs will be digested into peptides. After incubation, undigested protein (presumably the therapeutic mAb) is precipitated and removed, while HCP peptides in the supernatant are recovered and analyzed by LC/MS. There are a few concerns associated with this method, including risks that heat-labile HCP peptides may be lost, HCPs may co-precipitate with the mAb, and the method is designed to work optimally for digestion-resistant drug substances such as mAbs, thus it may not perform as well for other molecules such as fusion proteins [13, 14], which are known to be structurally flexible.

A novel hydrophilic interaction chromatography (HILIC) method based on a large pore size stationary phase has shown potential for characterization of product-related low molecular weight (LMW) impurities in mAb products, such as mAb fragments and subunits [15]. Upon HILIC separation, the elution order was observed to be mostly determined by the molecular weight, with LMW species eluting earlier [15].

Here, we demonstrate a new approach involving offline HILIC sample preparation to separate HCPs from therapeutic protein in order to improve LC/MS sensitivity for low-level HCPs. Our results indicate that most HCP species can be well-resolved from the therapeutic protein utilizing HILIC separation, collected in fractions and concentrated, then subjected to trypsin digestion and LC/MS analysis. The HILIC-enriched HCP method shows improved sensitivity to several HCPs in the NISTmAb (RM 8671) that were not reported or observed using other LC/MS strategies, and can serve as a complementary technique for HCP detection to previously published analytical strategies. This method is also demonstrated successfully for HCP analysis of non-mAb drug substances, in particular for a fusion protein.

## **5.2 Experimental**

### **5.2.1 Materials**

A recombinant IgG1 mAb (BMS mAb 1), a fusion protein (BMS fusion protein 1), and Chinese hamster ovary (CHO) null strain material (containing HCPs without drug substance) produced by Bristol-Myers Squibb (Hopewell, NJ) were used in this work. Humanized IgG1 $\kappa$  monoclonal antibody standard RM 8671 was purchased from the National Institute of Standards

and Technology (NIST, Gaithersberg, MD). All chemicals were reagent grade or better. Ammonium formate, ammonium hydroxide solution (~1 M in water), DL-dithiothreitol (DTT), dimethyl sulfoxide (DMSO), and Trizma pre-set crystals (pH 8.0) were purchased from Sigma-Aldrich Co. (St. Louis, MO). Water and acetonitrile (LC-MS grade), formic acid (FA), and trifluoroacetic acid (TFA) were obtained from Thermo Fisher Scientific (Rockford, IL). Urea (crystalline) was purchased from Alfa Aesar (Tewksbury, MA). Sequencing grade modified trypsin was obtained from Promega (Madison, WI). Pre-mixed chromatographic solvents (water containing 0.1% TFA, and acetonitrile containing 0.1% TFA), were from J. T. Baker Chemical Co. (Phillipsburg, NJ).

### **5.2.2 Offline HILIC Sample Preparation**

For initial method development, BMS mAb 1 material was diluted in water to a concentration of 2.50 mg/mL, with or without spiked HCP standard at a concentration of 2.35 mg/mL. A 4  $\mu$ L injection volume was utilized for aqueous samples. To increase mass loading on column, concentrated BMS mAb 1 drug substance (74.7 mg/mL in buffer) was mixed with CHO null strain material to produce 10,000 (10k) or 1,000 (1k) ppm spiked HCP in 37.5 mg/mL therapeutic protein.

For higher mass loading with lower concentration samples, organic solvents were added. NISTmAb (10 mg/mL) or BMS fusion protein 1 (25 mg/mL) were mixed with acetonitrile, DMSO, and TFA to a final ratio of 28/66/5/1 for therapeutic protein solution/acetonitrile/DMSO/TFA (v/v). The resulting concentration was 2.8 mg/mL for NISTmAb and 7.0 mg/mL for BMS fusion protein 1. For BMS mAb 1, 150  $\mu$ g was loaded onto the HILIC column per injection; for NISTmAb and BMS fusion protein 1, 700  $\mu$ g was loaded onto the HILIC column per injection. Samples were analyzed in duplicate.

### **5.2.3 HILIC Separation Parameters and Fraction Collection**

A Waters ACQUITY UPLC I-Class system was used for all HILIC separations with an ACQUITY UPLC BEH Glycoprotein Amide column (300  $\text{\AA}$ , 1.7  $\mu$ m, 2.1 x 150 mm, Waters, Milford, MA). The column was set at 60  $^{\circ}$ C and the LC solvents were 0.1% TFA in water as A

and 0.1% TFA in acetonitrile as B. For completely aqueous samples, the separation was performed with a 24-min gradient starting at 15% A for the first 0.5 min at 0.2 mL/min, ramping up to 28% A in another 0.5 min, and then linearly increasing from 28% to 42% A over the next 23 min. The gradient was then ramped to 99% A in 2 min with an increase of flow rate to 0.25 mL/min and held for 3 min before decreasing to 15% A in 3 min and then maintained at the initial condition for another 8 min to equilibrate the column. UV chromatograms were acquired at 215 and 280 nm.

For samples diluted in organic solvents, or for non-mAb samples, the gradient was modified slightly. For NISTmAb, the same gradient as above but with an initial condition of 28% A instead of 15% A was used. For BMS fusion protein 1, the 24 min LC gradient also commenced at 28% A but was held constant for 0.5 min before linearly increasing to 38% A in 12.5 min, then ramping to 58% A over another 11 min.

Based on the main UV peak location, indicating the therapeutic protein elution time, the HILIC eluate was collected in three separate fractions: pre-peak (Fraction #1); main peak (Fraction #2); and post-peak (Fraction #3). The main peak generally eluted between ~12 min and 15-19 min after injection. Fractions from two HILIC runs were combined for the BMS mAb 1 spiked samples. For NISTmAb and BMS fusion protein 1, a single injection of 700  $\mu$ g was performed and the fractions were collected from only one HILIC run.

Ammonium hydroxide solution (1 M) was added to each fraction to adjust pH to 6-7 (~18  $\mu$ L per mL) before each fraction was concentrated down to < 30  $\mu$ L using a centrifugal vacuum concentrator set to 40  $^{\circ}$ C coupled with a refrigerated vapor trap (Savant SPD111V and RVT5105, Thermo Scientific, Waltham, MA). Concentrated/dried samples were reconstituted with 100  $\mu$ L of digestion buffer containing 2 M urea and 50 mM tris-HCl (pH 8.0). Each sample was vigorously mixed by a vortex mixer, then combined with 50 mg/mL DTT solution. For BMS mAb 1 spiked samples, 2  $\mu$ L of the DTT solution was added to each fraction. For NISTmAb and BMS fusion protein 1, 3  $\mu$ L, 6  $\mu$ L, and 2  $\mu$ L of DTT solution was added to Fractions #1, 2 and 3, respectively. Fractions were then incubated for 20 min at 60  $^{\circ}$ C.

#### **5.2.4 Trypsin Digestion**

After cooling to room temperature, each fraction was treated with 0.5 mg/mL trypsin and incubated at 37 °C overnight (>15 h). For BMS mAb 1 spiked samples, the volume of the trypsin solution added was 2 µL, 3 µL and 1 µL to Fractions #1, 2 and 3, respectively. For NISTmAb and BMS fusion protein 1, the volume of the trypsin solution added was 5 µL, 10 µL and 3 µL to Fractions #1, 2 and 3, respectively. Digests were centrifuged at 13,000 x g for 2 min. The supernatant was transferred to an HPLC vial and 5 µL of 10% FA in water was added and mixed before LC MS/MS analysis. As control experiments, the aforementioned therapeutic protein samples were also prepared using the mAb-precipitation digestion method as described elsewhere [12].

#### **5.2.5 UPLC-MS/MS Analysis of Tryptically Digested HILIC Fractions**

The total volume of the digest for each HILIC fraction (100-120 µL) was injected for UPLC-MS/MS analysis unless otherwise specified. Tryptic digests were separated using a Waters ACQUITY UPLC CSH C18 column (1.7 µm, 2.1 x 100 mm) on a Waters ACQUITY UPLC system (Milford, MA). The mobile-phase solvent A was water with 0.1% FA and the solvent B was acetonitrile with 0.1% FA. Separation was performed at a column temperature of 60 °C with a mobile-phase gradient reported elsewhere [12]. On-line mass spectrometric analysis was conducted using an Orbitrap Fusion Lumos Tribrid Mass Spectrometer (Thermo Scientific, Waltham, MA) in positive ion mode utilizing orbitrap (OT) and ion trap (IT) detection for MS1 scans and MS2 scans, respectively. The MS1 full scan was conducted in a mass range of 230-1,500 *m/z* (resolution 120,000, AGC target 4.0e5, and maximum injection time 50 ms) followed by data-dependent HCD fragmentation (collision energy 32%, AGC target 1.0e4, and maximum injection time 300 ms) in a 3-s cycle time. Dynamic exclusion was applied after 1 scan for a duration of 60 s. The ion source (H-ESI) settings were as follows: ESI voltage 3,500 V, sheath gas flow rate 30, aux gas flow rate 7, sweep gas flow rate 1, ion transfer tube temperature 300 °C, and vaporizer temperature 150 °C. Precursor ions were selected in the quadrupole using a 1.4 *m/z* window.

### 5.2.6 Database Search Parameters

MS/MS data were searched for HCP identification using Byonic 3.1.0 (ProteinMetrics, San Carlos, CA) against a customized protein database including the therapeutic protein sequence and the CHO or mouse proteome, as appropriate, downloaded from UniProt.org. Search parameters were set as follows: mass tolerance as 10 ppm for precursors and 0.4 Da for fragments, fully specific peptide termini with  $\leq 3$  missed cleavages, and protein FDR cutoff at 1%. N-terminal glutamine formation of pyroglutamate was considered a common variable modification and oxidized methionine a rare variable modification (maximum 1 common and 1 rare modification). Protein hits with  $|\text{Log Prob}|$  score lower than 4.0, decoys, and common protein contaminants were excluded. Protein hits with only 1 or 2 unique peptides were manually verified to remove false positives.

### 5.3 Results and Discussion

Our HILIC-enriched HCP method was developed to address the dynamic range limitation of current LC/MS instrumentation when applied towards the detection of residual HCPs in biotherapeutic proteins. The separation capability of HILIC to dissociate and enrich HCP species from therapeutic proteins was explored to develop a protocol for collecting and reconstituting HCP fractions, followed by trypsin digestion and analysis by LC-MS/MS (Figure 5.1). This strategy takes advantage of the high loading capacity of the HILIC column to provide a semi-preparatory scale separation within 24 min. A large drying chamber helped fast concentration of HILIC fractions and a 2-h mobile-phase gradient was used for the UPLC-MS/MS analysis of trypsin digests of these fractions, enabling a comparable throughput for HCP detection to other LC/MS HCP methods [12] (particularly if only Fraction #1 is analyzed).

The HILIC chromatographic step can be advantageous for separation of HCPs from therapeutic proteins as compared with other strategies. The developed method allows up to 700  $\mu\text{g}$  per injection, with greater column loads possible. The denaturing conditions (high organic mobile phase) used are believed to facilitate disruption of protein-protein interactions between HCPs and

the drug substance, enabling separations that may not be achieved with other columns. The utilized amide column features wide pores and small particle size (300 Å and 1.7 µm, respectively) to achieve high resolution HILIC separation for intact proteins as compared with other types of HILIC columns. We selected the largest commercially available column diameter and length (2.1 x 150 mm) to maximize loading capacity.

Though protein precipitation may be problematic for high organic solvent concentrations, our HILIC method was optimized to maintain solubility. For example, 0.1% TFA not only improves separation resolution via ion pairing, but significantly increases solubility of therapeutic proteins in high acetonitrile mobile phases, and prevented column clogging observed with other additives such as formic acid (data not shown). Acetonitrile also facilitates concentration of fractions due to its higher vapor pressure than aqueous solvents.

Following fraction collection, the pH value of each fraction was adjusted to ~7 to prevent a decrease in pH from concentration of TFA during drying. Upon completion of the concentration step, white precipitation could be observed at the bottom of the microcentrifuge vial in a small amount of liquid for Fraction #2 samples and some Fraction #1 samples, but no precipitation was observed in the concentrated Fraction #3 samples. A chaotropic salt (urea) was added to the digestion buffer in order to improve reconstitution of the precipitated proteins. Subsequent heated reduction and overnight incubation with trypsin ensured thorough digestion of all present protein species into peptides.

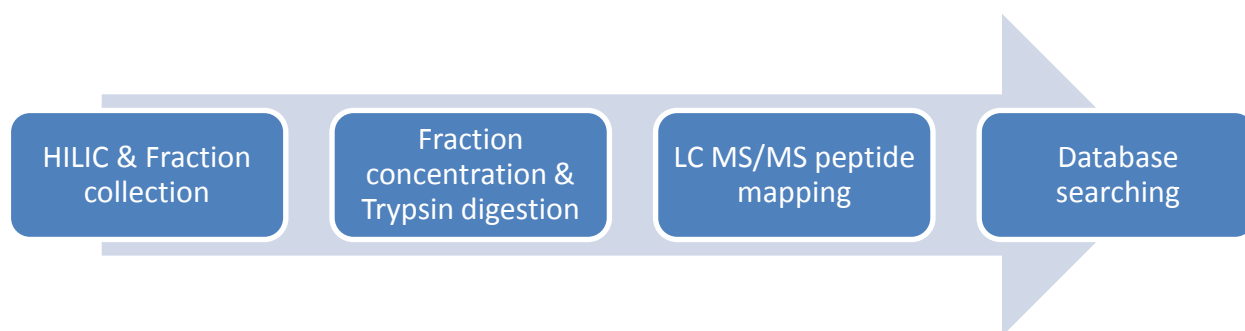


**Figure 5.1** Proposed protocol for our HILIC-enriched HCP LC/MS method.

### 5.3.1 Separation Profiles of HCPs and Therapeutic mAb using HILIC

As shown in the UV chromatogram in Figure 5.2, spiked HCPs (blue line) are well resolved from BMS mAb 1 (black line). This result agrees with the previously reported finding that LMW impurities (such as many HCPs [14]) in therapeutic mAbs can be characterized based on a size-related elution order when a similar HILIC strategy was used [15].

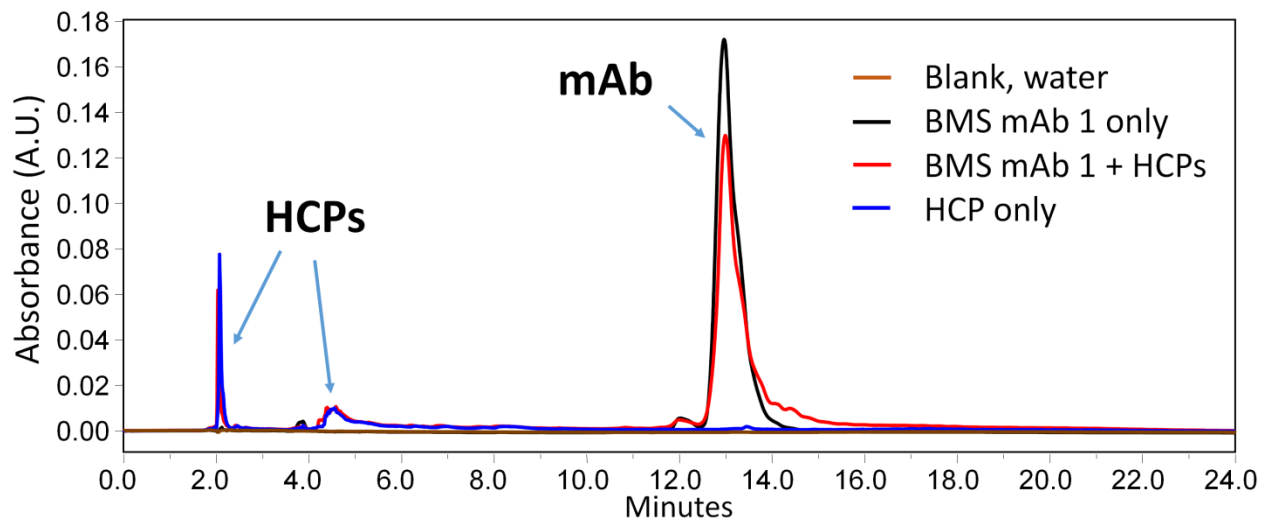


**Figure 5.2** 280 nm UV chromatograms from HILIC separation of 10.0  $\mu\text{g}$  BMS mAb 1 drug substance with (red line) and without (black line) addition of 9.4  $\mu\text{g}$  HCP standard from CHO null cell line. Blank (water, brown line) and null cell HCP material only (blue line) chromatograms are also shown for reference. A Waters UPLC BEH Glycoprotein Amide column (300  $\text{\AA}$ , 1.7  $\mu\text{m}$ , 2.1 x 150 mm) was used.

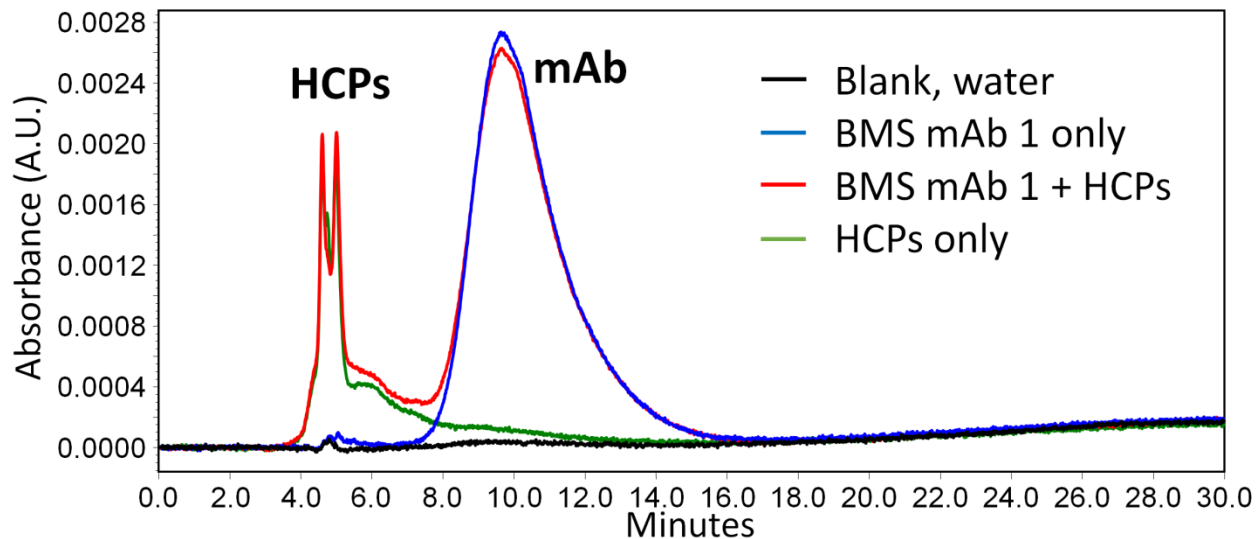


**Figure 5.3** 280 nm UV chromatograms from HILIC separation of 5.0  $\mu\text{g}$  BMS mAb 1 drug substance with (red line) and without (blue line) addition of 4.7  $\mu\text{g}$  HCP standard from CHO null cell line. Blank (water, black line) and null cell HCP material only (green line) chromatograms are also shown for reference. A Waters XBridge HILIC column (5  $\mu\text{m}$ , 4.6 x 150 mm) was used at an operating temperature of 45  $^{\circ}\text{C}$ . Mobile phase solvent A was 20 mM ammonium formate in water containing 0.1% formic acid and mobile phase solvent B was 20 mM ammonium formate in 90/10 acetonitrile/water containing 0.1% formic acid.

**Table 5.1** LC mobile phase gradient and flow rate used with the Waters XBridge HILIC column (data in Figure 5.3).

Time (min)	Flow rate (mL/min)	A%	B%
0	0.4	50.0	50.0
25	0.4	99.0	1.0
30	0.4	99.0	1.0
31	0.4	50.0	50.0
34	0.6	50.0	50.0
36	0.6	99.5	0.5
39	0.6	99.5	0.5
41	0.6	50.0	50.0
61	0.4	50.0	50.0
62	0.4	50.0	50.0

We also evaluated two other commercially available HPLC HILIC columns – a Waters XBridge HILIC column (150  $\text{\AA}$ , 5  $\mu\text{m}$ , 4.6 x 150 mm) and a Phenomenex Luna HILIC column (200  $\text{\AA}$ , 5  $\mu\text{m}$ , 4.6 x 150 mm). We observed that separation between the HCP standard and mAbs

could be achieved using the XBridge column with different mobile phase solvents and gradient (Table 5.1) compared with the Glycoprotein Amide column used in Figure 5.2; however, the loading capacity for the former column was limited, with the UV chromatogram showing significant tailing upon loading of just 5.0  $\mu\text{g}$  mAb and 4.7  $\mu\text{g}$  HCP standard (Figure 5.3). The Luna column did not show capability of separating intact proteins (data not shown). Because the Waters Glycoprotein Amide column provided the highest separation performance, it was used for all subsequent experiments.

### 5.3.2 HCP Detection with Spiked Samples

Highly purified drug substance BMS mAb 1 was spiked with HCP standard to evaluate the performance of the HILIC-enriched HCP method. Figure 5.4 shows the chromatographic profile from HILIC separation of 150  $\mu\text{g}$  drug material spiked with 10k ppm HCPs. The main peak area (Fraction #2) appeared at a retention time of 11.7–15.5 min, indicating that the therapeutic protein was well-retained on the column (retention factor  $\sim 5$ ). The spiked HCP species were barely visible on the UV chromatogram, probably due to the sensitivity limits of UV detection. However, based on the separation profile in Figure 5.2, it is probable that the majority of HCP species eluted into Fraction #1.

Respective fractions from two consecutive HILIC chromatograms were pooled for reconstitution, digestion, and LC/MS analysis. As indicated in Table 5.2, when 1k ppm HCP standards were spiked into BMS mAb 1, a total of 89 HCPs were identified from Fractions #1, #2, and #3, with 92% (82 out of 89) of HCPs observed from Fraction #1. In addition, there were 5 HCPs co-eluting with the mAb (Fraction #2). However, the mAb-precipitation method was only able to detect 41 HCPs. Of the 82 HCPs present in Fraction #1, 62 were not detected with the mAb-precipitation method. These results indicate that the HILIC-enriched HCP method showed improved sensitivity for many HCPs and provided complementary information for HCP detection compared with the mAb-precipitation method.

Interestingly, a different trend was observed with the 10k ppm HCP-spiked sample. While the mAb-precipitation method was able to detect 225 HCPs, a total of 193 HCPs were

observed from the three HILIC-enriched fractions. Even though the total number of HCPs identified by our method was lower than the mAb-precipitation method, the two methods showed sensitivity for different HCPs, thus providing complementary information and expanding the total number of HCPs identified to 294, as shown in Table 5.2. For example, 56 out of 162 (35%) identified HCPs from Fraction #1 were not observed using the mAb-precipitation method. Four out of 13 (31%) from Fraction #2 and 12 out of 35 (34%) from Fraction #3 were newly identified as well.

While the difference in selectivity of the two sample preparation strategies is evident from our study, the cause of these differences is not obvious. Potential sensitivity limitations of the mAb-precipitation method include risk of high background from over-digestion of the mAb, under-digestion of certain HCPs under non-denaturing conditions, co-precipitation of HCP peptides with the mAb, or degradation of thermally labile peptides during the precipitation step. Potential limitations of our HILIC enrichment method include risk of strong adsorption or precipitation of certain HCPs in the mobile phase, preventing elution; however our solvents were optimized to minimize this risk, and no column clogging or increase in back pressure was observed. Additionally, precipitate was observed in Fractions #1 and #2 after drying. Though pellets appeared to fully dissolve in the 2 M urea buffer utilized for digestion, it is possible that not all HCPs were fully reconstituted prior to digestion. Lastly, some HCPs may, by virtue of their size, hydrophobicity, or strong protein interactions (not disrupted by acetonitrile), co-elute with the therapeutic. As shown in Table 5.2, some HCPs were observed only in Fraction #2, which supports this hypothesis. The presence of high levels of therapeutic in Fraction #2 may limit sensitivity for low-level HCPs in that fraction.

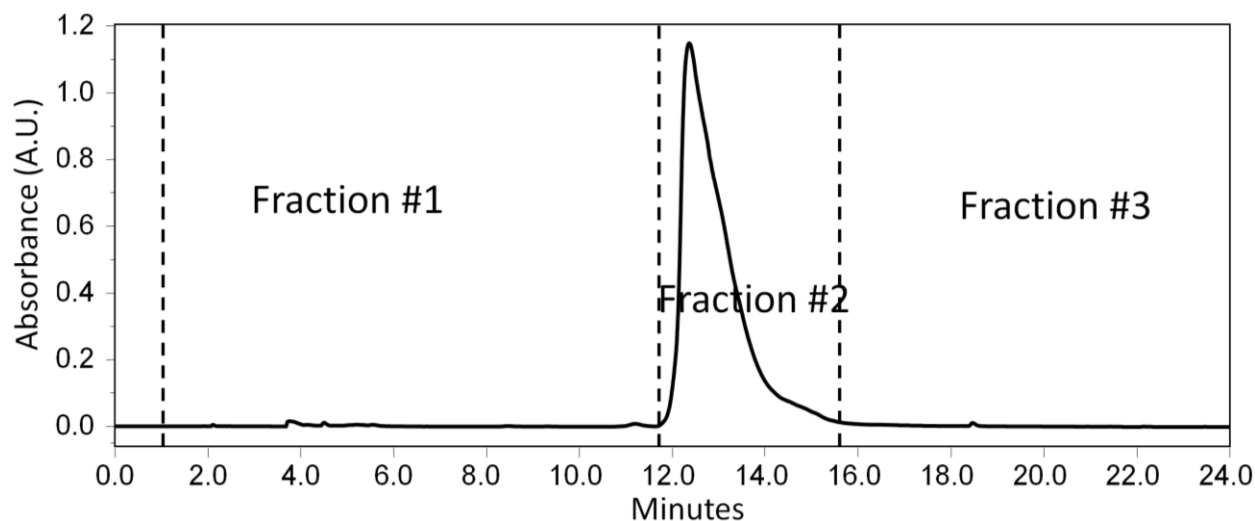


**Figure 5.4** The 280 nm UV chromatogram following HILIC separation of 150  $\mu$ g BMS mAb 1 drug substance spiked with 10k ppm HCPs. The LC eluate was collected as Fraction #1, #2, and #3 separately, as indicated by the different retention time ranges: 1.0–11.7 min for Fraction #1, 11.7–15.5 min for Fraction #2, and 15.5–24.0 min for Fraction #3.

**Table 5.2** The numbers of HCPs identified in the three HILIC-enriched fractions compared with those identified by the mAb-precipitation method for BMS mAb 1 spiked with 1k and 10k ppm HCP standards, NISTmAb, and BMS fusion protein 1. The numbers in parentheses indicate how many HCPs were uniquely identified by the HILIC-enriched HCP method but not by the mAb-precipitation method for each sample.

Method	BMS mAb 1 + 1k ppm HCP	BMS mAb 1 + 10k ppm HCP	NISTmAb	BMS fusion protein 1
<b><u>HILIC-enriched HCP method</u></b>	<b><u>89 (66)</u></b>	<b><u>193 (69)</u></b>	<b><u>71 (21)</u></b>	<b><u>22 (7)</u></b>
<b>Fraction #1 only</b>	<b>81 (62)</b>	<b>150 (54)</b>	<b>68 (21)</b>	<b>18 (6)</b>
Both Fractions #1 and #2	1 (0)	2 (0)	0 (0)	0 (0)
<b>Fraction #2 only</b>	<b>3 (2)</b>	<b>6 (3)</b>	<b>0 (0)</b>	<b>0 (0)</b>
Both Fractions #2 and #3	1 (1)	1 (1)	0 (0)	0 (0)
<b>Fraction #3 only</b>	<b>3 (1)</b>	<b>24 (9)</b>	<b>1 (0)</b>	<b>2 (1)</b>
Both Fractions #1 and #3	0 (0)	6 (2)	1 (0)	0 (0)
Fractions #1, #2, and #3	0 (0)	4 (0)	1 (0)	2 (0)
<b><u>mAb-precipitation method</u></b>	<b><u>41</u></b>	<b><u>225</u></b>	<b><u>91</u></b>	<b><u>17</u></b>
<b><u>Two methods combined</u></b>	<b><u>107</u></b>	<b><u>294</u></b>	<b><u>112</u></b>	<b><u>24</u></b>

### 5.3.3 HCP detection with NISTmAb

NISTmAb standard (RM 8671) is commonly used to evaluate LC/MS method performance, and is particularly informative for HCP characterization given its relatively low purity compared with most therapeutic mAbs [11, 12]. To analyze this standard by our method, a large injection volume was required to ensure a high loading amount of NISTmAb on the HILIC column, because its concentration was relatively low (10 mg/mL) compared with the BMS drug substances (74.7 mg/mL for BMS mAb 1 and 25.0 mg/mL for BMS fusion protein 1). A dilution strategy for NISTmAb (and other therapeutic proteins) was therefore developed, to overcome solubility risks with the HILIC mobile phase.

To prevent precipitation, DMSO and TFA were added to NISTmAb, enabling solubility in up to 72% acetonitrile. We also adjusted the HILIC mobile phase starting conditions to be aligned with the sample solvent strength, maintaining protein solubility. Figure 5.5 shows the UV chromatogram of the HILIC separation when 700  $\mu$ g NISTmAb material was loaded in one injection. While some increase in peak tailing was observed at high loading, the front of the mAb peak remained at about the same retention time as previous smaller injections (~12 min) and the peak returned to baseline at ~17 min. No change in peak shape or back pressure was observed after ~50 injections, supporting that high mass loading is not impacting the column adversely. As described above, most HCPs present in the sample are believed to elute earlier than the mAb, possibly within the solvent front as indicated by the small peak around 2 min, thus the peak tailing is not expected to impact separation of HCPs from NISTmAb.

The numbers of HCPs that could be identified from each fraction from NISTmAb are shown in Table 5.2, and are compared with the mAb-precipitation method. 71 and 91 HCPs were detected in total by our method and the mAb-precipitation method, respectively, for NISTmAb. 99% (70/71) of HCPs detected with the HILIC-enriched HCP method came from Fraction #1. A total of 21 new HCPs (Table 5.3) were identified by this method compared with the mAb-precipitation method, increasing the total identified HCPs to 112. These 21 new HCPs were detected in duplicate measurements.

A list of all 71 HCPs identified from the three HILIC fractions is shown in Table 5.4. To ensure that no protein identifications were the result of HCP carry-over, the HILIC column was washed with two water injections prior to NISTmAb injection. Additionally, a blank sample was analyzed with no sample protein but including the digestion protocol to assess false positive HCPs. As further precaution, the MS/MS spectra of the identified peptides from the 21 novel HCPs (Table 5.3) were all manually verified. Two of these MS/MS spectra (peptides from ubiquitin-60S ribosomal protein L40 and ATPase inhibitor, mitochondrial) are shown in Figure 5.6. To our knowledge, these 21 HCP species have not been previously reported within NISTmAb [11, 12]. In addition, the concentrations of the 50 HCPs commonly identified by our method and previous work are reported to range from less than 1 to over 200 ppm in NISTmAb [11, 12], demonstrating the great sensitivity of our method for HCP characterization in biotherapeutic protein drugs.

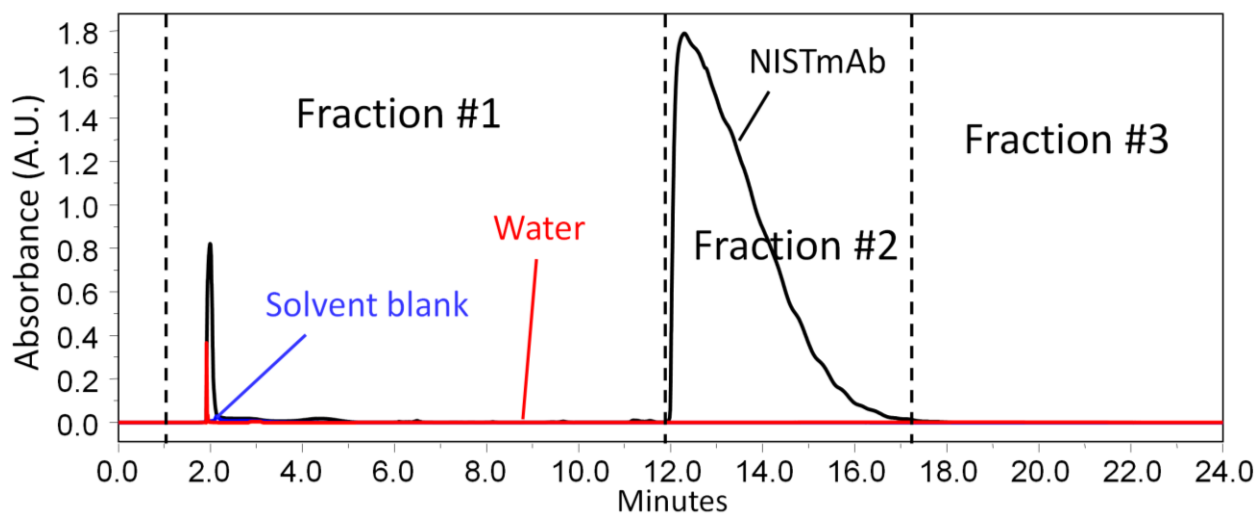


**Figure 5.5** 280 nm UV chromatograms following HILIC separation of 700  $\mu$ g NISTmAb. Two control injections are indicated with a red line (water) and blue line (solvent blank, H<sub>2</sub>O/ACN/DMSO/TFA 28/66/5/1 (v/v)). The LC eluate was collected in Fractions #1, #2, and #3 separately, as indicated by the different retention time ranges: 1.0–11.9 min for Fraction #1, 11.9–17.3 min for Fraction #2, and 17.3–24.0 min for Fraction #3.

**Table 5.3** NISTmAb HCPs uniquely identified with our HILIC-enriched HCP LC/MS method. These HCPs were not observed with the mAb-precipitation method and, to our knowledge, have not been reported previously.

<b>No.</b>	<b>Accession #</b>	<b>HCP Name</b>
1	<b>Q8K019</b>	Bcl-2-associated transcription factor 1
2	<b>P62984</b>	Ubiquitin-60S ribosomal protein L40
3	<b>O35143</b>	ATPase inhibitor, mitochondrial
4	<b>Q9CXW3</b>	Calcyclin-binding protein
5	<b>P70333</b>	Heterogeneous nuclear ribonucleoprotein H2
6	<b>Q9CQE1</b>	Protein NipSnap homolog 3B
7	<b>O35166</b>	Golgi SNAP receptor complex member 2
8	<b>P23116</b>	Eukaryotic translation initiation factor 3 subunit A
9	<b>Q61035</b>	Histidine--tRNA ligase, cytoplasmic
10	<b>P62897</b>	Cytochrome c, somatic
11	<b>Q62504</b>	Msx2-interacting protein
12	<b>Q99K48</b>	Non-POU domain-containing octamer-binding protein
13	<b>P62843</b>	40S ribosomal protein S15
14	<b>Q8CI11</b>	Guanine nucleotide-binding protein-like 3
15	<b>P54227</b>	Stathmin
16	<b>O08784</b>	Treacle protein
17	<b>D3Z0M9</b>	DEAD (Asp-Glu-Ala-Asp) box polypeptide 23
18	<b>Q3U0P5</b>	Ectonucleoside triphosphate diphosphohydrolase 6
19	<b>P51954</b>	Serine/threonine-protein kinase Nek1
20	<b>A2AFI3</b>	RNA binding motif protein, X chromosome, isoform CRA_b
21	<b>Q9DBG7</b>	Signal recognition particle receptor subunit alpha

**Table 5.4** A full list of identified HCPs in NISTmAb (RM 8671) using our HILIC-enriched HCP LC/MS method. For each identified HCP, the number of unique peptides observed, protein sequence coverage (%), and HILIC fraction are also listed.

No.	Accession #	HCP name	# of unique peptides	Coverage %	HILIC fraction
1	P05064	Fructose-bisphosphate aldolase A	32	63.46	1,2,3
2	P05063	Fructose-bisphosphate aldolase C	26	52.62	1
3	P06745	Glucose-6-phosphate isomerase	31	49.10	1
4	Q9CZ44	NSFL1 cofactor p47	14	37.84	1
5	Q922R8	Protein disulfide-isomerase A6	11	15.00	1
6	O88569	Heterogeneous nuclear ribonucleoproteins A2/B1	10	25.50	1
7	Q5SUH7	Clathrin interactor 1	7	12.52	1
8	Q9WTP6	Adenylate kinase 2, mitochondrial	11	43.51	1
9	Q9ER00	Syntaxin-12 OS=Mus musculus	6	24.45	1
10	Q68FL6	Methionine--tRNA ligase, cytoplasmic	3	4.66	1
11	P56812	Programmed cell death protein 5	4	38.89	1
12	Q923D2	Flavin reductase (NADPH)	5	33.98	1
13	Q8K4Z5	Splicing factor 3A subunit 1	6	8.22	1
14	Q8K019	Bcl-2-associated transcription factor 1	7	5.44	1
15	F6ZDS4	Nucleoprotein TPR	5	2.30	1
16	Q91YR9	Prostaglandin reductase 1	5	13.98	1
17	P49312	Heterogeneous nuclear ribonucleoprotein A1	4	15.94	1
18	P40142	Transketolase	4	10.43	1
19	P62984	Ubiquitin-60S ribosomal protein L40	4	34.37	1
20	Q9DBP5	UMP-CMP kinase	4	23.47	1
21	P45878	Peptidyl-prolyl cis-trans isomerase FKBP2	4	32.86	1
22	Q8BGD9	Eukaryotic translation initiation factor 4B	3	6.87	1
23	Q99PL5	Ribosome-binding protein 1	2	1.87	1
24	P21460	Cystatin-C	4	22.86	1
25	Q8BL97	Serine/arginine-rich splicing factor 7	6	24.72	1
26	Q68FF6	ARF GTPase-activating protein GIT1	6	6.62	1
27	Q9Z0X1	Apoptosis-inducing factor 1, mitochondrial	4	10.29	1
28	O08583	THO complex subunit 4	2	14.12	1
29	Q8K4F5	Protein ABHD11	5	18.24	1
30	O35143	ATPase inhibitor, mitochondrial	6	27.36	1
31	Q9D8B3	Charged multivesicular body protein 4b	4	16.96	1
32	Q9CXW3	Calcyclin-binding protein	3	9.61	1
33	Q60864	Stress-induced-phosphoprotein 1	4	6.81	1
34	Q03173	Protein enabled homolog	6	9.35	1

No.	Accession #	HCP name	# of unique peptides	Coverage %	HILIC fraction
35	P55302	Alpha-2-macroglobulin receptor-associated protein	4	11.67	1
36	P01887	Beta-2-microglobulin	7	26.05	1
37	Q8CGC7	Bifunctional glutamate/proline--tRNA ligase	2	2.31	1
38	P70372	ELAV-like protein 1	2	11.04	1
39	P70333	Heterogeneous nuclear ribonucleoprotein H2	2	4.90	1
40	Q99020	Heterogeneous nuclear ribonucleoprotein A/B	3	12.63	1
41	Q9CQE1	Protein NipSnap homolog 3B	4	17.41	1
42	Q9D2M8	Ubiquitin-conjugating enzyme E2 variant 2	5	32.41	1
43	Q61335	B-cell receptor-associated protein 31	4	11.43	1
44	P97855	Ras GTPase-activating protein-binding protein 1	5	12.26	1
45	Q3TLH4	Protein PRRC2C	2	1.05	1
46	Q9DB15	39S ribosomal protein L12, mitochondrial	3	15.92	1
47	P08249	Malate dehydrogenase, mitochondrial	3	10.65	1
48	P99029	Peroxisome oxidoreductin-5, mitochondrial	2	8.57	1
49	P10126	Elongation factor 1-alpha 1	2	4.33	1
50	O35166	Golgi SNAP receptor complex member 2	2	10.85	1
51	Q922I7	MCG13402, isoform CRA_c	4	5.77	1
52	P23116	Eukaryotic translation initiation factor 3 subunit A	4	2.23	1
53	Q61035	Histidine--tRNA ligase, cytoplasmic	2	3.93	1
54	P62897	Cytochrome c, somatic	1	10.48	1
55	Q62504	Msx2-interacting protein	3	0.96	1
56	Q792Z1	MCG140784	2	8.13	1,3
57	P40124	Adenylyl cyclase-associated protein 1	3	5.49	1
58	Q99K48	Non-POU domain-containing octamer-binding protein	3	5.92	1
59	P62843	40S ribosomal protein S15	1	8.97	1
60	Q62418	Drebrin-like protein	2	4.59	1
61	Q8CI11	Guanine nucleotide-binding protein-like 3	3	4.46	1
62	P54227	Stathmin	3	14.77	1
63	O08784	Treacle protein	1	1.06	1
64	D3Z0M9	DEAD (Asp-Glu-Ala-Asp) box polypeptide 23	3	3.42	1
65	Q9CQF3	Cleavage and polyadenylation specificity factor subunit 5	1	5.29	1
66	Q3U0P5	Ectonucleoside triphosphate diphosphohydrolase 6	1	2.20	1
67	P51954	Serine/threonine-protein kinase Nek1	3	1.50	1

No.	Accession #	HCP name	# of unique peptides	Coverage %	HILIC fraction
68	Q9JIX8	Apoptotic chromatin condensation inducer in the nucleus	4	5.16	1
69	A2AFI3	RNA binding motif protein, X chromosome, isoform CRA_b	1	4.32	1
70	Q9DBG7	Signal recognition particle receptor subunit alpha	1	1.89	1
71	Q62179	Semaphorin-4B	1	1.22	3

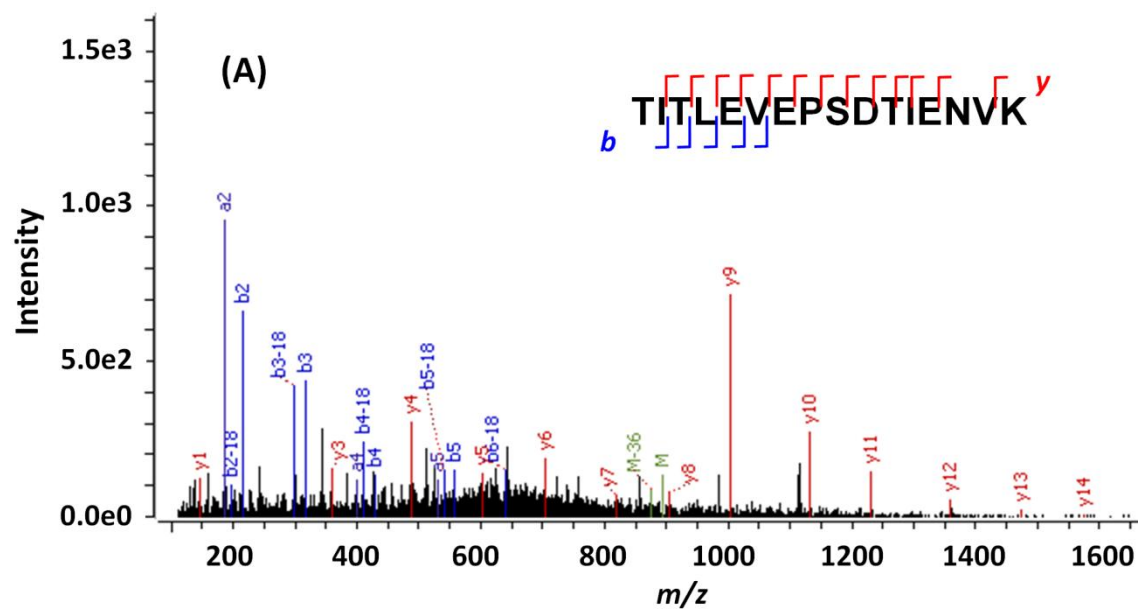


(Figure 5.6 continued on the next page)

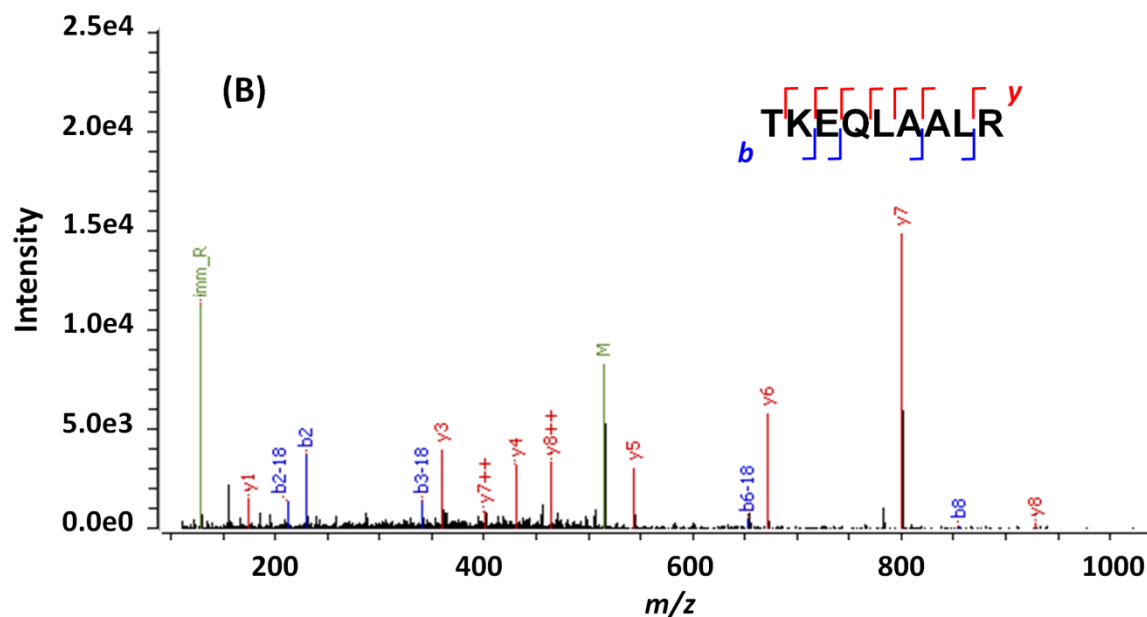


**Figure 5.6** MS/MS spectra for two identified peptides from two novel HCPs detected in NISTmAb, (A) ubiquitin-60S ribosomal protein L40 (P62984) and (B) ATPase inhibitor, mitochondrial (O35143).

### 5.3.4 HCP detection with fusion protein

BMS fusion protein 1 was analyzed using our HILIC-enriched HCP method. 700  $\mu\text{g}$  of the fusion protein drug product was loaded onto the HILIC column for HCP enrichment (UV chromatogram in Figure 5.7). For comparison, the mAb-precipitation method was also used in parallel. As indicated in Table 5.2, 22 HCPs were identified by the HILIC-enriched HCP method, showing a 30% increase compared with the precipitation method. Notably, 7 out of these 22 HCPs were unique to our method. For example, the HILIC method identified endoplasmic reticulum resident protein 29 (accession #: G3H284) with high confidence (28% sequence coverage), while it was undetected using the precipitation approach.

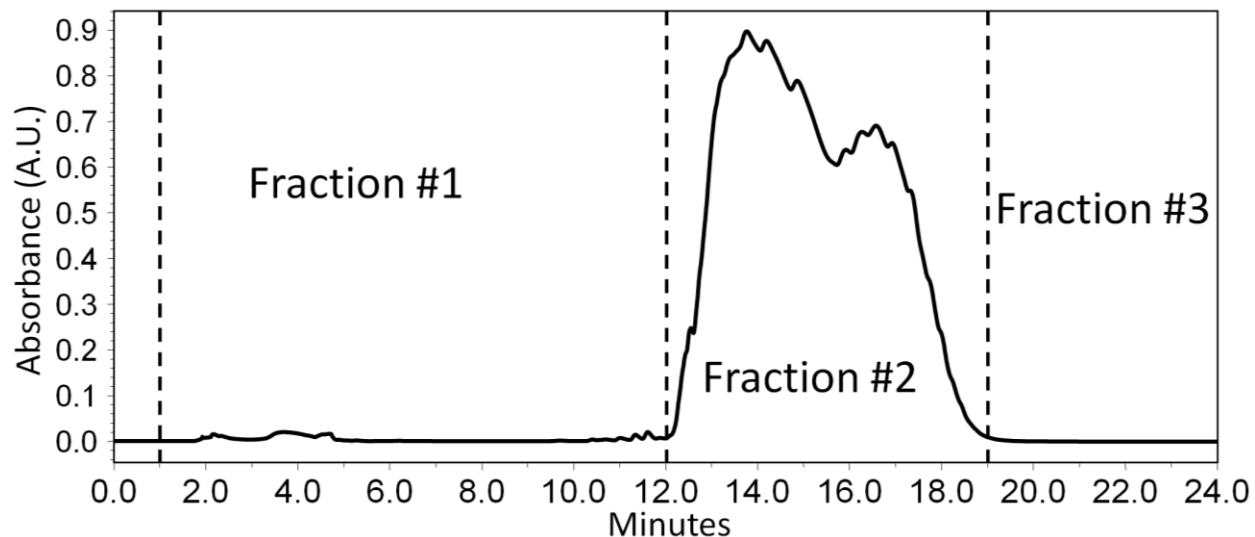


**Figure 5.7** 280 nm UV chromatogram from HILIC separation of 700  $\mu$ g BMS fusion protein 1. The LC eluate was collected in Fraction #1, #2, and #3 separately, as indicated by the different retention time ranges: 1.0–12.0 min for Fraction #1, 12.0–19.0 min for Fraction #2, and 19.0–24.0 min for Fraction #3.

The higher number of HCPs detected for BMS fusion protein 1 with the HILIC method may relate to the enrichment mechanism for the “mAb-precipitation” strategy. That approach relies on the resistance of antibodies to digestion, attributed to their stable higher-order structure under native conditions [12]. HCP enrichment is therefore achieved during sample preparation by removing the minimally digested therapeutic via precipitation. However, this method may not be effective for other kinds of therapeutic proteins that are less rigid in structure and, therefore, less resistant to trypsin digestion, e.g., fusion proteins. The “mAb-precipitation” and HILIC sample preparation methods again proved complementary, together detecting 24 HCPs, more than either technique alone.

## 5.4 Conclusions

The offline HILIC sample preparation method developed in this work can enrich HCPs and deplete high abundance therapeutic proteins and, therefore, improve the sensitivity for HCP detection in drug substances. This strategy takes advantage of high organic solvent concentration in the LC mobile phase to disrupt protein-protein interactions and consequently provide effective separation between HCPs and antibodies. The method enables characterization of HCPs in both

mAb and non-mAb drug substances with similar performance, which may be advantageous compared to other strategies.

Further benefits will be explored for improving HCP detection sensitivity with increased throughput. For future work, semi-preparatory scale HILIC columns (i.e., 4.6 mm i.d.) may provide higher sensitivity at similar throughput by allowing greater column loading. Further optimization in the drying and reconstitution steps may further improve recovery of HCPs. Lastly, a similar “mAb-precipitation” method to the published accounts may be performed on Fraction #2 to provide enrichment of any HCPs co-eluting with the mAb. This strategy should detect any HCPs currently observed with the “mAb-precipitation” technique but not with our approach. Quantification strategies can also be developed based on the current protocol by spiking in internal standards before or after the HILIC enrichment, or following digestion. This HILIC approach also provides another strategy for size or hydrophobicity-based separation of process and sample HCPs, and as future studies improve our understanding of the HILIC separation mechanism for intact proteins, a more detailed correlation with the physical properties of HCPs eluting before, with, and after the biotherapeutic protein will be achieved.

## 5.5 References

1. Wang, F., Richardson, D., Shameem, M.: Host-Cell Protein Measurement and Control. *BioPharm Int.* **28**, 32-38 (2015)
2. Abiri, N., Pang, J., Ou, J., Shi, B., Wang, X., Zhang, S., Sun, Y., Yang, D.: Assessment of the immunogenicity of residual host cell protein impurities of OsrHSA. *PLOS ONE.* **13**, e0193339 (2018)
3. Hogwood, C.E.M., Bracewell, D.G., Smales, C.M.: Host cell protein dynamics in recombinant CHO cells. *Bioengineered.* **4**, 288-291 (2013)
4. Schenauer, M., C Flynn, G., Goetze, A.: Identification and quantification of host cell protein impurities in biotherapeutics using mass spectrometry. *Anal. Biochem.* **428**, 150-157 (2012)
5. Bracewell, D.G., Francis, R., Smales, C.M.: The future of host cell protein (HCP) identification during process development and manufacturing linked to a risk-based management for their control. *Biotechnol. Bioeng.* **112**, 1727-1737 (2015)
6. Krawitz, D.C., Forrest, W., Moreno, G.T., Kittleson, J., Champion, K.M.: Proteomic studies support the use of multi-product immunoassays to monitor host cell protein impurities. *PROTEOMICS.* **6**, 94-110 (2006)
7. Berkelman, T., Harbers, A., Bandhakavi, S. Humana Press, New York, NY, Posch A. (eds) *Proteomic Profiling. Methods in Molecular Biology* (2015)

8. Zhang, Q., Goetze, A.M., Cui, H., Wylie, J., Trimble, S., Hewig, A., Flynn, G.C.: Comprehensive tracking of host cell proteins during monoclonal antibody purifications using mass spectrometry. *mAbs*. **6**, 659-670 (2014)
9. Madsen, J.A., Farutin, V., Carbeau, T., Wudyka, S., Yin, Y., Smith, S., Anderson, J., Capila, I.: Toward the complete characterization of host cell proteins in biotherapeutics via affinity depletions, LC-MS/MS, and multivariate analysis. *mAbs*. **7**, 1128-1137 (2015)
10. Doneanu, C., Xenopoulos, A., Fadgen, K., Murphy, J., Skilton, S.J., Prentice, H., Stapels, M., Chen, W.: Analysis of host-cell proteins in biotherapeutic proteins by comprehensive online two-dimensional liquid chromatography/mass spectrometry. *mAbs*. **4**, 24-44 (2012)
11. Doneanu, C.E., Anderson, M., Williams, B.J., Lauber, M.A., Chakraborty, A., Chen, W.: Enhanced Detection of Low-Abundance Host Cell Protein Impurities in High-Purity Monoclonal Antibodies Down to 1 ppm Using Ion Mobility Mass Spectrometry Coupled with Multidimensional Liquid Chromatography. *Anal. Chem.* **87**, 10283-10291 (2015)
12. Huang, L., Wang, N., Mitchell, C.E., Brownlee, T., Maple, S.R., De Felippis, M.R.: A Novel Sample Preparation for Shotgun Proteomics Characterization of HCPs in Antibodies. *Anal. Chem.* **89**, 5436-5444 (2017)
13. Lagassé H.A.D., Alexaki, A., Simhadri, V.L., Katagiri, N.H., Jankowski, W., Sauna, Z.E., Kimchi-Sarfaty, C.: Recent advances in (therapeutic protein) drug development. *F1000Research*. **6**, 113-113 (2017)
14. Moreland, L.W., Baumgartner, S.W., Schiff, M.H., Tindall, E.A., Fleischmann, R.M., Weaver, A.L., Ettlinger, R.E., Cohen, S., Koopman, W.J., Mohler, K., Widmer, M.B., Blosch, C.M.: Treatment of Rheumatoid Arthritis with a Recombinant Human Tumor Necrosis Factor Receptor (p75)-Fc Fusion Protein. *N. Engl. J. Med.* **337**, 141-147 (1997)
15. Wang, S., Liu, A.P., Yan, Y., Daly, T.J., Li, N.: Characterization of product-related low molecular weight impurities in therapeutic monoclonal antibodies using hydrophilic interaction chromatography coupled with mass spectrometry. *J. Pharm. Biomed. Anal.* **154**, 468-475 (2018)

## Chapter 6

### Conclusions and Future Directions

#### 6.1 Dissertation Summary

Chapters 2 through 4 in this dissertation explore alternative gas-phase fragmentation techniques and improve existing MS/MS methods for HDX MS experiments with the goal of elucidating protein higher-order structures. ECD and ETD have been demonstrated to proceed, under carefully tuned conditions, with minimal intramolecular H/D migration and are increasingly utilized in bottom-up and top-down HDX MS workflows to improve spatial resolution, i.e., to localize deuteriums down to the single amino acid residue level.

In Chapter 2, the feasibility of a series of negative ion mode MS/MS techniques for HDX MS/MS was examined. We focused on several regio-selectively deuterated peptide anions as probes to determine the extent of H/D scrambling associated with nCID, nFRIPS, EDD, and niECD. It was concluded that nCID induces extensive H/D scrambling within all peptides examined. In addition, unusual scrambling behavior was observed with histidine-containing peptides, presumably due to the involvement of histidine C-2 and C<sub>β</sub>-hydrogen atoms in H/D scrambling. nFRIPS, EDD, and niECD were also found to promote scrambling but to various extents. Complete randomization of the deuteration profile was observed upon nFRIPS, whereas EDD and niECD proceeded with moderate scrambling levels. niECD showed slightly lower H/D scrambling levels than EDD. In general, neither examined negative ion mode MS/MS technique is practical for improving spatial resolution in HDX MS/MS experiments, due to the energetics

of the fragmentation process itself and/or the negative ionization process. Nevertheless, my results provided new insights into the mechanisms of these anion fragmentation techniques.

In Chapter 3, we incorporated supercharging strategies into conventional ECD/ETD HDX MS workflows to enhance the extent of charging ( $\geq 3+$ ) for pepsin-derived peptides, with the goal of improving ECD/ETD fragmentation efficiency, sequence coverage, and, consequently improve spatial resolution in HDX MS experiments. By adding as little as 0.1% *m*-NBA to the LC mobile-phase solvents, a significant increase in average charge state was observed for all peptic peptides in a typical bottom-up HDX LC/MS workflow, although poorer chromatographic separation and increased chemical noise were also noted from the TICs. The presence of 0.1% *m*-NBA in the mobile phase shortened peptide retention times; however, these shifts could be avoided by injecting *m*-NBA through an external mixing tee located after the analytical column. Upon increasing the *m*-NBA concentration in the ESI solvent, the extent of charge enhancement further increased for myoglobin peptic peptides, but 0.1% appeared to be an optimal concentration for achieving a compromise between effective supercharging and acceptable S/N ratios. Sulfolane was found to be as effective as *m*-NBA for supercharging peptic peptides, while DMSO and propylene carbonate were not effective. As verified by LC ECD auto MS/MS on a SolariX FT-ICR instrument, the abundance of peptide peptides with  $\geq 3+$  charge states increased upon addition of *m*-NBA, which improved ECD fragmentation efficiency and peptide sequence coverage. We also verified that 0.1% *m*-NBA, either added to the LC mobile phase or injected post column, did not skew the deuterium contents of peptic peptide ions in HDX LC/MS experiments, suggesting that *m*-NBA can be used as an effective supercharging additive in ECD/ETD-based bottom-up HDX LC/MS workflows for improving HDX spatial resolution.

In Chapter 4, we specifically explored the occurrence of *b* ions, an unconventional type of fragment ion in ECD/ETD, of supercharged peptides. This work was inspired by the supercharging work in Chapter 3, as more fragments and associated more complex spectra were frequently observed upon ECD of highly charged peptide ions. To our knowledge, *b* ions have been reported to occur in ECD, but not in ETD, consistent with our findings that, for peptides

with few or no basic amino acid residues that yield abundant *b* ions upon ECD, ETD did not generate any *b* ions. Upon ECD of melittin and proteolytic peptides containing one or multiple basic sites, the number and abundance of *b* ions increased with the precursor ion charge state, suggesting that *b* ions are prominent in ECD spectra when the number of protons is higher than the number of basic sites in a peptide, e.g., following supercharging. Significantly less abundant *b* ions were observed in ETD spectra of supercharged peptides compared with ECD spectra. Nevertheless, these experiments are the first report of *b* ions from ECD/ETD as a function of precursor ion charge state. Our results provided insight into the different energy deposition and initial peptide temperature in ECD and ETD. We propose that, for supercharged peptide ions, a proton is likely located at a backbone amide, where electron attachment generates a hydrogen radical, which is preferentially ejected. The elevated internal energy of the remaining peptide is sufficient to generate *b*-type ions in ECD. Hydrogen radical ejection is less pronounced in ETD, thus *b* ion formation is much rarer in ETD. We suggest that *b* ions should be considered in ExD database searches for high peptide and protein charge states. Our data suggest that, for supercharging-assisted HDX MS/MS experiments, ETD is more suitable than ECD for minimizing deuterium loss and H/D scrambling.

Chapter 5 describes an offline HILIC sample preparation method that we developed for improving detection of residual-level host cell proteins in biotherapeutic proteins, as a work report for a six-month co-op program that I undertook at Bristol-Myers Squibb. This method utilizes the separation ability of HILIC to enrich HCPs while depleting highly abundant therapeutic proteins. The denaturing conditions used in the HILIC-based sample treatment facilitated disruption of protein-protein interactions between HCPs and therapeutic proteins to achieve efficient separation. This HILIC-enriched HCP LC/MS method enabled detection of HCPs in drug substances that had not previously been observed with other conventional flow rate LC/MS strategies, and is applicable to both mAb and non-mAb drug substances with similar performance.

Overall, the analytical strategies explored and developed in this dissertation contribute to

improving LC and MS tools for protein interaction analysis.

## 6.2 Future Directions

### 6.2.1 Hydrogen scrambling mechanisms in negative ion mode MS/MS

Following our study regarding H/D scrambling behavior in negative ion mode gas-phase fragmentation techniques presented in Chapter 2, there are several interesting questions worth further investigation. We have shown that radical-driven fragmentation methods can promote H/D scrambling, although to a smaller extent than collision-based fragmentation. However, the scrambling levels measured for different fragment ions from the same peptide upon EDD and niECD were different, indicating that intramolecular H/D scrambling might occur locally instead of evenly across the whole peptide anion. For example, the  $c_8$  ion exhibited a much higher hydrogen scrambling level than the  $c_2$  and  $c_3$  ions in niECD of peptide P4. Similar regio-selective H/D scrambling has been reported upon ETD for a smaller peptide, RPYIL [1]. It is implied that different chemical properties and steric effects of exchangeable sites within a fragment ion, as well as the gaseous conformation of the precursor ion may lead to different scrambling rates. Work by Rand *et al.* [2] shows another example: uneven distribution of deuteriums was observed in the Asp repeat of a selectively labeled peptide,  $K_2D_6$ IHKIK, upon ETD, which was not expected based on the known effect of primary structure on backbone amide hydrogen exchange [3]. Thus, to fully understand the mechanisms behind H/D scrambling, examination of multiple peptide models are needed for each type of MS/MS method.

A practical challenge for conducting hydrogen scrambling studies on selectively deuterated peptide anions is the reduced ionization efficiency and backbone fragmentation efficiency associated with radical-driven negative ion mode MS/MS, from which abundant neutral losses, such as water and ammonia, are frequently observed. It has been reported that the abundant  $NH_3$  loss upon ETD of peptide ions can indicate the extent of hydrogen scrambling during HDX ETD experiments [4], based on the several orders of magnitude higher solution-phase HDX rates of the N-terminal amine, the C-terminal carboxyl group, and the peptide side chains compared with backbone amide hydrogens [3]. Similarly, we may be able to

utilize ions originating from ammonia or water loss from the charge-reduced (or increased) peptide ion as a reporter of the extent of H/D scrambling upon negative ion mode MS/MS. This approach would provide higher confidence in determining the deuterium content of the reporter ion, particularly when inadequate numbers/abundance of backbone fragment ions are generated.

### **6.2.2 Supercharging combined with ECD HDX MS/MS for elucidation of structural changes of a modular polyketide synthase during its catalytic cycle**

We observed higher deuterium loss (increased back-exchange) with increasing peptide ion charge state, e.g. upon supercharging, compared with lower charge states. This observation is probably due to the in-source elevated kinetic energy at higher charge states, resulting in facilitated D/H exchange with residual gas molecules along the ion path, such as water, formic acid, and *m*-NBA. This result suggests that future experiments need to be carefully planned: even though highly charged ions often yield superior ECD/ETD spectra, extremely supercharged peptide ions should probably not be used for HDX measurements [5].

Although supercharging strategies have been previously reported in both bottom-up [6] and top-down [7, 8] HDX MS, Chapter 3 in this dissertation presents a detailed comparison between different supercharging reagents and various *m*-NBA concentrations. In addition, a post-column injection method for introducing supercharging reagent is described. One future application of this strategy is to facilitate ECD fragmentation in HDX LC MS/MS experiments to elucidate the structural rearrangements of a modular polyketide synthase, PikAIII, during its catalytic cycle [9, 10]. This prospective project is based on a collaboration with Life Sciences Institute researchers at Michigan. HDX coupled to ExD MS/MS holds potential for pinpointing conformational changes in PikAIII down to the level of individual residues. The newly-installed Agilent 6560 Ion Mobility Q-TOF LC/MS system equipped with a LEAP HDX PAL platform and an e-MSion ExD cell has the unique capability to perform this type of experiment. Given the size of the PikAIII polypeptide (over 1,500 amino acid residues), a middle-down method may be necessary. *m*-NBA, and other supercharging agents such as propylene carbonate and 1,2-butylene carbonate, can effectively supercharge small-to-medium size protein ions to promote top-down

ECD/ETD [11, 12] (one example is shown in Figures 6.1 and 6.2); therefore, they may also be ideal for larger peptides generated from a middle-down protocol.

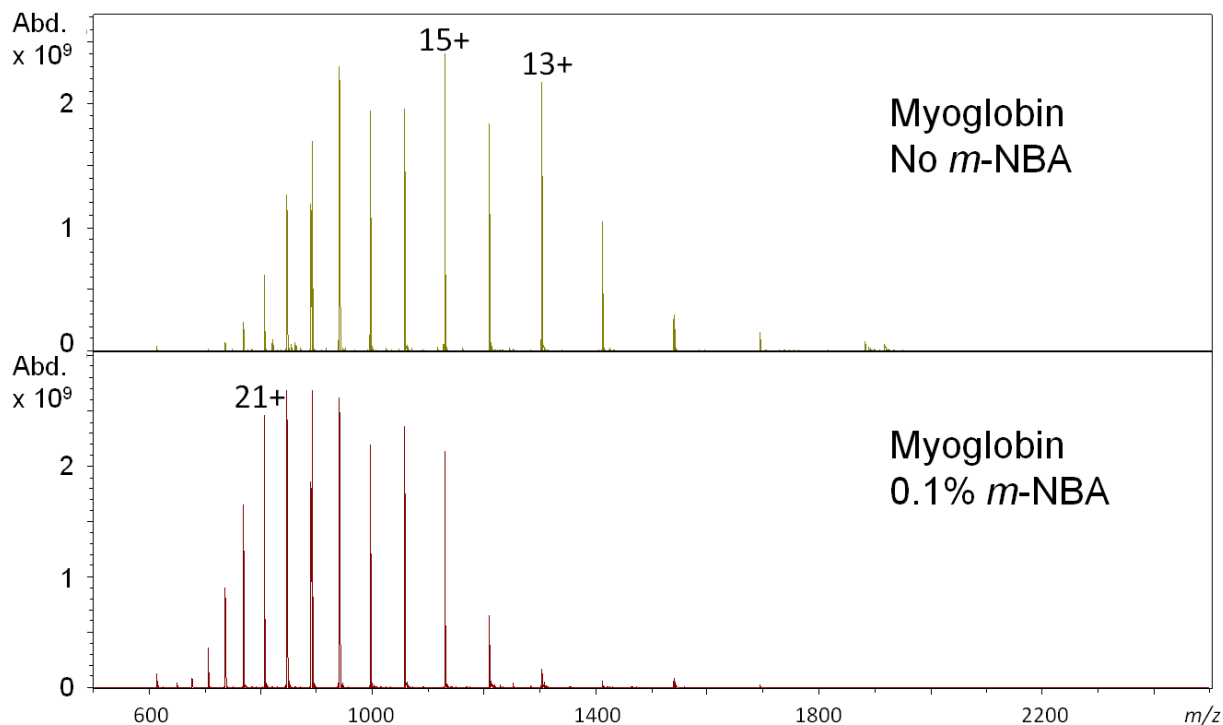
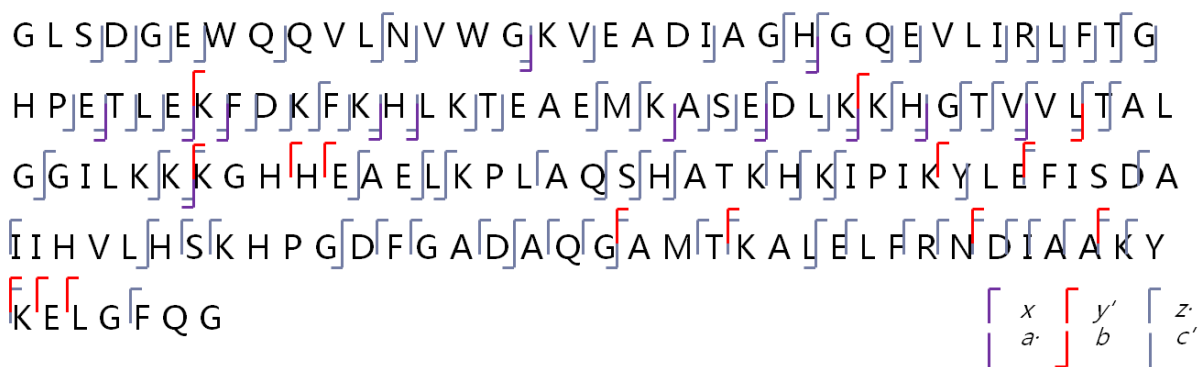


**Figure 6.1** Charge-state distributions of apo-myoglobin with (bottom) and without (top) addition of 0.1% *m*-NBA into the ESI solvent (50/50/0.2 water/methanol/formic acid). The mass spectra were collected on a Solarix FT-ICR mass spectrometer.

[Apo-myoglobin + 17H]<sup>17+</sup>; No *m*-NBA; 59%



[Apo-myoglobin + 22H]<sup>22+</sup>; 0.1% *m*-NBA; 72%

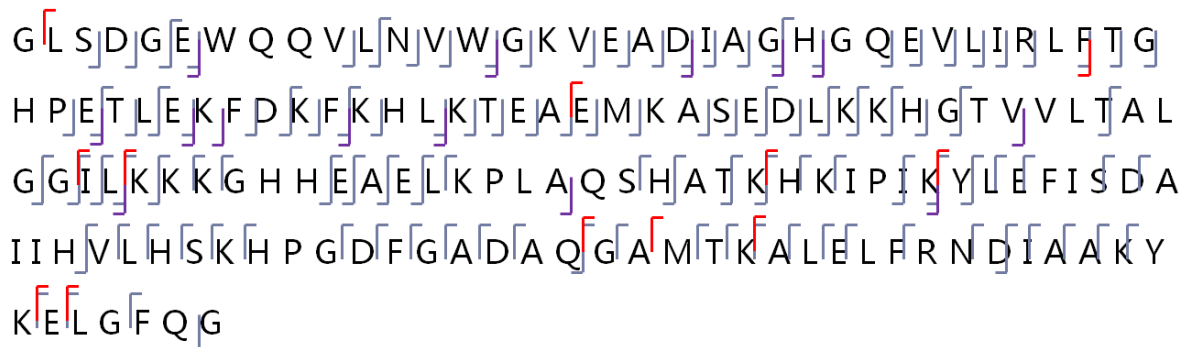


**Figure 6.2** Backbone cleavages in apo-myoglobin upon ECD of the 17+ charge state (top) versus the 22+ charge state (bottom).  $a^*/x$ ,  $b/y'$ , and  $c'/z'$  fragment ions are color-coded as shown in the legend. The addition of 0.1% *m*-NBA into the ESI solvent promoted the generation of more highly-charged protein ions, improving sequence coverage from 59% (17+) to 72% (22+).

### 6.2.3 Investigation of the occurrence of *b*-type ions in ECD/ETD of supercharged peptides

ECD is generally believed to be a “non-ergodic” process [13], but debates regarding its mechanisms have been ongoing since its invention in 1998. We believe that the work presented in Chapter 4 sheds light on a typically minor fragmentation pathway in ECD, but further investigation into the cause of *b* ions in ECD of supercharged peptides is warranted as it appears to be a major fragmentation pathway in such cases. One important question to answer is whether *b* ions occur from vibrational excitation upon H-desorption in ECD. Figure 6.3 presents an idea to support/reject this hypothesis. In Chapter 2, we showed that the extent of H/D scrambling in a selectively deuterated model peptide fragmented by ECD can be tuned by altering the “softness” of the ion source and the ion transport conditions, and that ECD can proceed with minimal hydrogen scrambling provided that the ion is not excessively heated. Similarly, we can use this

experimental method to measure the hydrogen scrambling levels of  $c'$ -,  $z'$ -, and  $b$ -ions, respectively, upon ECD of a supercharged model peptide. Under “harsh” conditions, both  $c'$ -/ $z'$ -ions and  $b$ -ions are expected to show high scrambling levels (~100%); whereas under “soft” conditions, minimal hydrogen scrambling (<10%) can be achieved for  $c'$ -/ $z'$ -ions. If  $b$  ions are generated from vibrational excitation in ECD, they should show extensive H/D scrambling despite the “soft” source conditions, and vice versa.

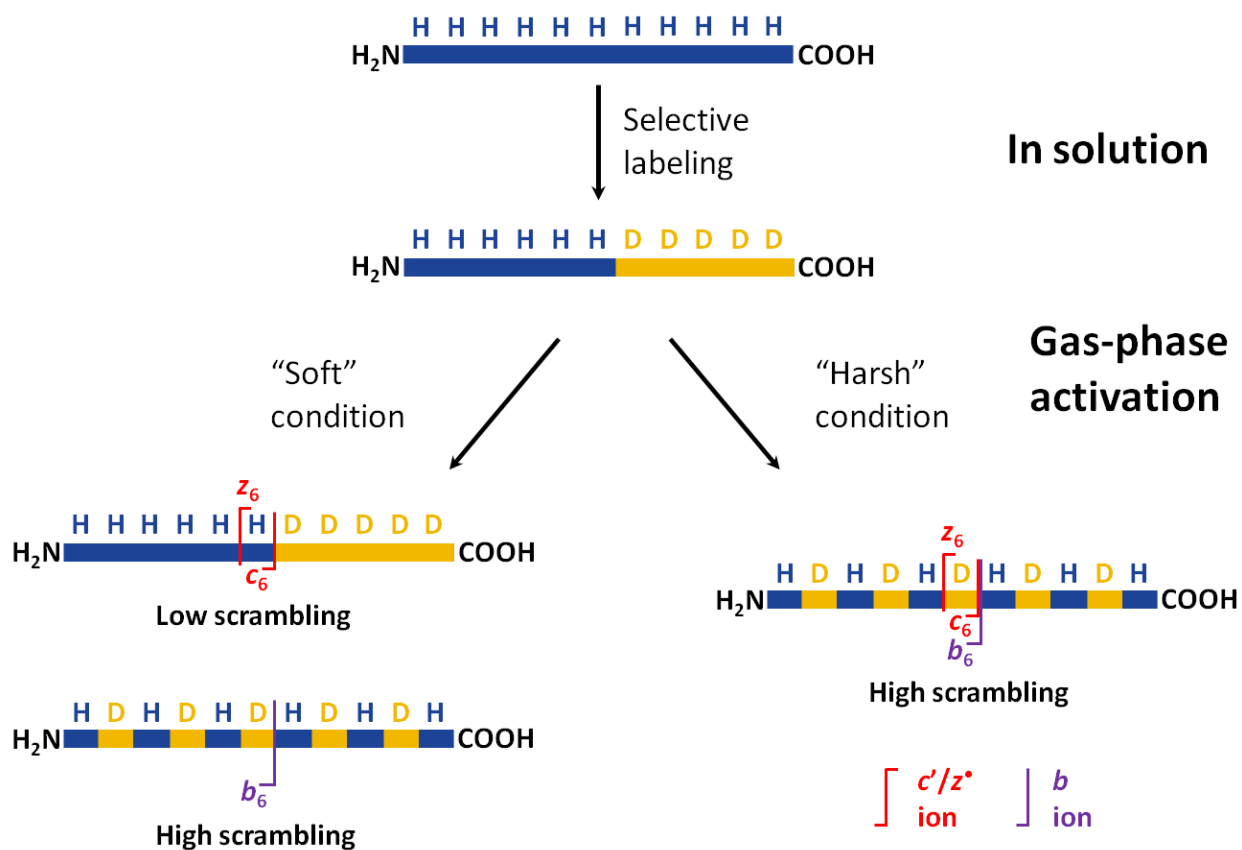


**Figure 6.3** Diagram of proposed H/D scrambling behaviors of  $c'$ -,  $z'$ -, and  $b$ -ions generated from ECD of a supercharged, selectively-deuterated peptide ion under “soft” and “harsh” conditions, respectively.

In addition, we can use other criteria to determine if  $b$  ions are formed via CID-like vibrational activation in ECD. Loss of labile modifications is frequently observed to a significantly greater extent in CID than in ECD/ETD spectra, e.g., for phosphorylation (due to the gas-phase lability of phosphoester bonds) [14]. We can perform ECD/ETD of high charge state phosphopeptides and examine how the extent of  $b$  ion formation correlates with

phosphate/phosphoric acid loss. Figure 6.4 shows example ECD/ETD spectra of a supercharged phosphopeptide ion, FQpSEEQQQTEDELQDK. The ECD spectrum of the 4+ charge state shows a plenitude of *b* ions, some with H<sub>3</sub>PO<sub>4</sub> neutral loss. However, no H<sub>3</sub>PO<sub>4</sub> loss is seen for *c* and *z* ions, or for the charge-reduced species generated upon ECD. On the contrary, ETD of the same peptide ion does not yield *b* ions or PTM losses. Phosphoric acid loss from *b* ions appears to occur only in ECD of supercharged phosphopeptides. Fundamental studies of this kind are valuable references for the design of MS experiments for which minimum vibrational activation is desirable, e.g., HDX ExD MS/MS.

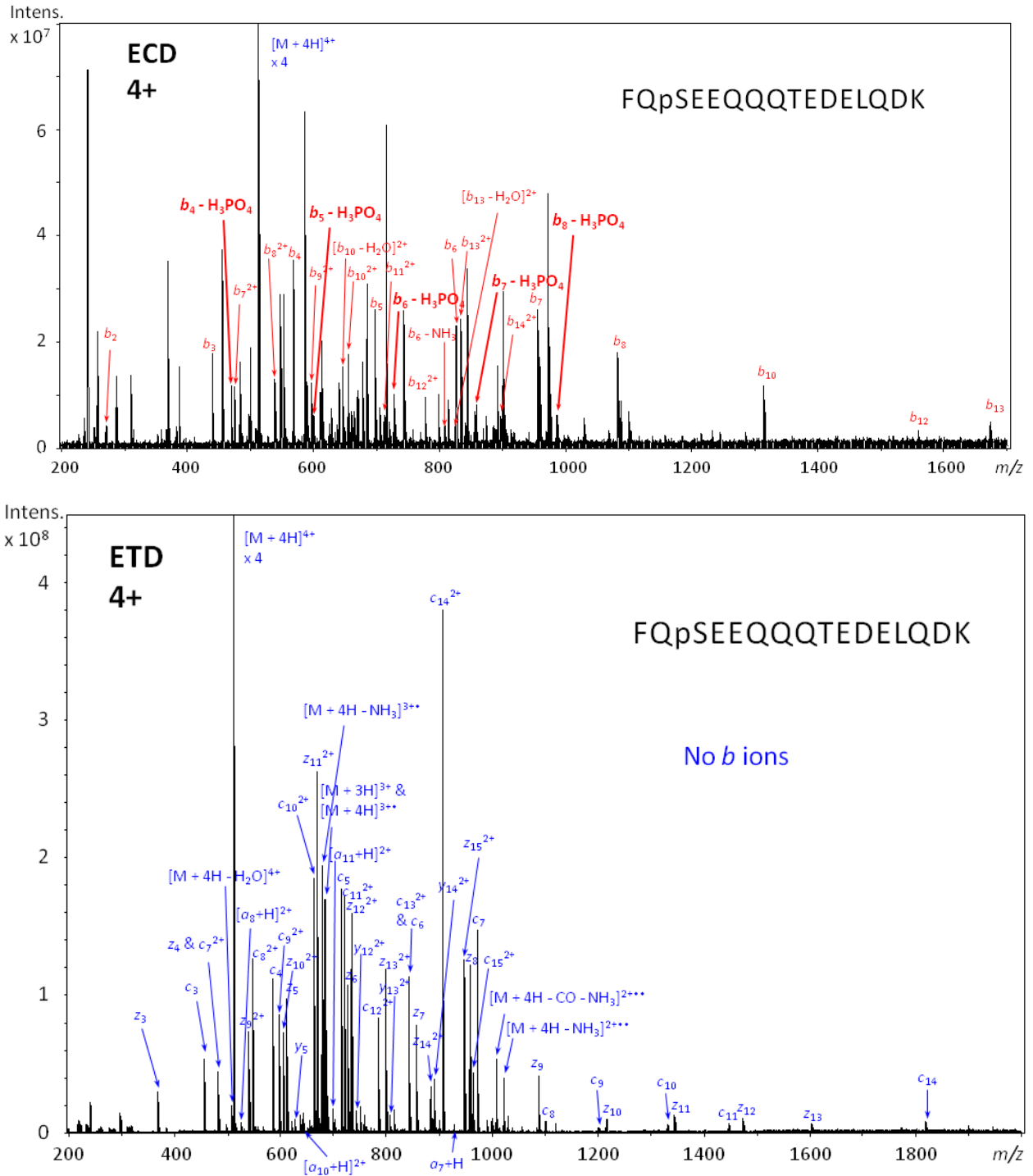


**Figure 6.4** ECD (top) and ETD (bottom) MS/MS spectra of a quadruply protonated monophosphorylated peptide from trypsin digestion of  $\beta$ -casein. This charge state is only observed following supercharging with *m*-NBA. In the ECD spectrum, only *b* ions and *b* ions with neutral loss are labeled (red).

#### **6.2.4 Further characterization and optimization of the offline HILIC method and the potential of utilizing HDX MS to investigate interactions between HCPs and biotherapeutic proteins**

When using the offline HILIC sample preparation method developed for HCP detection in biotherapeutics, samples are loaded onto an HILIC column and collected from eluates, followed by concentration, trypsin digestion, and LC/MS analysis. Potential HCP loss may be attributed to their adsorption on the HILIC column during chromatographic separation. This problem becomes more significant for HCPs present in the drug substance at very low ppm levels. For future work, the HCP recovery percentage of the current method needs to be evaluated by running more HCP-spiked drug substance samples. So far, only 10k and 1k ppm HCP spiked mAb samples have been characterized using our method. For future work, 100 and 10 ppm HCP spiked samples need to be analyzed to test the viability of our method for lower ppm level HCPs. Optimization of the current digestion protocol may also be necessary to further improve the sensitivity for low ppm level HCPs.

In addition, further benefits will be realized in the future if throughput can be increased. Currently, the first-step chromatography is conducted on a Waters HILIC column with the largest commercially available size, 2.1 x 150 mm. A semi-preparatory scale (i.e., 4.6 mm i.d.) custom column with the same packing material has been ordered and manufactured from Waters. This larger column may provide improved sensitivity at similar throughput by allowing greater column loading. Quantification strategies can also be developed based on the current protocol by spiking in internal standards before or after the HILIC enrichment, or after digestion. To improve our understanding of the principles of HILIC separation for intact proteins, we can examine the common/different physical properties of the HCPs eluting before, with, and after the therapeutic protein.

Also, characterizing interactions between HCPs and therapeutic proteins via HDX MS would be useful to elucidate the effects of coexisting HCP impurities toward the higher-order

structure of the therapeutic protein. One HCP candidate to study is phospholipase B-like 2 (PLBL2), a Chinese Hamster Ovary (CHO)-derived HCP that is challenging to remove in the purification processes for multiple antibody therapeutics [15]. It is of particular concern for being implicated in the literature as being potentially immunogenic [16, 17]. We have also identified PLBL2 in our HCP standard pool produced from CHO null cell line. The ultimate goal is to determine how these HCPs influence the stability and/or efficacy of the drug product and to develop powerful purification methods to achieve robust removal of these impurities.

With an increase in the number of protein therapeutics being pursued in the biopharmaceutical industry, there is an increasing demand for bioanalytical science to understand the characteristics of biotherapeutic proteins. Higher-order structural elucidation is a key aspect where HDX MS tools are valuable. Understanding the relationship between protein structure and function enables rational protein engineering to enhance therapeutic properties, improve safety and consistency of manufacturing, and reduce undesired interactions between impurities and biotherapeutic drug products. In the future, our ability to characterize the higher-order structure and interactions of large biomolecules on a routine level will be truly critical.

### 6.3 References

1. Hamuro, Y.: Regio-Selective Intramolecular Hydrogen/Deuterium Exchange in Gas-Phase Electron Transfer Dissociation. *J. Am. Soc. Mass. Spectrom.* **28**, 971-977 (2017)
2. Rand, K.D., Lund, F.W., Amon, S., Jørgensen, T.J.D.: Investigation of amide hydrogen back-exchange in Asp and His repeats measured by hydrogen (1H/2H) exchange mass spectrometry. *Int. J. Mass spectrom.* **302**, 110-115 (2011)
3. Bai, Y., Milne, J.S., Mayne, L., Englander, S.W.: Primary structure effects on peptide group hydrogen exchange. *Proteins: Structure, Function, and Bioinformatics.* **17**, 75-86 (1993)
4. Rand, K.D., Zehl, M., Jensen, O.N., Jørgensen, T.J.D.: Loss of Ammonia during Electron-Transfer Dissociation of Deuterated Peptides as an Inherent Gauge of Gas-Phase Hydrogen Scrambling. *Anal. Chem.* **82**, 9755-9762 (2010)
5. Duchateau, M., Jørgensen, T.J.D., Robine, O., Nicol, E., Malosse, C., Chamot-Rooke, J., van der Rest, G.: Ion source parameters and hydrogen scrambling in the ECD of selectively deuterated peptides. *Int. J. Mass spectrom.* **367**, 21-27 (2014)
6. Rand, K.D., Zehl, M., Jensen, O.N., Jørgensen, T.J.D.: Protein Hydrogen Exchange Measured at Single-Residue Resolution by Electron Transfer Dissociation Mass

- Spectrometry. *Anal. Chem.* **81**, 5577-5584 (2009)
7. Sterling, H.J., Williams, E.R.: Real-Time Hydrogen/Deuterium Exchange Kinetics via Supercharged Electrospray Ionization Tandem Mass Spectrometry. *Anal. Chem.* **82**, 9050-9057 (2010)
  8. Going, C.C., Xia, Z., Williams, E.R.: Real-time HD Exchange Kinetics of Proteins from Buffered Aqueous Solution with Electrothermal Supercharging and Top-Down Tandem Mass Spectrometry. *J. Am. Soc. Mass. Spectrom.* **27**, 1019-1027 (2016)
  9. Dutta, S., Whicher, J.R., Hansen, D.A., Hale, W.A., Chemler, J.A., Congdon, G.R., Narayan, A.R.H., Håkansson, K., Sherman, D.H., Smith, J.L., Skiniotis, G.: Structure of a modular polyketide synthase. *Nature.* **510**, 512 (2014)
  10. Whicher, J.R., Dutta, S., Hansen, D.A., Hale, W.A., Chemler, J.A., Dosey, A.M., Narayan, A.R.H., Håkansson, K., Sherman, D.H., Smith, J.L., Skiniotis, G.: Structural rearrangements of a polyketide synthase module during its catalytic cycle. *Nature.* **510**, 560 (2014)
  11. Teo, C.A., Donald, W.A.: Solution Additives for Supercharging Proteins beyond the Theoretical Maximum Proton-Transfer Limit in Electrospray Ionization Mass Spectrometry. *Anal. Chem.* **86**, 4455-4462 (2014)
  12. Zenaidee, M.A., Donald, W.A.: Extremely supercharged proteins in mass spectrometry: profiling the pH of electrospray generated droplets, narrowing charge state distributions, and increasing ion fragmentation. *Analyst.* **140**, 1894-1905 (2015)
  13. Zubarev, R.A., Kelleher, N.L., McLafferty, F.W.: Electron Capture Dissociation of Multiply Charged Protein Cations. A Nonergodic Process. *J. Am. Chem. Soc.* **120**, 3265-3266 (1998)
  14. Brown, R., Stuart, S.S., Houel, S., Ahn, N.G., Old, W.M.: Large-Scale Examination of Factors Influencing Phosphopeptide Neutral Loss during Collision Induced Dissociation. *J. Am. Soc. Mass. Spectrom.* **26**, 1128-1142 (2015)
  15. Tran, B., Grosskopf, V., Wang, X., Yang, J., Walker, D., Yu, C., McDonald, P.: Investigating interactions between phospholipase B-Like 2 and antibodies during Protein A chromatography. *J. Chromatogr. A.* **1438**, 31-38 (2016)
  16. Vanderlaan, M., Sandoval, W., Liu, P., Nishihara, J., Tsui, G., Lin, M., Gunawan, F., Parker, S., Wong, R.M., Low, J., Wang, X., Yang, J., Veeravalli, K., McKay, P., Yu, C., O'Connell, L., Tran, B., Vij, R., Fong, C., Krawitz, D.: Hamster phospholipase B-like 2 (PLBL2): A host-cell protein impurity in therapeutic monoclonal antibodies derived from chinese hamster ovary cells. *BioProcess International.* **13**, (2015)
  17. Jawa, V., Joubert, M.K., Zhang, Q., Deshpande, M., Hapuarachchi, S., Hall, M.P., Flynn, G.C.: Evaluating Immunogenicity Risk Due to Host Cell Protein Impurities in Antibody-Based Biotherapeutics. *The AAPS Journal.* **18**, 1439-1452 (2016)